Epidermal Function in the Nematode, *Caenorhabditis elegans*

Laura Mary McMahon

Wellcome Centre for Molecular Parasitology
Anderson College
University of Glasgow
56 Dumbarton Road
Glasgow
G11 6NU

This thesis is presented in submission for the degree of Doctor of Philosophy in the Faculty of Veterinary Medicine

May, 1999

ProQuest LLC.
789 East Eisenhower Parkway
P.O. Box 1346
Ann Arbor, MI 48106 – 1346

Abstract

Epithelial sheets create the forces which shape embryos during the development of all metazoans. The external epithelia, or hypodermis, of the nematode *Caenorhabditis elegans* plays an essential role in shape change during embryogenesis and also maintains body shape during postembryonic development. Embryonic shape change, known as elongation, is mediated by actin microfilaments in the hypodermis which align circumferentially and contract, causing the embryo to change from a ball of cells, to a long, thin worm shape. A prerequisite to elongation is the migration of the hypodermis around the embryo from the dorsal surface to completely cover the embryo in a layer of hypodermal cells, a process known as enclosure. At the end of embryogenesis, the hypodermis secretes a multi-layered, collagenous exoskeleton, known as the cuticle, which maintains the elongated worm shape postembryonically. In this thesis, I have characterised three elongation-defective mutants which arrest during embryogenesis, and have also looked at the pattern of a cuticular collagen, DPY-7, throughout development using a novel monoclonal antibody, DPY7-5a. One of the embryonic lethal mutations, *w4*, lies on Chromosome I, between positions 6.2 and 9.9 on the genetic map. The majority of *w4* homozygotes are defective in enclosure. The other two embryonic lethal mutations, *ijDf1* and *ijDf2* are the result of large deficiencies which have been physically mapped. *ijDf2* extends from around position -0.9 to 0.7 on chromosome V and is approximately 2.2Mb in size. *ijDf2* homozygotes appear to have a pre-enclosure defect in cell adhesion. *ijDf1* extends from around position 18 to 23.5 on the X chromosome and is approximately 1.6Mb in size. *ijDf1* homozygotes arrest as 1.5-fold stage embryos and this early elongation defect was rescued by injection of the genomic overlap of cosmids K09A9 and K09E9, plus the whole of cosmid C02C6. However, inhibition of the function of predicted genes contained in these cosmids did not produce the mutant phenotype seen in the deficiency. The characterisation of the DPY7-5a antibody suggests localisation of DPY-7 in the cortical layer of the cuticle. The study of the antibody pattern in a *dpy-7* mutant demonstrates a clear reduction in secreted DPY-7. These results suggest that there are many molecular components in the complex process of embryonic elongation and the DPY7-5a antibody provides a novel mechanism to study postembryonic shape change and mechanisms of cuticle organisation within the hypodermis.

Declaration

I declare that the work presented in this thesis is my own except where otherwise stated

Laura McMahon

1999

Acknowledgements

I would like to thank Iain Johnstone, my supervisor, for all his help and patience throughout these past few years. I am grateful to Joel Rothman, Julie Ahringer, Michel Labouesse, Johnathon Hodgkin, Michelle Coutu, Arnaud Labrousse and Alexander van der Bliek for antibodies, strains, protocols and much needed advice and to everyone who communicated results prior to publication. The work presented in this thesis was supported by a grant from the Wellcome Trust.

It has been a pleasure to work with all the people at WCMP (the department formerly known as WUMP) for the past few years. There are certain people who have become close friends and I would like to thank them individually. John 'Johnny doughnut' Gilleard has been a great help from the beginning and did not get to escape my questions even when he ran away to Canada. I would also like to thank Mary Gilleard for her support, for coffee and laughs and the 'Slasher-Logan' myth. Moira Watson has been the plate pixie, antibody pixie and Mini Prep pixie more times than I can remember and stopped me going mad on many occasions. I would like to thank Collette Britton for having a protocol for everything, even if nobody else does it the same way, for putting up with me at various conferences and for so much help. I would like to thank Caroline Clucas for helping me make sense of genetic crosses, cursing the bloody worms and always helping with my problems, no matter what they were. I would also like to thank Alan Winter for showing us all a glimpse of Winter-Wonderland and for making me feel like I know a lot about computers. Big thanks to the tea-time posse past and present for many surreal conversations and laughs.

In addition I would like to thank my parents, who have supported me more than I could have wished in every way. I only hope that if I have children I can be half as good a parent as they have been. And to my brother for lots of advice, a place to escape to for holidays, and for making up for all that childhood trauma he caused.

Finally, I would like to thank my non-wormy friends, especially Craig, Iain, Susanne, Tricia, Lucy, Lynne, Aiders, Lorna, Tara, Ruth, and Ross, for many good times and limitless support.

This thesis is dedicated to the memory of Eric John Stewart, for his support, big cheesy grin, bad jokes, disco-dancing, tuneless singing and recipe ideas. Life is just not the same without him.

Abbreviations

DIC	differential interference contrast
DNA	deoxyribonucleic acid
ds	double stranded
EMS	Ethyl methanesulphonate
GFP	green fluorescent protein
GTPase	guanosine triphosphatase
mRNA	messenger ribonucleic acid
PCR	polymerase chain reaction
RNA	ribonucleic acid
rpm	revolutions per minute
RT-PCR	reverse transcription polymerase chain reaction
ss	single stranded
STS	sequence-tagged site
ts	temperature-sensitive
UV	ultraviolet
UTR	untranslated region

measurements

bp	base pair
cm	centimetre
kb	kilobase
kDa	kilodalton
Mb	megabase
mg	milligram
µg	microgram
ng	nanogram
mm	millimetre
µm	micrometre
nm	nanometre
min	minute
ml	millilitre
µl	microlitre
M	Molar
mM	milliMolar
nM	nanoMolar
V	volt

Contents

Chapter 2
Materials and Methods

Chapter 3
Localisation of the cuticular collagen, DPY-7 in wild type and mutant animals using a novel monoclonal antibody, DPY7-5a

Figures for Chapter 3

Chapter 4
Characterisation of a zygotic embryonic lethal mutation, *w4*

Tables for Chapter 4

Chapter 5
Characterisation of a deficiency, *ijDf2*

Chapter 6
Characterisation of a deficiency, *ijDf1*

Tables for Chapter 6

Chapter 7
Concluding discussion

Chapter 1
Introduction

1.1. *Caenorhabditis elegans* - a member of the Phylum Nematoda

Nematodes make up the majority of all living animals and, although around 20,000 species have been described, estimates of the actual number range from 40,000 to as many as 10 million (Platt, 1994; Blaxter, 1998). These nematodes, or 'roundworms' as they are more commonly known, live almost anywhere. They inhabit all areas of the globe at all altitudes, from the tropics to the poles, and survive in salt-water, freshwater, and both fertile and desert terrestrial environments. Although the vast majority of nematodes are free-living, many species have adopted a parasitic lifestyle and in this they are equally diverse, parasitising practically all groups of plants and animals. Despite this range of diversity, all nematodes are composed of the same basic body plan with a circular cross section, which consists of two concentric tubes separated by a fluid filled space known as the pseudocoelom. The outer tube comprises the muscles, nerve cells, epidermis (known as the hypodermis in *Caenorhabditis elegans*) and the collagenous extracellular cuticle which is secreted by the hypodermis and is probably one of the reasons why the phylum Nematoda is so successful. The inner tube consists of the intestine and its lumen and in adult worms, the pseudocoelom contains the gonads. *Caenorhabditis elegans* is a nematode worm of the Rhabditida order and the Rhabditidae family and as such is a member of a very diverse and successful group of animals.

1.2. The biology of *C.elegans*

C.elegans is the most extensively studied and best characterised species of the phylum Nematoda. It is a free-living soil microbivore with a 3½-day life cycle and an adult length of 1.5mm. Sydney Brenner chose *C.elegans* as a model organism for the study of animal behaviour and development in 1965 for many reasons which will be discussed throughout this introduction, one being the ease of maintaining *C.elegans* in laboratories on agar plates or liquid culture using *Escherichia coli* as a food source (Brenner, 1974).

There are two sexes, hermaphrodite and male, which are of similar size but can be easily distinguished in later stages of the life cycle by their different reproductive structures (section 1.2.2). Hermaphrodites make up the vast majority of *C.elegans* animals in normal populations with a male incidence of around 0.2%. The mode of reproduction is therefore predominantly self-fertilisation by hermaphrodites and each has the potential to produce around 300-350 progeny per generation if not mated with a male. The fecundity of hermaphrodites is limited by the number of germ cells which differentiate into sperm as these are produced before the oocytes. The life cycle of *C.elegans*, like all other nematode species consists of four larval stages, L1-L4, followed by a moult into the adult and the eggs are fertilised inside the adult hermaphrodite.

1.2.1. *C.elegans* development

The egg shell of *C.elegans* embryos and the body wall of larvae and adults are transparent, allowing the cell lineage of the embryo and postembryonic stages to be followed accurately using Nomarski microscopy, a non-damaging, high resolution light microscopy technique (Sulston and Horvitz, 1977; Sulston *et al.*, 1983). It was found that the cell lineage was essentially invariant, producing a constant number of cells in the same positions in each animal. This has allowed the development of *C.elegans* to be studied in great detail and has resulted in an accurate description of the events that occur during the embryonic and postembryonic stages.

1.2.1.1. Embryogenesis in *C.elegans*

Embryogenesis in *C.elegans* takes around 14 hours (840mins) at 22°C and comprises three major stages (Figure 1.1)(Sulston *et al.*, 1983; Wood, 1988). The first stage occurs during the initial 2 hours after fertilisation and includes zygote formation and the generation of the founder cells. The second stage includes the majority of cell divisions, gastrulation, the beginning of organogenesis and the differentiation of cell types and continues until around midway through embryonic development. During the third stage of embryogenesis, organogenesis and cell differentiation are completed and the embryo changes shape from an almost spherical ball of cells to a thin cylindrical worm

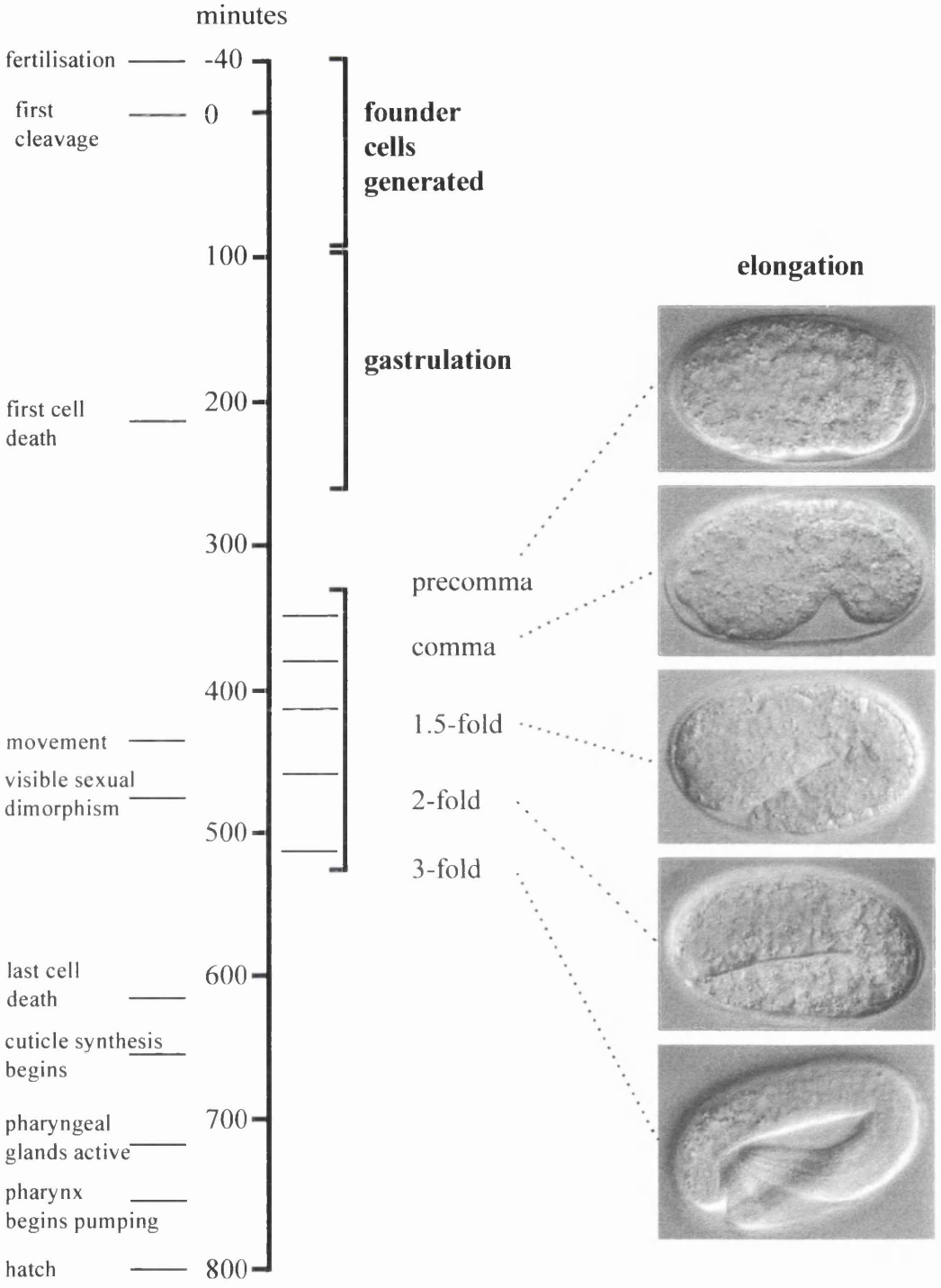

Figure 1.1

Stages, marker events, and body elongation during embryogenesis in *C.elegans*

The timescale is in minutes from first cleavage and refers to embryogenesis at 22°C. All embryos are approximately 50mm long and 30mm wide and before 3-fold elongation are orientated with the anterior to the left and the dorsal surface to the top of the image. (Adapted from Sulston *et al.*, 1983)

four times the original length. The third stage of development finishes at hatching when the pharynx of the embryo apparently pumps out enzymes which catalyse the breakdown of the eggshell from within (Wood, 1988). The timing of embryonic development is essentially invariant at any particular temperature and is usually measured from fertilisation or from first cleavage which occurs around 40 mins after fertilisation (Sulston *et al.*, 1983; Wood, 1988). Generally, early embryogenesis takes place in the uterus of the hermaphrodite and healthy wild type animals usually lay eggs when the embryos are undergoing gastrulation, around 120-180 mins after fertilisation.

The cell divisions which generate the founder cells and the tissues that arise from these cells are shown in Figure 1.2. The divisions that produce these founder cells are both asynchronous and unequal (Deppe *et al.*, 1978). Each founder cell and the cells it produces exhibit a characteristic rate of division which is fastest in the AB lineage and slowest in the D lineage. While the E, D and P_4 founder cells produce only gut, muscle and germline cells respectively, the AB, MS and C cells produce both ectodermal and mesodermal descendants (Sulston *et al.*, 1983).

Gastrulation is the process whereby mesodermal precursors migrate into the centre of the embryo from the surface through an opening known as the ventral cleft and thus form new cell-cell contacts which are essential for further development (Sulston *et al.*, 1983). This process begins around 140 mins after fertilisation at the 26 cell stage and continues until around 330 mins after fertilisation when the ventral cleft is closed. Gastrulation is discussed in more detail in section 5.1.2. Cell division and organogenesis occur during this stage and continue until around 390 mins after fertilisation. The terminally differentiated hypodermal cells are born on the dorsal surface of the embryo around 330 mins after fertilisation after the ventral cleft has closed and begin migrating bilaterally around the embryo to the ventral surface (Sulston *et al.*, 1983).

The active process of body morphogenesis begins at the end of cell proliferation around 390 mins after fertilisation when the embryo consists of around 550 cells and the hypodermal cells are continuous around the whole surface of the embryo (Sulston *et al.*, 1983; Wood, 1988; Williams-Masson *et al.*, 1997). From 390-690 mins the embryo elongates to a cylindrical shape which is three times narrower and four times longer than it was originally (Sulston *et al.*, 1983; Priess and Hirsh, 1986). The elongation of the

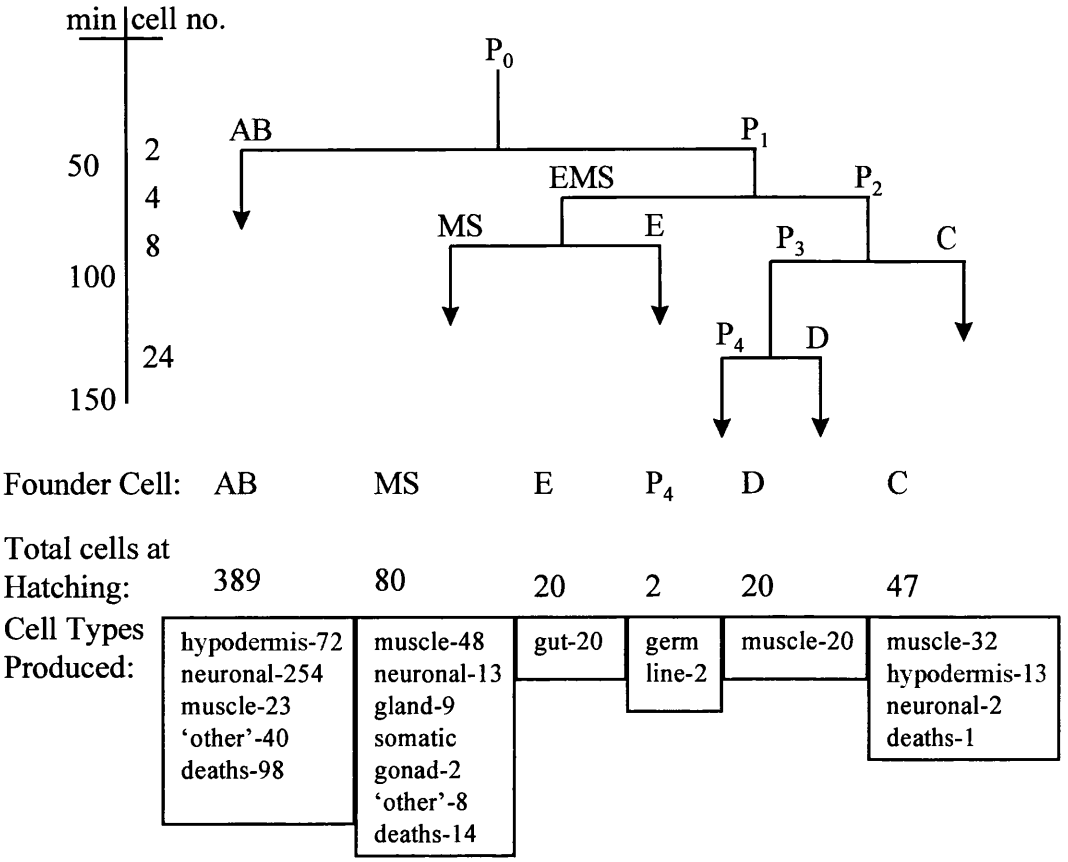

Figure 1.2

Generation of the founder cells during embryogenesis in *C.elegans*

The total number of cells at each stage and the time post-fertilisation (at 20°C) is shown at the top left and the different cell types produced by each founder cell is shown at the bottom. Founder cells which give rise to hypodermis are shown in green. (Redrawn from Sulston *et al.*, 1983).

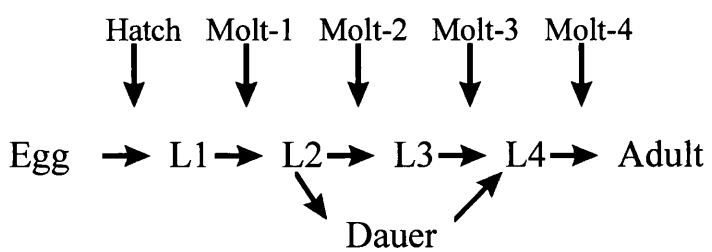

Figure 1.3

The life cycle of *C.elegans*

After hatching, development proceeds through four larval stages, L1-L4, to the adult. The entire process takes around 3 days at 20°C. The dauer stage is a developmentally arrested larva specialised to withstand adverse conditions. It is produced in response to environmental conditions at the L1 and L2 stages such as overcrowding or starvation.

worm and prior movements of the hypodermis are described in detail in section 1.7. The rate of elongation is invariant among wild type embryos and because there is a consistent relationship between age and shape of an embryo during elongation, the developmental stages can be described in terms of the physical length of the embryo (Sulston *et al.*, 1983; Priess and Hirsh, 1986; McKeown *et al.*, 1998). The main stages of elongation are shown in Figure 1.1 and are known as the precomma (or lima bean), comma, 1.5-fold, 2-fold, and 3-fold (or pretzel) stages of elongation and other increments of physical length are also used to denote development between these stages (Sulston *et al.*, 1983; Wood, 1988). Although the embryo elongates to around four times its original length, a fully elongated worm was initially termed 3-fold in the literature and so I will also use this terminology (Sulston *et al.*, 1983; Priess and Hirsh, 1986). At around 690 mins post-fertilisation, a collagenous exoskeleton or cuticle is secreted by the hypodermal cells surrounding the body which takes over the role of shape maintenance and acts as a barrier to the external environment after hatching (Singh and Sulston, 1978; Sulston *et al.*, 1983; Priess and Hirsh, 1986).

1.2.1.2. Postembryonic development in *C.elegans*

The worm hatches as an L1 larva and undergoes three more larval stages until it reaches adulthood, termed the L2-L4 stages of development (Figure 1.3). Each larval stage terminates in a moult when a new collagenous cuticle is secreted from the hypodermis underneath the old cuticle which is subsequently shed. Prior to the moult, when the new cuticle is being secreted, the pharynx of the larva stops pumping and the larva enters a developmental state known as lethargus (Singh and Sulston, 1978). Each of these larval stages differs in body size and the type of cuticle secreted although the morphology of the L1 larvae is superficially quite similar to the adult. The hypodermal control of post embryonic development is discussed in section 1.7.6.3 and the control of body shape by the cuticle postembryonically is discussed in sections 1.7.6.1 and 3.1.4. It takes around 3 days for an embryo to develop into an adult and adults can survive for around 2 weeks although they are only self-fertile for 2-3 days. In conditions of overcrowding or starvation, L2 larvae moult into a specialised stage known as the dauer stage (Cassada and Russell, 1975). Dauer larvae are specialised for dispersal and long-term survival. They do not feed but can survive for over 8 times the normal life span of

C.elegans (Klass and Hirsh, 1976). When conditions become favourable again, the dauer larvae moult into the L4 stage and resume normal development.

At the time of hatching, the L1 larvae contains 550 somatic nuclei, two of which will divide during larval development to produce the somatic gonad, and two of which will produce the germ line (Sulston *et al.*, 1983). Due to the postembryonic proliferation of both non-gonadal somatic blast cells and the gonadal primordia, the number of somatic nuclei at the adult stage is 959 for hermaphrodites and 1031 for males of which around 140 in the hermaphrodite and around 60 in the male are somatic gonadal nuclei (Sulston and Horvitz, 1977). The extra nuclei of the male adult are mostly neuronal and function in the control of male mating behaviour. Although gonadal development occurs from the L1 stage, gonadal structures are not visible until the L3 stage and their maturation concludes with the L4-adult moult when the hermaphrodite vulva is opened and the mail tail structures, which are used for copulation, become fully developed.

1.2.2. The anatomy of *C.elegans*

Each cell produced during the development of *C.elegans* which does not undergo programmed cell death has been followed to its terminal destination as part of a tissue or specialised structure in the body of the worm. The complete anatomy of the worm has been reconstructed using electron micrographs of serial sections and combined with the cell lineage data to produce a more complete picture (Sulston *et al.*, 1983; White, 1988). The basic nematode body plan has been mentioned in section 1.1 and I will now discuss the individual tissues in more detail. The anatomy of an adult hermaphrodite and male is illustrated in Figure 1.4.

The shape of the nematode, embryonically and postembryonically, is determined by the hypodermal cells, the external epithelia of *C.elegans,* and the cuticle they secrete. The main features of hypodermal cells are common to all epithelial cells: distinct apical and basolateral surfaces, a complex cytoskeleton, and tight adherens junctions between cells. The cuticle is always secreted from the apical surface forming a barrier between the worm and the external environment, and a basement membrane lies on the basolateral side of the cells between the hypodermis and the underlying body wall muscles. The hypodermis extends along the length of the body and at openings, such as

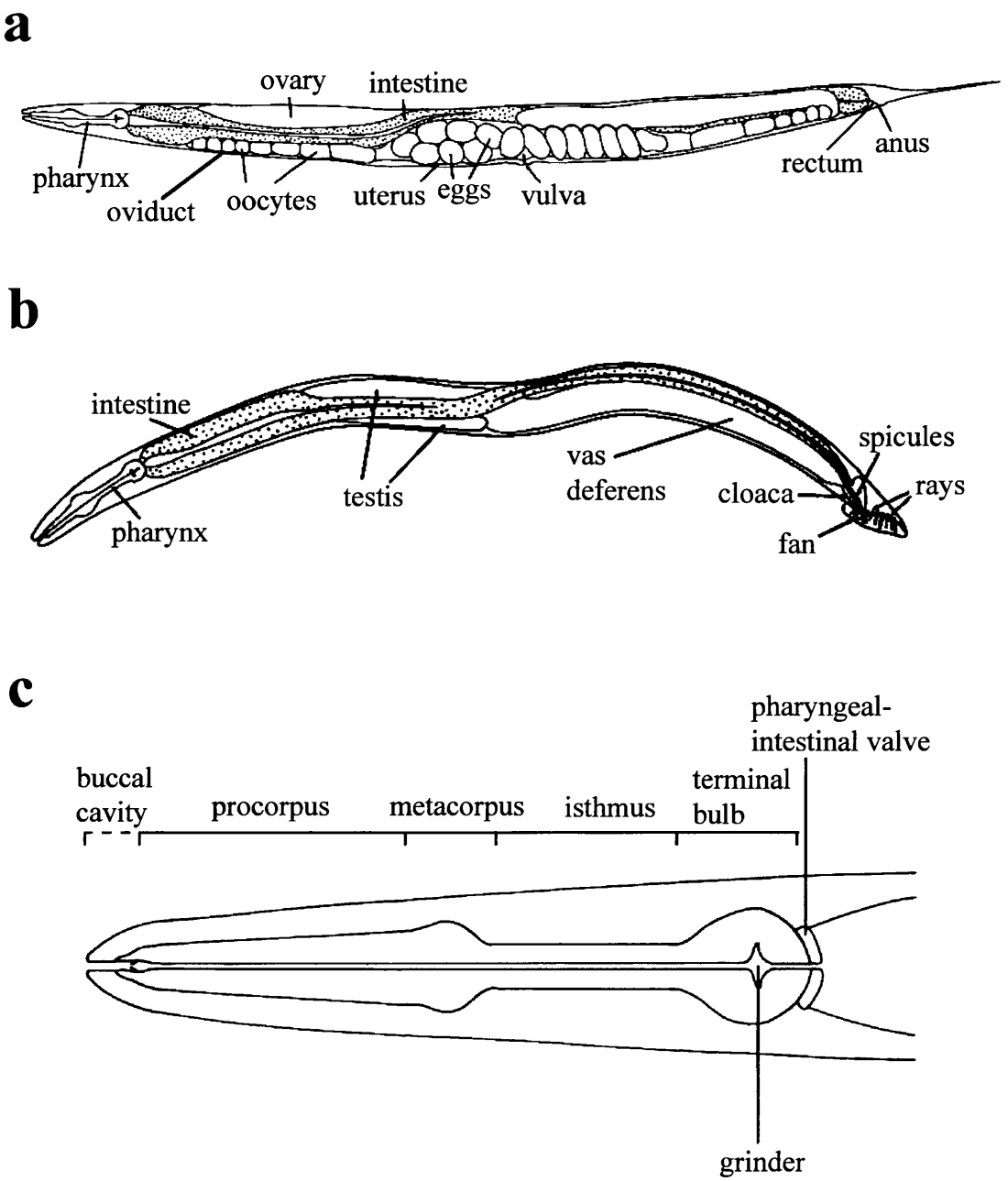

Figure 1.4

Diagrammatic representation of hermaphrodite and male anatomy and the principle regions of the pharynx

a	Hermaphrodite anatomy
b	Male anatomy
c	The principle regions of the pharynx: procorpus, metacorpus, isthmus, and terminal bulb

the buccal cavity, the rectum, the vulva and the excretory cell, the hypodermis connects to specialised cells which act as interfaces between the hypodermis and the organ to which the opening leads. Most of the hypodermal nuclei are arranged into multinucleate syncytia, the largest of which is hyp7. Smaller syncytia are present in the head and tail regions and at lateral regions there is a row of mononucleate hypodermal cells known as the seam cells. These cells are responsible for the cuticular structures called alae, present in L1, dauer and adult stages. On solid surfaces, *C.elegans* travels on one side with the alae contacting the surface during stages in which they are present. The four bands of body wall muscles that run longitudinally beneath the hypodermis, attach to the cuticle through the basement membrane and hypodermal structures called hemidesmosomes. The muscles that are attached to each side of the body contract alternately and, together with the internal hydrostatic pressure of *C.elegans*, create the characteristic sinusoidal movement.

The nervous system of *C.elegans* makes up 37% of hermaphrodite and 46% of male somatic nuclei (Chalfie and White, 1988). All connections and positions of the nerves in the nervous system have been reconstructed (White *et al.*, 1986). Most of the neuron cell bodies are organised into ganglia and the neuronal processes are organised into ordered bundles that run longitudinally (including the dorsal and ventral nerve cords) or circumferentially (the nerve ring). Synaptic contacts are made between adjacent neuronal processes within bundles. Most of the sensory neurons run from the nerve ring anteriorly and have their sensory endings in structures known as sensilla at the tip of the head. Motor neurons run posteriorly from the nerve ring and innervate the body wall muscle.

The alimentary canal is made up of the pharynx, the intestine, and the rectum. The pharynx is a self-contained system of muscles, epithelial cells and nerves demarcated by a basement membrane. Food is ingested through the most anterior section of the pharynx, the buccal cavity, and is concentrated and processed in the pharynx before being pumped into the intestine. During the life cycle, the pharynx pumps continuously except during the periods of lethargus prior to each larval moult. The complete structure of the pharynx has been described by Albertson and Thomson (1976). It is arranged into four regions (Figure 1.4c) termed the procorpus, the metacorpus, the isthmus, and the terminal bulb, all with a central lumen. The terminal bulb contains a structure known as the grinder and its function is to grind food as it

passes through. The junction between the pharynx and the intestine is marked by the pharyngeal-intestinal valve. The intestine consists of a tube of 20 cells with a dense layer of microvilli on the apical surface. At the anterior end of the intestine, the lumen is surrounded by 4 cells (int1) and more posteriorly by 8 pairs of cells (int2-int9). Intestinal cells can undergo endoreduplication of DNA without nuclear divisions at each stage of lethargus (Hedgecock and White, 1985). The primary function of intestinal cells is to secrete digestive enzymes into the lumen and absorb the processed nutrients but they also function as storage cells and play a major role in the nurture of germ cells by producing yolk proteins (Kimble and Sharrock, 1983). Some intestinal granules are refractile under polarised light and strongly autofluorescent under 300-400nm light which is very useful when identifying intestinal cells in living animals. The intestine is connected to the rectum by an intestinal-rectal valve, similar to the pharyngeal-intestinal valve. This valve is connected to hyp7 through endothelial cells which comprise the rectum. The rectum has 3 sets of associated muscles which control excretion. They are coupled together through gap junctions and innervated by a single neuron.

The excretory/secretory system consists of three cells: an excretory cell, a duct cell, and a pore cell which connects the excretory cell to hyp7. There are also excretory glands attached to the excretory and duct cells. The excretory cell is the largest mononucleate cell in *C.elegans* and is situated ventrally at the level of the pharyngeal terminal bulb.

The hermaphrodite reproductive structures comprise the gonad and the vulva. The gonad is bilobed and symmetrical with one arm extending anteriorly and one posteriorly from the centre of the worm (Hirsh *et al.*, 1976; Kimble and Hirsh, 1979). Each arm bends ventrally and then doubles back to meet at a common uterus in a ventral position at the centre of the worm. Each arm of the gonad can be divided into the distal ovary, the loop, the oviduct, the spermatheca, the spermathecal valve, and the uterus. The ovaries contain germ line nuclei which progress through meiosis as they travel along the gonad while being enclosed by membranes and are in diakinesis by the time they reach the oviduct. These nuclei have now formed oocytes which pass through, and are fertilised in, the spermatheca which contain amoeboid sperm. The fertilised eggs pass into the common uterus where they begin embryogenesis before being ejected through the vulva, a structure protruding from the ventral surface of the hermaphrodite,

made up of epithelial cells and muscles which connects the uterus to the outside environment.

The male reproductive structures are very different. The male gonad has one arm which is composed of the testis, the seminal vesicle, and the vas deferens. It begins in the central region of the worm and runs anteriorly before turning dorsally and running posteriorly until it meets the cloaca in the centre of the specialised reproductive structures at the male tail. The germ nuclei are mitotic at the beginning of the testis and become meiotic as they travel to the seminal vesicle. The sperm are stored in the seminal vesicle until copulation when they travel through the vas deferens and the cloaca. The mail tail is organised into a copulatory bursa which consists of many specialised neurons, muscles and hypodermal structures required for mating. A detailed description of the *C.elegans* anatomy is given in White (1988).

1.2.3. The genetics of *C.elegans*

In 1949, Nigon showed that wild type *C.elegans* hermaphrodites had five pairs of autosomes and one pair of X chromosomes while males contained five autosomes and just a single X chromosome. It has been shown that the primary sex-determining factor in *C.elegans* is the ratio of X chromosomes to autosomes by experimentally altering this ratio (Hodgkin *et al.*, 1979; Madl and Herman, 1979). The haploid genome is relatively small, consisting of 97 megabases (Mb) of DNA, which is only around eight times that of the yeast, *Saccharomyces* or around one-half the size of the *Drosophila* genome (The *C.elegans* Sequencing Consortium, 1998).

Many of the genes in *C.elegans* have been isolated and studied using classical genetic analysis and this research has been greatly aided by the short life cycle and the mode of reproduction in this nematode. Normal populations of *C.elegans* consist largely of hermaphrodites with less than 0.2% of males arising from non-disjunction of the X chromosome during meiosis (Wood, 1988). This predominantly hermaphrodite mode of reproduction allows the isolation and maintenance of recessive mutations, as 25% of the progeny of an heterozygous hermaphrodite will be homozygous for the mutation. It also allows easy maintenance of recessive lethal alleles, as 50% of the total progeny of an heterozygous hermaphrodite, or two-thirds of the viable progeny, will also be heterozygotes for the lethal mutation. At the same time, genetic crosses can be

carried out with ease by mating hermaphrodites with males. Mutations are often generated in *C.elegans* using chemical mutagenesis or radiation in large scale genetic screens. This forward genetic approach is useful when studying mutations producing a noticeable phenotype such as abnormal shape, movement, or death, and the mutation is subsequently mapped and cloned to discover the gene involved, its relationship to other genes, and the protein it encodes. *C.elegans* was first proposed as a model organism for the study of animal behaviour and development in 1965 and, by 1974, over 100 genetic loci comprising behavioural and morphological markers had been identified (Brenner, 1974). By 1997, Johnsen and Baillie reported that 1,503 loci had been genetically identified. The reverse genetic approach, which will be discussed in more detail in the next section, starts with a gene sequence and works backwards by attempting to elucidate the role of this gene, if any, in the worm. Clues of gene function can be found by comparing the sequence with known genes in other organisms and by observing the expression of the gene in the wild type worm.

1.3. *C.elegans* as an experimental system

Many features of *C.elegans* biology make it an excellent candidate for experimental analysis. Several of these, such as its size, short life cycle and transparency have been discussed above and the ease at which it can be maintained in the laboratory is another positive factor. The simplicity of this organism allows in-depth analysis of features such as the cell lineage and anatomy while it also shows many complex cellular, developmental and behavioural interactions. The constancy of cell number and the invariant cell lineage provide an ideal situation to enable the study of development. Virtually every cell in the body is accessible to laser microsurgery and the ability to selectively inactivate founder or blast cells and observe the effects on development provides an excellent opportunity to study the effects of cell positions, cell-cell interactions, and the determination of cell fate.

Initially, the study of the function and control of genes in *C.elegans* was restricted to the techniques available in the classical forward genetics approach (Brenner, 1974). However, many new techniques have become available over time which have increased the effectiveness of forward genetics while also allowing a reverse genetic approach to the study of *C.elegans* biology. Another reason for the increasing

trend towards reverse genetics is the sequencing of almost the entire genome by the *C.elegans* genome sequencing consortium which is discussed in section 1.4.2.

A powerful tool developed for several different uses is DNA transformation, which can be utilised when attempting to rescue a mutant phenotype and thus clone the wild type copy of the mutant gene, or may be used to study the temporal and spatial expression pattern of a gene during development (Stinchcomb *et al.*, 1985; Fire, 1986; Mello *et al.*, 1991). The generation of a physical map comprising overlapping clones (see section 1.4.1) along with the DNA transformation technique has produced a way of identifying a gene which has been mutated to create an observable phenotype in a genetic screen. After the mutation has been mapped to a specific region of the genetic map, clones from the physical map corresponding to this region can be injected into the gonad of a mutant worm. These injected clones can form heritable arrays and if the wild type copy of the gene which is mutated in the genome is present in the transgenic array, it may rescue the mutant phenotype in subsequent generations (Mello and Fire, 1995). Mutant phenotype rescue by transgenic arrays is discussed further in Section 4.4.1. DNA transformation is also of considerable use in reverse genetics when attempting to elucidate the function of a gene or when examining the expression pattern of a cloned gene. The gene of interest along with its flanking sequences is fused in frame to a reporter gene such as *lacZ* or the gene encoding the green fluorescent protein (GFP) of a jellyfish, *Aequorea victoria,* and the reporter gene fusion is injected into a wild type worm (Fire *et al.*, 1990; Fire, 1992; Chalfie *et al.*, 1994). This is especially useful when the GFP reporter gene is used as it allows the temporal and spatial expression pattern of the target gene to be followed in living animals using a UV source to detect the fluorescence produced by GFP (Chalfie *et al.*, 1994).

A technique which has proved to be invaluable in reverse genetics is gene-inactivation by insertion of the Tc1 transposon (Zwaal *et al.*, 1993). Insertion of Tc1 into a gene can interrupt that gene and therefore inactivate it and the presence of the Tc1 transposon in or near a gene can be detected by the polymerase chain reaction (PCR) using specific primers. This technique makes use of so called mutator strains which have mobile transposable elements and which activate Tc1 transposition and excision in the germ line at high frequency (Zwaal *et al.*, 1993; Plasterk, 1995). Genomic DNA from different populations of a mutator strain is screened using PCR with primers specific to Tc1 and the target gene. Siblings of the screened worms are kept alive in

order to maintain any Tc1 insertion found in the target gene. If an insertion is found in the target gene, further screening of sub-populations of the siblings is carried out until single worms carrying the Tc1 insertion are identified (Rushforth *et al.*, 1993). One feature of *C.elegans* biology is the ability to withstand freezing at -70°C under certain conditions, and this has allowed the generation of frozen Tc1 insertion mutant banks which can result in the isolation of Tc1 insertions in most genes (Zwaal *et al.*, 1993).

One of the most recent tools to be used in reverse genetics of *C.elegans* is RNA-mediated genetic interference (RNAi) which can specifically inhibit the function of a gene by the injection of double stranded (ds)RNA corresponding to a coding sequence of the gene and thus mimic the null phenotype of that gene (Fire *et al.*, 1991; Guo and Kemphues, 1995; Fire *et al.*, 1998; Tabara *et al.*, 1998). This is an invaluable tool when studying the function of a specific gene in *C.elegans* as it produces a very rapid effect and more recently it has been shown that simply soaking the worms in dsRNA can induce specific interference (Tabara *et al.*, 1998). RNAi is discussed in more detail in section 6.9.1.

These techniques, together with the extensive knowledge of *C.elegans* biology, an essentially completely sequenced genome, and experimental versatility make this organism an excellent experimental system for the study of gene function using both forward and reverse genetics and an ideal system for the study of development, both embryonically and postembryonically.

1.4. Genome Sequence of *C.elegans*

1998 was a landmark year in the history of *C.elegans* research with the announcement that the sequencing of the genome was essentially complete. It is the first multicellular organism genome sequence to be completed and the uses of such a resource of genomic information are manifold, not only for *C.elegans* biologists, but also for researchers interpreting other genomes, including the human genome.

1.4.1. The *C.elegans* physical map

A starting point for the sequencing of the genome was the generation of an ordered physical map of clones covering the genome which allowed sequence data obtained from these clones to be accurately linked together. Initially, a restriction enzyme fingerprinting method was used to assemble random cosmid and lambda clones into large sets called 'contigs' (Coulson *et al.*, 1986). Although this resulted in the coverage of 90-95% of the genome by 17,500 cosmids arranged into 700 contigs, there were still gaps present between these contigs due to the absence or under-representation of the linking clones in the cosmid libraries used. At this time, newly developed yeast artificial chromosomes (YAC) clones were used to bridge these gaps by generating a YAC library of *C.elegans* genomic DNA and this method proved to be very successful, rapidly reducing the number of contigs to 346 (Burke *et al.*, 1987; Coulson *et al.*, 1988). The YAC clones alone also covered almost all of the genome, forming a YAC grid of 958 clones, which enabled rapid screening of the entire genome using a hybridisation technique (Coulson *et al.*, 1991). At present, around 20% of the entire genome is only present in YAC clones (The *C.elegans* Sequencing Consortium, 1998).

Good alignment between the physical and genetic maps is also essential as this allows genes identified by sequence to be placed on the genetic map and mapped genes from mutant screens to be located in the physical map. Sulston *et al.* (1992) had positioned over 90Mb of sequence along the chromosomes using genetically mapped sequences and *in situ* hybridisation techniques and more recently a high resolution alignment of specific areas of the genetic, physical, and DNA sequence maps has been produced by the systematic rescue of lethal mutations in these areas using sequenced cosmids (Janke *et al.*, 1997; McDowall and Rose, 1997).

1.4.2. Sequencing the *C.elegans* genome

The *C.elegans* sequencing project began with the sequencing of the centres of the chromosomes where there was good cosmid coverage and the density of genetic markers was high (Sulston *et al.*, 1992). The sequencing process involved a shotgun phase where random subclones were sequenced and a finishing phase where gaps were closed and ambiguities solved using specialised techniques (The *C.elegans* Sequencing Consortium, 1998). Remaining gaps in the centres of the chromosomes were bridged by

screening fosmid and YAC clones and using long-range PCR (Kim *et al.*, 1992; Cheng *et al.*, 1994). Fosmids are similar to cosmids but are maintained at a single copy per cell as opposed to the multi-copies of cosmids and were therefore potentially more stable (Kim *et al.*, 1992). YAC sequencing recovered all the gaps in the outer regions of the chromosome and this also served as a check on the physical map arrangement as the YAC sequences were compared with previously made hybridisation links (The *C.elegans* Sequencing Consortium, 1998). 97Mb of sequence representing over 99% of the genome sequence is now represented by 2527 cosmids, 257 YACs, 113 fosmids, and 44 PCR products (The *C.elegans* Sequencing Consortium, 1998).

Running parallel with the sequencing project, other groups have been sequencing and mapping randomly selected complementary DNA (cDNA) clones from *C.elegans* (Waterston *et al.*, 1992; McCombie *et al.*, 1992; Kohara, 1996 [cited in: The *C.elegans* Sequencing Consortium, 1998]). These projects generate partial sequence from cDNA clones which have been mapped to the YAC grid to produce sequence tags. These can then be used to predict coding regions from the genomic sequence generated by the genome sequencing project. The Kohara group has produced 67,185 Expressed Sequence Tags (ESTs) which represent around 7432 genes and this information has been invaluable in identifying and elucidating the nature of genes in the genomic sequence (The *C.elegans* Sequencing Consortium, 1998).

1.4.3. The content of the *C.elegans* genomic sequence

In order to identify possible genes within finished *C.elegans* genomic sequences, the GENEFINDER program is used (P.Green and L.Hillier, unpublished software). These gene predictions are further adjusted or confirmed using information from protein, cDNA and EST matches. There are 19,099 predicted protein-coding genes in the 97Mb genomic sequence resulting in an average density of 1 predicted gene per 5kb (The *C.elegans* Sequencing Consortium, 1998). This number is around three times that found in yeast and around a third to a fifth of that predicted for humans (Goffeau *et al.*, 1996; The *C.elegans* Sequencing Consortium, 1998). Sequence comparisons of predicted protein products with known proteins has revealed that around 42% of predicted protein products show significant similarities to proteins in organisms outside the nematodes while 34% match proteins found only within the nematodes (The

C.elegans Sequencing Consortium, 1998). Significantly, 36% of predicted protein products in *C.elegans* match with human proteins, which is higher than the percentage matching with either *Escherichia coli* or *Saccharomyces cerevisiae* as expected from evolutionary relationships (Sonnhammer and Durbin, 1997).

The predicted genes in *C.elegans* are not evenly dispersed across the chromosomes, with a higher gene density at the centres of chromosomes compared to the chromosome arms, and an overall higher gene density in chromosomes I-V than in the X chromosome where the genes are also more evenly distributed. There are also many repeat and inverted sequences present throughout the *C.elegans* genome, accounting for 6.3% of the genome, and these are much more frequent on the chromosome arms than in the central regions or on the X chromosome. Another feature of the chromosomal organisation for the autosomes, chromosomes I-V, is that the amount of genes with similarities to organisms other than nematodes is lower on the chromosome arms than in the centres (Barnes *et al.*, 1995). As the rate of meiotic recombination is much higher on the autosome arms, it is suggested that the DNA on the arms may be evolving much more rapidly than in the central regions of the autosomes (The *C.elegans* Sequencing Consortium, 1998).

As expected from the genome of a multicellular organism, the *C.elegans* genome is predominantly non-coding with just 27% of sequence comprising predicted exons. The importance of determining the entire genome sequence rather than just the coding sequence, however, is that much of the information about biological function is located in the non-coding sequences. The completed genome sequence also shows the relationships between genes and contains the structural and control elements necessary for their correct function which is essential for the biological understanding of the entire organism.

1.5. *C.elegans* as a model organism

The simplicity of *C.elegans* and the wide range of experimental tools available for *C.elegans* research has already resulted in the accumulation of a wealth of biological information regarding its biology. The idea that information gained from research on this nematode species is relevant to mammalian biology is strengthened not only by the substantial homology seen between the encoded proteins of *C.elegans* and higher

eukaryotes but also by the discovery of several cellular pathways which appear to be shared between *C.elegans* and mammals. The detailed genetic analysis of these and other pathways which are clearly shared between *C.elegans* and mammalian pathways may eventually have an impact in the area of human health. This analysis may also link two pathways which were previously thought to be unrelated. I will discuss four such pathways as examples, two of which appear to be pathways important in aspects of human health.

The first example of a conserved pathway is the signalling pathway involved in the induction and development of the vulva in *C.elegans*. The vulva is the epithelial tube which connects the hermaphrodite uterus to the outside environment and which functions in egg laying and mating with males. It is generated by a special subset of ventral ectodermal blast cells and the induction pathway involved utilises molecules that are conserved between *C.elegans* and mammals as well as being present in many other organisms. The anchor cell present in the somatic gonad is the key organiser of vulval patterning and morphogenesis and it has been shown to be both necessary and sufficient to induce vulval development (Sulston and White, 1980; Kimble, 1981). The anchor cell produces an inductive signal, LIN-3, which is a transmembrane protein containing a single epidermal growth factor (EGF)-like motif (Sternberg and Horvitz, 1986; Thomas *et al.*, 1990; Hill and Sternberg, 1992; Katz *et al.*, 1995). The receptor for this signal is thought to be LET-23, a receptor tyrosine kinase of the EGF subfamily, which appears to positively regulate LET-60, a Ras protein, via an adapter, SEM-5 (Aroian *et al.*, 1990; Beitel *et al.*, 1990; Han and Sternberg, 1990; Clark *et al.*, 1992; Stern *et al.*, 1993). SEM-5 is a structural and functional homologue of the human GRB2 protein which functions as an adapter between receptor tyrosine kinases and Ras in humans (Clark *et al.*, 1992; Stern *et al.*, 1993; Greenwald, 1997). In turn, LET-60 activates a protein kinase cascade which includes LET-45, a Raf homologue, MEK-2, a MAP kinase kinase homologue, and MPK-1/SUR-1, MAP kinase homologues (Han *et al.*, 1993; Lackner *et al.*, 1994; Wu and Han, 1994; Church *et al.*, 1995; Kornfeld *et al.*, 1995; Wu *et al.*, 1995). Among targets of this signalling pathway are putative transcription factors, LIN-1 and LIN-31 (Miller *et al.*, 1993; Beitel *et al.*, 1995). LIN-1 acts as a negative regulator of vulval induction while LIN-31 is involved in the specification of vulval and non-vulval fates. Each of the proteins in this pathway is homologous to a protein in the mammalian receptor tyrosine kinase signalling pathway

which acts in the regulation of cell response to growth factors (Greenwald, 1997). The discovery of the LET-60 component in this system was also the first indication in any organism that Ras proteins are involved in specification and differentiation in addition to cell growth and proliferation.

During the development of the *C.elegans* hermaphrodite, 12% of generated cells undergo programmed cell death (Sulston and Horvitz, 1977; Sulston *et al.*, 1983). These deaths are highly reproducible and the same number of cells die in all individuals at the same developmental stage. The genetic pathway which controls programmed cell death results in the production of several proteins which have significant homology to proteins controlling cell death in vertebrates and so this appears to be another conserved pathway. Expression of the *ced-3* and *ced-4* genes are necessary for programmed cell death as mutations inactivating either gene result in the survival of almost all cells that normally die (Ellis and Horvitz, 1986). *ced-3* encodes a protein which has significant similarity to a new family of cysteine proteases, of which the mammalian interleukin-1β converting enzyme (ICE) is a member (Thornberry *et al.*, 1992; Yuan *et al.*, 1993). CED-3 exhibits a protease activity similar to that observed for ICE and it is thought that this protease activity is necessary for the ability of CED-3 to promote cell death (Xue and Horvitz, 1995; Xue *et al.*, 1996). Overexpression of ICE was found to induce programmed cell death in rat fibroblasts and so it is possible that this or a related protein may be involved in mammalian programmed cell death (Miura *et al.*, 1993). The *ced-9* gene is necessary and sufficient to protect cells from undergoing cell death in *C.elegans*. *ced-9* gain-of-function mutations or overexpression results in the survival of cells that would normally die and conversely, inactivation of *ced-9* causes the programmed cell death of many cells that would normally survive (Hengartner *et al.*, 1992). CED-9 has sequence similarity to the product of *bcl-2* the mammalian proto-oncogene involved in the control of mammalian programmed cell death and it has been shown that *bcl-2* can substitute for *ced-9* in *C.elegans* by preventing normal cell deaths and the extra cell deaths produced in *ced-9* loss of function mutants (Vaux *et al.*, 1992; Korsmeyer *et al.*, 1993; Hengartner and Horvitz, 1994). These results suggest that the genetic pathways controlling programmed cell death may be conserved between *C.elegans* and mammals.

The third example of a pathway showing homology between *C.elegans* and mammals is the *lin-12 Notch*-like signalling pathway which acts in the patterning of

equipotential cells by mediating cell-cell signalling (Levitan and Greenwald, 1995). Genetic analysis of the *lin-12 Notch*-like signalling pathway showed that a *C.elegans* orthologue of the human PS1 transmembrane protein implicated as having a role in Alzheimer's disease, regulates *lin-12* function (Levitan and Greenwald, 1995; Li and Greenwald, 1998; Greenwald, 1998). This placed the mammalian PS1 gene in a *Notch*-like signalling pathway as well as a neural degeneration pathway, and vice versa, implicating the *lin-12* pathway as a possible candidate for research into neural degeneration in Alzheimer's disease.

Another example of a shared pathway between *C.elegans* and mammals which may be important in human health is the DAF-2/AGE-1/DAF-16 insulin-like metabolic pathway which regulates metabolism, development and longevity (Morris *et al.*, 1996; Kimura *et al.*, 1997). DAF-2 is an homologue of the mammalian insulin receptor and AGE-1 encodes an homologue of the mammalian phosphatidylinositol 3-OH kinase [PI(3)K] catalytic subunit. *daf-2* and *age-1* mutants arrest development at the dauer stage although *daf-16* null mutations can suppress this effect (Ogg *et al.*, 1997; Riddle, 1997). DAF-16 encodes members of the Fork head family of transcription factors and it is thought that it acts downstream of DAF-2/AGE-1 to regulate the transcription of key metabolic and developmental control genes (Ogg *et al.*, 1997). DAF-2 and AGE-1 appear to negatively regulate DAF-16. It is thought that in the absence of DAF-2/AGE-1 signalling, DAF-16 represses metabolic genes and that this repression is lost in *daf-16* null mutants resulting in the suppression of the *daf-2* and *age-1* mutant phenotypes mentioned above. This DAF-2 pathway normally acts synergistically with a pathway activated by a TGF-β-type signal, DAF-7, and it appears that the action of this pathway may account for the fact that animals with defects in insulin-receptor-like signalling can live normally if they are also lacking *daf-16* (Ogg *et al.*, 1997; Riddle, 1997). In mammals, PI(3)K signalling activates protein kinase cascades which regulate metabolic enzymes and glucose transport (Tanti, 1996; Toker and Cantley, 1997). Human orthologues of DAF-16, FKHR and AFX, may also act downstream of insulin signalling and co-operate with TGF-β pathway components in order to mediate metabolic regulation. These genes may be abnormally regulated in diabetic patients and there is a possibility that if the DAF-16 homologues, FKHR and AFX are inhibited, the metabolic defects associated with a decline in insulin signalling may be lessened as is seen in *age-1/daf-16* or *daf-2/daf-16* mutants (Ogg *et al.*, 1997). This pathway also has similarities

to the vulval induction pathway discussed above as it involves a protein kinase cascade with a Fork head homologue as a suggested downstream target (Miller *et al.*, 1993; Ogg *et al.*, 1997).

These examples show to what extent pathways can be conserved between *C.elegans* and mammals and also how some of these pathways may be used to investigate new approaches to problems in human health. The high degree of homology between the systems supports the use of *C.elegans* as an important general model for metazoan biology.

1.6. Epithelial function and morphogenesis

C.elegans undergoes major body shape changes during embryogenesis and these changes are controlled and driven by the epidermis, the external epithelia, known as the hypodermis (Priess and Hirsh, 1986). Postembryonically, *C.elegans* larvae grow larger at each stage of the life cycle but do not undergo further body shape changes. The maintenance of the worm shape from the end of embryogenesis through the rest of the life cycle is performed by the exoskeleton, or cuticle, which is synthesised in, and secreted from, the hypodermis. I decided to study this dual function of the hypodermis in driving morphogenesis and maintaining body shape as it is an important developmental process in all metazoans. I will give a brief overview of the main process of epithelial shape change in metazoans and then look at the development and function of the hypodermis in *C.elegans* embryonically and postembryonically. Aspects of hypodermal function that are particularly relevant to individual chapters will be dealt with in the introductions to these chapters.

The shape of an organism is dictated by development of the epithelial tissue surrounding that organism which comprises a laterally continuous monolayer of cells with tight cell-cell junctions, a complex cytoskeleton, and apical basal polarity. Many factors are involved in the processes of cell signalling, cell adhesion and force generation in and between cells which mediate changes in the epithelial layer and transduce these changes into overall shape change or movement of the epithelium. There are four aspects of epithelial cells which practically all organisms have in common that are crucial for their function: apical-basal polarity, tight intercellular

junctions, a complex cytoskeleton, and molecules which mediate cell-cell adhesion (Fristrom, 1988).

1.6.1. Apical-basal polarity

The apical surface of epithelial cells either faces the exterior or luminal spaces and is never closely apposed to other tissues. In nematodes and many other invertebrates the apical surface is covered by an extracellular matrix known as the cuticle which is secreted from the epithelial cells and acts as an impermeable protective exoskeleton. The basal surface is often in close contact with internal tissues and is covered by another type of extracellular matrix, the basement membrane, which is made up from components secreted by the epithelium (the basal lamina) and the underlying tissues (Fessler *et al.*, 1984). The polarisation of these epithelial cells is also reflected in the distribution of cytoplasmic components and there are many molecules which act to maintain this polarity (Simons and Wandinger-Ness, 1990; Nelson, 1992; Mellman, 1996). The presence of two separate plasma membrane domains requires separate endocytic and biochemical pathways and a route for transport between the two cell surfaces (Rodman *et al.*, 1990; Mostov *et al.*, 1992). *In vitro* studies on cultured kidney epithelial cells have highlighted a structure present at the apical surface and known as the apical recycling compartment, as having a major role in sorting molecules within the cell in a polarised manner (Barroso and Sztul, 1994; Apodaca *et al.*, 1994). Small GTPases have been implicated in the function of polarised membrane transport and sorting within epithelial cells (Lütcke *et al.*, 1993; Zacchi *et al.*, 1998). Although basement membrane and extracellular matrix have been shown to be essential for some morphogenetic events, many epithelial sheet movements occur without the presence of a well defined basal lamina or extracellular matrix, and in some systems, the extracellular matrices must be separated from the epithelium before morphogenetic changes can occur (Brenner, 1974; Higgins and Hirsh, 1977; Cox *et al.*, 1980; Kusch and Edgar, 1986; Guo *et al.*, 1991; von Kalm *et al.*, 1995; Williams-Masson *et al.*, 1997).

1.6.2. Intercellular junctions

Epithelial cells are connected to their neighbours through circumferentially distributed apical junctions known as adherens junctions (Fristrom, 1988). These junctions perform an essentially adhesive role and are often associated with circumferentially distributed actin filaments and molecules involved in cell adhesion such as cadherins (Gieger and Ayalon, 1992; Gumbiner, 1996). The tight proximity of epithelial cells also serves to transmit local forces across the entire cell sheet which is essential for any morphogenetic process (Gumbiner, 1996).

1.6.3. The epithelial cytoskeleton

The cytoskeleton of epithelial cells comprises actin-based microfilaments, intermediate filaments and microtubules (Fristrom, 1988). Another component is a plasma-membrane skeleton which is often made up mostly of spectrin, an actin binding heterodimer, that assembles into an extensive network along with actin (Luna and Hitt, 1992). It is linked to the plasma membrane on one side and to the cortical cytoskeleton on the other and has been implicated in stabilising the plasma membrane and maintaining cell shape (Elgasaeter *et al.*, 1986). Microtubules and intermediate filaments have also been implicated in maintaining cell shape and the tensile strength of the epithelial sheets (Joshi *et al.*, 1985; Janmey *et al.*, 1991; Fuchs and Weber, 1994). Microtubules also play a role in cell vesicle transport, polarity maintenance, and actively mediate certain cell shape changes while intermediate filaments also have roles in attachment of other tissues to the epithelium (Bamburg *et al.*, 1986; Francis and Waterston, 1991; Solnica-Krezel and Driever, 1994; Williams-Masson *et al.*, 1998). Apart from microtubules, the component of the cytoskeleton which has been implicated in many different aspects of epithelial motility and cell shape change is the actin microfilament network. Actin microfilaments polymerise and depolymerise rapidly in response to external signals and thus mediate cell movement (Schmidt and Hall, 1998). In response to activation by small GTPases, actin microfilaments organise into protrusions such as lamellopodia and filopodia during cell movement and they also assemble into contractile stress fibres along with myosin (Ridley and Hall, 1992; Ridley *et al.*, 1992; Kozma *et al.*, 1995; Nobes and Hall, 1995). They drive cell shape change

during *Drosophila* leg elongation along with myosin and during *C.elegans* embryonic elongation (Priess and Hirsh, 1986; Condic *et al.*, 1991; von Kalm *et al.*, 1995). I will discuss different aspects of actin-mediated epithelial shape change and movement later in this introduction.

1.6.4. Molecules involved in intercellular adhesion in epithelial sheets

As has been mentioned before, morphogenesis would be impossible without tight adhesion between the cells that make up the epithelium. There are many different adhesion molecules which maintain cell-cell contacts but one of the most important and ubiquitous types of adhesion complexes is made up of the classical cadherin molecules and their catenin counterparts. These have been found to play a major role in *C.elegans* embryonic morphogenesis and although they have been shown to have many roles in cell sorting during development, I will focus solely on their function in cell adhesion and actin cytoskeleton anchorage (Takeichi, 1991; Costa *et al.*, 1998). Cadherins are transmembrane Ca^{2+}-dependent adhesion molecules which are either present over the entire cell surface or localised to epithelial adherens junctions depending on the cell type and state and which maintain adhesion through homophilic interactions with the extracellular domains of cadherin molecules on adjacent cells (Takeichi, 1991; Shapiro *et al.*, 1995). In order to function in this manner, cadherins must form intracellular connections with cytoplasmic catenin proteins and, through these, with the actin cytoskeleton (Figure 1.5) (Kemler *et al.*, 1989; Gumbiner, 1993). α-Catenin has actin-binding activity and is thought to function in linking the actin cytoskeleton to the intracellular cadherin domain (Rimm *et al.*, 1995). This is achieved through interaction with β-catenin which binds to cadherin and α-catenin although another protein, plakoglobin, may take the place of β-catenin in the complex (Aberle *et al.*, 1994; Näthke *et al.*, 1994). The most important role of cadherin/catenin complexes in most systems is general cell adhesion. During *C.elegans* morphogenesis, however, it appears that this role may be performed by other molecules, while a putative cadherin/catenin complex performs the important role of anchoring the actin cytoskeleton to the adherens junctions (Laure *et al.*, 1994; Costa *et al.*, 1998). In any system that requires active organisation of the actin cytoskeleton for morphogenesis, especially when a contractile mechanism is involved, the anchorage of the active components must be essential.

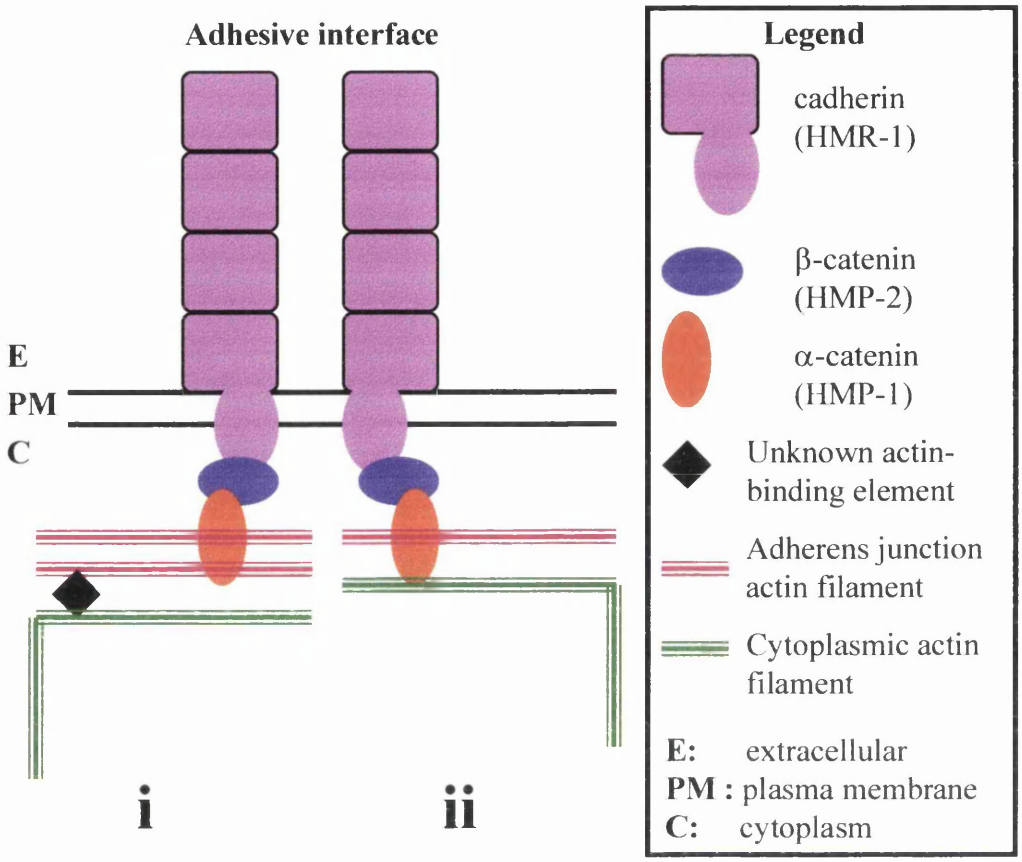

Figure 1.5

Possible models of cell adhesion and actin filament binding by the cadherin-catenin complex at epidermal adherens junctions

It is known that α-catenin binds to cadherin via β-catenin and that the cadherin-catenin complex is linked to the actin cytoskeleton but it is unknown whether α-catenin links directly to cytoplasmic actin filaments (model **ii**) or if there is an unknown component which links the α-catenin-associated adherens junction filaments with cytoplasmic actin filaments (model **i**). The *C.elegans* homologues of cadherin, α-catenin, and β-catenin are noted in brackets. They are thought to play a major role in the anchorage of cytoplasmic actin filaments during embryonic elongation (see section 1.7.5.4).

The extracellular cadherin domain is thought to mediate cell adhesion through a zipper-like mechanism with extracellular cadherin domains on neighbouring cells.

There clearly must be other adhesive molecules acting in *C.elegans* in order to maintain general cell adhesion but it is unknown whether these molecules are cadherin-related or of a completely different nature (Costa *et al.*,1998). There are many other cell-cell adhesion molecules which may mediate general cell interactions in *C.elegans* and in other systems (Prieto and Crossin, 1995).

1.6.5. Mechanisms of epithelial morphogenesis

There are several mechanisms whereby an ectodermal sheet can change the shape of the organism or structure it covers and the main processes used to achieve morphogenesis are: cell shape change, cell rearrangements and the addition or deletion of cells (Fristrom, 1988). All of these mechanisms are dependent completely or in part on the aspects of epithelial structure and function outlined above.

The orientation of cell divisions in *C.elegans* and in the leech are very important in mediating cell-cell contacts and in this way could be considered as contributing to morphogenesis but cell divisions are essentially complete within the embryo when actual body morphogenesis occurs and so the addition of cells is not used as a morphogenetic process as it is in other systems (Sulston *et al.*, 1983; Zackson, 1984; Hartenstein and Campos-Ortega, 1985). Cell death has also been shown to have a role in shaping epithelia in vertebrate neural tube morphogenesis and separating digits in developing limbs (Fristrom, 1988).

Cell shape change appears to be of paramount importance in the shaping of the *C.elegans* embryo and in the elongation of the *Drosophila* leg as well as in morphogenesis of many other tissues (Priess and Hirsh, 1986; Condic *et al.*, 1991). As discussed above and in other sections of this introduction, this cell shape change appears to be almost entirely driven by actin microfilaments within the epithelial cytoskeleton which are often associated with myosin (Spooner *et al.*, 1973; Priess and Hirsh, 1986; Young *et al.*, 1993). The individual cell shape changes are often channelled in one direction by restricting movement in one plane, thus causing the cells to elongate. The force produced by this individual cell shape change is transmitted across the epithelial sheet via tight cell-cell junctions to produce an overall morphogenetic change. The mechanism of cell flattening has also been shown to be an essential component to epiboly in some organisms, where the epithelial cells spread around the embryo in order

to cover it completely, and in the process of wound healing (Radice, 1980; Trinkaus, 1984). Cell flattening is also a component of *Drosophila* wing imaginal disc development and sea urchin embryogenesis (Ettensohn, 1985; Milner and Muir, 1987).

Cell rearrangement is another mechanism resulting in the spreading of epithelial cells and in shape change in many organisms (Keller and Trinkaus, 1987; Schoenwolf and Alvarez, 1989; Wilson and Keller, 1991; Williams-Masson *et al.*, 1998). This is the process whereby epithelial cells change position within the epithelial sheet while maintaining tight junctions and cell-cell contacts with neighbouring cells (Keller and Trinkaus, 1987; Fristrom, 1982). It is involved in the elongation of certain structures during sea urchin and *Drosophila* development and also is responsible for the first obvious shape change during *C.elegans* morphogenesis, the bending of the dorsal surface (Fristrom, 1976; Ettensohn, 1985; Hardin, 1989; Williams-Masson *et al.*, 1998). The mechanism of cell rearrangement is not well understood although a recent report in *C.elegans* has implicated both actin microfilaments and microtubules as being involved (Williams-Masson *et al.*, 1998).

1.7. Hypodermal development and function in *C.elegans* embryonic and postembryonic body morphogenesis

I will now look at the processes involved in *C.elegans* morphogenesis in detail from the cell fate specification of hypodermal cells through to the actual mechanisms that shape the embryo into the worm and maintain this shape throughout the life cycle.

1.7.1. Establishment and maintenance of the hypodermal cell fate in early embryos

1.7.1.1. Establishment of the hypodermal cell fate

Hypodermal cells are derived from two of the *C.elegans* founder cells, AB and C (Sulston *et al.*, 1983). 72 hypodermal cells are descendants of the AB founder cell, while 13 are descendants of the C founder cell (Figure 1.2)(Sulston *et al.*, 1983). The specification of cell fate in the AB lineage is quite complicated and arises from several binary switches early in development (Schnabel and Priess, 1997). These switches are

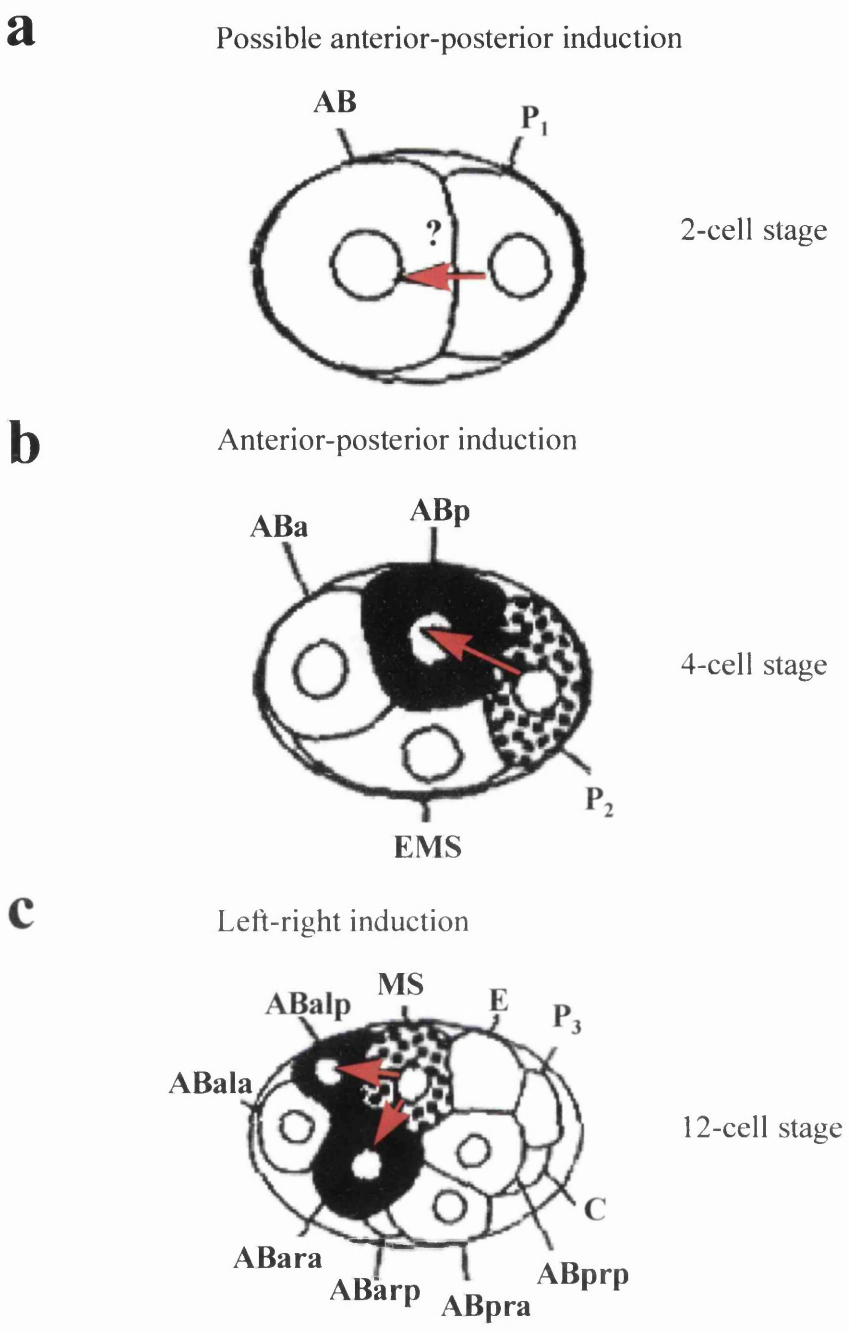

Figure 1.6

Summary of the main inductions that occur in the early AB lineage to specify cell fate

a Possible anterior-posterior induction in the 2-cell stage embryo by the P_1 cell on the AB founder cell which may establish different identities in the anterior and posterior descendants of AB.

b Anterior-posterior induction in the 4-cell stage embryo by the P_2 founder cell which affects the ABp cell and establishes different identities in the previously equivalent ABa and ABp daughters of AB.

c Left-right induction in the 12-cell stage embryo by the MS founder cell which establishes a pharyngeal fate in ABalp and ABarp descendants of AB. (adapted from Schnabel and Priess, 1997)

summarised in Figure 1.6. They all depend on cell-cell contacts, establish blastomere lineage fates and act to differentiate otherwise equivalent cells (Schnabel and Priess, 1997).

There is disagreement as to whether there is an interaction between the AB and P1 cells at the two cell stage in the embryo which polarises the AB cell and is involved in anterior-posterior patterning (Hutter and Schnabel, 1995b), or whether this anterior posterior asymmetry is already present in the AB blastomere by the first cleavage of the embryo (Gendreau *et al.*, 1994). However, it is generally agreed that at the 4 cell stage of the embryo, there is an interaction between P_2 and ABp (the posterior daughter of AB) which changes the ABp blastomere from one equivalent to ABa (the anterior daughter of AB) to a blastomere with an unique fate (Priess and Thomson, 1987). This interaction depends on direct contact between ABp and P_2 and it has been shown that if the orientation of cells in a 4 stage embryo is perturbed so that ABa contacts P_2 and ABp does not, then ABa acquires the usual ABp cell fate and vice versa (Mango *et al.*, 1994b; Hutter and Schnabel, 1994). This interaction has two main consequences: firstly it infers the ability on ABp to produce certain unique cells and products not produced by ABa, and secondly, it causes ABp to become largely unresponsive to the later induction from the MS founder cell which induces anterior pharynx in descendants of ABa (McGhee, 1995).

It has been proposed that each of the four granddaughters in the AB lineage has an intrinsic ability to produce one neuronal and one hypodermal precursor from each division and that the default state of cells in the AB lineage is neuronal (Gendreau *et al.*, 1994). The hypodermal precursors produce mostly the major hypodermis: seam (lateral hypodermal cells), P cells (ventral hypodermal cells), and the major hypodermal syncytia. The minor epidermal cells (small head and tail hypodermal syncytia as well as neuronal support cells) are produced from both hypodermal and neuronal producing cells. It has been suggested that the ABa cell produces anterior granddaughters which are predisposed to become neurons and posterior granddaughters which are predisposed to become hypodermis and that this is reversed in the granddaughters of the ABp cell (Gendreau *et al.*, 1994; Moskowitz *et al.*, 1994). This fate disposition was thought to be an intrinsic feature of the AB blastomere at the first cleavage and it was reported that when P_1 was ablated at the 2 cell stage then this patterning remained (Gendreau *et al.*, 1994). Hutter and Schnabel (1995b), however, have reported that when P_1 is ablated at

the 2 cell stage then the posterior granddaughters of both ABa and ABp change their fate to that of the anterior granddaughters, while the fate of the anterior granddaughters does not change. In both models, it was shown that the normal left-right asymmetry of the AB lineage was absent after P_1 removal for reasons explained below.

The interaction, involving the MS founder cell, which establishes left-right asymmetry is illustrated in Figure 1.6c. The MS founder cell which is a descendant of P_1 contacts three cells at the 12 cell stage of development and two of them, descendants of the ABa cell (shown in black in Figure 1.6c), are induced to form pharyngeal cells (Sulston *et al.*, 1983; Priess *et al.*, 1987; Hutter and Schnabel, 1994; Moscowitz *et al.*, 1994). The third contacting cell is a descendant of the ABp cell and as mentioned before, is normally unresponsive to the MS induction due to an earlier interaction between ABp and P_2. When the MS cell is removed, extra neuronal and hypodermal cells are produced from the cells which would have been induced by contact with MS (Priess *et al.*, 1987). This interaction between MS and two of the ABa granddaughters establishes a left-right asymmetry in the embryo which is modified by two later interactions (Schnabel and Priess, 1997). These final two cell-cell interactions affect ABp descendants on the left side of the embryo only, one occurring at the 24 cell stage between an ABa and ABp descendant, and one occurring at the 26 cell stage between an MS descendant and an ABp descendant (Hutter and Schnabel, 1994, 1995a). They specify further left-right asymmetries in the AB lineage.

In the C lineage, each daughter of the C blastomere also divides to produce one hypodermal and one non-hypodermal precursor although the non-hypodermal precursor produces body wall muscle rather than nervous tissue (Sulston *et al.*, 1983; Gendreau *et al.*, 1994). It also seems that the C founder cell has the intrinsic ability to produce hypodermis in isolation (Gendreau *et al.*, 1994). The genes involved in the induction of hypodermis appear to be completely separate in the two systems however and are discussed below.

1.7.1.2. Genes involved in specifying hypodermal cell fates

Many genes have been implicated as regulators in the inductions described above or as specifiers of hypodermal cell fate. Most events of *C.elegans* embryogenesis from fertilisation to gastrulation are thought to be controlled by maternally provided

products and so most of the genes found to be involved in early cell-cell interactions in the AB lineage are maternally expressed (McGhee, 1995). *glp-1* is a maternally expressed gene which is a homologue of *lin-12* and the *Drosophila Notch* gene and which has been implicated in several cell-cell interactions during development (Austin and Kimble, 1987; Priess *et al.*, 1987; Yochem and Greenwald, 1989). The protein encoded by *glp-1* is present on the surface of AB but not P_1 descendants and has been implicated as the receptor in both the P_2 and MS cell interactions. In the P_2 interaction, the ligand for GLP-1 is thought to be APX-1 which is a homologue of the *Drosophila* Notch protein, Delta (Mello *et al.*, 1994; Schnabel and Priess, 1997). APX-1 is expressed in P_2 and is localised to the junction between P_2 and ABp (Mickey *et al.*, 1996). The ligand for GLP-1 in the MS interaction is unknown although it does not appear to be APX-1 or the product of two of its homologues (Schnabel and Priess, 1997). GLP-1 is also thought to function with LIN-12 in the minor left-right asymmetry interactions at the 24 and 26 cell stage (Schnabel and Priess, 1997).

The *pal-1* gene is expressed both maternally and embryonically and appears to be involved in specifying the correct development of the C lineage and it seems that the expression of PAL-1 is regulated by the product of the *mex-3* gene (Schnabel and Priess, 1997). In *mex-3* mutants, PAL-1 is expressed ectopically in the granddaughters of the AB lineage whereby each of them produces body wall muscles and hypodermal cells as in the wild type C lineage (Draper *et al.*, 1996; Schnabel and Priess, 1997). MEX-3 contains two domains which are thought to mediate interactions with RNA and it has been suggested that MEX-3 binds to the *pal-1* mRNA and prevents its translation in AB descendants in the wild type embryo but not in the P_1 lineage where PAL-1 is normally expressed (Schnabel and Priess, 1997).

Several genes have been implicated in the specification of hypodermis. These genes generally act later in embryonic development and are usually zygotically expressed although they are probably controlled by maternal products. *elt-1* is an embryonically expressed gene which encodes a GATA-like transcription factor and is required for the production of major hypodermal cells from both the AB and C lineages (Spieth *et al.*, 1991; Page *et al.*, 1997). In *elt-1* homozygous lethal mutants, cells that become epidermal cells in wild type embryos become either neurons (AB lineage) or muscle cells (C lineage) (Page *et al.*, 1997). ABp descendants differentiate into an as of yet unknown cell type which is neither hypodermal, neuronal or muscle. ELT-1 is

expressed in hypodermal precursors from the 44 cell stage and in their hypodermal descendants and it appears that *elt-1* is required for the specification of hypodermal cell fate. In the C lineage, it is possible that ELT-1 is regulated by PAL-1 which is expressed in the hypodermal precursors before and during the time of ELT-1 expression. LIN-26, a presumptive zinc-finger transcription factor, is present in the nuclei of all non-neuronal ectodermal cells and appears to be involved in the maintenance of cell fate in this group which includes hypodermal cells (Labouesse *et al.*, 1994; Labouesse *et al.*, 1996). *lin-26* expression is first seen in cells of the AB and C lineages that give rise to hypodermal cells around 2 cell divisions prior to the generation of these cells. In homozygotes of one mutant allele, *lin-26(n156)*, a subset of hypodermal cells, the P cells, differentiate into neurons rather than hypodermis, and in mutants homozygous for strong loss of function alleles *mc1* and *mc4,* hypodermal cells are abnormal and degenerate rapidly (Labouesse *et al.*, 1996). *elt-1* mutants and chromosomal deficiencies deleting the *elt-1* region prevent the normal expression of LIN-26 (Chanal and Labouesse, 1997; Page *et al.*, 1997). Another GATA-like transcription factor, ELT-3, is localised to the nuclei of all hypodermal cells except the lateral seam cells immediately after the final cell division that gives rise to their terminal fate (Gilleard et al, 1999). *elt-1* is required for the formation of most *elt-3* expressing cells but *lin-26* function does not appear to be necessary for *elt-3* expression. Ectopic expression of *elt-3* in early blastomeres produces additional hypodermal cells (J.Gilleard, pers. comm.). However, worms homozygous for a deletion which removes the DNA-binding domain of *elt-3* appear to have a normal hypodermis which suggests that *elt-3* has a redundant role in hypodermal differentiation (J.Gilleard, pers. comm.).

Several embryonically expressed genes also appear to specify the fate of a particular subset of hypodermal cell, the lateral seam cells. *hln-2* encodes a zinc finger protein and is expressed exclusively in seam cells from the precomma stage until adulthood. This gene may play a role in specifying and patterning seam development. However, inhibition of the function of *hln-2* by RNAi does not appear to give a noticeable phenotype which suggests that it could be redundant (K.Koh, pers. comm.). Another gene encoding a GATA factor, *elt-8*, is expressed at high levels in seam cells and in lower levels in many other cells, mostly derived from the AB lineage. Inhibiting *elt-8* function using RNAi resulted in lumpy worms with fewer than normal seam cells (K.Koh, pers. comm.). Another gene which acts in the seam cells is *lin-22* (Wrischnik

and Kenyon, 1997). Anterior seam cells (V1-V4) are blast cells which generate only hypodermis postembryonically in the wild type *C.elegans*, while a pair of seam cells to the posterior (V5 and V6) produce neuronal as well as hypodermal cells in males. *lin-22* appears to act in V1-V4 to prevent them from following a more posterior-like fate and also seems to act in a branch of the V5 lineage to prevent excess neurons from being produced. In order to repress the production of excess neurons, *lin-22* inhibits the expression of the posterior Hox gene *mab-5* in both V5 and V1-V4 cells as well as inhibiting the activity of *lin-32* and another as yet unidentified gene involved in the regulation of stem cell division in cells V1-V4. Interestingly, *lin-22* is a homologue of the transcriptional regulator *hairy* and the *Enhancer of split* complex genes of *Drosophila* (Wrischnik and Kenyon, 1997). These genes regulate multiple components of anterior-posterior patterning and neural development in *Drosophila* and some of the *lin-22* activities are similar to those of its homologues.

1.7.2. Enclosure of the hypodermis in the *C.elegans* embryo

As cell divisions are occurring and cell fates are being specified, the precursors of the future internal structures of *C.elegans* migrate internally, a process known as gastrulation, producing novel cell-cell contacts and positioning the cells in the correct place within the embryo. Gastrulation is described in more detail in section 5.1.2. At the end of cell division, terminally differentiated hypodermal cells arise on the dorsal surface of the developing *C.elegans* embryo around 290 mins after first cleavage at 20°C (Sulston *et al.*, 1983). They organise into a monolayer of 6 rows of cells which then extends laterally around the embryo until the migrating edges meet at the ventral midline and form adherens junctions so that the entire embryo is enclosed in a continuous hypodermal layer. This process of epiboly, or spreading of epithelial sheets, is known as enclosure in *C.elegans* and occurs in two stages. The first stage involves a quartet of hypodermal cells, the leading cells, migrating around the embryo bilaterally towards the anterior using actin-rich filopodia to achieve movement (Williams-Masson *et al.*, 1997). The other hypodermal cells are pulled around the embryo by this leading cell movement and eventually the leading cells from either side meet and fuse, forming adherens junctions, at the ventral midline. The second process of enclosure occurs at the ventral midline when the hypodermal cells from the anterior and posterior meet in a

circular 'pocket'. The cells at the edge of this pocket are known as the ventral pocket cells and appear to close in a 'purse-string' manner involving a contractile actin band similar to that employed in *Drosophila* dorsal enclosure or the healing of small wounds (Martin and Lewis, 1992; Young *et al.*, 1993). Enclosure is discussed in more detail in section 4.1.2.

1.7.3. Cell rearrangement during intercalation of the dorsal hypodermis in *C.elegans*

Cells forming the two rows of the dorsal hypodermis undergo a process of intercalation which starts at around 330 mins after fertilisation as hypodermal cells are migrating around the embryo, and ends during ventral enclosure (Sulston *et al.*, 1983; Williams-Masson *et al.*, 1998). The tip of each intercalating cell produces a thin protrusion which wedges underneath and between the adherens junctions of its two contralateral cells and as the tip widens dorsoventrally and in the anterior-posterior direction, the cell pushes completely between the two cells resulting eventually in one row of dorsal hypodermal cells (Figure 1.7) (Williams-Masson *et al.*, 1998). Prior to dorsal intercalation the embryo is a relatively spherical shape but this process produces a slight bend in the embryo by creating a longer dorsal surface with the merging of two hypodermal rows (Priess and Hirsh, 1986; Williams-Masson *et al.*, 1998). The embryo is now at the precomma or lima-bean stage. This mechanism of cellular rearrangement is dependant on the presence of microtubules for its initiation and also requires actin microfilaments for successful completion. It is thought that the microtubules are necessary for the formation of the initial tip-protrusion and provide the rigidity needed for it to furrow between the two contralateral cells. The role of actin microfilaments in the process is less clear. There does not seem to be specific microfilament localisation or organisation in the intercalating tips like those seen in the leading edges of enclosing cells (Williams-Masson *et al.*, 1997; 1998). Instead, it is possible that the disruption of the actin cytoskeleton of the cell may be enough to cause the defects seen in intercalating cells when cytochalasin D is used to interfere with actin filaments (Priess and Hirsh, 1986; Williams-Masson *et al.*, 1998). It has been suggested that the cue for dorsal hypodermal intercalation may come from signals produced by the basement membrane or underlying muscles (Williams-Masson *et al.*, 1998). This is because

Figure 1.7

Dorsal intercalation of hypodermal cells

The two rows of dorsal hypodermal cells are the central two rows in the diagrams, the cells of one side are shaded to illustrate intercalation into a single row. The anterior is towards the top of the figure. Cells are shown as if the central region of the hypodermis was cut open along the ventral midline and viewed from above. Progression from **a** to **c** occurs as the hypodermal cells migrate ventrally around the embryo during hypodermal enclosure. The embryo illustrated in **b** would be a precomma embryo and in **c** would be a comma stage embryo. (Adapted from Podbilewicz and White, 1994).

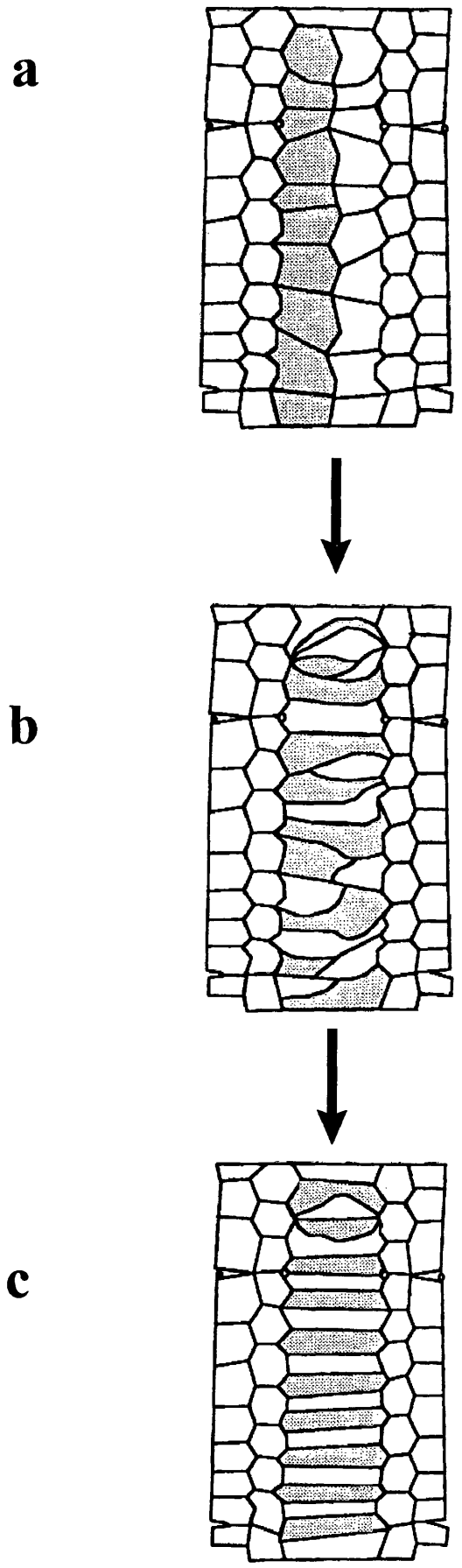
a
b
c

intercalation of the dorsal hypodermis is not blocked by the removal of neighbouring lateral hypodermal cells and it does not seem that the intercalating ability of individual dorsal cells is prevented by the ablations of any neighbouring cell of the dorsal hypodermis.

1.7.4. The relation of enclosure and dorsal intercalation to subsequent morphogenesis in *C.elegans*

It is obvious that complete hypodermal enclosure is necessary for subsequent elongation of the *C.elegans* embryo as embryos with enclosure defects rupture when elongation is initiated, probably because of pressure exerted on internal cells by the contracting hypodermis (Mango *et al.*, 1994a; Labouesse, 1997; Williams-Masson *et al.*, 1998; Costa *et al.*, 1998). It is possible that the tension and hypodermal cell movements during enclosure help to organise the circumferentially oriented actin filaments responsible for elongation (Williams-Masson *et al.*, 1998). It is also obvious that correct junctions must be formed along the ventral midline before morphogenesis can occur (Costa *et al.*, 1998). Whatever the function of enclosure relating to subsequent morphogenesis, it is evident that it is an essential prerequisite to normal elongation.

The intercalation of the dorsal hypodermis also appears to be necessary for subsequent normal elongation. Mutants homozygous for a mutation in the *die-1* gene show incomplete dorsal intercalation and arrest at the 1.5 to 2-fold stage (P.Heid, pers.comm.). Enclosure and fusion do occur in these mutants, although fusion appears to be initiated prematurely and enclosure is not completely normal. *die-1* encodes a zinc finger protein which is interesting as several putative transcription factors in *Drosophila* are involved in cell rearrangement in ovary and embryo development (Godt and Laski, 1995; Oda *et al.*, 1998; P.Heid, pers.comm.). It is possible that the intercalation of the dorsal hypodermal cells is necessary for the alignment of the microtubule framework which in turn may allow the circumferential alignment of actin microfilaments and subsequently elongation of the worm (Priess and Hirsh, 1986; Williams-Masson *et al.*, 1998).

1.7.5. Elongation of the *C.elegans* embryo

1.7.5.1. Mechanism of elongation in wild type embryos

During mid-embryogenesis, from around 390-690 mins after fertilisation, the *C.elegans* embryo elongates from a relative spheroid to a cylindrical worm shape four times the original length and with a decrease in width of around threefold (Sulston *et al.*, 1983; Wood, 1988). Active elongation begins after the intercalation of the dorsal hypodermal cells produce a slight bend in the embryo and is thought to be driven by the contraction of actin-rich microfilament bundles which circumferentially align throughout the hypodermis prior to elongation (Priess and Hirsh, 1986). Microtubules in the hypodermal cells also align circumferentially and are thought to maintain the tensile strength of the cells during elongation. There is also an extracellular sheath present over the surface of the embryo from the beginning of elongation which may act to transmit stresses across the hypodermis. Actin-mediated elongation is described in detail in section 6.1.1.

1.7.5.2. Hypodermal cell fusions during embryonic elongation

There are 78 hypodermal nuclei in the *C.elegans* embryo at the end of elongation but only 42 hypodermal cells (Sulston *et al.*, 1983; Podbilewicz and White, 1994). This arises due to the extensive cell fusions which occur in the hypodermis prior to and during embryonic elongation. After dorsal intercalation, 17 cells from the dorsal hypodermis fuse with 4 cells at the anterior of the ventral hypodermis and 2 cells at the posterior anus to form hyp7, the largest hypodermal syncytium (Figure 1.8)(Podbilewicz and White, 1994). To the anterior of hyp7, hypodermal cells fuse to form 6 smaller syncytia, hyp1-hyp6 with 3,2,2,3,2 and 6 nuclei respectively (White, 1988). To the posterior of hyp7, hypodermal cells fuse to form 4 smaller syncytia, hyp8-hyp11, containing 1,1,2 and 1 nuclei respectively (White, 1988). The 10 lateral hypodermal cells on either side of the embryo and the 6 pairs of P cells on the ventral surface of the embryo do not fuse during embryogenesis but remain mononucleate (Podbilewicz and White, 1994). Recently, a cold sensitive mutant with defects in dorsal fusion of the hypodermis has been characterised and homozygous embryos arrest at a

Anterior

hyp1
hyp2
hyp3

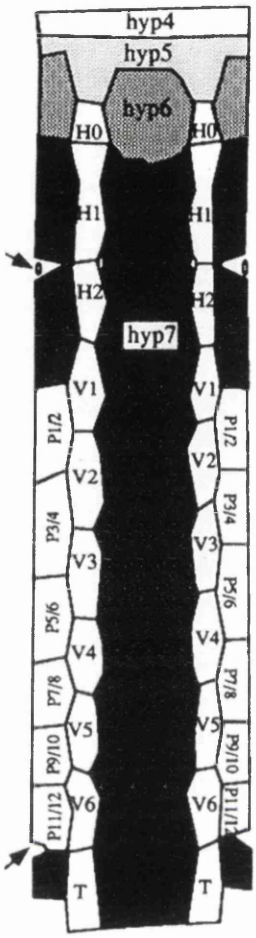

hyp11
hyp10 (dorsally)
hyp8
hyp9
hyp10 (ventrally)

Posterior

Figure 1.8

Hypodermal cell positions at hatch

This diagram is a representation of an embryo hypodermis at hatch which has been cut open along the ventral midline and viewed from above. It illustrates the fusion of the hypodermis into 11 syncytia (hyp1-hyp11), which contain 3, 2, 2, 3, 2, 6, 23, 1, 2, 2 and 1 nuclei respectively. The ventral P cells (1-12) and the lateral paired seam cells (H1, H2, V1-V6, and T) remain mononucleate during embryogenesis. (Adapted from Podbilewicz and White, 1994).

1.5- to 2-fold stage of elongation indicating that normal hypodermal fusion is necessary for the completion of elongation (B.Podbilewicz, pers. comm.). Viral-induced cell fusion and invasion are cold-sensitive processes and the nature of this *duf-1* mutation suggests that hypodermal cell fusion is also a cold-sensitive process. It has also been reported recently that cell fusion between hypodermal cells occurs by a similar mechanism to virus-cell fusion (Mohler *et al.*, 1998). Hypodermal cell fusion initiates at a single point or pore restricted to the adherens junctions, and then widening basally and laterally in a radial wavefront as the fusing membranes are internalised by vesiculation.

1.7.5.3. Hypodermally expressed genes involved in embryonic elongation

Despite the evidence implicating the hypodermis as the tissue responsible for driving cell shape change and elongation in the *C.elegans* embryo, there remain very few elongation defective mutants which show mutations in hypodermally expressed genes. Most of the elongation defective mutants characterised to date have mutations in genes expressed in the body wall muscle which is attached to the hypodermis, or in genes encoding proteins present in the basement membrane between hypodermal and muscle cells. These observations indicate that the presence of normal body wall muscles, muscle-hypodermis basement membrane, and muscle-hypodermis attachments are essential for complete elongation of the embryo although the role of the muscle in elongation is still unknown (Guo *et al.*, 1991; Lundquist and Herman, 1994; Sibley *et al.*, 1994; Williams and Waterston, 1994; Gupta *et al.*, 1997). I will discuss mutations in genes expressed in both hypodermis and body wall muscle which result in an elongation-defective phenotype.

Priess and Hirsh (1986) proposed that the circumferentially oriented microfilaments within hypodermal cells were connected to the adherens junctions at each side of the cell they traversed and recently this idea has been reinforced by the characterisation of mutations in the genes *hmp-1, hmp-2* and *hmr-1* which encode homologues of the cell adhesion proteins α-catenin, β-catenin/Armadillo, and classical cadherin respectively (Costa *et al.*, 1998). Mutants homozygous for *hmp-1* and *hmp-2* arrest as embryos with severe defects in elongation although all other tissues and structures show terminal differentiation. This is also true for around 40% of *hmp-2*

homozygotes and 2% of *hmr-1* homozygotes. The other *hmp-2* homozygotes arrest with less severe elongation defects while 98% of *hmr-1* homozyogtes undergo abnormal ventral hypodermal enclosure as discussed in section 4.1.2.2. The elongation defective mutants begin to elongate as normal although subsequently only the ventral cells are seen to elongate significantly and dorsal folds appear as the dorsal hypodermis retracts along with the ventral elongation. Immunofluorescence studies have shown that the actin microtubule bundles align as normal and appear to be anchored to the adherens junctions on either side of the hypodermal cells. However, during elongation, actin microfilaments in the dorsal hypodermis detach from the adherens junctions and retract towards the dorsal midline so that further contractions no longer draw opposing sides of the hypodermal cell together and therefore do not result in elongation of the cell. Detachment of actin microfilaments does not occur in the much smaller lateral or ventral hypodermal cells and it is thought that the attachments are under much more stress in the dorsal hypodermis which is mostly made up of the single large hyp7 syncytium. In lateral and ventral cells there are adherens junctions between unfused cells which run parallel to the circumferential actin microfilaments down the length of the embryo while in the dorsal hypodermis there are only two adherens junctions parallel to the contractile microfilaments, one at either end of the hyp7 syncytium. These adherens junctions may help withstand the stretching forces created by microfilament contraction in lateral and ventral hypodermal cells. HMP-1, HMP-2 and HMR-1 all localise to adherens junctions between hypodermal cells. Wild type *hmr-1* is required to localise HMP-1 and HMP-2 to adherens junctions and wild type *hmp-2* is required to localise HMP-1 to adherens junctions.

From the characterisation of these mutations it appears that the actin microfilaments are anchored to the adherens junctions via a putative cadherin/catenin system (see Figure 1.5)(Costa *et al.*, 1998). This system is used extensively in both vertebrate and invertebrate epithelial cells for cell-cell adhesion, signal transduction and the organisation of the actin cytoskeleton and so it seems that it plays a similar role in *C.elegans* during embryonic elongation (Aherle *et al.*, 1996; Gumbiner, 1996). Another cadherin-related gene in *C.elegans, cdh-3*, shares homology with the *Drosophila dachsous* gene (see below) and has been shown to have a role in the morphogenesis of a single hypodermal cell, hyp10 (Pettitt *et al.*, 1996). It is expressed in developing hypodermal and neuronal cells throughout development and null mutations in *cdh-3*

result in an abnormal tail phenotype. It was proposed that *cdh-3* acts to maintain the connection between hyp10 and hyp11 cells during elongation of the tail in embryos and that disruption of this connection results in abnormal tail morphogenesis. Because *cdh-3* is expressed in many more hypodermal cells than are affected in a *cdh-3* null mutation, there must be other cadherin-related or general adhesion molecules which can substitute for *cdh-3* function in these cells. Severe mutants of the *Drosophila dachsous* gene, which encodes a protein with 27 cadherin domains, have abnormal legs with shorter, thicker leg segments (Clarke *et al.*, 1995). The mechanism of *Drosophila* leg elongation is also thought to be driven by cell shape change caused by the contraction of an apical actin-myosin belt and so would also require a mechanism to transmit this contractile force across a sheet of epidermal cells in order to cause shape change on a larger scale (Condic *et al.*, 1991; von Kalm *et al.*, 1995). It is thought that the contractile actin-myosin belt is connected to the adherens junctions via a cadherin/catenin system as in vertebrates (von Kalm *et al.*, 1995).

Another gene which is involved in elongation and is expressed in the hypodermis is *sma-1* which encodes a β_H-spectrin homologue, a novel isoform of β-spectrin which was first identified in *Drosophila* (McKeown *et al.*, 1998). *sma-1* homozygotes are viable and elongate for the same length of time as wild type embryos but they have a decreased rate of elongation and result in short, wide larvae with a blunt anterior, abnormally elongated pharynx, and a twisted tail. Different *sma-1* alleles elongate at different rates specific to each allele and *sma-1* RNA is located in hypodermal cells from the start of hypodermal migration around the embryo prior to enclosure. As embryos elongate, the level of *sma-1* RNA in hypodermal cells rapidly decreases and cannot be detected after the 2-fold stage. Spectrin is a heterodimeric actin-binding protein which is composed of α- and β-spectrin subunits and forms a cytoskeletal network with the plasma membrane (Bennett and Gilligan, 1993). β_H-spectrin differs from β-spectrin in that it does not contain an ankyrin binding sequence that is present in β-spectrin and it does contain SH3 domains which are not present in β-spectrin (Thomas *et al.*, 1997). In polarised epithelia, α-spectrin is generally distributed on plasma membranes while β-spectrin is restricted to the basolateral surface and β_H-spectrin is localised at the apical surface at the adherens junction (Lee *et al.*, 1993; de Cuevas *et al.*, 1996; Thomas *et al.*, 1997). A pair of α-spectrins can form tetramers with a pair of either β- or β_H-spectrins and both can crosslink actin (Dubreuil *et al.*, 1990). It

is proposed that SMA-1 acts as a component of the hypodermal actin cytoskeleton to regulate the elongation of the *C.elegans* embryo (McKeown *et al.*, 1998). SMA-1/α-spectrin tetramers could link the actin fibres in the hypodermis to each other and to the apical membrane thus stabilising the actin cytoskeleton during elongation. SMA-1 may play a regulatory role as well as a structural role in embryonic elongation as indicated by the decreased rate of elongation of *sma-1* mutants. It is suggested that SMA-1 may play a role in the interaction between muscle and hypodermis at the attachment sites, possibly as a binding site for signal transduction molecules. In *Drosophila,* β_H-spectrin, encoded by the *karst* gene, co-localises with *D*E-cadherin (Thomas *et al.*, 1998). It is thought to play a role in mediating tight cell-cell adhesion in order to facilitate cell signalling through the close association with the cadherin cell adhesion complex and is essential for eye development. β_H-spectrin is associated with regions of apical contraction resulting in cell shape change and movement during morphogenesis of the *Drosophila* embryo although no *karst* mutants have shown matching morphological defects to date (Thomas and Kiehart, 1994; Thomas *et al.*, 1998). Interestingly, a mutation in the gene encoding an homologue of α-spectrin, *spc-1*, has recently been isolated in *C.elegans* and it produces a phenotype of 1.5- to 2-fold arrest (K.Norman, pers. comm.). There appears to be no disorganisation in the hypodermal actin filament pattern but instead these mutants show abnormalities in the body wall muscle and overlying basement membrane, which are twice as wide as normal, and in pharyngeal muscle, resulting in abnormal pumping (K.Norman, pers. comm.).

The third *C.elegans* hypodermally expressed gene with an apparent function in embryonic elongation is *let-502*, which encodes a Rho-binding serine/threonine kinase and which interacts with *mel-11*, a gene encoding a protein similar to regulatory subunits of smooth muscle myosin-associated phosphatase (Wissmann *et al.*, 1997). LET-502 is expressed in the hypodermal seam cells and the gain of function mutations in *let-502* resulted in embryonic arrest with no elongation although other tissues and structures appeared to have differentiated terminally (Wissmann *et al.*, 1997; A.Piekny, pers.comm.). These results may implicate a myosin component of the microfilament contraction which drives elongation.

Smooth-muscle myosin II is composed of two heavy chains and two pairs of light chains (Allen and Walsh, 1994). In smooth muscle, and non-muscle cells, phosphorylation of either muscle or non-muscle myosin light chain (MLC), one of the

pair of two myosin light chains, results in the formation of myosin cross-bridges along actin filaments and subsequently either contraction of the smooth muscle, or the assembly of contractile acto-myosin stress fibres in non-muscle cells (Allen and Walsh, 1994; Giuliano and Taylor, 1995; Huttenlocher et al, 1995; Kimura et al, 1996; Gong et al, 1996). Phosphorylation of MLC is carried out by Myosin light chain kinase (MLCK) and Myosin light chain phosphatase (MLCP) reverses this effect by dephosphorylating MLC resulting in the relaxation of muscle cells or inhibition of stress fibre formation depending on the cell (Allen and Walsh, 1994; Giuliano and Taylor, 1995). The process of MLC phosphorylation is regulated mainly by intracellular Ca^{2+} levels as Ca^{2+} regulates MLCK activity. However, it has been found that the state of MLC phosphorylation can be altered while Ca^{2+} levels remain constant and therefore there must be other regulatory mechanisms involved (Bradley and Morgan, 1987). Many studies have since implicated small GTPases such as Rho in the regulation of MLC phosphorylation and thus the control of myosin contraction in smooth muscle (Kimura *et al.*, 1996; Gong *et al.*, 1996). Rho activates several serine/threonine kinases including rho-binding kinase which inactivate MLCP by phosphorylating their myosin-binding subunits thus preventing the dephosphorylation of MLC (Kimura *et al.*, 1996). In this way, activation of Rho can trigger or maintain myosin contraction. Rho, and Rho-binding kinases have also been implicated in non-muscle cells in cytoskeletal reorganisation of actin and myosin to form contractile stress fibres which run throughout the cytoplasm and are anchored at the plasma membrane by cell adhesion molecules in sites known as focal adhesions (Ridley and Hall, 1992; 1994; Hall, 1998).

A possible model was proposed for the function of the *let-502* and *mel-11* genes which suggested that a small GTPase could activate LET-502 which would then phosphorylate MEL-11 preventing dephosphorylation of non-muscle MLC (nmMLC) and may in fact phosphorylate nmMLC itself, leading to myosin contraction and thus elongation. In the absence of Rho activation, MEL-11 would dephosphorylate nmMLC and result in myosin relaxation. However, all the *let-502* alleles identified by Wissmann *et al.* (1997) were gain of function alleles with a maternal component and it has been subsequently shown that both RNAi for *let-502* and loss of function alleles produce variable phenotypes which are near wild type (A.Piekny pers.comm.). Although this strongly suggests that the *let-502* and *mel-11* pathway is redundant, it does not remove the possibility that other serine/threonine kinases or MLCP homologues may be

interacting in a similar pathway active in *C.elegans* elongation. The mutant LET-502 protein which results in a blockage of elongation may disrupt the function of another Rho-binding kinase in an active contractile pathway.

An embryonic morphogenetic process which apparently utilises an actin-myosin mechanism to drive cell shape changes and thus elongation is the morphogenesis of the *Drosophila* leg (Condic *et al.*, 1991; von Kalm et al, 1995). During the prepupal period of *Drosophila* morphogenesis the leg imaginal disc evaginates from its larval position on the inner surface of the epidermis, and the femur and tibia undergo significant elongation via changes in the epidermal cell shape (Condic *et al.*, 1991). Several mutations in two genes, *zipper* and *spaghetti squash*, result in abnormally elongated and malformed leg and wing discs (Gotwals and Fristrom, 1991). These two genes encode homologues of non-muscle myosin heavy chain (nmMHC) and nmMLC respectively and the zipper protein localises to the actin-myosin belt present around the apical edge of many epithelial cells forming the *Drosophila* leg (Gotwals and Fristrom, 1991; Young *et al.*, 1993). This suggests that *Drosophila* leg elongation results from the cell shape change caused by the contraction of a myosin motor in the actin-myosin belt (Condic *et al.*, 1991; von Kalm *et al.*, 1995).

1.7.5.4. Genes encoding proteins present in basement membrane and muscle which are involved in embryonic elongation

Muscle cells arise in two lateral rows adjacent to the lateral hypodermal cells at around 290 mins after first cleavage and migrate dorsally and ventrally until there are two longitudinal rows to each side of the embryo midline on both the dorsal and ventral surfaces immediately underlying the hypodermis (Hresko *et al.*, 1994). A basement membrane forms between adjacent muscle cells and between the muscle cells and the hypodermis. The embryo is at the precomma stage when the muscle cells have arranged in this way and the muscle and hypodermal cells remain in close contact during embryonic elongation with muscle cells forming attachments to the hypodermis as the embryo elongates from the comma to the 1.5-fold stage (Goh and Bogaert, 1991; Hresko *et al.*, 1994). As the embryo continues to elongate, the myofilaments of the muscle cells attach through the basement membrane to hemidesmosome structures in the hypodermis containing intermediate filaments. It is thought that these

hemidesmosomes are formed in response to signals from the underlying muscle cells as they do not form in hypodermal cells when the precursors of the underlying muscle cells have been ablated (Hresko *et al.*, 1994). Around the 3-fold stage of wild type elongation, the hemidesmosomes attach the muscle cells through the hypodermis to the cuticle so that their contractions will be manifested as body movements (Francis and Waterston, 1991). At the 1.5-fold stage of elongation the muscle cells are organised into sarcomeres and as elongation progresses, they become flattened and more closely aligned to the hypodermis (Guo and Bogaert, 1991; Hresko *et al.*, 1994). Muscle cells usually begin contraction as the embryo elongates from 1.5- to 2-fold and result in the embryo vigorously rolling around inside the eggshell during the latter stages of elongation.

Both the correct assembly and organisation of muscle components and the formation of adequate connections between the body wall muscle and hypodermis appear to be essential for the normal completion of elongation. Mutations in genes encoding basement membrane proteins have also shown that this plays an essential role in the attachment of muscle to the hypodermis during elongation. Mutations in various genes encoding proteins present in the muscle and basement membrane produce severe defects in body wall muscle organisation and attachment leading to what is termed the Pat phenotype (Gilchrist and Moerman, 1992; Rogalski *et al.*, 1993; Williams and Waterston, 1994). This phenotype is the paralysed arrest of embryos at a two-fold stage of elongation and is lethal. Embryos do not start muscle contractions as normal but instead exhibit irregular twitching around the 1.5- to 2-fold stages and cease elongation and movement around the 2-fold stage. These mutants often hatch but are inviable. Genes which can be mutated to produce this phenotype include *myo-3*, which encodes myosin heavy chain A, *unc-52*, which encodes a homologue of the mammalian basement membrane protein perlecan; and *pat-3*, which encodes a homologue of β-integrin, a protein involved in the attachment of muscle structures to the membrane as well as many other genes which have not been studied at a molecular level (Waterston, 1989; Rogalski *et al.*, 1993; Williams and Waterston, 1994; Gettner *et al.*, 1995). Certain alleles of the *mec-8* gene also show a variably penetrant cold sensitive Pat phenotype and *mec-8* has been shown to encode a protein with two RNA binding motifs which regulates alternative splicing of the *unc*-52 gene (Lundquist and Herman, 1991; Lundquist *et al.*, 1996).

Mutations in other genes affecting muscle or basement membrane function show arrest at an equivalent or slightly longer stage of embryonic elongation with variable defects in muscle contraction. Certain *mup-1* mutant alleles produce inviable short and lumpy 3-fold embryos or L1 larvae as a result of abnormal or ectopic muscle-hypodermis attachments (Goh and Bogaert, 1991). Mutants homozygous for null mutations in the *hlh-1* gene, which encodes a homologue of the vertebrate myoD DNA-binding protein have defects in muscle sarcomere organisation and muscle cell placement and arrest as lumpy 2-fold embryos or larvae with weak muscle contractions and uncoordinated movement (Chen *et al.*, 1994).

Type IV collagen forms a branched network that is a major component of the basement membranes which surround the pharynx, intestine, gonad, and is present on the basolateral surface of the hypodermis, between muscle-muscle and muscle-hypodermis junctions (Albertson and Thomson, 1976; Francis and Waterston, 1991; Kramer, 1994a). Temperature sensitive point mutations in the genes *emb-9* and *let-2,* which encode two different chains of type IV collagen, result in a vast reduction of collagen secretion into basement membranes and a build up of the collagen in the producing muscle cells at the restrictive temperature (Guo *et al.*, 1991; Sibley *et al.*, 1994). This is manifested as a lethal phenotype with embryonic arrest at around the 2-fold stage of development. At the permissive temperature the phenotype is less severe with a higher proportion of secreted collagen and less retention of the mutant collagen in muscle cells (Gupta *et al.*, 1997). The phenotype of homozygous null *emb-9* embryos is embryonic arrest at around the 2.5- to 3-fold stage. In these null mutants, body wall muscles are seen to detach from the hypodermis as elongation progresses indicating that type IV collagen is essential for normal muscle attachment to the hypodermis (Williams and Waterston, 1994; Gupta *et al.*, 1997). The temperature sensitive mutants show a semi-dominant embryonic lethal phenotype with embryonic arrest at an earlier stage and it appears that this phenotype is due to the accumulation of collagen within the muscle cells (Waterston, 1989; Williams and Waterston, 1994; Gupta *et al.*, 1997). This collagen build-up may be disrupting the muscle cell function to some degree by interfering with the synthesis or processing of other proteins.

Clearly there is a relationship between muscle and hypodermal tissues which is essential for normal embryonic elongation. The mechanism of muscle-hypodermis attachment appears to be involved in the later stages of elongation when there appears to

be a stronger pull from the muscles as the embryos elongate. The role of this muscle-hypodermal interaction in elongation is still unknown as the longitudinal contraction of muscles would oppose the direction of elongation. However, it has been proposed that the hemidemsomes, apparently recruited in the hypodermis by signals from the underlying muscle cells, may act to stabilise the actin cytoskeleton during elongation and so defects in the signalling cells or the attachment structures themselves may disrupt elongation in this way (Costa *et al.*, 1998; McKeown *et al.*, 1998).

1.7.5.5. Genes involved in pharyngeal organogenesis which may play a role in embryonic elongation

The *pha-4* and *glp-1* genes will be discussed in connection with embryonic enclosure by the hypodermis in section 4.1.2.2. Mutations in *glp-1* have been shown to result in extra hypodermal cells due to the failure of the pharyngeal fate induction in the AB lineage (Priess *et al.*, 1987). As well as producing variable defects in hypodermal cell enclosure, these embryonic mutants also have variably penetrant defects in elongation and prominent bulges often form along the length of the embryo. In many of these embryos the hypodermis does not divide into the usual dorsal, lateral and ventral rows and in those embryos which do show hypodermal subdivisions, the extra hypodermal cells are always present in the lateral rows. Another gene involved in the development of the pharynx is *pha-1* which encodes a transcription factor (Granato *et al.*, 1994). Mutant embryos homozygous for certain *pha-1* alleles are often shorter than wild type embryos and have hypodermal bulges although there do not seem to be any abnormalities in the number or arrangement of hypodermal cells (Schnabel and Schnabel, 1990). It has been proposed that the morphogenetic defects in the body shape of these mutant embryos are secondary effects of the absence of a pharynx. Since the pharynx usually fills the anterior third of the developing embryo, the absence of a normal pharynx may indirectly influence anterior body shape. However, certain *pha-4* mutants which completely lack a pharynx can elongate relatively normally and so the general morphogenetic defects seen in *pha-1* mutant embryos may be the result of a more direct effect (Mango *et al.*, 1994a).

1.7.6. The maintenance of body shape after embryonic elongation

1.7.6.1. The role of the cuticle

During the life cycle of *C.elegans* the cuticle, the impermeable exoskeleton, is synthesised 5 times, once at the end of embryogenesis and once at each subsequent moult with the final cuticle secreted at the L4 to adult moult (see Figure 1.3)(Singh and Sulston, 1978; Cox *et al.*, 1981c). Starting at the precomma stage of embryonic development, structural proteins that will form the multi-layered cuticle are transcribed and translated in the hypodermis (Singh and Sulston, 1978; Johnstone and Barry, 1996; Gilleard *et al.*, 1997). These proteins are known as cuticular collagens and are expressed in temporally distinct waves throughout embryogenesis and each subsequent stage of the life cycle (Cox et al, 1981b; Johnstone and Barry, 1996). After elongation of the embryo is complete, cuticular collagens and other components of the cuticle are secreted from the apical membrane of the hypodermal cells forming the extracellular cuticle and after this stage the cuticle takes over the role of shape maintenance in the embryo (Sulston *et al.*, 1983; Priess and Hirsh, 1986). Genes that encode cuticular collagens and the mutations found in these genes which have uncovered their various roles in the maintenance of body shape are discussed at length in section 3.1.4. The actin microfilaments which drive the process of elongation and the embryonic sheath which covers the embryo during elongation are both thought to play a role in the formation and patterning of the first cuticle and actin microfilaments have also been implicated in cuticle patterning at each moult during post embryonic development (Costa *et al.*, 1997). The external layer of each cuticle is patterned into a series of rings, known as annulae, by shallow circumferentially oriented furrows (Cox *et al.*, 1981a). These furrows correspond to the pattern of actin filament bundles during elongation and are first manifest in the embryonic sheath (Costa *et al.*, 1997). The sheath furrows and ridges are found at close proximity to the hypodermal membrane and patches of electron-dense material are present in regions of the hypodermis underneath sheath ridges which may represent the secretion of extracellular materials from the hypodermis at these points. At the end of embryogenesis, prior to hatching, the sheath appears to separate from the hypodermal membrane and develops a trilaminar appearance which is identical to the external layer of the cuticle in hatched L1 larvae. Thus, the sheath,

which is patterned by the hypodermal actin filaments during elongation becomes the outermost layer of the first secreted cuticle of the life cycle resulting in the annular patterning of the cuticle. Annulae extend along the dorsal and ventral sides of the L1 cuticle but do not traverse the lateral areas which instead have longitudinally arranged ridges known as the alae (Cox *et al.*, 1981a,c). Although the actin microfilaments also align circumferentially in the lateral seam cells during elongation, they do not appear to be closely associated with the apical membrane as the dorsal and ventral microfilaments are and therefore do not pattern the sheath and thus the cuticle at these areas (Costa *et al.*, 1997). Postembryonically, during each moulting period, actin microfilaments again align circumferentially in the hypodermis but only in the dorsal and ventral regions. These actin bundles appear to join the adherens junctions on either side of the hypodermal cells they traverse as during embryonic elongation, and the pattern of these filaments is coincident with the pattern of annulae in each subsequent cuticle. It is thought that the actin filaments contract at postembryonic moults as the hypodermal cells add new cuticle material to the surface between the bundles thus allowing the new cuticle to form beneath the old cuticle but have a larger surface area to accommodate the increase in growth between each stage.

During normal moults, after the new cuticle is synthesised underneath the old cuticle, the old cuticle is expelled from the anterior half of the pharynx and then the whole anterior cuticle separates from the body (Singh and Sulston, 1978). The animal rotates inside the old cuticle rupturing it at the anterior and subsequently emerges in its new cuticle. The molecules that control the process of moulting in *C.elegans* are not well understood as yet but recently there have been reports of two genes which may be involved in cuticle shedding. *nhr-23* is a gene encoding CHR3, an nuclear hormone receptor, which is homologous to the *Drosophila* ecdysone-inducible DHR3 protein involved in metamorphosis (Koelle *et al.*, 1991; Lam *et al.*, 1997; Kostrouchova *et al.*, 1998). During late embryogenesis, *nhr-23* transgene fusion constructs are expressed in hypodermal cells. CRH3 function was inhibited using RNAi and the phenotypes produced included small size, dumpyness, and an inability to shed or degrade old cuticle properly after moulting. It has been proposed that CHR3 plays a role in cuticle detachment although, as with the *Drosophila* DHR3 protein, this involvement in moulting may be indirect.

A second gene *lrp-1* has also been implicated as having a role in moulting (Yochem *et al.*, 1999). *lrp-1* encodes a lipoprotein receptor-related protein homologous to megalin, a membrane protein which is expressed on the apical surface of epithelia and which regulates lipid homeostasis and the activity of extracellular proteases (Strickland *et al.*, 1995). Animals homozygous for mutations in *lrp-1* produce phenotypes with high similarity to *nhr-23* RNAi (Kostrouchova *et al.*, 1998; Yochem *et al.*, 1999). Many of these mutants are slow growing or dumpy and they often arrest at the L3-L4 stages encased in old cuticles or with pieces of old cuticle still attached to their bodies (Yochem *et al.*, 1999). *lrp-1* mutants do not appear to rotate inside the old detached cuticles or be able to degrade them. These mutants are also very slow moving and are thought to have feeding defects due to the obstruction of old cuticle at the buccal cavity and pharynx. LRP-1 is present at the apical surface of hyp6 and hyp7 and is thought to endocytose dietary sterols which are needed for an as yet unknown function during moulting. Another possible role for LRP-1 could be the activation of collagenases or other proteases that might be secreted during moults. As the study of moulting control in *C.elegans* is in its infancy, many of the proposed roles for these genes are highly speculative and a clearer picture of the molecules involved in cuticle moulting awaits the characterisation of further genes.

1.7.6.2. Postembryonic hypodermal cell fusions

The lateral seam and the ventral P cells are blast cells which go through several stages of cell divisions after hatching throughout post embryonic development (Sulston and Horvitz, 1977). The postembryonic fate of these cells differs between the hermaphrodite and the male because different sets of sex organs must develop in each, so I will only describe hypodermal postembryonic lineage in the hermaphrodite. At each round of cell divisions one of the daughter cells generally fuses with hyp7, the largest hypodermal syncytium, and the other daughter cell either remains as a blast cell, as in the case of the seam, or V, cells or becomes neuronal or a vulva precursor cell, as in the case of the P cells depending on their position (Sulston and Horvitz, 1977; Podbilewicz and White, 1994). P cells 1,2 and 9-12 undergo a cell division at the end of the L1 stage after which the anterior daughters fuse to hyp7 and the posterior daughters eventually migrate into the ventral nerve cord. At the end of the L3 stage, the posterior

daughters of P3-P8 divide once and while half of these cells fuse with hyp7 also, the other half become vulva precursor cells (Podbilewicz and White, 1994; Sharma-Kishore *et al.*, 1999). The lateral seam cells undergo a stem cell division at the beginning of each larval stage and half fuse to hyp7 at each division. Around the middle of the L4 stage, the seam cells to either side fuse longitudinally, in the final postembryonic cell fusion event, forming two continuous lateral syncytia and cease cell division (Podbilewicz and White, 1994). Overall, 12 P cell descendants and 98 seam cell descendants fuse to hyp7 throughout postembryonic development (Sulston and Horvitz, 1977).

The significance of these fusions is not well understood although it is known that the cells stop cell division once they have fused and certain genes have been discovered which appear to be involved in this fusion process. *lacZ* fusion constructs containing two genes encoding novel transmembrane tyrosine kinases were shown to be expressed in hyp7 from the L1 stage and in each subsequent cell which fused to hyp7 during postembryonic development at the time of fusion (Morgan and Greenwald, 1993). It was proposed that these genes, *kin-15* and *kin-16* which appear to have arisen from a gene duplication event, may regulate the fusion of mononucleate cells with hyp7 throughout postembryonic development or may function in maintaining the nuclei of these cells in a mitotically quiescent state after fusion. The transgene constructs showed expression in all hyp7 nuclei from the L1 stage, when there are 23 hyp7 nuclei, to the adult stage when hyp7 comprises 133 nuclei.

1.7.6.3. Postembryonic control of hypodermal function

The pathway that controls many aspects of postembryonic hypodermal cell fate including hypodermal gene fusions and the transcription of several stage-specific cuticular collagens is known as the heterochronic gene pathway and to date comprises at least 6 genes: *lin-4, lin-14, lin-28, lin-42, lin-58* and *lin-29* (Figure 1.9)(Ambros, 1989; Abrahante *et al.*, 1998). *lin-29*, which encodes a zinc-finger type transcription factor is the most direct regulator of the larval to adult switch, which comprises the fusion of lateral hypodermal cells, secretion of the adult specific cuticle, and cessation of the moulting cycle (Liu *et al.*, 1995; Rougvie and Ambros, 1995; Bettinger *et al.*, 1996). LIN-29 accumulates in the hypodermis during the L4 stage of development (Rougvie

and Ambros, 1995; Bettinger *et al.*, 1996). *lin-14, lin-28, lin-42* and *lin-58* all act upstream of *lin-29* and act as negative regulators of *lin-29* activity, restricting LIN-29 production to the L4 stage (Abrahante *et al.*, 1998). The associations between these genes has been elucidated by the study of many heterochronic mutants which either precociously moult into adults, or never undergo the larval to adult moult depending on the mutation. Null *lin-4* mutants reiterate the L1 hypodermal pattern at each moulting stage and never moult into adults (Chalfie *et al.*, 1981; Ambros and Horvitz, 1987). Null *lin-14* mutants conversely adopt precocious L2 hypodermal patterns at the L1 stage and subsequently moult into adults one stage early (Ambros and Horvitz, 1984;1987). *lin-4* encodes two small RNAs which interact directly with the 3'UTR region of the *lin-14* transcript and negatively affect its translation therefore actively downregulating *lin-14* (Lee *et al.*, 1993). Null mutations in *lin-28* result in mutants which undergo a moult straight from the L1 to L3 stage, completely skipping the L2 stage of hypodermal development, and subsequently moult to adult one stage early (Chalfie *et al.*, 1981; Ambros and Horvitz, 1984). As expected, *lin-29* null mutants develop to the L4 stage but never moult into adults, instead moulting into successive L4 stages (Ambros, 1989). It is thought that *lin-14* and *lin-28* do not directly regulate *lin-29* and it is unknown whether *lin-42* or *lin-58* control *lin-29* directly although it is known that *lin-42* prevents the early expression of the adult hypodermal program and that *lin-14* requires the action of *lin-58* in order to prevent the larval to adult switch (Abrahante *et al.*, 1998).

As mentioned above and described in detail in section 3.1.2, hypodermal cells synthesise collagens during each larval stage (Cox and Hirsh, 1985). These collagens are expressed in temporally distinct waves within each stage and many collagens have been found to be specific to a particular larval or adult stage (Cox and Hirsh, 1985; Kramer *et al.*, 1985; Johnstone and Barry, 1996). The expression patterns of certain larval or adult-specific collagen reporter transgenes have been examined in heterochronic mutants. These have shown that heterochronic mutations which cause precocious formation of the adults cuticle also cause precocious transcription of the adult-specific collagen genes *col-7* and *col-19* (Liu *et al.*, 1995; Abrahante *et al.*, 1998). They also showed that heterochronic mutations which prevented the larval-adult switch caused continued expression of a larval collagen gene *col-17* and prevented the activation of *col-7* and *col-19* transcription (Liu *et al.*, 1995). It is not known whether *lin-29* directly controls the transcription of these collagens although it is thought that

cuticle collagen genes are controlled largely by tissue specific transcriptional enhancers rather than repressors in other tissues (Liu *et al.*, 1995; Gilleard *et al.*, 1997; Abrahante *et al.*, 1998). It is possible that other heterochronic genes also have a role in regulating cuticular collagens specific to different stages of the life cycle.

Figure 1.9 The heterochronic gene pathway

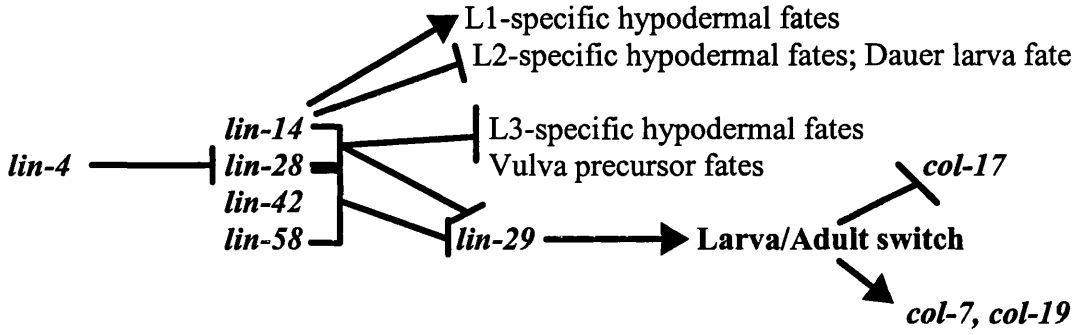

During wild type development these genes are up- or down-regulated depending on the larval stage in order for the correct sequence of hypodermal developmental events to occur. However, an interesting discovery was made when observing heterochronic mutants that had passed through the dauer stage instead of the normal L2 stage (Liu and Ambros, 1991). *lin-4, lin-14*, and *lin-28* mutants which had gone through a dauer stage in response to lack of food exhibited wild type post-dauer development (Cassada and Russell, 1975; Liu and Ambros, 1991). During wild type development, *lin-14* activity must decrease between the L1 and L2 stages of development in order to specify the proper timing and sequence of events which ultimately lead to the larval/adult switch (Ambros and Horvitz, 1987; Ambros, 1989). Since *lin-4* and *lin-28* interact with *lin-14*, they too are likely to be under precise temporal control (Liu and Ambros, 1991). Dauer development is a period of indefinite developmental arrest and so it may be that *lin-4, lin-14,* and *lin-28* are rendered ineffective due to this period of arrest and are no longer of use in post-dauer developmental control.

1.8. Aims of the project

It is clear that there are many factors involved in the process of hypodermally-mediated body shape change in *C.elegans*. The mechanism of morphogenesis relies on correct cell fate specification in the very early embryo, through correct cell migrations at the time of gastrulation and enclosure, to correct cell-cell contacts during the active process of elongation between hypodermal cells and between muscle and hypodermal cells, and correct synthesis and secretion of an extracellular cuticle which takes over the role of body shape maintenance from the end of embryogenesis onwards. Each stage in the control of this process may involve several pathways which must co-ordinate properly in order for the correct series of events to take place and as yet the molecules involved in elongation are largely unknown. My aim in this project was to elucidate some of the molecules involved in the enclosure and elongation of the *C.elegans* embryo by characterising embryonic lethal mutants defective in these processes and to examine postembryonic shape change using an antibody specific to a cuticular structural protein which is essential for the maintenance of body shape.

Chapter 2

Materials and Methods

Unless otherwise stated, all chemicals / reagents were purchased from BDH (Merck House, Poole, Dorset, UK), Fisher Scientific (Fisher Scientific UK Ltd., Loughborough, Leicestershire, UK). GibcoBRL (Life Technologies Ltd., Paisley, Renfrewshire, UK) or Sigma (Sigma-Aldrich Company Ltd., Poole, Dorset, UK). Restriction enzymes were obtained from New England Biolabs (New England Biolabs [NEB], Ltd.,Hertfordshire, UK).

2.1. Chemical abbreviations and common names

BSA:	Bovine Serum Albumin
BME:	β-mercaptoethanol
DABCO:	1,4-diazabicyclo-2,2,2-octane
DEPC:	Diethyl pyrocarbonate
DTT:	Dithiothreitol
diH_20:	Deionized water
FITC:	Fluorescein isothiocyanate
IPTG:	Isopropyl-β-D-thiogalactoside
Na_2EDTA:	Ethylenediaminetetraacetic acid disodium salt
Na_2EGTA:	Ethyleneglycoltetraacetic acid disodium salt
Pipes:	1,4-piperazinediethanesulphonic acid
RITC:	Rhodamine B isothiocyanate
sdiH_20:	Sterile deionized water
SDS:	Sodium dodecyl sulphate
Tris-HCl:	2-Amino-2-(hydroxymethyl)-1,3-propanediol-hydrochloride
Tween-20:	Polyoxyethylenesorbitan monolaurate
X-gal:	5-bromo-4-chloro-3-indolyl-β-D-galactopyranoside (Boehringer Mannheim, Ltd., Diagnostics and Biochemicals, East Sussex, UK)

2.2. Commonly used stocks, solutions and media

Antibody Buffer A (AbA): 1x PBS, 1% BSA, 0.5% Triton X-100, 0.05% NaAzide and 1mM EDTA in diH_2O. Stored at 4°C.

Antibody Buffer B (AbB): As AbA but with 0.1% BSA. Stored at 4°C.

Ampicillin (1,000x): 100mg/ml solution in sdiH_2O. Aliquoted and stored at -20°C.

Blocking solution (1x): 1% milk powder in 1xPBST. Made fresh before use.

BO_3 buffer (20x): 1M H_3BO_3, 0.5M NaOH in diH_2O. Stored at room temperature.

Chitinase solution: 20mg/ml chitinase in 50mM NaCl, 70mM KCl, 2.5mM $MgCl_2$. Aliquoted and stored at -20°C.

Chloramphenicol (1,000x): 17mg/ml solution in sdiH_2O. Aliquoted and stored at -20°C

DEPC Treated di$H_2$0: DEPC added to diH_2O to a final concentration of 0.1%, mixed vigorously for 10min and autoclaved. Stored at room temperature.

DTT: 1M stock in 0.01M Na acetate, adjusted to pH 5.2. Aliquoted and stored at -20°C.

Egg Salts: 118mM NaCl and 48mM KCl in diH_2O. Stored at room temperature.

Ethidium Bromide: 10mg/ml stock in diH_2O, final concentration 0.5µg/ml in agarose gels. Stored, protected from light, at room temperature.

Injection mix (10x): 20% Polyethylene glycol (MW 6000-8000), 200mM KPO_4, pH7.5 and 30mM $C_6H_5K_3O_7$ in DEPC Treated diH_2O. Stored at room temperature.

IPTG: O.5M stock in sdiH_2O. Aliquoted and stored at -20°C.

Kanamycin (1,000x): 50mg/ml in sdiH_2O. Aliquoted and stored at -20°C.

L-Broth: 1% Bacto tryptone (Difco, Michigan, USA), 0.5% yeast extract (Difco), 0.5% NaCl, in diH_2O. Autoclaved and stored at room temperature.

L-Broth Agar: as for L-Broth + 1.5g/100ml bacto-agar (Difco). Autoclaved then allowed to cool (antibiotics were added at this stage, if required) poured with sterile technique on to plastic plates, allowed to set, dried by inversion in sterile flow hood (microflow) and stored, for short periods, at 4°C.

M9 Buffer (1x): 0.3% KH_2PO_4, 0.6% Na_2HPO_4, 0.5% NaCl, 1mM $MgSO_4$, in diH_2O. Autoclaved and stored at room temperature.

Mounting Solution: 50% glycerol, 1xPBS, 2.5% DABCO. Made fresh prior to use.

Na_2EDTA: 0.5M stock in diH_2O pH8.0 with NaOH. Autoclaved and stored at room temperature

NGM Agar: 0.3% NaCl, 1.7% agar (Difco), 0.25% peptone (Difco), 0.0003% cholesterol (1ml/L of 5mg/ml stock in ethanol), in diH_2O. Autoclaved and then 1ml/L of 1M $CaCl_2$, 1ml/L of 1M $MgSO_4$ and 25ml/L of 1M potassium phosphate buffer pH6.0 added. Poured with sterile technique on to plastic plates, allowed to set, dried by inversion in sterile flow hood (microflow) and stored at room temperature.

Phenol: Purchased liquified and pre-equilibrated at pH8. Stored at 4°C.

Phenol / Chloroform: Mix of equal volumes of phenol and chloroform. Stored at 4°C.

Phosphate Buffered Saline [PBS] (100mM): 7.31g NaCl, 2.36g Na_2HPO_4, 1.31g NaH_2PO_4 $2H_2O$ in 1L diH_2O, adjusted to pH 7.2. Autoclaved and stored at room temperature.

PBST: As PBS but with the addition of 0.2% Tween 20. Stored at room temperature.

Potassium Phosphate Buffer (1M): Prepared from 1M KH_2PO_4 and 1M K_2HPO_4, mixed in appropriate ratio for desired pH. Autoclaved and stored at room temperature.

Proteinase K: 10mg/ml stock in diH_2O. Aliquoted and stored at -20°C.

Ruvkun Fixation Buffer [RFB] (2x): 160mM KCl, 40mM NaCl, 20mM Na_2EGTA, 10mM spermidine-HCl, 30mM NaPipes (pH7.4) in 50% methanol. Stored at -20°C.

Single Worm Lysis Buffer (SWLB): 50mM KCl, 10mM Tris (pH 8.3), 2.5mM $MgCl_2$, 0.45% Tween 20, 0.01% (w/v) gelatin. Autoclaved and stored in aliquots at -20°C. Proteinase K (Boehringer-Mannheim) added to 60μg/ml just prior to use.

SDS: 10% stock solution in $sdiH_2O$. Stored at room temperature

SOC medium: 20g Bacto-tryptone, 5g Bacto-yeast extract, 0.5g NaCl in 950ml diH_2O. 10ml of 250mM KCl added and pH adjusted to 7. Autoclaved and then 5ml of 2M $MgCl_2$ and 20ml of 1M glucose added before use. Stored at room temperature.

Sodium Phosphate Buffer (1M): Prepared from 1M NaH_2PO_4 and 1M Na_2HPO_4, mixed in appropriate ratio for desired pH. Autoclaved and stored at room temperature.

TE: 1mM EDTA, 10mM Tris-HCl, (pH as required) in diH_2O. Autoclaved and stored at room temperature. TE at pH 8.0 was used for all DNA manipulations, unless otherwise indicated.

Tetracycline (1,000x): 12.5mg/ml in 50% $sdiH_2O$, 50% ethanol. Aliquoted and stored at 4°C.

TBE (10x): 0.9M Tris-HCl, 0.9M Boric acid, 25mM Na_2EDTA pH8.0, in diH_2O. Stored at room temperature.

Tris-Triton buffer [TTB]: 100mM Tris-HCl, pH7.4, 1% Triton X-100, 1mM EDTA. Stored at room temperature.

X-Gal (100x): 2% in dimethyl formamide (DMF). Stored in aliquots, protected from the light, at -20°C.

Note: All media and most heat insensitive solutions were autoclaved using the following conditions: 120°C, 15lbs/in^2 for 15min.

2.3. *C.elegans*, yeast and bacterial strains

C.elegans: All Obtained from the *Caenorhabditis* Genetics Center (University of Minnesota, St Paul, Minnesota, USA)

N2:	Wild-type Bristol stock (Brenner, 1974).
BA671:	*spe-9(hc88)*I
BC1785:	*dpy-18(e364)/eT1* III; *unc-46(e177) sDf30/eT1* V
CB88:	*dpy-7(e88)*X
CB151:	*unc-3(e151)*X
CB458:	*dpy-13(e458)*IV
CB224:	*dpy-11(e224)*V
CB1410:	*unc-84(e1410)*X
CX51:	*dyn-1(ky51)*X
DR210:	*dpy-5(e61) daf-16(m26) unc-75(e950)*I
DR293:	*dpy-5(e61) unc-101(m1)*I
MT309:	*lin-15(n309)*X
MT465*:	*dpy-5 (e61)*I; *bli-2(e768)*II; *unc-32(e189)* III
SP219:	*mnDp1(*X;V*)*/+V; *unc-3(e151)*X
SP511:	*mnDp1(*X;V*)*/+V;*mnDf43* X
SP261:	*mnDp1(*X;V*)*/+V;*mnDf2* X
SP262:	*mnDp1(*X;V*)*/+V;*mnDf1* X
SP268:	*mnDp1(*X;V*)*/+V;*mnDf7* X
SP275:	*mnDp1(*X;V*)*/+V;*mnDf17* X

SP277: *mnDp1(*X;V*)*/+V*;mnDf19* X

SP278: *mnDp1(*X;V*)*/+V*;mnDf20* X

RW7000: RW subclone of Bergerac BO

*MT465 was previously known as CB4166

Other strains:

IA022: *dpy-7*::GFP*(ijIs9)* (Generated by I.Johnstone).

IA023: *egl-23(n601)*IV; *dpy-7*::GFP*(ijIs5)* (Generated by I.Johnstone).

IA060: *ijDf1*/+ X (Generated by I.Johnstone).

IA061: *ijDf2*/+ V (Generated by I.Johnstone).

IA105: *unc-76(e911)*V;*dpy-7*::GFP, *unc-76(+)(ijIs12)* (Generated by E.Stewart).

MQ375: *dpy-7(qm63)*X (Gift from S.Hekimi).

Alleles:

w4: Gift from J.Rothman. No designated strain name.

dyn-1(cq4) Gift from A.van der Bliek. No designated strain name.

E.coli strains:

Name	Genotype
OP50	The strain used in the our laboratory is a variant of the uracil requiring OP50 strain (Brenner, 1974) which has been transformed with a plasmid containing the Tet^r marker (I.L.Johnstone, pers. comm.).
NovaBlue	*endA1, hsd17($r_{k12}^-m_{k12}^+$), supE44, thi-1, recA1, gyrA96, relA1, lac* [F′, *proA*$^+$*B*$^+$ *lacI*^{q}*Z–M15*::Tn*10*] Obtained from Novagen,Inc.via R&D systems Europe, Abingdon, UK.
XL1-Blue	*recA1*, *endA1*, *gyrA96*, *thi-1*, *hsdR17*, *supE44*, *relA1*, *lac* [F′, *proAB*, *lacI*^{q}*Z–M15*, Tn*10* (Tet^r)] Obtained from Stratagene Ltd., Cambridge, UK.

2.4. Vectors and clones

2.4.1. Plasmid vectors

pBluescript II SK-: pUC19 derived phagemid. Obtained from Stratagene Ltd.

pTAg: pUC derived phagemid. Obtained from Novagen, Inc.

2.4.2. Clones

pRF4: Contains the dominant *rol-6(su1006) C.elegans* cuticular collagen mutation (Mello *et al.*, 1991). Gift from J.Kramer.

pMW0002: Consists of the *dpy-7* cuticular collagen gene promoter in frame with the GFP coding sequence contained in the pPD95.67 Fire Vector (A.Fire, pers.comm.). Constructed by M.Watson.

pMW0003: Consists of the *col-12* cuticular collagen gene promoter in frame with the GFP coding sequence contained in the pPD95.67 Fire Vector (A.Fire, pers.comm.). Constructed by M.Watson.

Cosmid Clones:

Chromosome I: W02B9, F36D1, F56G4, T02A8, W06H12, F46A8, AA2, F28D9, C27D12.

X Chromosome: C11G10, T10B10, F46F2, C02D4, C33A11, F47C8, F39D8, R03A10, C02C6, K09A9, K09E9, H08J19, F59D12, ZK662, ZK678.

Gifts from J.Sulston and A.Coulson.

2.5. Culture maintenance

2.5.1. *C.elegans* culture

2.5.1.1. Wild type culture

Bristol N2 wild-type strains carrying non-temperature sensitive mutations and transgenic *C.elegans* strains were maintained in a 20°C incubator (Jencons LT3, Jencons Scientific Ltd., Leighton Buzzard, UK) on NGM agar plates (3.5 or 5cm in diameter- Griner Labortechnik Ltd., Stonehouse, Gloucestershire, UK) with *E.coli* OP50 as a food source according to standard methods (Sulston and Hodgkin, 1988).

2.5.1.2. Culture of strains carrying temperature sensitive or lethal mutant alleles

Strains carrying temperature-sensitive (ts) alleles were maintained at the permissive (16°C) or restrictive (25°C) temperature, in Jencons LT3 incubators (Jencons Scientific Ltd.), depending on what they were being used for. If males hemizygous for a ts allele on X which prevented mating were required for crosses, the cross was generally carried out at 15°C and the progeny then moved to 20°C or 25°C. Strains carrying recessive lethal mutations were maintained as a heterozygous stock and at each generation individual hermaphrodites from the strain were left to self fertilise separately on agar plates (3.5cm in diameter - Griner). As soon as the embryos laid began to hatch, the hermaphrodites were removed. After around 24 hours, the plates were scored for embryonic death and larvae from plates which contained carriers of the mutant allele were plated out separately as before to maintain the mutation. All worms were viewed and scored using an Olympus SZ40 dissecting microscope (Olympus Optical Co. (UK) Ltd., London, UK).

2.5.2. Bacterial culture

2.5.2.1. Bacterial culture on plates

All *E.coli* bacterial strains were grown at 37°C (in a Heraeus incubator; Heraeus

Equipment Ltd., Brentwood, Essex, UK) on L-agar plates (9cm - Griner), supplemented with the appropriate antibiotic at the appropriate concentration. The final concentrations of the antibiotics used were as follows:

i)	*E.coli* strains transformed with plasmids:	100μg/ml ampicillin or 12.5μg/ml tetracycline
ii)	*E.coli* strains transformed with cosmids:	100μg/ml ampicillin, 25μg/ml kanamycin or 17μg/ml Chloramphenicol

2.5.2.2. Bacterial liquid culture

Unless otherwise stated, all liquid cultures were grown at 37°C with vigorous shaking. The media, antibiotics and antibiotic concentrations used in these cultures were as follows:

i) *E.coli* strains transformed with plasmids:
L-broth supplemented with 100μg/ml ampicillin or 12.5μg/ml tetracycline.

ii) *E.coli* strains transformed with cosmids:
L-broth supplemented with 100μg/ml ampicillin, 25μg/ml kanamycin or 17μg/ml Chloramphenicol.

2.6. DNA preparation

2.6.1. Plasmid and Cosmid DNA mini preparation

Qiagen plasmid Mini DNA Preparation kits (Qiagen Inc., via Hybaid Ltd., Teddington, Middlesex, UK), were used for cosmid and plasmid DNA mini preparations from an appropriate volume of overnight culture of *E.coli* cells, according to the manufacturer's protocols supplied with these kits. To get an equivalent DNA yield from cosmid preparations, 9mls of overnight culture were used per column instead of the recommended volume. Approximately 5μg of DNA was recovered from each column for cosmids and 15-20μg for plasmids. The cosmid or plasmid DNA was

resuspended in an appropriate volume of TE or sterile deionized water, usually 15-20μl for cosmids and 50μl for plasmids.

2.6.2. Cosmid and plasmid DNA medium scale preparations

Qiagen Plasmid Midi DNA Preparation kits (Qiagen Inc.) were used for medium and large scale plasmid DNA preparations respectively, from an appropriate volume of overnight culture of *E.coli* cells according to the manufacturer's protocols. I used 150mls of overnight culture for cosmids per column to obtain a higher DNA yield. Cosmid preparations yielded around 30μg of DNA, and plasmid preparations, around 66μg.

2.7. Standard molecular biology techniques

2.7.1. Restriction endonuclease digests

Single enzyme digests were carried out at 37°C in 1x enzyme reaction buffer supplied with the restriction endonuclease for 3 hours to overnight. Double digests were performed in the recommended buffer for that specific double digest (yielding over 75% activity for each enzyme - NEB). In situations where the enzymes used required incompatible reaction conditions single digests were done sequentially with phenol/chloroform extraction and ethanol precipitation steps between the two digests using standard protocols (Sambrook *et al.*, 1989) and adding 0.5μg of 20mg/ml glycogen (Boehringer Mannheim) to each extracted sample to aid ethanol precipitation. After precipitation, the DNA was resuspended in sterile deionized water containing 1x reaction butter appropriate for the next restriction endonuclease to be used. In some cases heat inactivatable enzymes were used first and the organic extraction step above was replaced by inactivation of the enzyme by heating at the recommended temperature for that enzyme, usually 65°C, for 10min on a heating block (Grant instruments, Cambridge, England). The quantity of enzymes used varied depending upon the source of the DNA and also upon its required usage, however a general rule was observed which states that 1 unit of enzyme digests 1μg of lambda DNA in 1 hour in a 20μl volume at the appropriate temperature.

2.7.2. Agarose Gel electrophoresis of DNA and RNA samples

Restriction endonuclease digested DNA and PCR amplified DNA samples were electrophoresed through agarose gels. Samples of purified single- and double-stranded RNA was visualised in the same way. DNA samples from STS marker PCRs were electrophoresed through special MetaPhor agarose (FMC corporation, via Flowgen, Lichfield, Staffordshire) to allow greater separation of the STS marker bands. Gels ranging from 0.6% to 2% agarose were prepared by dissolving the appropriate amount of agarose in 1x TBE. MetaPhor agarose gels were prepared according to the manufacturer's protocol and 3% gels were used for separation of STS bands. These gels, which were normally 15cm in length, were run in 1x TBE using gel electrophoresis tanks from GibcoBRL or Pharmacia (Milton Keynes, UK). The gels were generally run at a voltage equivalent to 3-10V/cm. All DNA samples were loaded into the wells of these gels using DNA sample buffer (see below). Gels were post-stained by placing in a container of 1xTBE plus 0.2μg/ml ethidium bromide on a moving platform for 20-40 mins and then washed in deionized water before visualising. The electrophoresed DNA or RNA was visualised using a UV transilluminator (Appligene Oncor, Durham, UK) and a record of the gel made using a digital imaging system (Appligene). Each gel contained at least one lane of DNA size standards, either 1 kb ladder or 50bp ladder (both from GibcoBRL).

Fragment Sizes

1kb ladder	12.216	11.198	10.180	9.162	8.144
(in kilobases)	7.126	6.108	5.090	4.072	3.054
	2.036	1.636	1.018	0.517	0.506
	0.396	0.344	0.298	0.220	0.201
	0.154	0.134	0.075		

50bp ladder	800-50 in multiples of 50bp. The 350bp band is 2-3 times
(in bases)	brighter than the other bands for internal orientation.

10x DNA Sample buffer

20mM EDTA
25% Ficoll
0.2% Bromophenol blue
in diH_20

2.7.3. Gel and PCR purification

DNA fragments generated from restriction endonuclease digests or PCR reactions were purified in two ways. Specific fragments from restriction endonuclease digests or PCR reactions resulting in non-specific fragments as well as the target DNA fragment were electrophoresed through agarose gels run in 1x TBE. Where there were high molecular weight fragments that required extra separation from surrounding fragments before they could be excised cleanly, a 0.7% gel 30cm in length was used to separate these fragments. The appropriate fragments were excised using a scalpel blade and the DNA extracted from the gel using the QIAquick Gel Extraction kits (Qiagen Inc.) according to the manufacturer's protocol. The PCR purification method allows separation of 100bp-10kb products from primers, nucleotides, polymerases and salts. If a clean PCR fragment of the correct size was obtained, it was purified using the QIAquick PCR purification kit (Qiagen Inc.) according to the manufacturer's protocol.

2.7.4. Ligation reactions

Ligation reactions were performed in a 10µl volume using 1x T4 DNA ligase buffer (NEB) and 1-2 units of T4 DNA ligase (NEB). Generally, 250ng of vector DNA were used in each ligation. The amount of insert DNA used varied with the molar concentration of free ends in the reaction and I used the following equation as a guideline with a molar ratio of around 1:1:

$$\frac{\text{ng of vector x kb size of insert}}{\text{kb size of vector}} \times \text{molar ratio of } \frac{\text{insert}}{\text{vector}} = \text{ng of insert}$$

Ligations were performed overnight at 16°C.

2.7.5. Transformation of *E.coli*

Transformations were performed using either *E.coli* XL1-blue (Stratagene, Ltd.) or Novablue (Novagen, Inc.) supercompetent cells and 25-100ng of ligated DNA according to the manufacturers protocols with the following exceptions: only 25µl of supercompetent cells were used for the transformations with XL1-blue and the volumes of all solutions required for the transformation were adjusted accordingly; also, when transforming with Novablue, 200µl of SOC medium was added to each transformation rather than 80µl.

The transformed cells were selected using the antibiotic resistance marker carried by the plasmid (Amp^r). Where applicable, blue / white colony selection was also used to select transformants with plasmids containing inserts. This selection makes use of α-complementation of the *lacZΔM15* mutation in appropriate *E.coli* strains. In these instances, the agar media was also supplemented with 0.004% X-gal and 34µM IPTG (final concentrations).

2.8. Preparation of slides for observations of living embryos and adults

2.8.1. Slide preparation for short-term Nomarski and fluorescence microscopy of live embryos

Slides used for microscopy of living embryos were overlaid with an agarose pad to prevent squashing of the specimens. A 0.4mm thick pad of agarose was prepared by flattening a large drop of a molten 2-5% agarose solution on a microscope slide (BDH) with a second slide placed across it at right angles to its longitudinal axis. The flattening slide was supported on either side by another slide perpendicular to the mounting slide resting on 2 layers of autoclave tape (approximately 0.4mm thickness) which raises it the required amount above the mounting microscope slide with the agarose overlay. The agarose pad was usually around 15 mm in diameter and was left sandwiched between these two slides while preparing the specimens. Embryos were washed off the surface of an agar plate onto a watchglass using M9 buffer. A 1mm

capillary was drawn out to 0.1-0.2mm and used to transfer embryos from the watchglass to the mounting slide using a mouth pipettor. Once the transfer was complete, a 22x22mm coverslip (thickness 1, BDH) was carefully lowered over the agarose pad using a scalpel blade. Care was taken to transfer enough M9 along with the embryos so that they would not be squashed when the coverslip was lowered (around 10-20µl). After the specimens were mounted, slides were kept in closed humid boxes at 20°C until viewed under the microscope. These humid boxes were plastic boxes with close fitting lids, containing tissue paper soaked in deionized water.

2.8.2. Slide preparation for short-term Nomarski and fluorescence microscopy of live larvae and adults

The preparation of slides for microscopy of live larvae and adults was essentially the same as for embryos but the problem of movement across the agarose pads had to be overcome. To enable microscopy of stationary worms, 10mM sodium azide was added freshly to the agarose when molten. This anesthetises the worms so that they can be examined at length. Worms were washed off plates, mounted, and stored in the same way as for embryos.

2.8.3. Slide preparation for time course observations of live embryos

Embryos examined over a longer period of time, such as for timecourse microscopy were prepared in a different manner. A small drop of 5% agarose was used to make the agarose pad on a microscope slide in the same manner as before, although for time course microscopy a smaller pad was used, around 10mm in diameter. 1ml of the 5% agarose was prepared in an eppindorf and was placed on an heating block at 80°C to melt. In this way, each slide could be prepared individually without the agarose solidifying. Gravid hermaphrodites were washed off plates onto a watch glass with M9 buffer and cut open using two sharp needles (microlance 26G1, Becton Dickinson S.A., Madrid, Spain) so that the embryos were released into the buffer. Embryos of a particular age were selected to synchronise the observed population, usually 2- or 4-cell embryos were chosen. Capillaries were drawn out to a diameter just wider than that of an embryo and the selected embryos were transferred to the centre of the agarose pad

along with a small amount of M9. A 22x22mm coverslip (thickness 1, BDH) was then lowered carefully on top using a scalpel blade. For preliminary timecourse observations which were carried out at a lower magnification, it was preferable to view groups of embryos at a time. To position embryos close together, 22x22mm coverslips (thickness 1, BDH) were subbed by immersing in 0.1% Poly-L-lysine for 5-10 mins and leaving to dry at room temperature. Embryos were transferred from the watchglass to the centre of the coverslip in a small amount of M9 and, once they had settled onto the surface, it was lowered carefully using a scalpel blade onto the microscope slide with the 5% agarose pad. To prevent the slides drying out, the edges of the coverslip were sealed with molten soft paraffin. White soft paraffin BP (Pinewood laboratories, Clonmel, Ireland) was melted in a 1.5ml eppindorf tube on a heating block (Grant instruments) at 80°C and loaded into a 1ml syringe with a $26G^{3}/_{8}$ microlance needle (Becton Dickinson S.A.). This allowed the soft paraffin to be precisely placed underneath the edges of the coverslip without any damage to the specimens.

2.8.4. Nomarski and Fluorescence optics used in microscopy of living embryos and larvae

The live embryos, larvae and adults were viewed using a Zeiss Axioplan microscope (Carl Zeiss, Oberkochem, FRG). Embryos were examined at 1000x magnification using the 100x/1.5 Zeiss Plan-Neofluar air objective. For embryos containing a reporter GFP transgene, the GFP fluorescence was viewed using a Tungsten halogen lamp (240V 500W, Osram) UV source and Zeiss filter set 09 (487909-0000). Larvae and adults were examined at 200x, 400x, and 1000x magnification, using the 20x/0.5, 40x/0.75, and 100x/1.5 Zeiss Plan-Neofluar air objectives respectively. For timecourse microscopy, embryos were viewed at 40x or 100x magnification using the objectives detailed above and photographed across a period of around 10 hours at hourly or half-hourly time points depending on the onset of the defect seen (estimated from preliminary low-resolution time course observations). Between time points, slides were kept in a humid box at 20°C. Images were taken with either a Panasonic wv-CL700 colour digital camera and Digitalvision 1.0.6 video capture software or a Hamamatsu C4742-95 (Hamamatsu photonics, Hamamatsu City, Japan) monochrome digital camera and Openlab 2.0.2 software.

2.9. Fluorescence microscopy of embryos and adults

Except where noted, all these protocols are variations on staining protocols obtained from J.Ahringer, and M.Labouesse (pers. comm.) and from Albertson (1984). Mutant embryos were stained with each antibody at least twice and always along with a wild type control slide. The DPY7-5a staining pattern was examined in over 50 wild type embryos, over 50 larvae of various stages and in over 20 adult specimens. When examining the DPY7-5a staining pattern in CB88, CB458 and MQ375 strains, I observed more than 30 embryos and over 30 larvae and adult stages.

2.9.1. Preparation of slides for fluorescence microscopy of embryos, larvae and adults

Slides used for fluorescence microscopy were first cleaned with 70% ethanol and subbed by immersing the slide in a 0.1% poly-L-lysine solution for 5-10 mins and then allowing the slide to dry at room temperature. Embryos, larvae or adults were washed separately off agar plates into eppindorf tubes using M9 buffer and pelleted at 5000rpm for 30 seconds in a Heraeus microfuge. Depending on the amount of bacteria washed off with the worms, they were washed and pelleted 1-3 times and then transferred to a watchglass. Capillaries drawn out to around 0.2-0.3mm for embryos and around 0.4-0.5mm for larvae or adults were used to transfer large numbers of embryos, larvae or adults onto the subbed slide. Large amounts of embryos were transferred in around 30µl of M9 and allowed to settle on the subbed surface of the slide. A 22x22mm coverslip (thickness 1, BDH) was lowered over the buffer using a scalpel blade and the excess M9 buffer was wicked off the edge of the coverslip under a dissecting microscope until the embryos were seen to be under a slight pressure but not rupturing (J. Ahringer, pers. comm.). Larvae and adults were transferred in around 10-20µl of M9 buffer and overlaid with a 64x22mm coverslip (thickness 1, BDH). Pressure was applied to the coverslip using forceps until the larvae or adults were slightly ruptured (otherwise they do not stick to the slides) and excess M9 buffer was again wicked off at the edge of the coverslip.

2.9.2. Permeablisation of embryos, larvae and adult specimens on slides

Immediately after preparing the embryos, larvae or adults under pressure on the slides they were snap frozen by placing on an aluminium block pre-cooled and maintained at -20°C on dry ice. After 5-10 mins, the coverslip was 'popped' off using a clean scalpel blade while the slides were still frozen.

2.9.3. Fixation of embryos and adults on slides

Freeze-cracked slides were immediately placed in coplin jars filled with methanol at -20°C and left at -20°C for 10 mins. The slides were then transferred to acetone at -20°C for 10 mins and rehydrated in 1xPBS.

2.9.4. Antibody staining protocol for embryos, larvae and adults fixed on slides

For all washing steps in the staining protocol, embryos were usually washed in coplin jars filled with 1xPBST while slides containing larvae or adults were washed by carefully pipetting 1xPBST onto the slide placed flat in a humid box and then removing it by tilting the slide gently onto a tissue. This is because embryos generally adhere to the slides strongly whereas larvae and adults tend to be loosened easily. The staining protocol is as follows:

i) Excess 1xPBS was removed from slides containing fixed and rehydrated specimens using a tissue and the slides were placed in humid boxes. Around 500µl of blocking solution was placed on the slides and they were left at 20°C for 20-30 mins.

ii) The blocking solution was removed by tilting the slides at an angle onto some tissue and primary antibody dilutions were prepared in fresh blocking solution. The dilutions differed slightly for each primary antibody used. Table 2i details the antibodies used with their localisation, and staining conditions. 100µl of antibody + blocking solution was placed on each slide in the humid box and the slides were placed at 4°C overnight.

iii) The antibody + blocking solution mix was removed by wicking it off the tilted slides using a tissue and the slides were washed 2x15 mins with 1xPBST.

iv) Excess PBST was removed using a tissue and secondary antibody dilutions were prepared in blocking solution. Fluorescent secondary antibodies were used at 1/100 dilution and around 100µl of antibody + blocking solution was placed on each slide. The slides were placed in an humid box at 37°C for 2-3 hours.

v) Again, the antibody + blocking solution mix was wicked off the slide and the slides were washed 2x15 mins with 1xPBST. This time, the washing receptacles were covered in foil to prevent exposure of the slides to light.

(vi) After washing, the slides were allowed to dry completely and around 5µl (for embryos) or 20µl (for larvae/adults) of mounting solution was placed on top of the specimens. A 22x22 (thickness 1, for embryos) or 64x22mm (thickness 1, for larvae/adults) coverslip was placed over the mounting solution and lowered very carefully with a scalpel blade to avoid the production of bubbles. The edges of the slide were sealed with clear nail polish and the slides stored in a covered box at 4°C.

2.9.5. Alternative protocol for permeabilsation, fixation and staining of adults in tubes

An alternative protocol to freeze-fracturing for larvae and adults, is the Finney and Ruvkun method (Finney and Ruvkun, 1990). This allows larvae and adults to be stained completely intact without rupturing on a slide. I used the modified Finney and Rufkun method (Miller and Shakes, 1995). Fixation was performed by incubating in 4% formaldehyde for an hour and incubation with 1% β-mercaptoethanol was carried out at 37°C for 1 hour. Antibody staining times were the same as indicated above.

Table 2i Monoclonal antibodies used in immunofluorescence microscopy

Antibody name	Antibody type	Localisation	Dilution used in staining	Secondary antibody used	Notes and References
3NB12	monoclonal	a subset of pharyngeal muscles from 6 hours of development	1/10 (ascites fluid)	goat-anti-mouse FITC	A gift from J.Hodgkin. (Okomoto and Thomson, 1985; Priess and Thomson, 1987)
DM5.6	monoclonal	myosin A within the central region of body wall muscle thick filaments	1/100	goat-anti-mouse FITC	A gift from M.Coutu. (Miller *et al.*., 1983)
DPY7-5a	monoclonal	DPY-7 collagen present within or secreted on the apical surface of hypodermal cells	1/50	goat-anti-mouse FITC	Produced by I.Johnstone
anti-LIN-26	polyclonal	LIN-26 nuclear protein present in all epithelial cells	1/100	goat-anti-rabbit FITC or TRITC	A Gift from M.Labouesse (Labouesse *et al.*, 1996)
MH3	monoclonal	UNC-52 in junctions between adjacent muscle cells, and between muscle cells and the hypodermis	1/50	goat-anti-mouse FITC	A gift from M.Coutu (Francis and Waterson, 1991)
MH4	monoclonal	intermediate filaments (components of the hemidesmosome) within the hypodermis	1/200	goat-anti-mouse FITC	A gift from M.Coutu (Francis and Waterson, 1991; Hresko *et al.*, 1994)
MH27	monoclonal	A component of adherens junctions between hypodermal cells and within the intestine	1/500	goat-anti-mouse FITC	A gift from R.Waterson (Francis and Waterson, 1991)

2.9.6. Fluorescence microscopy of stained specimens

Stained specimens were viewed 400x or 1000x magnification using a Zeiss Axioplan microscope and Zeiss Plan-Neofluar 40x/0.75 or 100x/1.5 air objectives. The UV source was a tungsten halogen lamp (240V 500W, Osram) and Zeiss filter sets 09 (487909-0000) or 15 (487915-9901) specific to green and red excitation/emission spectra specifically. Images were taken using either a Panasonic wv-CL700 colour digital camera with Digitalvision 1.0.6 software or Hamamatsu C4742-95 monochrome digital camera plus Openlab 2.0.2 software.

2.10. Expression of collagen::GFP transgenes in mutant strains

The *Aequorea victoria* green fluorescent protein (GFP) is a widely used fluorescent marker which is active in many prokaryotic and eukaryotic organisms (Chalfie *et al.*, 1994; Dopf and Horiagon, 1996). GFP can acquire fluorescent activity without exogenous substrates or cofactors and is therefore a valuable tool which can be used to monitor gene expression or protein localisation in living specimens. Gene fusions can be made by placing the gene under observation, or its promoter sequence, in frame upstream and in *cis* to the GFP primary sequence. These transgene fusions can be injected into worms using the methods described in section 2.14 and the pattern of fluorescence can be examined in the transgenic lines obtained. I examined the expression of cuticular collagen::GFP reporter transgenes in mutant embryos by either crossing the mutant chromosome into a strain carrying an integrated collagen::GFP transgene, or injecting the collagen::GFP construct directly into the mutant strain.

2.10.1. Crossing mutant strains with integrated lines carrying collagen::GFP transgenes

IA022 and IA105 are strains carrying integrated copies of the *col-12* promoter::GFP (IA022) or the *dpy-7* promoter::GFP reporter construct (IA105). Chromosomes carrying either *w4* or *ijDf2* were crossed into the collagen::GFP transgene integrated background and homozygous lethal mutants carrying the transgenes were examined for their expression patterns.

2.10.2. Injecting collagen::GFP transgenes into mutant strains

Because I could not cross the *ijDf1* carrying X chromosome into the integrated strains, I injected the pMW0003 plasmid into hermaphrodites heterozygous for *ijDf1*. pMW0003 was injected at 10ng/µl along with100ng/µl pRF4 (see section 2.14). *ijDf1* homozygote embryos from transgenic lines were examined for *col-12*::GFP expression.

2.11. Classical genetic mapping

2.11.1. Generation of males

Male worms (carrying only one X chromosome) occur spontaneously in the wild type population of *C.elegans* at a frequency of around 0.2% (Sulston and Hodgkin, 1988) but this frequency can be increased 10 fold or more by heat shock to produce males for mating. 6-10 L4 hermaphrodites were incubated at 30°C for 4-6 hours on a small NGM agar plate (5cm diameter) seeded with OP50 and then were left to self at 20°C. The progeny usually contains 2-5% males. To generate a male stock for mating, these males are mated with wild type hermaphrodites. Generally around 10-15 L4 males and 2-3 L4 hermaphrodites were placed on a 5cm plate containing NGM agar and an approximately 2cm diameter spread of OP50 in the centre of the agar at 20°C. These are the normal conditions for all crosses and unless noted otherwise, other crosses mentioned were carried out in this way. L4 males are transferred for crossing in all cases as the male mating apparatus is enclosed in cuticle until the adult stage and is therefore not damaged when transferring between plates. These plates were maintained at 15-20°C and F1s were almost 50% males depending on the success of the mating. L4 males from each subsequent generation were mated with wild type L4 hermaphrodites as before to maintain the male stock.

2.11.2. Setting up crosses to map mutations

Initial crosses were carried out between old adult hermaphrodites heterozygous for the lethal mutant allele and 10-15 wild type males, using the same conditions as the cross above. To obtain hermaphrodites heterozygous for the recessive lethal alleles

being mapped, individual animals from the strain carrying the lethal mutation were left to self fertilise on separate plates. As soon as the resulting embryos began to hatch, the parent hermaphrodites were transferred separately onto fresh plates which were marked in the same way as the original plates. After about 24 hours, the original plates were scored and the hermaphrodites transferred from that plate were used in crosses. Male F1s from the mutant/wild type cross were picked and used to cross the mutant allele into mapping strains. Where the mutant allele was found to be linked to the X chromosome, as in the case of *ijDf1*, subsequent crosses were carried out by crossing the mapping strain with wild type males, and crossing the F1 males produced with an hermaphrodite heterozygous for the mutant allele under study.

2.11.3. Using the results from mapping crosses to position mutant alleles

These mapping crosses rely on the generation and detection of recombinant animals in order to position the mutant alleles genetically in relation to other genes contained within the genome.

2.11.3.1. Chromosome assignment crosses

For the initial chromosome assignment cross, males heterozygous for the lethal alleles (not linked to the X chromosome) were crossed into the triply mutant strain, MT465 (*dpy-5 (e61)*I; *bli-2(e768)*II; *unc-32(e189)* III) and the F1 hermaphrodites were allowed to self. The progeny of hermaphrodites carrying the *w4* or *ijDf2* alleles were then examined for recombinants homozygous for only one of the visible marker mutations. These recombinants were then allowed to self on individual plates and their progeny were scored for the presence or absence of the lethal mutant allele. If the allele was unlinked to the marker mutation, then $^{2}/_{3}$ of the recombinants should be positive for the lethal mutation. This is because the homozygous *ijDf2* or *w4* progeny are dead therefore, of the living progeny, $^{2}/_{3}$ will be heterozygous for *ijDf2* or *w4* and $^{1}/_{3}$ should be homozygous for the wild type chromosome. If the lethal mutation was linked to the marker mutation, however, then the number of marker recombinants which carry the lethal mutation would be significantly reduced. I calculated whether the differences

were significant or non-significant using a χ^2 test with 1 degree of freedom (Parker, 1991).

2.11.3.2. Two-Factor crosses

In order to measure the genetic distance between two genes I used a formula which allows for the production of recombinant classes of progeny and also takes into account that certain classes of progeny may be subviable (Sulston and Hodgkin, 1988). Mutants that were heterozygous for the lethal allele and a marker allele present in *cis* on the same chromosome, were allowed to self on individual plates. If the two mutations are known as a and b, where a is the visible marker mutation and b is the lethal mutation to be mapped, and p is the recombination distance, then the gamete proportions will be as shown below:

ab	++	a+	b+
$\frac{1-p}{2}$	$\frac{1-p}{2}$	$\frac{p}{2}$	$\frac{p}{2}$

And subsequently, the proportion of each type of progeny produced will be as follows:

W(wild type)	A(marker phenotype)	B(lethal)	AB(lethal)
$\frac{3-2p+p^2}{4}$	$\frac{2p-p^2}{4}$	$\frac{2p-p^2}{4}$	$\frac{(1-p)^2}{4}$

This gives the equation :

$$\frac{(A+B)}{(W+A+B+AB)} = \frac{2p-p^2}{2}$$

where p is the total frequency of recombinant phenotypes. But where progeny classes B and AB are both lethal, they cannot be distinguished and are removed from the viable population so it is better to calculate p from the modified equation:

$$\frac{A}{(A+W)} = \frac{(2p-p^2)}{3}$$

I calculated p separately for each brood scored and then looked at the deviations of the means of each brood to see if the results could be pooled (Parker, 1991). In each case, the means were shown to be from within the same population and the results could be pooled.

2.11.3.3. Three-factor crosses

The main aim of three-factor crosses is to order the mutant allele with respect to two other known mutations. These crosses are less informative about the genetic map distance of the mutant allele from any particular gene. Males heterozygous for the lethal allele (*l*) under study (not linked to the X chromosome) were crossed into a strain homozygous for two visible marker mutations (*a* and *b*) on the same chromosome and the resulting F1 hermaphrodites heterozygous for all mutations with the lethal allele in *trans* to the marker mutations (*a + b/+ l +*), were allowed to self on individual plates. Recombinant F2 hermaphrodites homozygous for only one of the marker mutations (*a + b/ a ? + or a + b/ + ? b)* were picked separately onto plates and each was scored for presence or absence of the lethal allele. The proportion of these recombinants carrying or not carrying the lethal allele indicated the position of the lethal allele relative to the marker alleles and the genes were positioned in this way. For example, if 8 recombinants homozygous only for marker *a* carried the lethal allele *l* (*a + b/ a l +)* and 4 did not (*a + b/ a + +)*, and if 6 recombinants homozygous only for marker *b* carried the lethal (*a + b/ + l b)* and 12 did not (*a + b/ + + b)*, then the genes would be positioned thus:

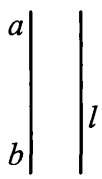

with *l* being between the two genes and lying approximately twice as close to *b* as it is to *a*.

2.11.4. Complementation tests

For complementation tests with the *ijDf2* allele, wild type males were first crossed into a strain (CB224) homozygous for *dpy-11(e224)*. The resulting F1 males were crossed with old adult hermaphrodites heterozygous for *ijDf2* and the progeny were examined for visible phenotypes.

For complementation tests with *ijDf1*, a different approach had to be taken. The *unc-3(e151)* allele on X was balanced by the duplication mnDp1 (strain SP219) and when wild type males were crossed into this strain, only F1 males appearing wild type (that is carrying the duplication) were picked to cross with old adult hermaphrodites heterozygous for *ijDf1*. Males hemizygous for *unc-3(e151)* without the balancing duplication were unable to mate. *lin-15(n309)* homozygotes, used in the complementation test, have the multivulva (Muv) phenotype and did not carry a balancing duplication but the *lin-15(n309)* allele is temperature sensitive and could be crossed at the permissive temperature of 15°C. At 25°C, wild type males cannot mate with *lin-15(n309)* hermaphrodites as none of their vulvas function normally and hemizygous *lin15(n309)* males have a significantly reduced mating efficiency. At the permissive temperature (15°C), however, mating can occur both between wild type males and *lin-15(n309)* hermaphrodites, and between *lin-15(n309)* hemizygote males and other hermaphrodites. *lin-15(n309)* hemizygote males and *ijDf1* heterozygote hermaphrodites were crossed at 15°C and after 1-2 days, the plates were moved to 25°C so that any visible phenotype would be seen in the F1 generation.

2.12. Sequence tagged sites (STS) mapping

STS mapping is a PCR-based mapping system which utilises known Tc1 insertions in the genome of the Bergerac strain, RW7000, as dominant markers to map a mutation (Williams *et al.*, 1992; Williams, 1995). The principle of STS mapping is outlined in section 5.3.2.

2.12.1. Preparation of custom made primers

Custom oligonucleotide primers for Polymerase Chain Reaction (PCR) in this section and elsewhere, were supplied ready to use by Genosys (Genosys Biotechnologies Europe Lts., Pampisford, Cambridgeshire, UK).

2.12.2. STS mapping protocol

I carried out STS mapping of the mutant alleles *ijDf1* and *ijDf2* using essentially the same protocol as Williams *et al.*, 1992, but with several changes. The differences in the mapping crosses due to *ijDf1* being present on the X chromosome are detailed in chapter 6.3.2.. I used a slightly modified PCR reaction mixture and slightly different PCR conditions. These are both detailed below:

STS PCR reaction mixture

Reagent	Final Concentration
10x*Taq* polymerase buffer (made up as in Williams *et al.*, 1992)	1x
dNTPs (Promega Corporation)	0.1mM
Tc1 primer 618 (Table 2ii)	125pM
Each STS specific primer used (Table 2ii)	25pM
Taq polymerase (NEB)	0.5U/25µl

The reactions were made up in a final volume of 25µl using sdiH_2O. Each reaction was overlaid with an approximately equal volume of mineral oil and the PCR was performed using a Crocodile III thermocycler (Appligene) using the following conditions:

Step	Cycles	Temp°C	Time(min)
1	1	94	3
2.1	38	94	0.5
2.2	38	58	1

Step	Cycles	Temp°C	Time(min)
2.3	38	72	1

STS-specific primers used for mapping *ijDf2* on chromosome V and *ijDf1* on the X chromosome are shown in Table 2ii. 10µl of each reaction was run on a 3% MetaPhor agarose (FMC corporation) gel as detailed in section 2.7.2.

2.13. Physical mapping of deficiencies using PCR

In order to physically map deficiencies, I designed primers specific to small regions of the genomic sequences within the cosmids tested and then used PCR to detect the presence or absence of these cosmid sequence markers (CSMs).

2.13.1. Design of cosmid sequence marker (CSM) primers

Primers were designed to amplify between 100 and 400bp of genomic sequence within each cosmid tested. I used Vector NTI to design primers specific to each cosmid genomic sequence and the sequences are listed in tables 2iii and 2iv

2.13.2. Preparation of embryos and PCR conditions for CSM assay

ijDf1 or *ijDf2* homozygote embryos and wild type controls were lysed in SWLB in the same way as in Williams *et al.*, 1992 with one exception: I lysed each embryo in 12.5µl of SWLB rather than 2.5µl so that I could use the DNA from one embryo to test several CSMs at one time, including positive and negative control markers. The PCR reaction mixture and conditions were the same as detailed above for STS mapping. Each CSM was tested using at least ten mutant embryos on at least two separate occasions and many more repetitions were carried out where there was ambiguity with the results obtained. For each CSM tested, I carried out a positive and negative control at the same time on the same mutant embryo DNA and on wild type embryo DNA.

Table2ii Primer sequences for STS assays

Primer	Polymorphism	Band size (bp)	Sequence (5′-3′)
618*			GAACACTGTGGTGAAG TTTC
Chromosome I			
734	hP4	130	CGGAAATATTATCAGC ACAGC
Chromosome II			
723	maP1	234	CCAATTTTCCGGAAGTT TTCG
Chromosome III			
587	mgP21	165	GGAACAAAAGTGCCTT GGG
Chromosome IV			
653	sP4	179	TTTCTGTTTTGTGCTTA GACG
Chromosome V			
813	stP3	153	GTCGCATTTCCATTCAT GCAG
440	stP192	290	GCACGCTGAGAGTAAG TGC
997	stP23	135	TTGTCAACTATTTTACA GCGAG
736	Bp1	119	AACACATTTAGGTAAT GTAGCAC
998	stP6	170	TCACAATCGATGACTA AGTACTGG
862	stP18	203	TTGAACTTCTCCCACTC CTC
438	stP108	135	AAAGATAAACGCGCTT TTTGG
439	stP105	152	GGGTAGTTGTTCATGTC TCG
652	stP128	200	GCAACGCTTTGTGGAT CTG
Chromosome X			
930	stP41	193	TGTCTACTTACCTTAAC TTACC
888	stP40	229	GTATGAGCTAATTGTA CCCTC
112	stP33	260	CGTCTAGTCGTGTGTTT CC
454	stP129	160	CCACTTATTGCCACTTT TTGG
452	stP72	112	CTTGAAAATACCATGG CATAC
887	stP2	127	CAAAACGGTATACTCT GGTG

*618 is a primer specific to Tc1 which is used in all reactions

Table 2iii CSM primers for physical mapping of Chromosome V deficiencies

CSM Primer name	Primer (Read 5′-3′)	Sense of primer	Position of 5′ and 3′ end bases of each primer in published cosmid sequence		Fragment size produced by each primer pair (bp)
			5′ end	3′ end	
C52A10-S	GCGGCGACCAGC AAAAC	sense	93	110	210
C52A10-A	TTCCCCACATCCC CAAC	antisense	303	286	
C35A11-S	TCATTCTTGTCCC GCCC	sense	3668	3685	280
C35A11-A	TGGTTGTGCTGGT CTCGC	antisense	3948	3930	
M03E7-S	TGTCGTCCTCCAC CACCG	sense	12435	12453	150
M03E7-A	ATGCTCCGCCAAA GTCG	antisense	12585	12568	
F29G9-S	TCCGTTGTCTTTTC ATTTCG	sense	6113	6133	153
F29G9-A	TCCTTCTACTCCC TTGTTTCTTC	antisense	6266	6243	
K08B12-S	ATTTGGCAGACCG AGCG	sense	19909	19926	129
K08B12-A	GGCGACGATTTCA CTGG	antisense	20037	20020	
W01A11-S	CGATGGTGGTTCC TTGTTCC	sense	24377	24397	333
W01A11-A	ATGATGTGAGATT TTATTCCCG	antisense	24710	24688	
K04A8-S	AGGAGCCGCACTT TTCTTCACAC	sense	720	743	208
K04A8-A	CGCGTATTTCGGA TTCATCACAGTC	antisense	928	903	
F44C4-S	GCGGTTTGATGGA GGATAGTGGAAG	sense	16180	16205	210
F44C4-A	CGGTGTTTTTGGC GAGAAGGTG	antisense	16390	16386	
W02F12-S	GACCAGATTCATA CTCAAACCACC	sense	4489	4513	220
W02F12-A	TCTTCTACCCCAA CATTTCTCC	antisense	4709	4687	
K11C4-S	TTGGTTTAGGGGT TAGAAGGG	sense	24833	24854	330
K11C4-A	TCATTTACTCAGC GGTGGAA	antisense	25163	25143	

Table 2iii CSM primers for physical mapping of Chromosome V deficiencies (continued)

CSM Primer name	Primer (read 5′ to 3′)	Sense of Primer	Position of 5′ and 3′ end bases of each primer in published cosmid sequence		Fragment size produced by each pair (bp)
			5′ end	3′ end	
F10G2-S	ATCCCAACCACCA ACGG	sense	132	149	333
F10G2-A	CCTGAGCCACCAA AGCC	antisense	465	448	
C12D5-S	ATCACTTCTCATT TCTATTCTCCCAT C	sense	6869	6896	217
C12D5-A	CCCATTCATCACC ATCACTCTG	antisense	7086	7064	
T05B11-S	GGTGCCCCATCAA AATCAG	sense	2897	2916	332
T05B11-A	TCAAACTTCCGCC AACAAC	antisense	3229	3210	

Table 2iv Cosmid primers for physical mapping of X Chromosome deficiencies

CSM Primers	Primer (Read 5′-3′)	Sense of primer	Position of 5′ and 3′ end bases of each primer in published cosmid sequence		Fragment size produced by each primer pair (bp)
			5′ end	3′ end	
K02B9-S	ATTACTGTAAGTT GAGCGCGGCTGA	sense	18118	18143	238
K02B9-A	TGACGGATGGCA GTATACTTCGAGG	antisense	18356	18331	
E02H4-S	TGATTCTCCGTGT AAGGAAGAGGCC	sense	21123	21148	208
E02H4-A	AACTGACGACCA CCCATAGAAACC G	antisense	21331	21306	
T14C1-S	AAACCCAACCAA TCGCC	sense	11570	11587	239
T14C1-A	GCAAATGAATAG CAGAACAACAAG	antisense	11809	11785	
T24C2-S	TGACCAGGTAGC GGAAAACG	sense	7758	7778	239
T24C2-A	GGTAGAGGGGGA AAGGAGTATTGTG	antisense	7997	7972	
F54E4-S	ACTCTTTATGTCT GTGTTGCCC	sense	16034	16056	194
F54E4-A	ACTGTATCCTTCG CTCCCC	antisense	16228	16209	
F42D1-S	CCCACAATCAGCT CACTCCAAGAAC	sense	14589	14614	299
F42D1-A	CGGAGGCAAGAA CGACATCATC	antisense	14888	14866	
C18B12-S	TGGACAACAAGC GATGAATAG	sense	3852	3873	293
C18B12-A	AGAAACGACGAC AGGAGGG	antisense	4145	4126	
T10B10-S	AAAACACCCAGG CAGCAACAGGT	sense	708	731	155
T10B10-A	GGTTATCGAGCGC TTTGTGGTCAAC	antisense	863	838	
F39D8-S	GTAGGAAATAAT GGTGATAGCGATG	sense	16414	16439	161
F39D8-A	AACTGTAGGGGTA ATGATAACGAC	antisense	16575	16551	
ZK662-S	CGAGAAGAGTTC AACTACCGAGTGC	sense	22113	22138	235
ZK662-A	CACTTTGATGGGA AGATTTCTGAAA	antisense	22323	22298	

Table 2iv Cosmid primers for physical mapping of X Chromosome deficiencies (continued)

CSM Primers	Primer (Read 5′-3′)	Sense of primer	Position of 5′ and 3′ end bases of each primer in published cosmid sequence		Fragment size produced by each primer pair (bp)
			5′ end	3′ end	
ZK678-S	ATGCAATGCTTGC AAACTGTTTT	sense	15741	15764	218
ZK678-A	TCAAATCATAAAT TCGATCGGAAGT	antisense	15959	15934	
E03G2-S	TCTCCAGGGATTC CGTCCTC	sense	4754	4774	305
E03G2-A	GGCCAACGTCAA CTTCTATGCC	antisense	4996	4974	
F09C8-S	TCTAATGTCTTGT CACCTCCGGC	sense	27271	27295	227
F09C8-A	TCTTCTGGCGGCT TGGTAGTT	antisense	27498	27477	
F52E10-S	CTTGAATGATGTC GTGC	sense	10958	10975	181
F52E10-A	TTTCGCAAGCTCA TCTG	antisense	11139	11122	
C11G6-S	ACATTGACTCTGC TCCG	sense	14120	14137	166
C11G6-A	ATCAGCGGCAAC AGATG	antisense	14224	14207	
F01G12-S	GTCGGTGGACTTG ACGCAAACTTG	sense	21123	21148	208
F01G12-A	TGGCTTACCACCA TCGACAATGACT	antisense	21331	21306	

2.13.3. Visualisation of PCR results

10µl of each PCR reaction was loaded onto a 2% agarose gel and run according to the conditions detailed in section 2.7.2.

2.14. Generation of transgenic *C.elegans* lines

2.14.1. Preparation of materials and worms for microinjection

Cosmid and plasmid DNA for microinjection was extracted and purified using the Qiagen Plasmid Mini or Midi DNA kits (Qiagen Inc.) and was resuspended in TE. In some cases additional organic extraction and ethanol precipitation steps were carried out if the DNA was suspected of containing impurities. One or both of two marker plasmids were used in cosmid rescue injections, pRF4 which carries the dominant *rol-6(su1006)* mutation, and pMW0002 which carries a *dpy-7* promoter::GFP transgene fusion. The *rol-6(su1006)* mutation causes animals that carry the pRF4 plasmid to have a helically twisted cuticle and body resulting in rolling about the longitudinal axis and movement in circles which is easily detected using a dissecting microscope (Mello *et al.*, 1991). Animals carrying the pMW0002 plasmid express the *dpy-7* promoter::GFP transgene fusion in hypodermal cells from the comma stage of elongation and so its presence could be detected by observations using a tungsten halogen lamp (240V 500W, Osram) UV source and Zeiss filter set 09 (487909-0000). The pRF4 marker plasmid was diluted to a final concentration of 100ng/µl in sterile deionized water and the pMW0002 *dpy-7* promoter::GFP marker transgene was diluted to 5ng/µl where used. Concentrations of cosmids and plasmids used in rescue experiments of *w4* and *ijDf1* are shown in Tables 2v and 2vi. pTAg (Novagen, Inc.) is a vector containing both ampicillin and kanamycin resistance providing areas of homology to cosmids carrying ampicillin or kanamycin resistance.

Needles for microinjection were prepared from Borosilicate glass capillaries (Clark Electromedical Instruments, Pangbourne, Reading, UK) which possessed glass filaments along their internal length to aid loading of the injection solution to the tip of the needle. Needles were pulled to the desired shape using a model 773 electrode puller (Campden Instruments Ltd., Sileby, Loughborough, UK). Immediately before use, the

Table 2v Concentration of cosmids and plasmids used in the 9 cosmid mix to attempt cosmid rescue of *w4*.

Cosmid or plasmid name	Antibiotic resistance marker	Stock concentration of cosmid DNA (μg/μl)[§]	Final concentration of DNA in mix (ng/μl)
W02B9	Kan	0.349	23
F36D1	Kan	0.986	66
F56G4	Kan	0.483	32
T02A8	Kan	0.082	5
W06H12	Kan	0.033	2
F46A8	Kan	0.090	6
AA2	Amp	0.205	14
F28D9*	Kan	0.100	7
C27D12*	Amp	0.100	7
pTAg	Amp and Kan	500	50
pRF4	Amp	400	100

[§] These concentrations were OD readings from a Beckman DU 650 Spectrophotometer which appears to be inaccurate at low concentrations. Because of this, the cosmid stocks were diluted so that 1μl of each stock run out on a gel gave an approximately equivalent band concentration.

* These cosmids concentrations were estimated only from gels.

injection solution was centrifuged at 15,000rpm for 5-10 mins in a microcentrifuge (Heraeus Equipment Ltd.) and loaded into hand pulled borosilicate capillary tubes (Clark Electromedical Instruments) by drawing the injection solution up using a mouth pipettor. The DNA was then loaded into the needles by inserting the hand pulled capillary tube down the wide bore of the needle and depositing the injection solution just behind the needle tip, using gentle pressure with a mouth pipettor.

Worms to be injected were immobilised on dried agarose pads under paraffin oil essentially as described by Fire (1986). The dried agarose pads were prepared on 64mm x 22mm glass coverslips (Thickness 1, BDH), by placing a single drop of a 3% agarose solution onto the coverslip, placing a 22mm x 22mm glass coverslip (Thickness 1, BDH) on the drop and applying gentle pressure. The smaller coverslip was removed and the agarose plug dried by baking at 80°C for 10min.

Young adult *C.elegans* hermaphrodite worms heterozygous for *w4* or *ijDf1* (Table 2vii) were transferred to a partially desiccated NGM agar plate prior to injection. When the injection apparatus was ready, a sharpened platinum wire pick was used to transfer 5-12 of these worms to a dried agarose plug, overlaid with 2-3 drops of paraffin. The picked worms were allowed to touch the dried agarose plug and the pick was gently removed once a portion of the worm had adhered to the surface of the dried agarose. The immobilised worms were placed on the microscope stage and the injection procedure started immediately.

2.14.2. Microinjection procedure

The microinjection procedure and apparatus are essentially the same as that described by Mello *et al.*, 1991. Needles containing the injection solution were loaded into the microtool collar of a Narishige MO-202 Joystick Hydraulic Micromanipulator (Narishige Co Ltd., Tokyo 157, Japan) and were pressurised using an attached bottled nitrogen source. A pressure regulator and solenoid valve attached to the nitrogen cylinder were used to obtain the desired rate of flow of the injection solution. Pressure was activated by means of a foot operated switch linked to the solenoid valve.

Table 2vi Concentration of cosmids and plasmids used in the cosmid rescue of *ijDf1*.

Cosmid or plasmid name/group	Antibiotic resistance marker	Final concentration of DNA in mix (ng/µl)
pRF4 (in all mixes)	Amp	100
pMW0002 (in all mixes)	Amp	5
15 cosmid mix [1]	all Amp, Kan or Chlor	5 (each cosmid)
6 cosmid group L[2]	all Amp, Kan or Chlor	5 (each cosmid)
6 cosmid group L[3]	all Amp, Kan or Chlor	5 (each cosmid)
F29D12	Kan	10
H08J19	Chlor	10
K09E9	Kan	10/5 [4]
K09A9	Kan	10/5 [4]
C02C6	Amp	10
ZK678	Kan	10
5 cosmid group [5]	all Amp, Kan or Chlor	5 (each cosmid)
K09A9 + K09E9	Kan	5 (each cosmid)
K09A9 + C02C6	Kan, Amp	5 (each cosmid)
K09E9 + C02C6	Kan, Amp	5 (each cosmid)
pKA1,pKA2, C02C6	Amp	1 (each plasmid), 5 (C02C6)
pKEO and C02C6	Kan, Amp	5 (each cosmid)
pKENO and C02C6	Kan, Amp	5 (each cosmid)

[1] The 15 cosmids injected in this mix were, from left to right: C11G10, T10B10, F46F2, C02D4, C33A11, F47C8, F39D8, R03A10, F59D12, H08J19, K09E9, K09A9, C02C6, ZK662, ZK678.

[2] The cosmids in the 6L mix were, from left to right: C33A11, F47C8, F39D8, R03A10, F59D12, H08J19.

[3] The cosmids in the 6R mix were, from left to right: F59D12, H08J19, K09E9, K09A9, C02C6, ZK678.

[4] K09A9 and K09E9 were both injected singly at 5 and 10 ng/µl

[5] The cosmids in the 5 cosmid mix were :F59D12, H08J19, K09E9, C02C6, ZK678.

Table 2vii Genotype of worms used in cosmid rescue injections

Lethal allele under study	Genotype of injected worms	ts alleles present
w4	*spe-9(hc88)/w4,unc-75(e950)*	*spe-9(hc88)* is ts. Strain maintained at 25°C
ijDf1	*ijDf1/unc-84* or *ijDf1/+*	*unc-84* is ts. Strain maintained at 25°C *ijDf1/+* strain maintained at 20°C

Each large coverslip, carrying worms immobilised on the agarose plugs, was taped to the free sliding oil cushioned stage of a Zeiss Axiovert 100 inverted microscope fitted with Nomarski optics. Microinjections were performed at 400x magnification using a Zeiss Achroplan 40x air objective lens. Pressure was applied to the needle containing the injection solution using the foot operated switch. The micromanipulator was used to open the sealed needle by repeatedly touching the tip of the needle onto a piece of capillary tube placed on the agarose plug until a suitably high flow rate was observed, indicating that the needle possessed a sufficiently large bore to reduce blocking. Injections were performed by first focusing on the grainy cytoplasm in the centre of the distal gonad. The needle was then brought into the same focal plane and the microscope stage moved by hand to push the worm into the needle tip. Once the needle was touching the surface of the worm, the microscope stage was tapped and this usually resulted in the needle penetrating the cuticle and gonad. Nitrogen pressure was then applied to force the injection solution into the gonad immediately after penetration. The needle was rapidly withdrawn from the worm without reducing the nitrogen pressure, once the gonad had swollen visibly.

After injection, the worms were recovered by adding a drop of 1xM9 buffer onto the agarose pad, causing the worms to float off the pad. The injected worms were then collected from the drop using a platinum wire pick and approximately 10 worms seeded onto a fresh NGM agar plate supporting an *E.coli* OP50 food source, by floating the worms onto a drop of sterile 1xM9 buffer. The injected worms were incubated for 3-4 days at 20°C (or overnight at 20°C and 2 days at 25°C in cases where the injected hermaphrodites carried the lethal mutation, *w4* or *ijDf1*, balanced by a ts allele -see Table 2vii) until F1 progeny with the *rol-6* phenotype were observed.

2.14.3. Isolation of transgenic lines and examining for signs of cosmid rescue

F1 progeny from the injected worms which exhibited the *rol-6* phenotype, conferred by the pRF4 marker plasmid, were seeded to fresh NGM agar plates supporting an *E.coli* OP50 food source (3 worms/plate). These plates were incubated for 3-4 days at 20°C (or 2 days at 25°C in cases where the injected hermaphrodites carried the lethal mutation, *w4* or *ijDf1*, balanced by a ts allele - see Table 2vii) until F2 progeny with the *rol-6* phenotype were observed. Around 10 F2 roller progeny were

picked from each F1 plate that transmitted the *rol-6* phenotype to the F2 progeny and these worms were seeded onto fresh NGM agar plates supporting an *E.coli* OP50 food source (1 worm/plate). This process generated at least 10 populations of worms derived from a single animal from each original plate of transmitting F1 progeny. Each of the populations generated from each F1 plate were scored for the presence of the lethal allele under study and these populations were examined for signs of rescue. For cosmid rescue of *w4*, signs of rescue were observed by scoring the progeny of the transformed lines and noting any changes in the percentages of Uncs seen that did not correspond to recombination between *w4* and *unc-75(e950).* The signs of rescue for the *ijDf1* deficiency, however, were more subtle. Because I was only adding back a small number of cosmids to a large deficiency which deletes several essential genes, the *ijDf1* homozygotes would still be arresting as embryos but, if rescued by a gene involved in elongation, the arrested embryos would have a noticeably longer end phenotype. The *dpy-7*::GFP transgene was co-injected to act as a marker in the arrested embryos so I could distinguish between transformed and untransformed embryos under UV light. *ijDf1* homozygote embryos from transmitting lines were examined at 1000X magnification using a Zeiss Axioplan microscope and Zeiss Plan-Neofluar 100x/1.5 air objective, with Tungsten halogen UV source (240V 500W, Osram). Images were taken using a Panasonic wv-CL700 colour digital camera and the Digitalvision 1.0.6 program.

2.15. Diagnostic restriction digests of injected cosmids

The usual method of testing that cosmids are intact before injecting is to prepare DNA from at least 2 separate colonies containing the cosmid using a Qiagen plasmid Mini kit (Qiagen Inc.) and compare the restriction patterns of a common restriction endonuclease, for example *EcoR*I. However, when I began looking at the digest fingerprint in detail for cloning purposes, I realised that many of these cosmids were deleted significantly and in order to be certain that an intact cosmid was being injected, it appeared to be necessary to examine the digests in detail. Before the restriction endonuclease digests of each injected cosmids could be analysed properly, I had to determine what cosmid backbone was present and the full genomic sequence contained within the cosmid. A. Coulson *et al.*, 1995 lists the cosmid backbones for all cosmids used and the full genomic sequence was determined from details within the separate

published sequences. I used Vector NTI version 4.0 to construct the entire cosmid backbone plus contained genomic sequence and thus calculate what fragments any diagnostic digest should yield.

2.16. Subcloning of Cosmids involved in phenotype rescue of *ijDf1*

2.16.1. Restriction digests of Cosmids

The complete genomic plus cosmid backbone sequence was determined for each cosmid as in section 2.15 and the restriction endonuclease enzymes required to cleave fragments of the correct size were selected. Digests were carried out as in section 2.7.1.

2.16.1.1. Fragments containing gene clones and vector digests

In order to isolate the fragment containing the predicted gene K09A9.1, cosmid K09A9 (accession number Z79601) was digested with *Pvu*II and *Kpn*I. These digests were carried out sequentially as in section 2.7.1 and a sample was taken at the end of the initial digest to ensure that the DNA was cut completely. The digest reaction was run out on a 0.7% agarose gel (see section 2.7.2) and a 4701bp fragment, corresponding to the sequence between positions 36409bp and 41113bp in the complete genomic sequence contained within K09A9, was excised and purified as in section 2.7.3. K09A9.1 is predicted to run from 37183bp (ATG)-40467bp (TAA) in the complete genomic sequence within the K09A9 cosmid and so the excised fragment also contained 774bp of upstream flanking sequence and 646bp of downstream flanking sequence from the predicted gene. Since there are two *Pvu*II sites within the pBluescript pSK- plasmid used to clone the gene, both outwith the polylinker, another blunt cutting restriction endonuclease, *EcoR*V, was used along with *Kpn*I to cut this vector. The digest was run on an agarose gel and the correct fragment gel purified as before.

A fragment containing the predicted gene K09A9.2 was isolated from cosmid K09A9 by digesting with *Bam*HI and *Xho*I. The digest reaction was run out on a 0.7% agarose gel as before and a 4492bp fragment containing sequence between positions 33279bp and 37770bp of the complete genomic sequence within cosmid K09A9 was excised and purified. The predicted gene K09A9.2 runs complementary from 36864bp

(ATG) to 35531bp (TAG) and so the fragment containing K09A9.2 also has 906bp upstream flanking sequence and 2252bp downstream flanking sequence from the gene. The pBluescript SK- vector was also cleaved with *Xho*I and *Bam*HI within the polylinker. The digest was run out on an agarose gel, excised and gel purified as before.

2.16.1.2. Specific deletions of cosmids

I wanted to subclone the K09E9 cosmid (accession number: Z79602) so that I was only injecting the genomic overlap between K09A9 and K09E9, or the non-overlap genomic region. In order to do this I used restriction endonucleases to specifically delete the area of the genomic DNA I did not want and then re-ligated the rest of the cosmid sequence plus the backbone to produce a new smaller cosmid clone containing the genomic sequences of interest.

The pKEO cosmid subclone was produced by deleting the non-overlap sequences containing predicted genes and leaving the overlap sequence which contained predicted genes K09A9.1 and K09A9.2. In order to create this subclone, I digested cosmid K09E9 with *Avr*II, ran the digest reaction and gel purified the 15625bp fragment corresponding to the region containing the K09A9/K09E9 genomic overlap plus the LoristB cosmid backbone. This fragment comprised the 5551bp LoristB cosmid backbone, the genomic sequence from 1bp to the *Avr*II sites at 8312bp in the complete K09E9 genomic sequence, and the sequence from the *Avr*II site at 37447bp to the end (39209bp) of the K09E9 genomic sequence.

The pKENO cosmid was produced as a result of deleting the genomic sequence contained in the K09E9/K09A9 genomic overlap from cosmid K09E9 and re-ligating the linearised deleted cosmid so that only the non-overlap genomic sequence remained. The K09E9 cosmid was digested with *Pme*I and *Bam*HI endonucleases and the digest run out on an agarose gel as before. The 38246bp fragment containing the 5551bp LoristB cosmid backbone, genomic sequence from 1bp to the *BamHI* site at position 478bp in the complete K09E9 genomic sequence, and genomic sequence from the PmeI site at position 6992bp to the end (39209bp) of the complete K09E9 genomic sequence was gel purified as before. This fragment contained the cosmid backbone and the genomic sequence that was not shared between cosmids K09A9 and K09E9. Before I re-ligated this fragment, I used klenow DNA polymerase I (NEB) in the supplied

EcoPol buffer plus recommended amounts of dNTPs (Promega Corporation) to fill in the *Bam*HI 5′ overhang and then heat-inactivated the enzyme according to the manufacturer's instructions .

2.16.2. Ligation reactions for gene and cosmid deletion subcloning

Ligation reactions between genomic inserts and pBluescript vector DNA were carried out with molar ratios and conditions as section 2.7.4 (using around 20ng of both insert and vector). To ligate the pKENO fragment I cleaned up the klenow reaction using a Qiaquick PCR clean-up kit (Quiagen, Inc) to remove unused dNTPs and other impurities. This reaction was resuspended in around 8µl of deionized water, to which T4 ligase (NEB) and T4 ligase buffer (NEB) were added as in section 2.7.4.

2.16.3. Transformation of subcloned plasmid and cosmids

The ligations involving fragments containing predicted genes plus pBluescript SK- (Stratagene Ltd.) vectors were transformed using Novablue (Novagen, Inc.) supercompetent cells. Of the deleted cosmid self-ligations, pKEO was transformed using Novablue (Novagen, Inc.) supercompetent cells and pKENO was transformed using XL1-blue (Stratagene Ltd.) supercompetent cells. Transformations were carried out as in section 2.7.5.

2.16.4. Screening of Transformed colonies

2.16.4.1. Colony Lysis

Colony lysis is a method used to screen transformed *E.coli* colonies during the generation of subclones for genes K09A9.1 and K09A9.2. The same buffer and protocol was used in all cases and is outlined below:

<u>Colony lysis buffer</u>

2% Ficoll

1% SDS
0.2% Bromophenol Blue
in 1x TBE buffer

1) Isolated colonies from transformation plates were picked using a wooden tooth pick.
2) The pick was dipped into 30µl of lysis buffer in a 0.5ml eppindorf and left at room temperature for 15-20 min.
3) Samples were microfuged at 13,000rpm for 25 min
4) Samples were then placed at 4°C for at least 30 min to enable subsequent easy loading of an agarose gel
5) The sample supernatant was loaded onto a 1.2% agarose gel, being careful to avoid loading the loose pellet, and the gel was run at around 5V/cm

Colonies containing an insert ran more slowly than control colonies containing the vector only.

2.16.4.2. DNA preparation from colonies and diagnostic digests

DNA was prepared from transformed colonies using Quiagen plasmid Mini DNA preparation kits (Quiagen, Inc.). Blue-white selection was used to identify positive colonies where pBluescript SK- (Stratagene Ltd.) was used as a vector (see section 2.7.5). Diagnostic digests were performed on around 200ng of prepared DNA using suitable endonucleases for each subclone with conditions as 2.7.4.

2.17. RNA interference (RNAi)

RNAi information and general protocols were taken from the Fire lab website (http://elegans.swmed.edu/Worm-labs/Fire/) version 1.0, 1 February, 1998 (also Fire *et al.*, 1998; Tabara *et al.*, 1998). The protocol I used differed in many respects from the protocols outlined on the website so I will describe it in detail.

2.17.1. Generating the target DNA fragment using PCR

Primers were designed specific to each cloned or predicted gene used in the RNAi analysis. K09A9.1, K09A9.2, C02C6.2 and C02C6.3 are predicted genes from the published sequences of the *C.elegans* genomic DNA contained within cosmids K09A9 and C02C6, and C02C6.1 is *dyn-1* which has been cloned (Clark *et al.*, 1997). RNA prepared from genomic DNA inclusive of intron sequence is effective, as long as there is also an exon sequence present, and for most genes, any RNA segment of around 200-1000 nucleotides or more seems to be capable of inducing interference (Tabara *et al.*, 1998). Each of these primers also had either T3 or T7 sequences at their 5′end to enable RNA synthesis of the amplified fragment after PCR. Primer sequences, cloned and predicted genes, and intron/exon sequences amplified are shown in Table 2viii. Reagents and conditions used in PCR are shown below. Genomic fragments were amplified from K09A9 or C02C6 cosmid DNA which had been prepared using Quiagen Mini or Midi plasmid DNA preparation kits (Quiagen, Inc.).

PCR reaction mix

Reagents	Final concentrations
Taq Polymerase 10x buffer (NEB)	1x
Taq Polymerase (NEB)	1U/25µl
$MgCl_2$	2.5mM
dNTPs (Promega Corporation)	0.1mM
gene T3 oligo (Table 2viii)	4ng/µl
gene T7 oligo (Table 2viii)	4ng/µl
cosmid DNA	0.8ng/µl

The reactions were made up in a final volume of 25°C using sdiH_2O. Each reaction was overlaid with an approximately equal volume of mineral oil and the PCR was performed using a Crocodile III thermocycler (Appligene) with the following conditions:

Table 2viii Primers for the amplification of gene sequences for RNA synthesis

Primer Name	Sequence (5′-3′) T3 and T7 sequences in bold, Genomic sequence in regular text	Sense of Primer	Size of fragment amplified (bp) (Includes T3 and T7 sequences)	Position of 5′ End and 3′ End bases of genomic sequence in each primer with respect to predicted ATG Initiation codon		Total size of exon sequences contained within amplified fragment (bp)	Total size of intron sequences contained within amplified fragment (bp)
				5′End	3′End		
K09A9.1-T3	**AATTAACCCTCACTAAAG GGAGA**TGTTGGAAATAC	sense	1450	+1168	+1180	1126	278
K09A9.1-T7	**TAATACGACTCACTATAG GGAGA**AGGATATAAAAT	antisense		+2572	+2560		
K09A9.2-T3	**AATTAACCCTCACTAAAG GGAGA**ATGACGGCTGCT	antisense	1380	-1	+11	630	704
K09A9.2-T7	**TAATACGACTCACTATAG GGAGA**CTAGCAGTTGCA	sense		+1333	+1321		
C02C6.1-T3	**AATTAACCCTCACTAAAG GGAGA**TCATTCTTGCCG	sense	1477	+760	+772	1261	170
C02C6.1-T7	**TAATACGACTCACTATAG GGAGA**ATGTGGAAAGAA	antisense		+2191	+2179		
C02C6.2-T3	**AATTAACCCTCACTAAAG GGAGA**CTCGTGGTCGTC	sense	1026	+1244	+1256	863	117
C02C6.2-T7	**TAATACGACTCACTATAG GGAGA**CCAGGTTCGCA	antisense		+2224	+2212		
C02C6.3-T3	**AATTAACCCTCACTAAAG GGAGA**CAGCGTGCCAAT	antisense	1773	+1249	+1261	635	1092
C02C6.3-T7	**TAATACGACTCACTATAG GGAGA**TGCTACCCAGCA	sense		+2976	+2964		

Step	Cycles	Temp°C	Time(min)
1	1	94	4
2.1	35	52	0.5
2.2	35	72	3
2.3	35	94	1
3.1	1	52	4
3.2	1	72	5

The PCR reactions were run out on 0.7% agarose gels as in section 2.7.2 and target fragments were gel purified as in section 2.7.3.

2.17.2. T3 and T7 polymerisation

RiboMAX large scale RNA production systems (Promega Corporation) were used for T3 and T7 synthesis of single stranded RNA from around 1-2μg of the purified PCR fragments. The manufacturers protocol was followed except that I used 50μl reactions rather than 1000μl reactions and all the reagents were scaled accordingly. I also added 80U extra rNAsin ribonuclease inhibitor (Promega Corporation). After RNA synthesis, the DNA template was removed by DNase treatment. The RNA was cleaned by an organic extraction and isopropanol precipitation according to the RiboMAX protocol. All reagents and tips used were RNase free.

2.17.3. Annealing reaction

Equal amounts (around 25μg) of sense RNA and antisense RNA were incubated in 12μl of 1x injection buffer along with 40U rNAsin ribonuclease inhibitor (Promega Corporation) at 68°C for 10min and 37°C for 30min. The annealing was checked by running a sample from each reaction on a 0.7% agarose gel as in section 2.7.2. Clean tanks and RNase free TBE were used. The reactions were stored at -70°C until needed for microinjection

2.17.4. dsRNA microinjections

Injection mixes with double stranded (ds)RNA specific to different combinations of predicted genes were made as in Table 2ix. The injection procedure used was identical to that in section 2.14.2, with the same needles and equipment. Young adult wild type hermaphrodites were injected with each of the dsRNA mixes, except for mix 10 which was injected into hermaphrodites heterozygous for the *dyn-1*(null) allele, and were placed 10 to a 5cm plate (Griner) for 6-12 hours at 20°C to recover.

2.17.5. Examination of the phenotype produced by RNAi

Wild type worms that appeared healthy after the recovery period were plated out separately on 3.5cm plates (Griner) at 20°C and the plates were numbered. These hermaphrodites were transferred around every 12 hours to similarly numbered plates and around 14-20 hours after transfer, the original plates were examined. Any visible phenotype such as lethality (Let), dumpy (Dpy), uncoordinated (Unc) etc. was scored quantitatively and arrested embryos were viewed on agarose mounted slides using Nomarski optics were scored quantitatively also. The plates were all followed through to adulthood for any later death or visible markers which only became obvious at later stages.

2.18. Statistics

A number of statistical tests were used to determine whether the percentage death from hermaphrodites heterozygous for a mutation or deficiency could be attributed to homozygote death alone and to compare results from classical genetic mapping crosses with expected results for unlinked genes. An analysis of variance (ANOVA) test was carried out comparing the deaths in 33 broods from hermaphrodites heterozygous for *w4*, *ijDf1* and *ijDf2* (Appendices 4.1,5.1 and 6.1)(Parker, 1991). This gave an F value of 1.13 which was not significant at 2 numerator (k-1) and 66 [k(n-1)] denominator degrees of freedom for 3 (k) treatments and 33 (n) replicates for each treatment. This showed that there was no significant difference in the percentage of deaths for each mutation and suggested that the deaths were unlikely to be due to

Table 2ix Genes and dsRNA used in RNAi injections

Gene specific dsRNA	Abbreviations used in mixes	Concentration in all mixes except mixes 2 and 9 (ng/µl)	Concentration in mix 2 and 9 (ng/µl)	Mix	dsRNA present
K09A9.1	K1	315	32	1	all genes
K09A9.2	K2	307	31	2	all genes
C02C6.1 (*dyn-1*)	C1	285	29	3	K1,K2,C1
C02C6.2	C2	296	30	4	K1,K2,C2
C02C6.3	C3	292	29	5	K1,K2,C3
				6	K1,C1,C2, C3
				7	K2,C1,C2, C3
				8	C1
				9	C1
				10	K1,K2

anything other than homozygosity for the recessive lethal mutation. For each classical mapping cross, a χ^2 test was carried out with the appropriate degrees of freedom as detailed in Parker (1991) as in section 2.8.1.

2.19. Computer programs

All images were taken using either Digitalvision software version 1.0.6 © 1993-1994 Graphics unlimited, or Openlab 2.0.2 software © 1998 Improvision (Coventry, UK) for Macintosh computers. Primers and subclones were designed using Vector NTI software, version 4.0 © 1994-1996 InforMax Inc.. The ACeDB *C.elegans* was used for all *C.elegans* genetic and physical map computer analyses (Thierry-Mieg and Durbin, unpublished software). DNA sequence comparisons were done using the WU-blast 1.4 BLASTN search. WU-BLAST 1.4 is based on NCBI-BLAST version 1.4 (Gish and States, 1993; Altschul and Gish, 1996) . *C.elegans* clone sequences were obtained from EMBL or genbank sources using either <http://www.sanger.ac.uk/Projects/c_elegans/Genomic_Sequence.shtml> or <http://www .ncbi.nlm.nih.gov/Entrez/nucleotide.html>.

Chapter 3

Localisation of the cuticular collagen, DPY-7 in wild type and mutant animals using a novel monoclonal antibody, DPY7-5a

3.1. Introduction

3.1.1. Cuticular collagens of *C.elegans* and the structure of the cuticle throughout the life cycle

Caenorhabditis elegans is covered by a cuticle which acts as a barrier between the worm and the environment, and an exoskeleton which maintains and defines the shape of the nematode (Johnstone, 1994). The predominant constituents of this cuticle are the extensively crosslinked cuticular collagens which are synthesised and secreted by the underlying hypodermal cells (Singh and Sulston, 1978; Cox *et al.*, 1981a; Kramer, 1994a). Collagens are the most abundant and ubiquitous extracellular proteins of metazoans although nematode collagens are notably smaller than vertebrate collagens being around 30-40kDa compared to >150kDa in size (Adams, 1978; Kramer *et al.*, 1988; Johnstone, 1994). The structure of *C.elegans* cuticular collagens are most similar to the non-fibrillar FACIT collagens of vertebrates (Shaw and Olsen, 1991). The genome of *C.elegans* contains 170 collagen genes and most of these are thought to be cuticular collagens (Johnstone, 1994; The *C.elegans* sequencing consortium, 1998). It is clear therefore that in *C.elegans* many collagens must be assembled from the hypodermal cytoplasm into a complex macromolecular extracellular structure, the cuticle, and the mechanism by which this happens is not well understood.

C.elegans nematodes, in common with other nematodes, undergo 4 larval stages between hatching from the egg and becoming adults, named the L1-L4 stages (Singh and Sulston, 1978; Cox *et al.*, 1981c). During embryogenesis and at each of the transitions from one larval stage to the next, a new cuticle is synthesised in the hypodermal cells and secreted from them. In all stages after embryogenesis this new cuticle is secreted underneath the old one which is then sloughed off from the worm (Singh and Sulston, 1978). To allow for growth at each stage, it has been proposed that the hypodermal surface contracts during cuticle secretion forming a folded surface under the old cuticle so that a new cuticle can be synthesised beneath the old one but have a

larger surface area (Costa *et al.*, 1997). Under conditions of overcrowding or lack of food, L2 stage larvae moult into a specialised L3 stage called the dauer stage (Cassada and Russell, 1975). These longer, thinner larvae are specialised for withstanding harsh environments and they do not feed. They can survive for 8-16 weeks and only moult into an L4 larvae when better conditions are presented, such as the addition of food (Klass and Hirsh, 1976). Each of the larval and adult stages has a different cuticle structure adapted to its needs, for example, the dauer cuticle is thicker in proportion to its circumference and the adult cuticle allows it to grow considerably larger without an additional moult (Cox *et al.*, 1981c).

The cuticle is composed of several layers differing at every stage. The main layers characterised in the adult cuticle are the epicuticle, external cortical, internal cortical, medial and basal layers (Figure 3.1a)(Cox *et al.*, 1981a,c; Peixoto and Souza, 1992). The adult-specific medial layer is fluid-filled and contains filamentous struts which connect the cortical and basal layers (Figure 3.1a)(Kramer, 1997). The cuticles of L2-L4 larvae are all very similar and contain an epicuticle, external cortical, internal cortical, and basal layers (Cox et all, 1981c). L1 and dauer cuticles have a striated layer in place of the basal fibre layer of other stages (Cox *et al.*, 1981c). The localisation of collagens and other components of the cuticle is largely unknown. Exceptions are the SQT-3 collagen which is thought to localise to the basal layer, and the BLI-1 and BLI-2 collagens which are thought to be components of the medial layer struts in the adult cuticle (Priess and Hirsh, 1986; J.Kramer, pers.comm.). There are also insoluble components of the cuticle known as cuticlins which are localised to the cortical layer (Ristoratore *et al.*, 1994; Favre *et al.*, 1995). These proteins are discussed in more detail below.

The external cortical layer of the different cuticles secreted throughout the life cycle of *C.elegans* contain circumferentially orientated furrows, named annulae (Figure 3.1), which are coincident with the organisation of actin filaments in the underlying hypodermis during embryogenesis and at each moult (Cox *et al.*, 1981c; Costa *et al.*, 1997). These annulae are present on the dorsal and ventral cuticular surfaces but not at the lateral surfaces overlying the specialised hypodermal cells known as seam cells. This can be explained postembryonically by the fact that, at each moult, membrane associated actin fibres in the hypodermis align only in dorsal and ventral regions and in embryos the aligned actin filaments in the seam cells are never found on the apical

Figure 3.1

Structure of the cuticle in *C.elegans*

a Schematic diagram of the adult cuticle of *C.elegans* showing the different component layers. The outermost layer, the epicuticle, is not shown. The predominantly collagenous layers are the internal cortical, struts, and basal layers.

b Cross section of the adult worm showing the cuticle and underlying hypodermis. This shows the difference in the thickness of the hypodermis at different places. The thickest regions of the hypodermis are at the seam cells and the dorsal and ventral cords. In other regions the hypodermis is very thin. Hypodermal nuclei tend to lie in thick areas of the hypodermis.

(Johnstone, 1994)

a

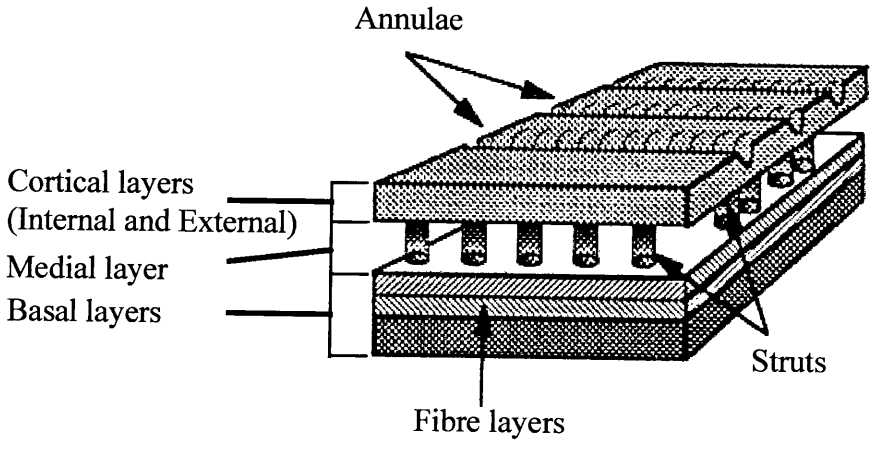
Annulae
Cortical layers
(Internal and External)
Medial layer
Basal layers
Struts
Fibre layers

b

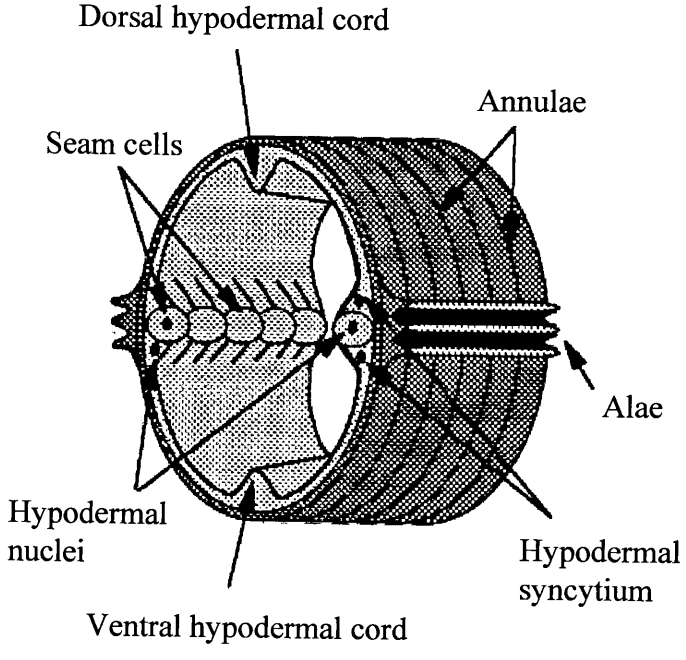
Dorsal hypodermal cord
Annulae
Seam cells
Alae
Hypodermal
nuclei
Hypodermal
syncytium
Ventral hypodermal cord

surface and so do not influence the patterning of the cuticle above in the same way as the dorsal and ventral hypodermis (Costa *et al.*, 1997). Seam cells are responsible for another structural aspect of the cuticle. In three different life cycle stages; L1, dauer and adult, there are additional surface cuticular structures, known as alae, which are thickenings of the cuticle running longitudinally along the lateral regions of the worm, above the seam cells (Figure 3.1b)(Singh and Sulston, 1978; Cox *et al.*, 1981c). These are produced by the seam cells at each of these specific stages and differ in their structure between each stage. They are apparently generated by circumferential contraction of the seam-specific cuticle after secretion at these stages (Singh and Sulston, 1978; Sulston *et al.*, 1983). *C.elegans* nematodes travel across substrates on their lateral surfaces and so the alae contact the substrate directly when they are present (Cox *et al.*, 1981a). As yet, none of the collagen genes are known to be alae-specific although the *col-7* collagen gene is expressed only in the lateral hypodermal cells (Liu *et al.*, 1995). However, there are two insoluble cuticle proteins, CUT-1 and CUT-2, which are present in high amounts within a 2μm-wide band underlying the alae of the dauer stage (Sebastiano *et al.*, 1991; Lassandro *et al.*, 1994). These proteins, known as cuticlins (Fujimoto and Kanaya, 1973), are present in very low amounts in the cortical layers of the cuticle in all stages but are not concentrated at the alae region in any stage other than dauer (Ristoratore *et al.*, 1994; Favre *et al.*, 1995).

3.1.2. Stage specific and temporal expression of cuticular collagens

It was originally thought, from radiolabelling studies, that the cuticular collagens in *C.elegans* were synthesised just prior to moulting between each developmental stage (Cox *et al.*, 1981b) but looking at the mRNA abundance of 6 different collagen genes this was found not to be the case (Johnstone and Barry, 1996). Instead, it was discovered that there are several different, temporally distinct, waves of collagen gene expression during each developmental stage (Johnstone and Barry, 1996). Some collagen genes, including *dpy-7*, are expressed at the start of the cycle four hours before the next cuticle is secreted. Others, including *dpy-13* and *col-1* are expressed two hours before the next cuticle is secreted while *col-12* and *col-14* are expressed coincident with the secretion of the new cuticle (Johnstone and Barry, 1996). This is thought to be a possible mechanism of restricting the number of collagens being translated and

processed at any time, to facilitate a more straightforward assembly into a multi-layered cuticle (Johnstone and Barry, 1996). Another interesting finding was that some collagen genes, *sqt-1* and *col-12*, were also expressed during the adult stage while others, *dpy-7*, *dpy-13*, *col-1* and *col-14*, were not. Adults of *C.elegans* increase significantly in length and circumference without moulting and this is also seen in nematodes such as *Ascaris* (Figure 3.2) (Watson, 1965). The mechanism of adult growth is not understood in *C.elegans* but it is possible that the synthesis of certain collagens at the adult stage relates to growth of the adult cuticle and also may indicate that only a restricted set of collagens are responsible for adult cuticle growth (Johnstone and Barry, 1996). There have been several studies examining collagen gene expression throughout development which have identified other stage-specific collagens. Certain collagens, *col-2* and *col-6*, are expressed only during the specialised L3 dauer larval stage and other collagens, *col-7* and *col-19*, are primarily adult specific (Cox and Hirsh, 1985; Kramer *et al.*, 1985).

3.1.3. Structural and sequence similarities among *C.elegans* cuticular collagens

Collagens are all rich in the amino acids: glycine, proline and the hydroxylated form of proline, hydroxyproline, and are characterised by blocks of Gly-X-Y amino acid repeats where X and Y can be any amino acid but are often proline and hydroxyproline respectively (Bornstein and Traub, 1979). Collagens typically form a triple helical structure (Ramachandran, 1967; Ramachandran and Ramakrishnan, 1976). Gly-X-Y repeats form a helix in the collagen monomer with the glycines being stacked on top of one another down one side of the helix. These helices then join with two other helices by hydrogen bond interaction so that the glycine residues all face into the centre of the newly formed triple helix (Figure 3.3b). Spatial constraints in the centre of the helix restrict the size of the side chains of amino acids present here while no such constraints are placed on the side chains of amino acids elsewhere in the helix. This results in the necessity of a glycine, which has a side chain of hydrogen, as every third residue to form the centre of the helix. Nematode collagens contain a number of cysteine residues at conserved positions which are thought to stabilise this triple helical structure, via disulphide bonding, and possibly maintain the correct positioning of different collagen chains (Cox *et al.*, 1981a; Johnstone, 1994; Kramer, 1994). Although the

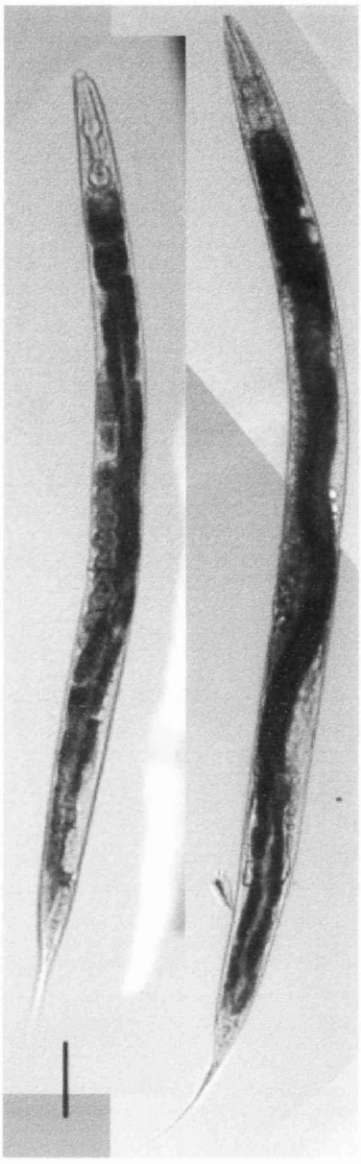

Figure 3.2

Young and old adult wild type hermaphrodites

Image showing the difference in size between a young, gravid hermaphrodite (left) and an old hermaphrodite past the reproductive age (right). The old adult is both broader and longer than the young adult. The anterior is to the top and the dorsal surface to the left of the image.

Scale bar is 0.1mm

Figure 3.3

The general structure of *C.elegans* cuticular collagens and the coiled structure of the collagen triple helix

a General structure of *C.elegans* cuticular collagens derived from the sequences of 38 collagen genes. The dashed lines indicate the regions that show the greatest length and sequence divergence among the collagens. The number of amino acids in different domains are indicated above the lines at the top of the figure. (Kramer, 1997).

b The coiled structure of the collagen triple helix. Three chains, labelled 1,2 and 3 are indicated. Size constraints of amino acid side chains in the core of the triple helix (R1 and R4) dictate that every third residue of the collagen chains (C1 and C4) must be glycine. There are no size constraints on the side chains (R2 and R3) of the other residues in the Gly-X-Y repeats and they are usually proline and hydroxyproline(C2 and C3).
(Johnstone, 1994).

a

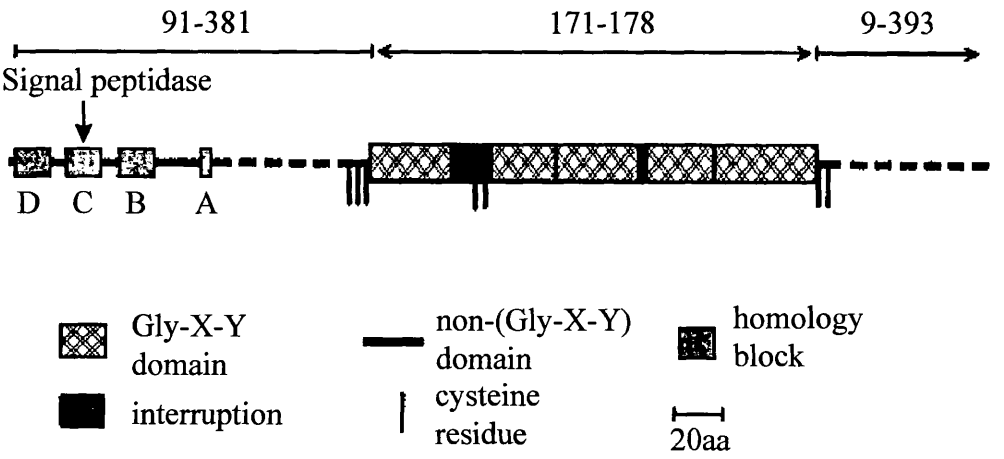
91-381
171-178
9-393
Signal peptidase
D C B A
Gly-X-Y domain
non-(Gly-X-Y) domain
homology block
interruption
cysteine residue
20aa

b

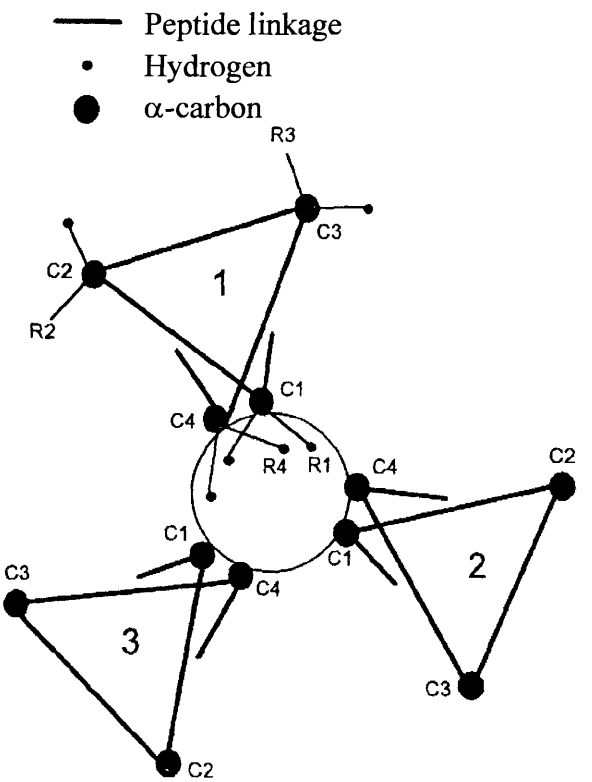
Peptide linkage
Hydrogen
α-carbon
R3
C3
C2
1
R2
C1
C4
R4
R1
C4
C2
C1
C1
C3
C4
2
3
C3
C2

overall structures of the cuticular collagens are very similar (Figure 3.3a), they differ in the organisation and lengths of the Gly-X-Y repeat blocks, the number and spacing of cysteine residues and the sequence of the non-repetitive amino- and carboxy-terminal domains (Cox *et al.*, 1989). The collagens fall into groups based on the differences between the Gly-X-Y blocks and the cysteine residues. Interestingly, there are some similarities between the groupings of collagens based on structure and those based on temporal expression. Two of the genes expressed mid-cycle, *dpy-13* and *col-1,* belong to the same structural group, as do the collagen genes expressed at the moult, *col-12, col-13* and *col-14* (Johnstone and Barry, 1996; J.Muriel, pers.comm.). There are also specific sequence homologies in the presumptive promoter regions of collagens expressed at the same stage in the life cycle. The dauer larva-specific genes, *col-2* and *col-6*, and the primarily adult-specific genes, *col-7* and *col-19*, show two distinct conserved sequences in the 5′ flanking sequence presumably involved in stage specific regulation (Cox *et al.*, 1989). However, genes within a particular structural group do not always share similar temporal or developmental patterns which suggests that structural and regulatory regions of these genes evolve separately.

In addition to the Gly-X-Y repeats and the conserved cysteine residues, there are also 4 blocks of homology in the amino-terminal domain (Figure 3.3a), one of which (HBA) contains two highly conserved arginines that are thought to function as a subtilisin-like proteinase cleavage site (Yang and Kramer, 1994). There is a *C.elegans* gene, *bli-4* which encodes a protein with strong similarity to the subtilisin family of endoproteases and certain mutations in this gene result in disruptions to the cuticle as described below (Peters *et al.*, 1991; Kramer, 1994a).

3.1.4. Mutations in *C.elegans* cuticular collagens and their affect on body shape

During embryogenesis in *C.elegans*, the embryo elongates from a ball of cells to a cylindrical worm shape more than four times longer and three times narrower (Sulston *et al.*, 1983). It is thought that contractions of actin microfilaments within the hypodermal cells drive the elongation process until the worm is fully elongated and at what is known as the 3-fold stage of development (Priess and Hirsh, 1986). Structural elements that can effect organism morphology are often found in the extracellular matrix. There is strong evidence that the extracellular cuticle of *C.elegans* plays a role

in maintaining the shape of the body from the end of embryogenic elongation onwards (Kusch and Edgar, 1986; Priess and Hirsh, 1986; Kramer *et al.*, 1988). Mutations in the *sqt-3* gene, which encodes a collagen, cause mutant embryos to initially elongate normally but then retract significantly in length as they cannot maintain the elongated shape (Priess and Hirsh, 1986; van der Keyl *et al.*, 1996). Also, many cuticular collagens have been shown to alter the postembryonic body shape drastically when mutated, resulting in phenotypes such as roller (*rol-6*, *sqt-1*: Cox *et al.*, 1980; Kramer *et al.*, 1988; Kramer *et al.*, 1990), dumpy (*dpy-7*, *dpy-13*: von Mende *et al.*, 1988; Johnstone *et al.*, 1992), and long (*sqt-1*: Kramer *et al.*, 1988). Roller mutants have a helically twisted cuticle and internal organs and move in circles, rotating about their longitudinal axes (Brenner, 1974; Higgins and Hirsh, 1977). Dumpys are short and fat, and the long mutants are abnormally long and thin (Brenner, 1974).

It has been suggested that the dumpy phenotype could arise from a cuticle that had greater inherent extensibility and would therefore become more spherical when subjected to the high internal hydrostatic pressure of the worm resulting in a short, fat animal (Kramer *et al.*, 1988). This may indicate that collagens which can be mutated to produce the dumpy phenotype have a function in maintaining the strength or relative rigidity of the cuticle. Conversely, the long phenotype could arise from a cuticle which had a more restricted radial extensibility resulting in a longer, narrower worm than normal (Kramer *et al.*, 1988). The roller phenotypes are interesting as mutations in different genes can result in either a right roller or left roller phenotype (Kusch and Edgar, 1986; Kramer *et al.*, 1988; Levy *et al.*, 1993; Park and Kramer, 1994). The basal layer of the *C.elegans* cuticle has two fibrous sublayers containing helically oriented fibres that spiral in opposite directions offset from the anterior-posterior axis by 65°C (Cox *et al.*, 1981a; Bergmann *et al.*, 1998). The outer fibre layer has a right-handed screw direction while the inner fibre layer has a left-handed screw direction. It has previously been proposed that the roller phenotypes were due to defects in these layers and that the handed-ness of the roller phenotype seen depended on which layer was disrupted. However, there is not a wide body of evidence for this view (Peixoto *et al.*, 1998). Certain *rol-6* mutants which exhibit the roller phenotype have unchanged orientations of the apparently normal fibre layers while other mutants seem to have clearly altered fibre orientations (Bergmann *et al.*, 1998; Peixoto *et al.*, 1998). Bergmann *et al.* (1998) have proposed a model in which the assembly of the first (outer)

fibre layer involves interactions of the fibres with each other and with other cuticle components while the assembly of the second (inner) fibre layer is affected by interactions with the overlying fibre layer. In this model, mutations which alter the first layer by interfering with the self assembly or interactions with other cuticle components would affect the orientation of both layers while mutations which alter the interaction between the two fibre layers should only change the orientation of the second layer. In this way, different mutations could be expected to produce either left or right roller phenotypes. There are also mutations in the collagen genes *bli-1* and *bli-2* which cause blistering of the adult cuticle due to the production of fluid-filled swellings (J.Kramer, pers.comm.). The blister phenotype is only seen in adult cuticles due to the stage specific fluid-filled medial layer (Cox *et al.*, 1981c). The dense columns or struts of material which traverse the fluid-filled medial layer connecting the outer layers, are absent or abnormal in *bli-1* and *bli-2* mutants causing the fluid to flow out into swellings on the surface of the cuticle (J.Kramer,pers.comm.).

Mutations in certain collagen genes, including *sqt-1*, *rol-6* and *dpy-10*, result in completely different phenotypes depending on whether the mutation in the gene is dominant or recessive (Kramer *et al.*, 1990; Kramer and Johnson, 1993). This suggests that the different types of mutation may produce mutant phenotypes for completely different reasons, for example, a recessive mutation may result in a phenotype due to the absence of the wild type collagen in the mutant cuticle while a dominant mutation could result in a phenotype caused by the presence of an aberrant collagen in the mutant cuticle. The different mutations also interact in unpredictable ways both intra- and intergenically. These observations are typical of genes encoding structural components which interact with each other forming complex multimeric structures (Kusch and Edgar, 1986; Kramer *et al.*, 1988).

3.1.4.1. Null mutations in *C.elegans* cuticular collagen genes

The effects of null mutations are the most easily interpreted for these genes and they appear to fall into two different classes. Null mutations in certain collagen genes, for example *sqt-1* and *rol-6* (Kramer *et al.*, 1988; Kramer and Johnson, 1993), show a very weak or apparently wild type phenotype while null mutants of other collagen genes, such as *dpy-7* (Figure 3.4c)(J.Ewbank, pers. comm.), *dpy-10* (Levy *et al.*, 1993)

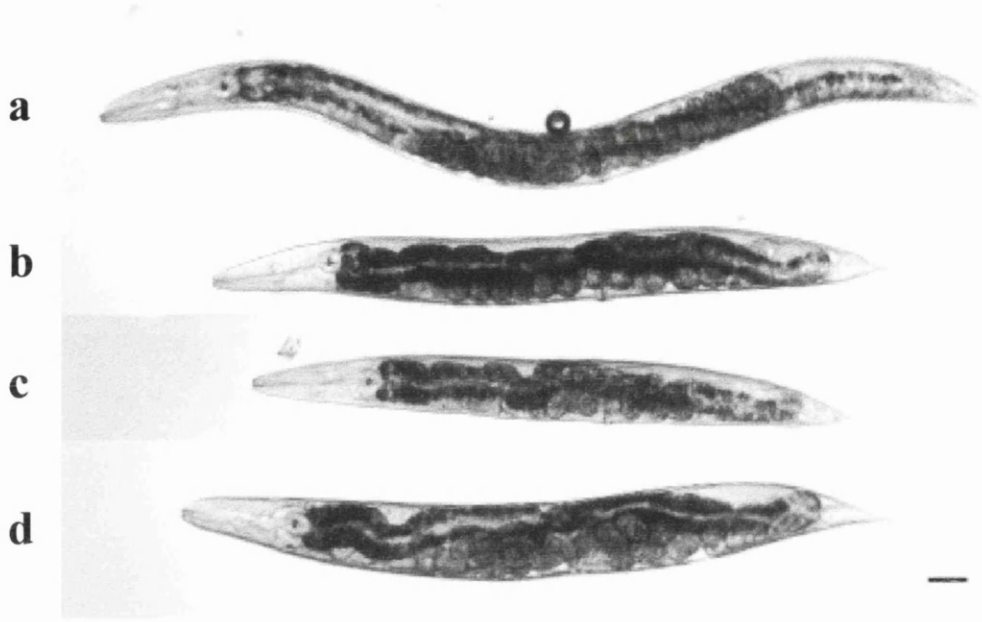

Figure 3.4

Size differences between egg-laying wild type and dumpy adult hermaphrodites

In all images, the anterior is to the left and the dorsal region to the top of the page

a	wild type hermaphrodite
b	homozygous *dpy-7(e88)* hermaphrodite
c	homozygous *dpy-7(qm63)* hermaphrodite
d	homozygous *dpy-13(e458)* hermaphrodite

Scale bar is 0.1mm

and *dpy-13* (Figure 3.4d)(Kramer, 1994a) can cause severe morphological defects. This indicates that the wild type copies of SQT-1 and ROL-6 may have partially overlapping functions or functions that are not easily detected by the observation of phenotypes under laboratory conditions, whereas the wild type DPY-7, DPY-10 and DPY-13 collagens are clearly required to achieve or maintain normal cuticle function.

3.1.4.2. Glycine substitutions in the Gly-X-Y repeats of cuticular collagens

Studies of mammalian fibrillar collagens have shown that mutations causing the substitution of glycine residues in Gly-X-Y repeats result in a dominant phenotype (Prockop *et al.*, 1989; Engel and Prockop, 1991). These dominant glycine substitution mutations cause the inhibition of triple helix assembly and, as a result, mutant and wild type collagen chains are subsequently degraded intracellularly. This is a common effect of glycine substitutions and as a result, a reduced amount of abnormal collagen is secreted into the matrix (Kramer, 1997). The dominant effects seen in these mutants could therefore either be due to a reduced amount of wild type collagen in the cuticle or the result of small amounts of mutant collagen incorporated into the closely packed fibrillar collagen matrix. In contrast, glycine substitutions in Gly-X-Y repeats of nematode cuticular collagens often result in recessive phenotypes similar to the null phenotype (Johnstone *et al.*, 1992; Levy *et al.*, 1993; Kramer, 1994a, J.Ewbank, pers.comm.). This suggests that the presence of mutant glycine substitution cuticular collagens does not prevent the production and secretion of wild type collagens, allowing the formation of an apparently normal cuticle. It also strongly suggests that the recessive nature of these mutations in cuticular collagen genes is due primarily to the absence of the wild type collagen in the secreted cuticle rather than the presence of any mutant collagen within it. In two cases, however, the recessive phenotype resulting from glycine substitutions in cuticular collagens differs from the null phenotype. Two *sqt-1* glycine replacement mutations, *sc107* and *sc99,* result in a weak long or weak left roller phenotype compared to a very weak abnormal tail phenotype or wild type phenotype for the null (Kramer *et al.*, 1988; Kramer and Johnson, 1993). Also, several recessive glycine substitution alleles of *dpy-10* result in a dumpy phenotype which differs from the null dumpy LRol phenotype (Levy *et al.*, 1993). These results suggest that the incorporation of a glycine replacement mutant collagen into the mutant cuticle

can contribute to the phenotype seen. An interesting effect is seen in *dpy-2* glycine substitutions as identical amino acid substitutions at sites in close proximity can result in different phenotypes (Levy *et al.*, 1993). For example, *dpy-2(e489)* which creates a Gly to Arg substitution at position 247 in *dpy-2* results in a temperature sensitive dumpy left roller (DpyLRol) phenotype whereas the same substitution at position 253 [*dpy-2(q292)*] results in a dumpy phenotype alone.

C.elegans glycine substitution collagens do not noticeably disrupt the cuticle in animals heterozygous for the mutation which indicates that either there is a mechanism which completely blocks secretion of these mutant collagens, or small amounts of the mutant collagen incorporated into the cuticle do not disrupt the normal function of this complex matrix. An explanation for the absence of glycine substitution collagens in the cuticle could be that mutant collagens do not trimerise normally due to the disruption of the triple helix caused by the missing glycine and as a result are degraded intracellularly, as happens with the vertebrate collagens discussed above (Johnstone *et al.*, 1992; Johnstone, 1994). However, due to the recessive nature of cuticular collagen glycine substitution mutations, any triple helix disruption among mutant collagens does not appear to prevent the trimerisation of wild type collagen chains and secretion of sufficient wild type collagen to produce a functioning cuticle.

3.1.4.3. Dominant mutations in the HBA domain of cuticular collagens

One set of typically dominant mutations in *C.elegans* cuticular collagens are point mutations resulting in the substitution of one of two highly conserved arginine residues at positions 1 and 4 in a block of homology at the amino-terminal domain known as HBA (Yang and Kramer, 1994; Kramer, 1994b). Dominant mutations have been discovered in the HBA domain of *sqt-1, rol-6* and *dpy-10* (Kramer and Johnson, 1993; Levy *et al.*, 1993). These were all found to be arginine to cysteine substitutions at one of the two conserved arginines and it was thought that the mutant collagens produced could form ectopic disulphide bonds because of the extra cysteine residues. However, transgenic analysis of *rol-6* and *sqt-1* genes mutagenised *in vitro* indicated that the substitution of other nonbasic amino acids for arginine at these conserved positions also produced a dominant effect (Yang and Kramer, 1994). The phenotypes produced by these synthetic mutations differ from the null phenotype in the type of

morphological abnormality produced and therefore seem to result from the incorporation of mutant collagen into the cuticle rather than, or in addition to, the absence of wild type collagen in the cuticle (Kramer, 1994a). It seems that even a small amount of mutant collagen is enough to disrupt the cuticle structure by being incorporated into it. An exception was seen where the arginine residues are replaced with another amino acid with a strong positive charge such as lysine as these mutant collagens produce a wild type phenotype (Yang and Kramer, 1994). In fact some wild type collagen genes that have been sequenced encode collagens with lysine at positions 1 or 4 rather than arginine (Kramer, 1994b; Yang and Kramer, 1994). An arginine to histidine replacement at the conserved Arg-4 site in *rol-6(e187)* results in a recessive phenotype which, together with the lysine data suggest that a strong basic residue is required at the conserved arginine positions (Yang and Kramer, 1994). A closely related motif to the HBA homology block functions as a cleavage site for subtilisin-like serine proteinases which are involved in endoproteolytic processing of proproteins and prohormones (Barr, 1991; Yang and Kramer, 1994). The HBA motif could therefore be the cleavage site for a subtilisin-like protease with cleavage required for normal functioning of the cuticle (Yang and Kramer, 1994). One explanation for the different severity of phenotypes seen could be that the substitution of arginine with a non-positively charged residue completely blocks cleavage at the HBA site while substitution with His, a weakly positively charged residue, only partially blocks cleavage (Yang and Kramer, 1994). It seems likely that the incorporation of incorrectly cleaved cuticle collagens could dominantly disrupt collagen function and lead to the phenotypes seen in *rol-6* and *sqt-1* arginine substitution mutants.

The *bli-4* gene of *C.elegans* has been shown to encode a subtililsin-like protease as mentioned above (Peters *et al.*, 1991; Yang and Kramer, 1994). Mutations in *bli-4* usually cause early larval lethality but one viable mutation causes incompletely penetrant blistering of the adult cuticle indicating a role for the wild type gene involved in cuticle function (Peters *et al.*, 1991). These two defects are independently mutable suggesting that *bli-4* plays more than one role during the life cycle of *C.elegans*. Unlike mutations in cuticular collagens which are structural components of the cuticle, the mutations of *bli-4* do not produce many different morphological phenotypes and are all recessive (Peters *et al.*, 1991). This points more to an enzymatic function of cuticle assembly or maintenance which agrees with the idea that *bli-4* may be involved in

cleaving collagens prior to their assembly into the cuticle (Kusch and Edgar, 1986; Yang and Kramer, 1994).

3.1.5. Background of DPY7-5a production and DPY-7 expression

DPY7-5a is a mouse monoclonal antibody which reacts against the carboxy terminal domain of DPY-7 (Figure 3.5) (I.Johnstone, pers.comm.). The target epitope is within the protein region shown in Figure 3.5b. Blastp searches using WU-Blast 1.4 suggest that the DPY-7 carboxy terminal is not similar to other *C.elegans* collagens and so the DPY7-5a antibody should specifically recognise DPY-7. Previous studies using GFP and *lacZ* reporter constructs have shown that *dpy-7* is expressed in hypodermal cells from the precomma stage of embryogenesis before elongation begins (Johnstone and Barry, 1996; Gilleard *et al.*, 1997). Also, mRNA studies using RT-PCR indicate that this is the first collagen expressed among those studied (Johnstone and Barry, 1996). The majority of animals expressing the *dpy-7*::GFP or *lacZ* reporter constructs, showed expression in all hypodermal cells except the lateral seam cells, although in around 20% of animals, much fainter expression was also seen in seam cells (Gilleard *et al.*, 1997). More recently, *dpy7*::GFP transgenes have been constructed in our laboratory that are expressed in the seam cells as brightly as in the dorsal and ventral hypodermis (E.Stewart, pers.comm.). Figure 3.6 shows the early onset of *dpy-7*::GFP transgene expression during embryogenesis.

3.2. Specificity of the DPY7-5a monoclonal antibody

The *dpy-7(qm63)* allele is a deletion of approximately 6.6kb which removes the *dpy-7* locus although it has not been accurately characterised (J.Ewbank, pers.comm.). The *dpy-7(qm63)* homozygotes are dumpy, as expected from the phenotype of the GLY-X-Y glycine substitution mutants (Figure 3.4c)(Johnstone *et al.*, 1992; Johnstone, 1994; Kramer, 1997). No staining was found at any embryonic or postembryonic stage in *dpy-7(qm63)* homozygotes indicating that the DPY7-5a antibody was indeed specific to the DPY-7 collagen (Figure 3.7). Control wild type slides were prepared and stained under

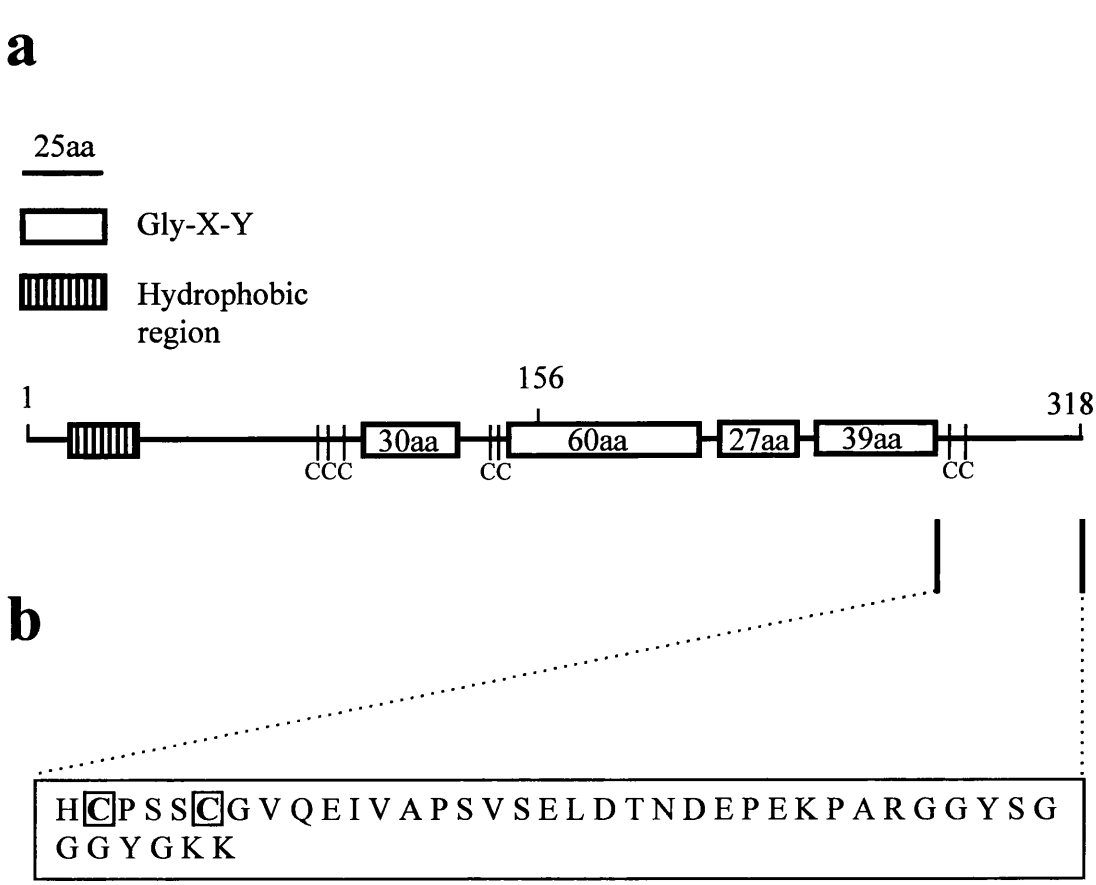

Figure 3.5

Schematic representation of the predicted DPY-7 protein and the amino acid sequence of the carboxy terminal domain

a Schematic diagram of the predicted DPY-7 protein. Numbers refer to amino acid residues. The *dpy-7(e88)* mutant allele has a residue substitution of glycine to arginine at position 156 which is indicated. Cysteine residues are indicated as vertical bars denoted by the letter C. The lengths of the Gly-X-Y repeat domains are indicated within the boxes.

b Amino acid sequence of the carboxy terminal domain of the predicted DPY-7 protein which contains the epitope recognised by the monoclonal antibody DPY7-5a. The conserved cysteine residues are indicated in boxes.

(Adapted from Johnstone *et al.*, 1992).

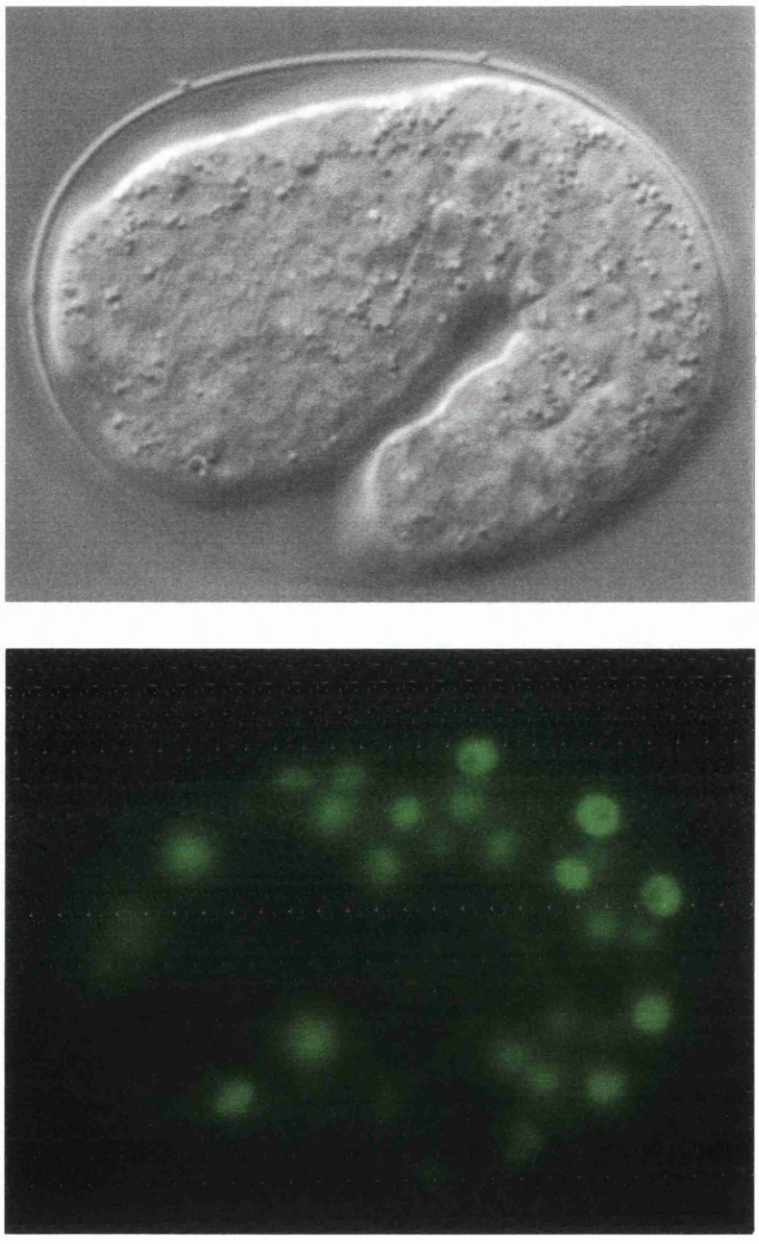

Figure 3.6

***dpy-7* promoter::GFP reporter gene expression in an embryo of strain IA105 which contains an integrated copy of a *dpy-7* promoter::GFP*lacZ* construct.**

The embryo is positioned with the anterior to the left and the dorsal surface to the top of the image. In this and in all subsequent images, embryos are approximately 50μm in length and 30μm wide.

a DIC image of a 1.5-fold IA105 embryo

b UV image of a 1.5-fold IA105 embryo showing expression of a *dpy-7*::GFP reporter gene construct long before the first cuticle is secreted.

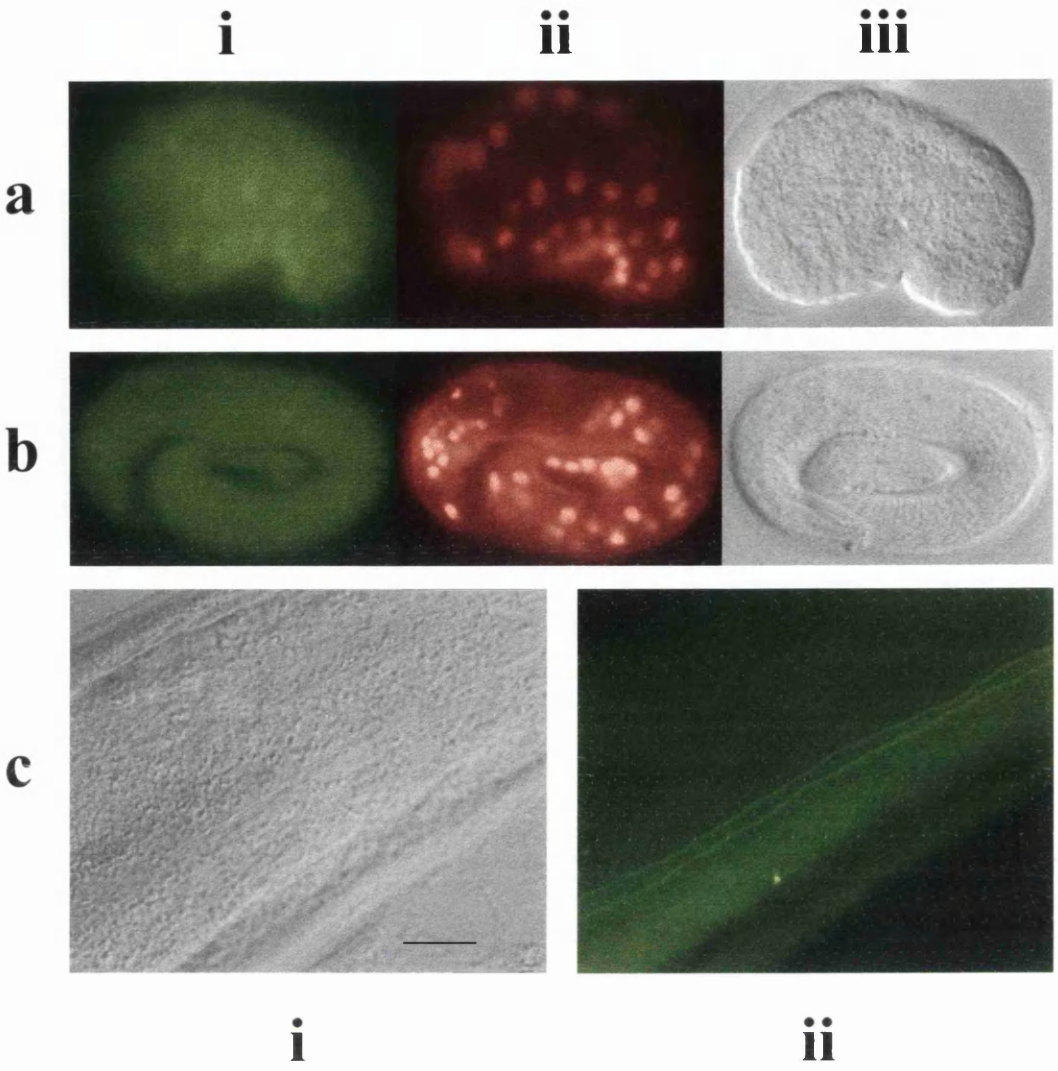

Figure 3.7

Illustration of the specificity of the DPY7-5a antibody

All embryos are orientated with the dorsal region to the top and the anterior to the left of the page.

a *dpy-7(qm63)* homozygous comma stage embryo

- **i** DPY7-5a staining (showing bleed-through of anti-LIN-26 staining).
- **ii** anti-LIN-26 staining
- **iii** DIC image

b *dpy-7(qm63)* homozygous 3-fold stage embryo

- **i** DPY7-5a staining
- **ii** anti-LIN-26 staining
- **iii** DIC image

c Section from a *dpy-7(qm63)* homozygous adult hermaphrodite

- **i** DIC image
- **ii** DPY7-5a and MH27 staining

The scale bar in **c** is 10μm and applies only to the images in **c**

the same conditions as the *dpy-7(qm63)* homozygote slides and usually the *dpy-7(qm63)* embryos and postembryonic stages were also co-stained with the anti-LIN-26 polyclonal antibody, which recognises the nuclear protein LIN-26 present in all epidermal cells in *C.elegans,* or the MH27 monoclonal antibody which recognises a component of epidermal adherens junctions, to ensure that they were completely permeabilised (Priess and Hirsh, 1986; Waterston, 1988; Labouesse *et al.*, 1996). The wild type DPY7-5a staining pattern in each case was as described below and for *dpy-7(qm63)* homozygotes that were co-stained with DPY7-5a and either anti-LIN-26 or MH27 respectively, the anti-LIN-26 or MH27 patterns were as wild type.

3.3. Spatial and temporal pattern of DPY7-5a during embryogenesis

The intracellular spatial and temporal localisation of DPY-7 was observed extensively during embryogenesis as this is the only stage of the life cycle where there is not a secreted cuticle to obscure the pattern of the collagen within the hypodermal cells. The timing of each embryonic stage, from precomma through to comma, 1.5-fold, 2-fold and 3-fold has been well documented and so the onset of antibody staining is easily estimated with respect to the stage of embryo elongation (Sulston *et al.*, 1983; Wood, 1988). Intracellular staining of DPY-7 was observed easily using the monoclonal antibody DPY7-5a and could be followed from before the initiation of elongation through to the secretion of cuticle at the end of embryogenesis.

3.3.1. Temporal occurrence of DPY-7 during embryogenesis

DPY7-5a staining was first observed at the early comma stage of embryogenesis at around 350 mins after first cleavage (Figure 3.8a) . The time was not measured absolutely but estimated by comparing the stage of embryogenesis with previously published results (Wood, 1988). The staining was quite faint at this time but grew more intense as the embryo developed (Figure 3.8b,c). Extracellular staining was first seen at the 3-fold stage of embryogenesis, around 650mins, and was clearly different from the fainter intracellular staining pattern (Figure 3.8d). Extracellular staining was observed in every postembryonic stage including the adult stage (results shown later) although this brighter staining of secreted DPY-7 obscured the intracellular staining and so the

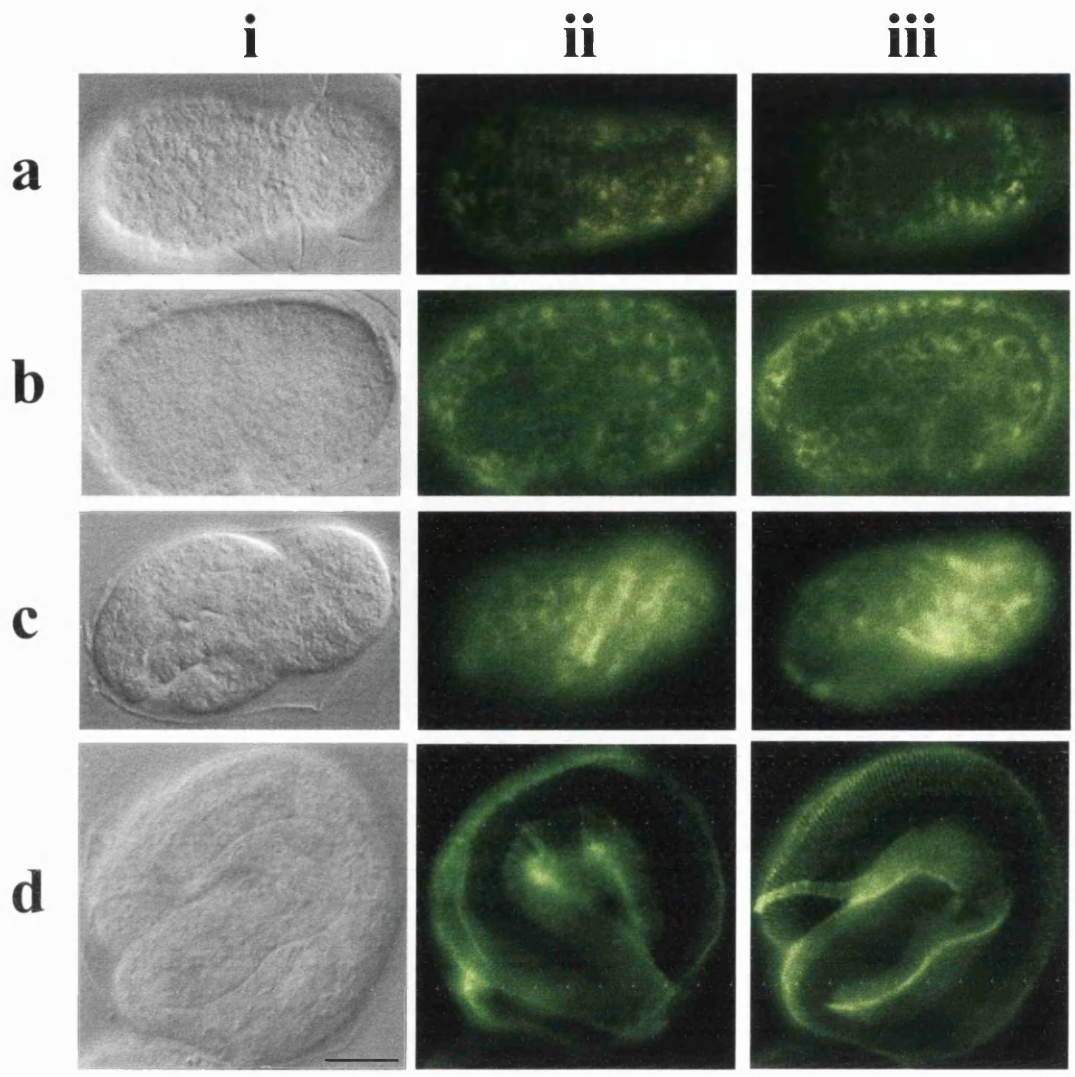

Figure 3.8

Localisation of DPY-7 in wild type embryos

DIC images are shown in column **i**

a precomma stage embryo (anterior to the left, lateral sides to top and bottom of the page)

ii Internal DPY7-5a staining of the dorsal region

iii Internal DPY7-5a staining of the ventral region

b 1.5-fold stage embryo (anterior to the left, dorsal region to the top of the page)

ii and **iii** Internal DPY7-5a staining on either side of the embryo

c 2.5-fold stage embryo (anterior to the left)

ii and **iii** Internal DPY7-5a staining of either side of the embryo

d 3-fold stage embryo (anterior facing the bottom right of the image)

ii and **iii)** External DPY7-5a staining on either side of the embryo

Scale bar in **d** is 10μm and only applies to the images in **d**.

timing of intracellular DPY7-5a staining was not followed after embryogenesis.

3.3.2. Spatial localisation of DPY-7 during embryogenesis

DPY7-5a staining was observed only in hypodermal cells. The monoclonal antibody, MH27, and the polyclonal antibody anti-LIN-26, were used to visualise the cell junctions or nuclei of hypodermal cells respectively. The easiest stage to see the staining clearly was the comma stage of development as the 3 rows of hypodermal cells are seen clearly on each side of the embryo. DPY7-5a staining is present in the cytoplasm of hypodermal cells and is brightest around the nucleus although it is absent within the nucleus. The anti-LIN-26 and DPY-7 co-staining is shown in Figure 3.9a for an embryo homozygous for the *dpy-7(e88)* point mutation (see section 3.5). There was no detectable difference in these staining patterns between *dpy-7(e88)* and wild type embryos (not shown). It was initially difficult to determine if there was staining in both hypodermal syncytia and seam cells as the nuclei of hypodermal cells which will form the hyp7 syncytia to the dorsal side and the P cells to the ventral side, lie very close to the borders of the seam cells (see Figure 3.1b). From further observations, however, it appears that there is DPY7-5a staining within the cytoplasm surrounding the nuclei of the seam cells as well as in the cells to either side. Co-staining with MH27 helped to clarify the matter (Figure 3.9b) although the majority of intracellular DPY7-5a staining is observed on a more internal focal plane than distinct MH27 staining and is only present faintly towards the apical surface of the hypodermis where MH27 lies. It appears therefore that the DPY-7 collagen is localised predominantly to a subapical position in the hypodermal cell. DPY7-5a staining appears to be present throughout the cytoplasm of mononucleate hypodermal cells and is brightest around the nucleus. In hypodermal syncytia such as hyp7, DPY7-5a staining is only apparent at regions where nuclei are present and there are two dark bands where staining is absent to each side of the dorsal midline (Figure 3.10). The DPY-7 protein may be translated near nuclei in thicker regions resulting in an absence of DPY7-5a staining where the hypodermis is thin (see Figure 3.1b).

The transition from internal to external staining is abrupt and occurs after the embryo has elongated to the 3-fold stage (Figure 3.8c-d). External DPY7-5a staining is much brighter than internal staining which is why it is so difficult to see intracellular

Figure 3.9

Localisation of DPY-7 within hypodermal cells of *dpy-7(e88)* and wild type embryos

Both embryos are positioned with the anterior to the left and the dorsal region to the top of the page. DIC images are shown in row **i**.

a Homozygous *dpy-7(e88)* 1.5-fold embryo showing DPY7-5a and anti-LIN-26 co-staining

ii Anti-LIN-26 staining which recognises the LIN-26 nuclear protein present in hypodermal and other epithelial cells.

iii DPY7-5a staining showing that DPY-7 localises to the cytoplasm around the nucleus of hypodermal cells.

b Wild type comma stage embryo showing DPY7-5a and MH27 co-staining

ii and **iii** DPY7-5a and MH27 co-staining of lateral sides of the embryo. Arrows point to either side of the row of seam cells which runs from right to left in each image. DPY7-5a staining can be seen within the row of seam cells at each side. The boundaries of the seam cells are stained by the MH27 antibody which recognises a protein in the adherens junctions of hypodermal cells.

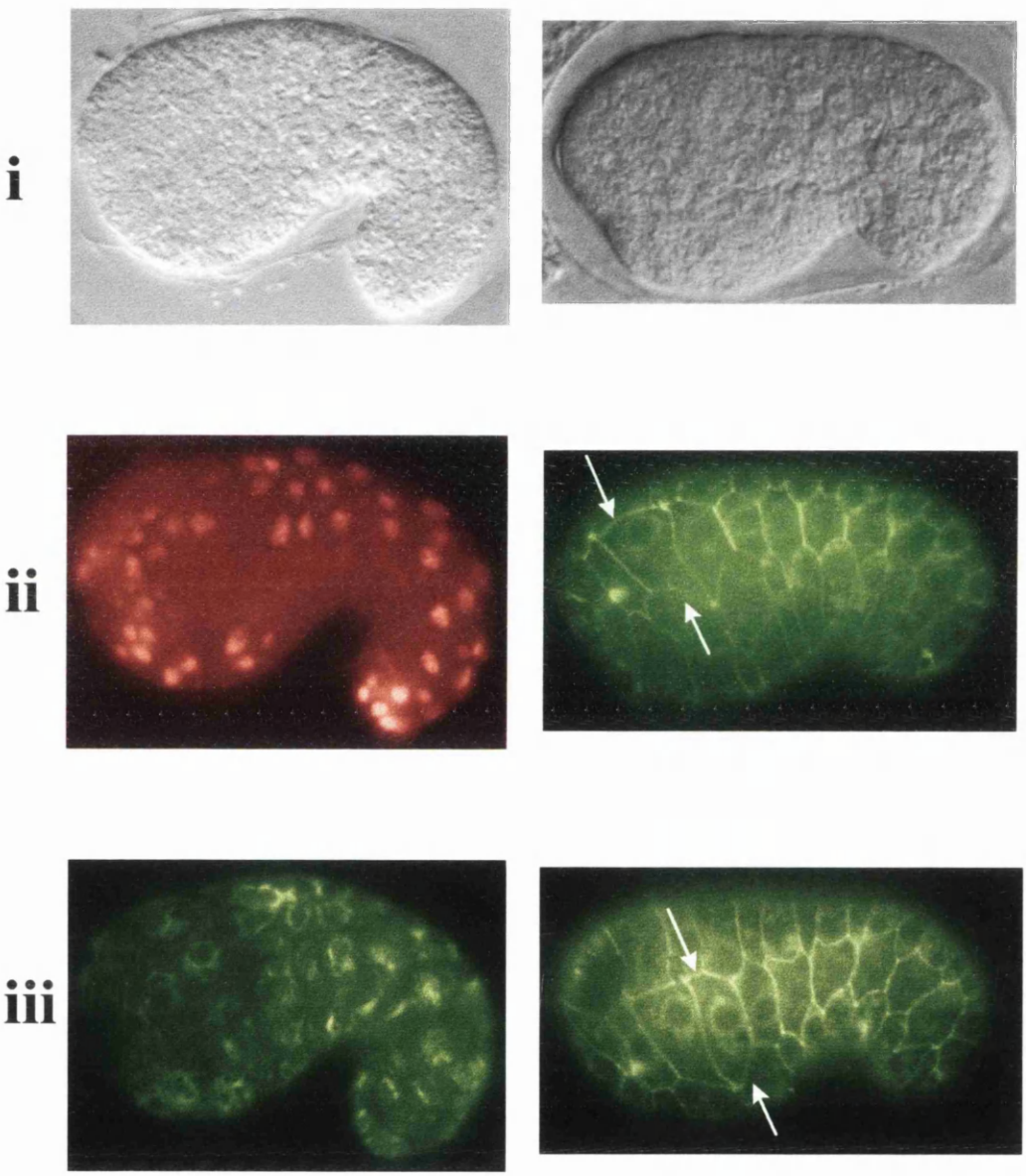
a
b
i
ii
iii

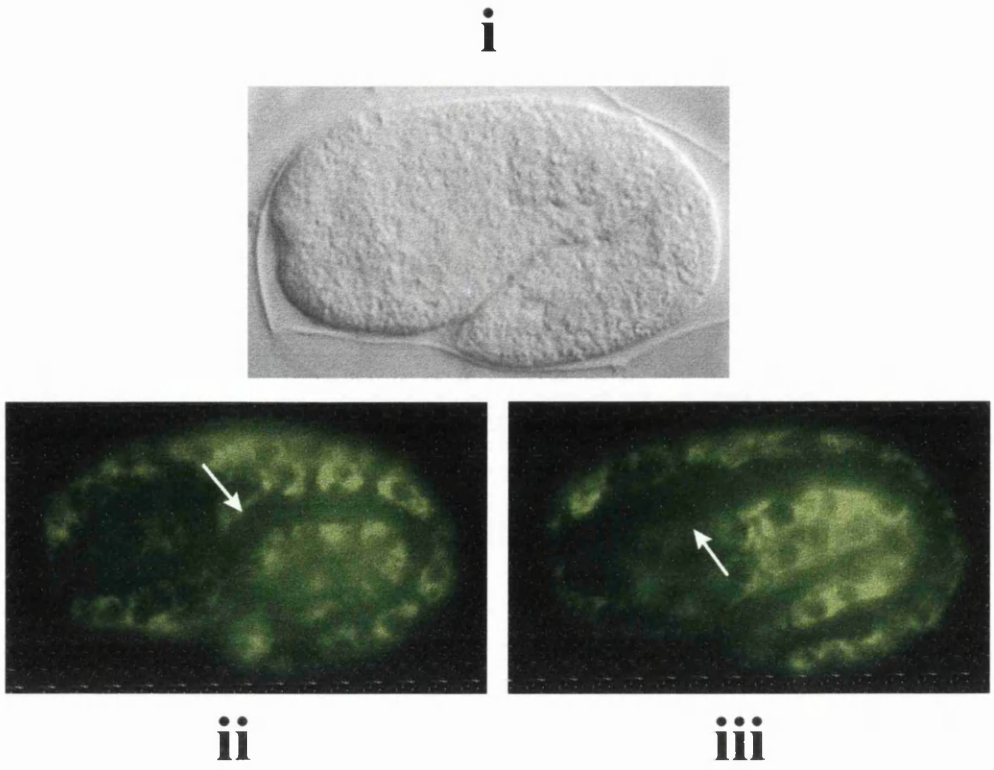

Figure 3.10

The absence of DPY7-5a staining from either side of the dorsal midline where hypodermal nuclei are present

The embryo is positioned with the anterior to the left and dorsal region to the top of the page.

DPY7-5a staining of a wild type 1.5-fold stage embryo showing an absence of staining to either side of the dorsal midline. The embryo is positioned with the dorsal region tilted out of the page and so the bands showing an absence of staining are not symmetrical about the top of the image.

i DIC image

ii View of the left side of the embryo showing DPY7-5a staining

iii View of the right side of the embryo showing DPY7-5a staining

Arrows indicate the regions where DPY7-5a is absent.

staining in later stages. Co-staining with MH27 suggests that DPY-7 is present extracellularly everywhere but above the seam cells (Figure 3.11). This is a surprising result as the internal staining shows the presence of DPY-7 within the cytoplasm of the seam cells. Because the longitudinal ridges, or alae, are positioned above the seam cells at the L1 stage, it is clear that DPY-7 collagen is not present in these structures and it is possible that it is the presence of the alae which prevents the localisation of DPY-7 in this region. It is also possible that DPY-7 is present above the seam cells but the epitope recognised by DPY7-5a is masked by the presence of the alae. The time of secretion of DPY-7, taken as the switch of DPY7-5a staining from an intracellular to an extracellular position, is consistent with the assumption that the cuticle is secreted at the 3-fold stage of elongation (Sulston *et al.*, 1983; Priess and Hirsh, 1986; Wood, 1988).

3.4. Postembryonic localisation of secreted DPY-7 cuticular collagen

3.4.1. Spatial localisation of DPY7-5a in postembryonic stages

After the 3-fold embryonic stage and postembryonically, cuticular annulae are obvious as alternate fluorescing and dark bands running circumferentially around the worm at regular intervals in animals stained with DPY7-5a antibody. The fluorescing bands coincide with the annular ridges while the dark bands coincide with annular furrows (Figure 3.12). This may indicate a subcuticular localisation of DPY-7 in the annular ridges. Measurements taken of the distance between annular ridges of a fixed adult under Nomarski optics also correspond to measurements taken of the distance between DPY7-5a bright bands in the same region (Table 3.1; Appendix 3.1). The pattern of secreted DPY-7 is very similar in each developmental stage but there are some interesting differences. As has been mentioned, the cuticular structures known as alae, which run longitudinally along the worm above the hypodermal seam cells, are only present in the L1 and adult stages in the normal life cycle. While the pattern of DPY7-5a staining in L1 and Adult stages clearly shows that DPY-7 localisation is either outwith the alae or undetectable where the alae are present (Figure 3.13a,b), DPY7-5a staining in L2-L4 stages indicates that DPY-7 is localised above the seam cells (Figure 3.13c,d). This can be seen more clearly using the MH27 monoclonal antibody to highlight the boundaries of the seam cells (Figure 3.14). The DPY7-5a staining pattern

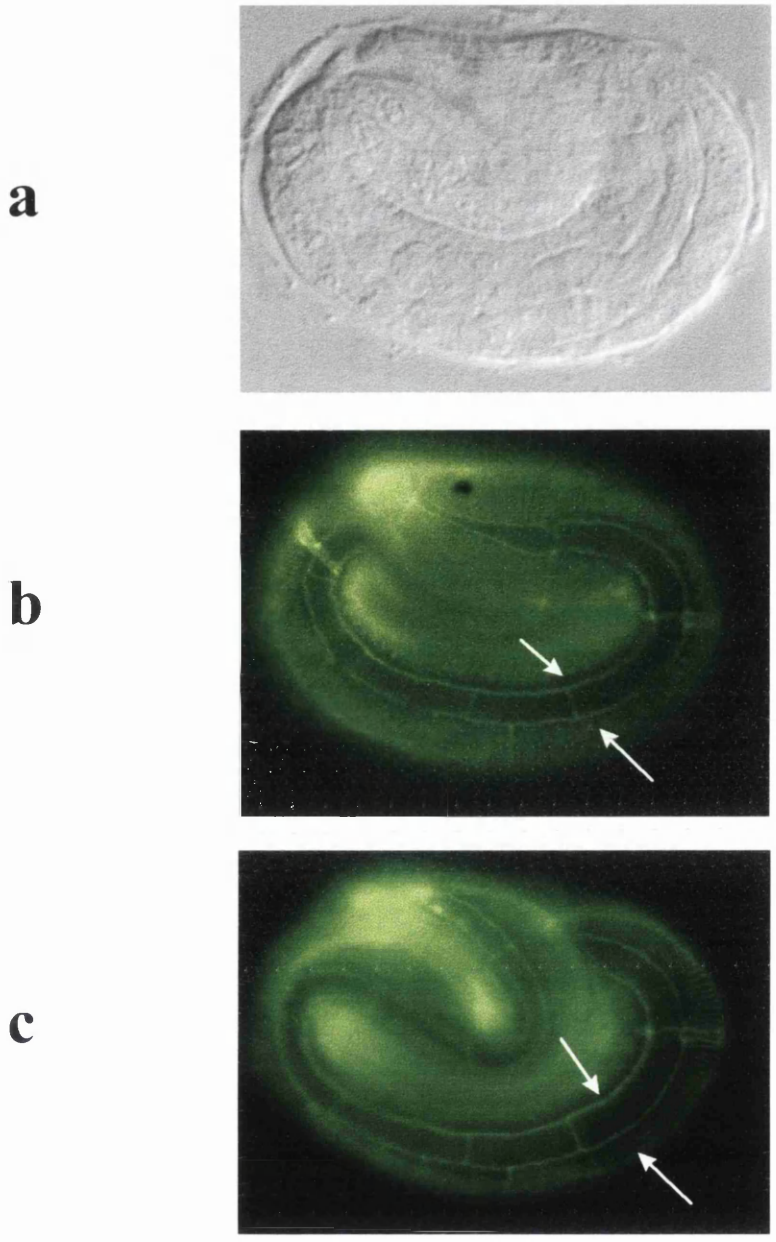

Figure 3.11

Absence of extracellular DPY7-5a staining over the lateral seam cells in wild type 3-fold embryos

The anterior of the embryo is facing to the left of the page at the top of the image

a DIC image

b and **c** DPY7-5a and MH27 antibody staining on both sides of the 3-fold embryo. DPY7-5a staining is absent from above the lateral seam cells. Hypodermal cell boundaries are visualised by the MH27 antibody. The row of seam cells is indicated with white arrows

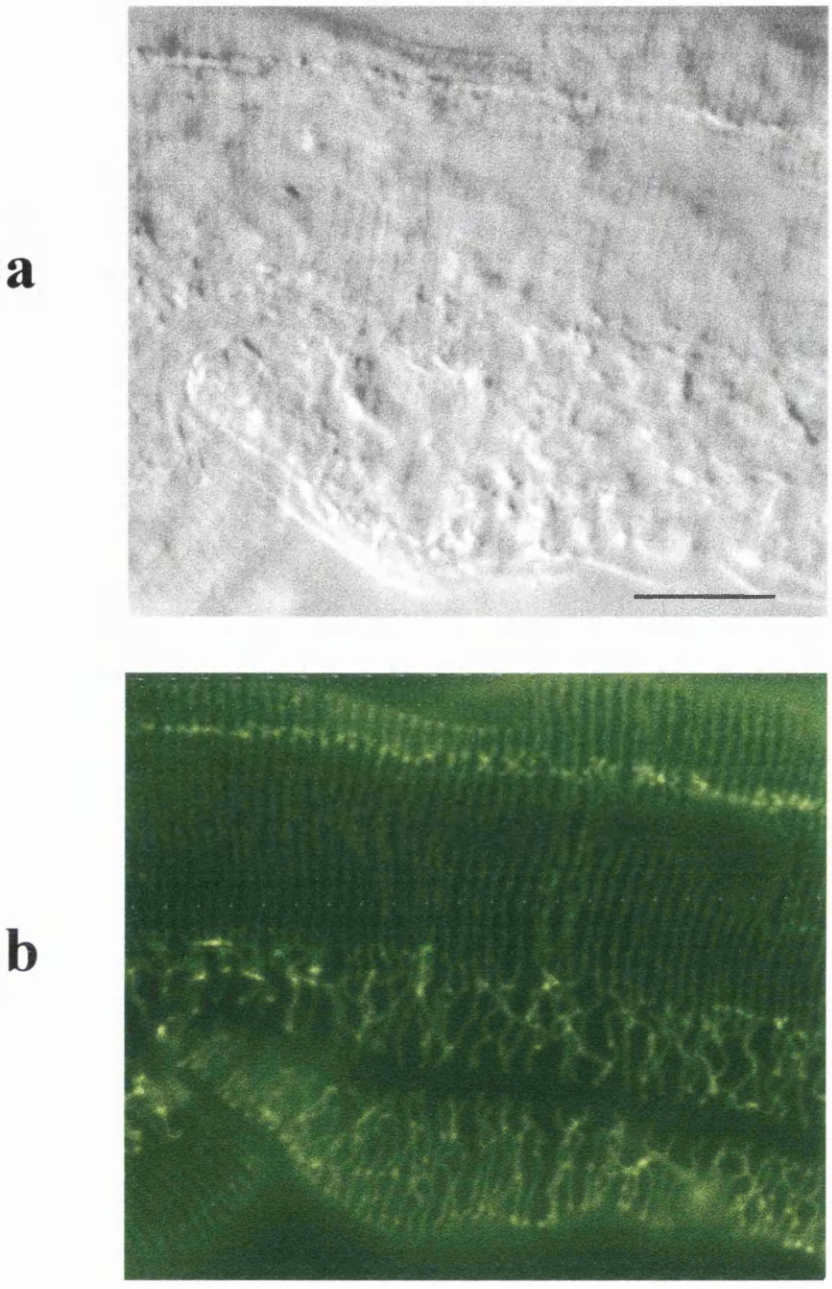

Figure 3.12

A section from a larval stage of a wild type hermaphrodite showing the coincidence of DPY7-5a bright bands with cuticular annulae ridges.

a DIC image of a wild type larval section showing cuticular annulae ridges as stripes running longitudinally down the plane of the image.

b UV image of a wild type larval section which has been stained with the DPY7-5a monoclonal antibody and an FITC-labelled secondary antibody showing bright bands coincident with the annular ridges.

Scale bar is 10μm

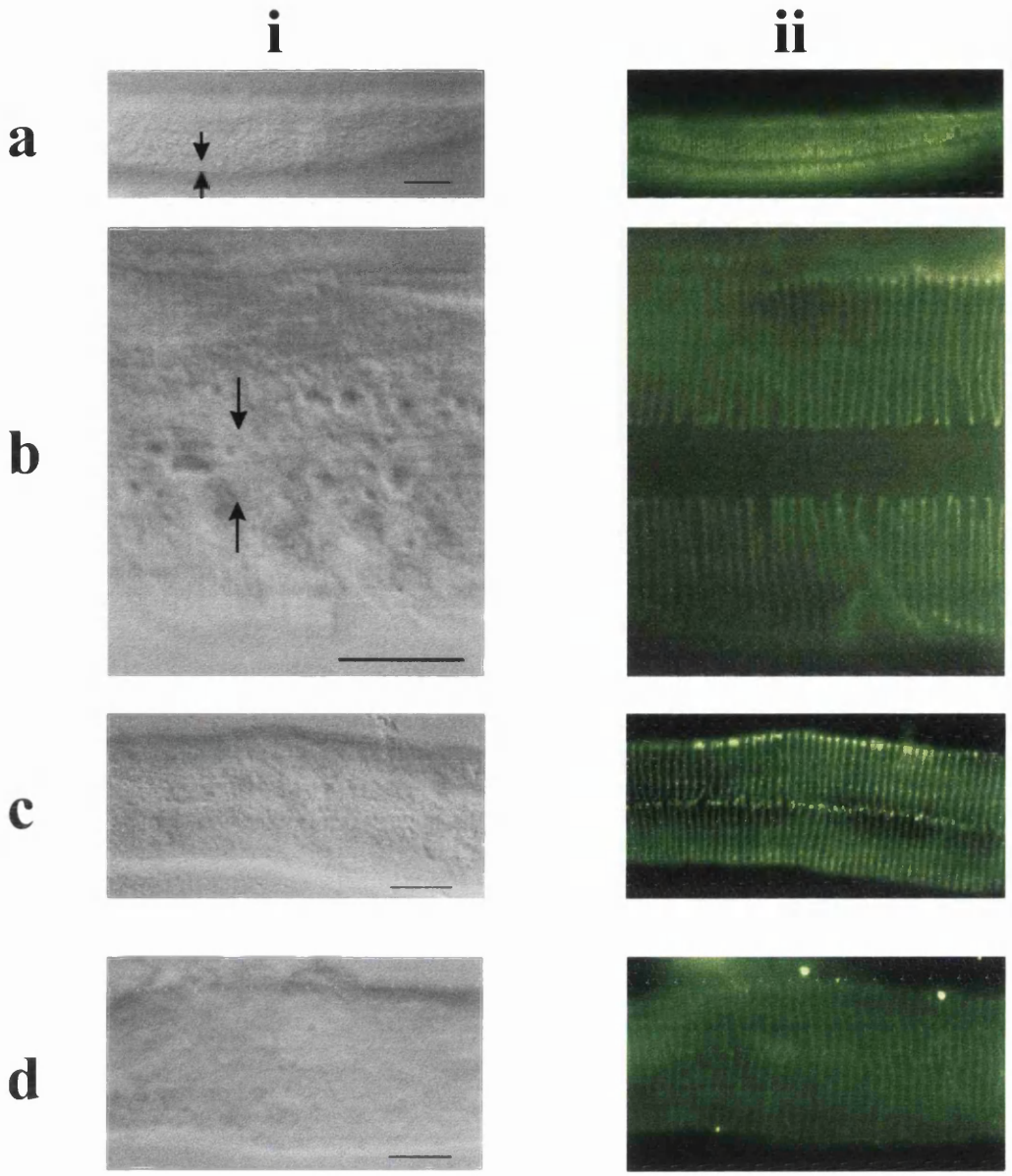

Figure 3.13

Postembryonic extracellular localisation of DPY-7 in wild type hermaphrodites

In all cases **i** shows the DIC image and **ii** shows DPY7-5a staining.

a Lateral view of an L1 larva showing an absence of DPY7-5a staining where the lateral alae are present. The extent of the alae dorsally and ventrally is indicated by arrows.

b Lateral view of an adult showing an absence of DPY7-5a staining where the lateral alae are present. Again the extent of the alae is denoted by arrows.

c and **d** Postembryonic stages between the L1 and adult stage which do not possess alae along their lateral surfaces. These images show lateral views of the larvae and indicate that DPY7-5a staining is not absent from above the lateral hypodermal seam cells in these stages.

Scale bars are all 10μm

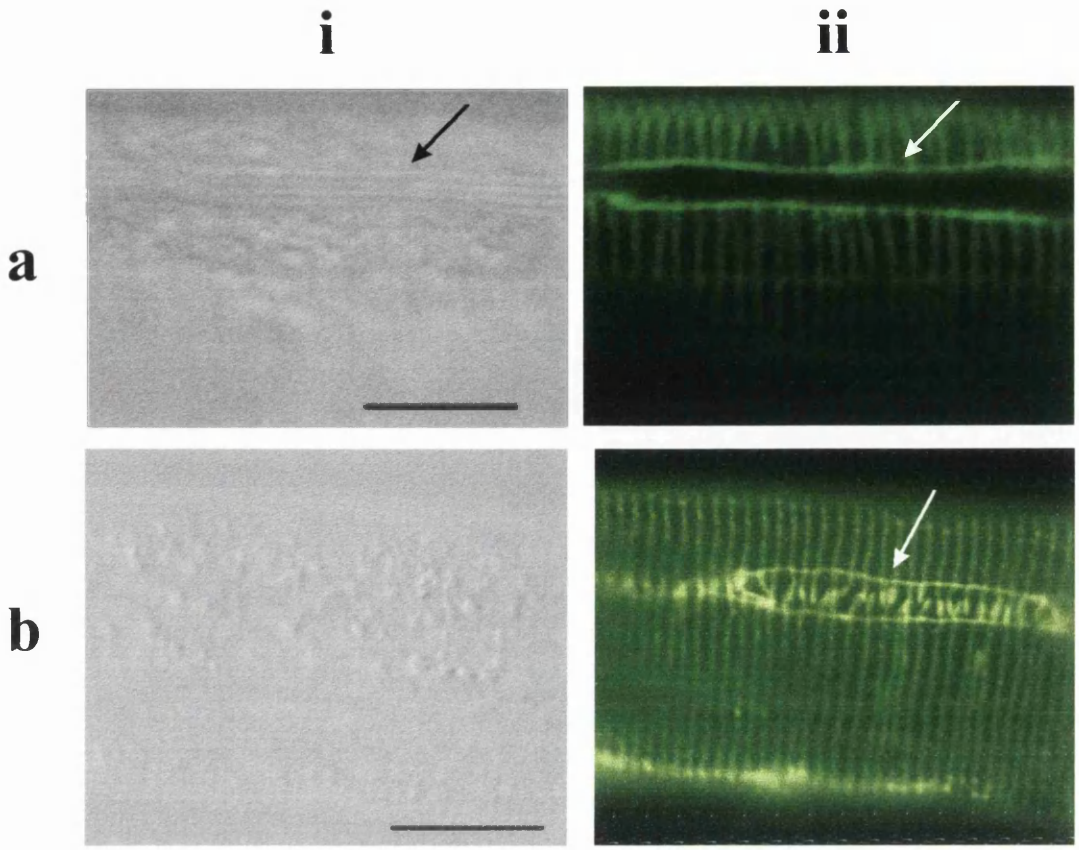

Figure 3.14

Postembryonic localisation of DPY-7 in wild type adults and in larval stages without alae

a Lateral section of an adult hermaphrodite

i DIC image. Alae indicated with an arrow.

ii DPY7-5a and MH27 staining. MH27 denotes the boundaries of the lateral seam cells running from right to left across the page which are fused in the adult. The seam is indicated with an arrow. The DPY7-5a bright bands of staining which is running from the top to the bottom of the page is clearly absent from within the seam cells.

b Lateral section of a larval stage without alae

i DIC image

ii DPY7-5a and MH27 staining. MH27 again denotes the boundaries of the lateral seam cells running from right to left and is indicated with an arrow. The DPY7-5a bright bands of staining, which run from top to bottom, can be seen to traverse the boundaries of the seam cells and interdigitate above the centre of this row of cells.

Scale bars are 10μm

in postembryonic stages without alae shows a pattern coincident with the annulae which traverses the borders of the seam cells as visualised by MH27 and almost interdigitates rather than stopping clearly to either side of them. This difference in DPY7-5a pattern between the stages with and without alae seems to suggest that it is the presence of the alae that completely prevents DPY-7 localisation or the detection of DPY-7 localisation above the seam cells rather than the presence of the seam cells alone. Johnstone and Barry, (1996) have shown that *dpy-7* is not expressed in adults. However, it is expressed in the L4 larvae which synthesise the adult cuticle and so it is not surprising that DPY7-5a is seen in the adult cuticle as well as the other stages.

Table 3.1 Coincidence of DPY7-5a bright band staining with annular ridges

Measurements made between:	Distance between annular ridges (mean ± standard error)	Number of annulae measured
Annular ridges viewed under Nomarski optics	1.474±0.02μm	22
DPY7-5a bright staining bands	1.505±0.03μm	22

One of the staining methods used to visualise DPY7-5a staining, the modified Ruvkun method (section 2.9.5), caused damage to the cuticle so that individual 'threads' of DPY7-5a staining were seen to peel away from the animal (Figure 3.15). The Ruvkun method uses freeze-fracture to permeabilise the worms and then consists of a series of fixation, reduction and oxidation reactions. The 'threads' of DPY7-5a staining could be another indication that the DPY-7 protein is localised to structures within the annular ridges. However, it may be a result of reducing disulphide bonds in the cuticle between annular ridges so that any material in the furrows is degraded more easily during the staining process.

3.4.2. Annular spacing in young and old N2 adults

Measurements were made in several pre-egg-laying and egg-laying adults ('young' adults) between the bright DPY7-5a staining bands and compared with old adults that had stopped egg laying (Table 3.2; Appendix 3.1). Because the wild type adult increases considerably in size, both in length and width, between the L4-adult moult and death, I would expect to see an increase in the spacing of annular ridges

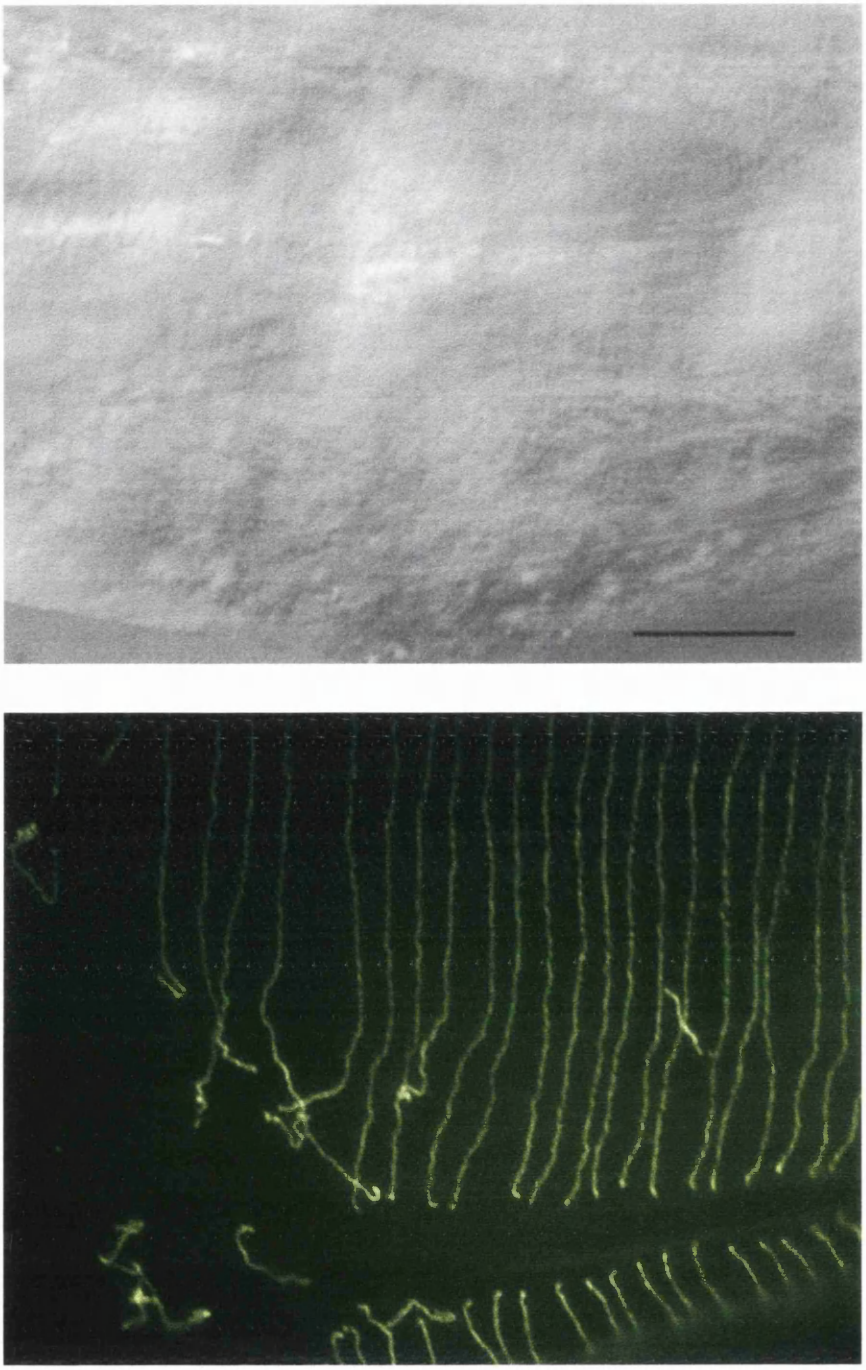

Figure 3.15

Damaged cuticle of a wild type adult hermaphrodite showing DPY-7 localisation

a DIC image

b DPY7-5a staining. The cuticle has been damaged by oxidation and reduction stages and the DPY7-5a staining bands appear to be peeling off as 'threads' rather than sheets of stained tissue.

Scale bar is 10μm

between young adults and very old adults. This is because the annular ridges are thought to arise from actin filament patterning at the L4-adult moult and would therefore be fixed in number throughout the adult stage (Costa *et al.*, 1997). If the annulae were fixed in number but the worm increased significantly in length, the annulae width should increase, which would be reflected as an increase in the distance between annular ridges. Although these measurements were made on fixed animals and therefore may not indicate a true spacing of annular ridges in living animals, the results were comparable with the annular widths given by Cox *et al.* (1981c) and therefore do seem to be indicative of the actual annular spacing. There was as much variation in annular width among the group of 'young' N2 adults as there was between the 'young' and 'old' N2 adults. However, this variation among the 'young' adults may have arisen as some of them had just moulted into adults and contained no eggs, while others were slightly older and were egg-laying. There does seem to be a general increase in annular width between adults just after the L4-adult moult and adults which have passed reproductive age but a more tightly controlled comparison would need to be carried out before the significance of this difference can be tested properly.

Table 3.2 Comparisons between young and old N2 adults and between N2 and *dpy-13(e458)* homozygote adults of a similar age.

Adult age and strain	Distance between annular ridges (mean ± Standard error)	number of annulae measured per animal
N2 young adults		
young adult A	1.249±0.022μm	40
young adult B	0.825±0.020μm	51
young adult C	0.927±0.020μm	48
young adult D	1.050±0.015μm	48
young adult E	1.127±0.018μm	48
N2 old adults		
old adult A	1.505±0.026μm	22
old adult B	1.526±0.019μm	47
old adult C	1.697±0.028μm	47
CB458 (*dpy-13[e458]*) old adults		
old dumpy adult A	0.676±0.12μm	29
old dumpy adult B	0.766±0.09μm	44

3.5. Embryonic spatial localisation and temporal pattern of DPY7-5a in a Gly-X-Y glycine substitution mutant, *dpy-7(e88)*

The *dpy-7(e88)* point mutation is at base 648 from the ATG initiation codon in *dpy-7* resulting in the substitution of the fourth glycine with arginine in the second Gly-X-Y repeat block of the encoded DPY-7 mutant collagen. *dpy-7(e88)* homozygous mutants have a dumpy phenotype slightly longer than the *dpy-7(qm63)* homozygotes (Figure 3.4b,c). homozygous *dpy-7(e88)* embryos were stained with DPY7-5a and compared with wild type embryos. DPY7-5a staining was detected from the same time in mutant embryos and wild type embryos and there was no detectable difference in the intracellular pattern observed (Figures 3.16 and 3.9a). It was not until the 3-fold stage of embryogenesis that a difference in the staining pattern was observed (Figure 3.17). While wild-type embryos have a clear secreted collagen pattern showing annulae, *dpy-7(e88)* homozygotes show very speckled surface staining which is significantly different to the wild type pattern. This speckled staining appears, in places, to be arranged into an annular pattern.

3.6. Postembryonic localisation of DPY-7 collagen in *dpy-7(e88)* mutants

The speckled appearance of DPY7-5a staining within the secreted cuticle appears similar in postembryonic stages (Figure 3.18a). The pattern of staining seen in this mutant is consistent with the idea that the mutant DPY-7 collagen resulting from a glycine substitution in a Gly-X-Y repeat block is predominantly degraded within the hypodermis and not secreted into the cuticle (Johnstone *et al.*, 1992). Because the DPY7-5a staining shows the same speckled pattern in later *dpy-7(e88)* stages as in L1 larvae, intracellular DPY-7 localisation can be seen clearly (Figure 3.18b). The spatial organisation of the intracellular pattern appears to be the same as seen in embryogenesis with cytoplasmic staining of hypodermal cells and an absence of nuclear staining.

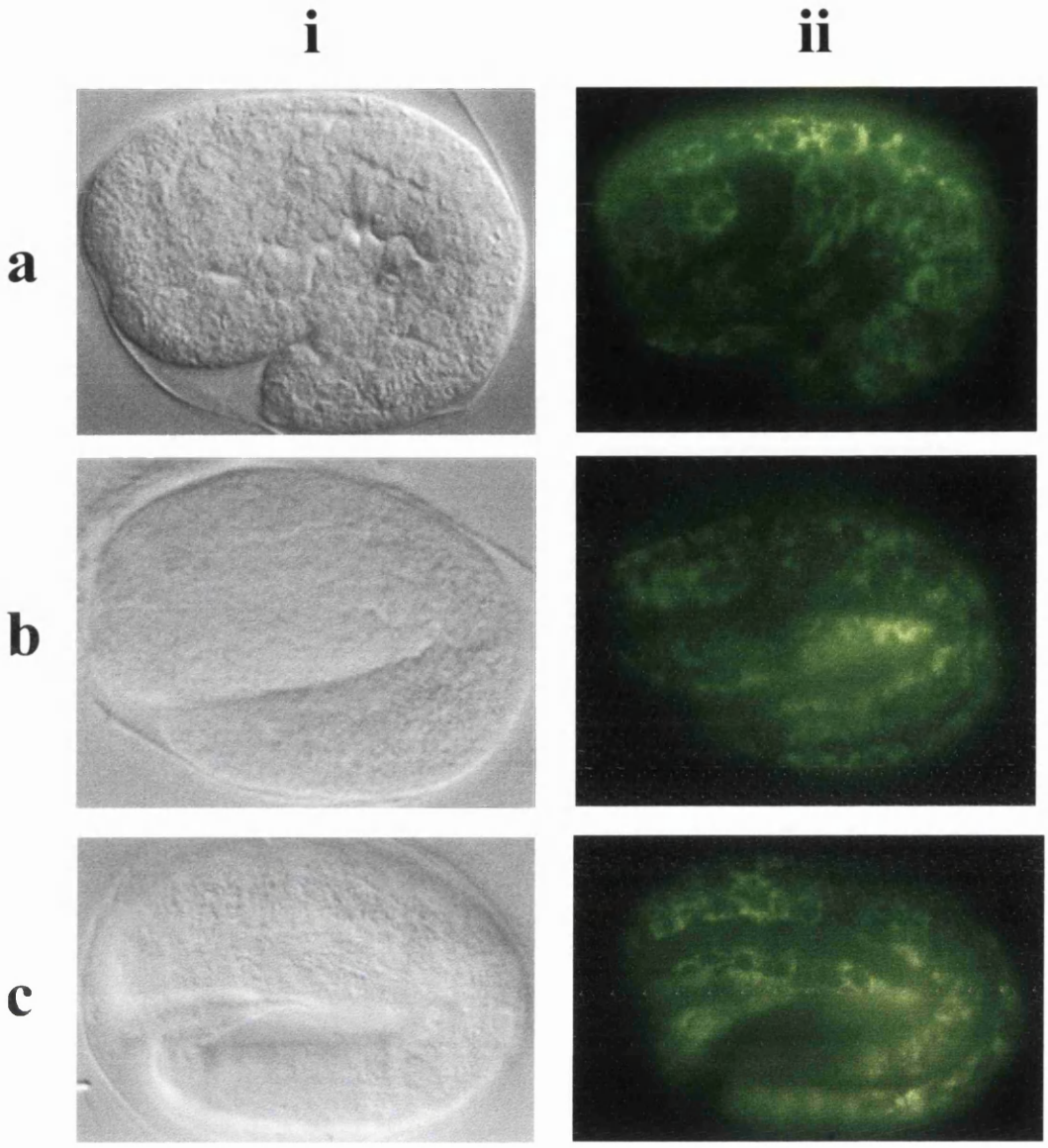

Figure 3.16

Intracellular localisation of DPY-7 in homozygous *dpy7(e88)* embryos

In all cases the DIC image is shown in column **i** and DPY7-5a staining is shown in column **ii**. All embryos are positioned with the anterior to the left and the dorsal surface to the top of the image.

a 1.5-fold homozygous *dpy7(e88)* embryo

b 2-fold homozygous *dpy7(e88)* embryo

c 2.5-fold homozygous *dpy7(e88)* embryo

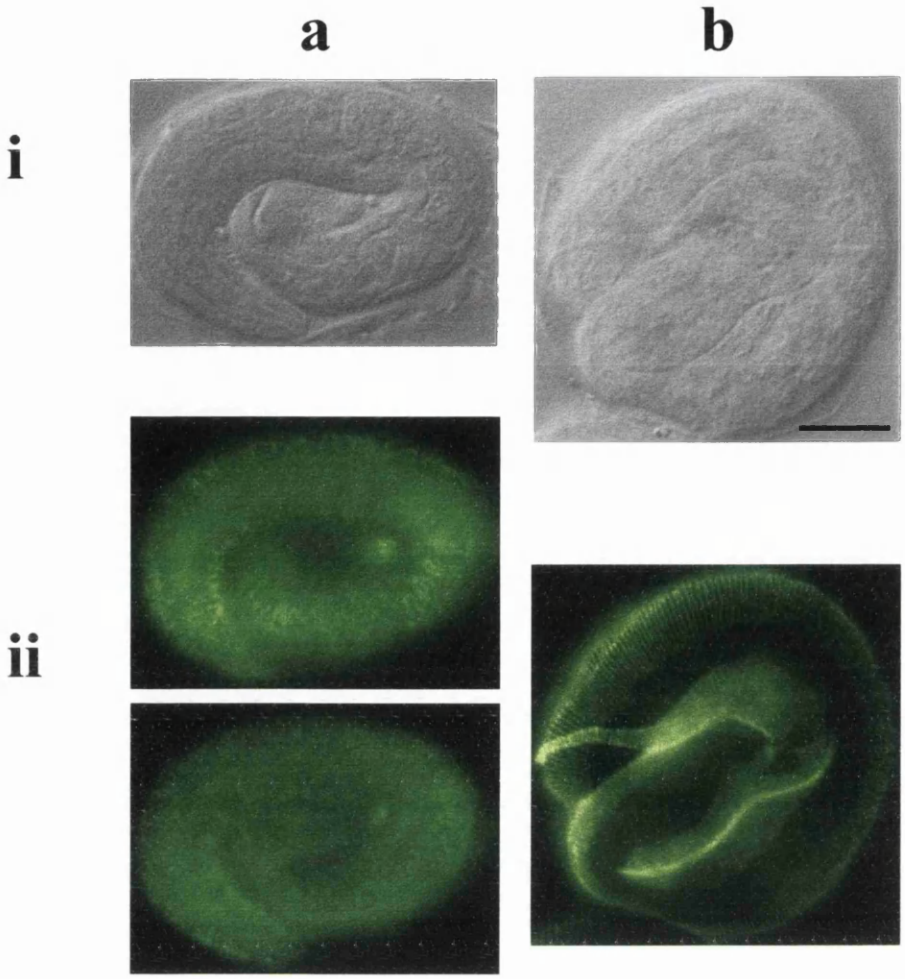

Figure 3.17

Extracellular localisation of DPY-7 in homozygous *dpy-7(e88)* and wild type 3-fold embryos

In both embryos, the anterior of the worm is facing the bottom right of the image

a homozygous *dpy-7(e88)* 3-fold embryo

i DIC image

ii DPY7-5a staining of the two sides of the embryo showing a speckled appearance unlike the bright bands seen in the wild type 3-fold embryo

b DPY7-5a staining in a wild type 3-fold embryo

i DIC image

ii DPY7-5a staining showing the bright bands running circumferentially around the embryo. There is a clear difference between the extracellular localisation of DPY7-5a in the wild type and *dpy-7(e88)* 3-fold embryo.

The scale bar in **b** is 10μm and refers only to image **b**

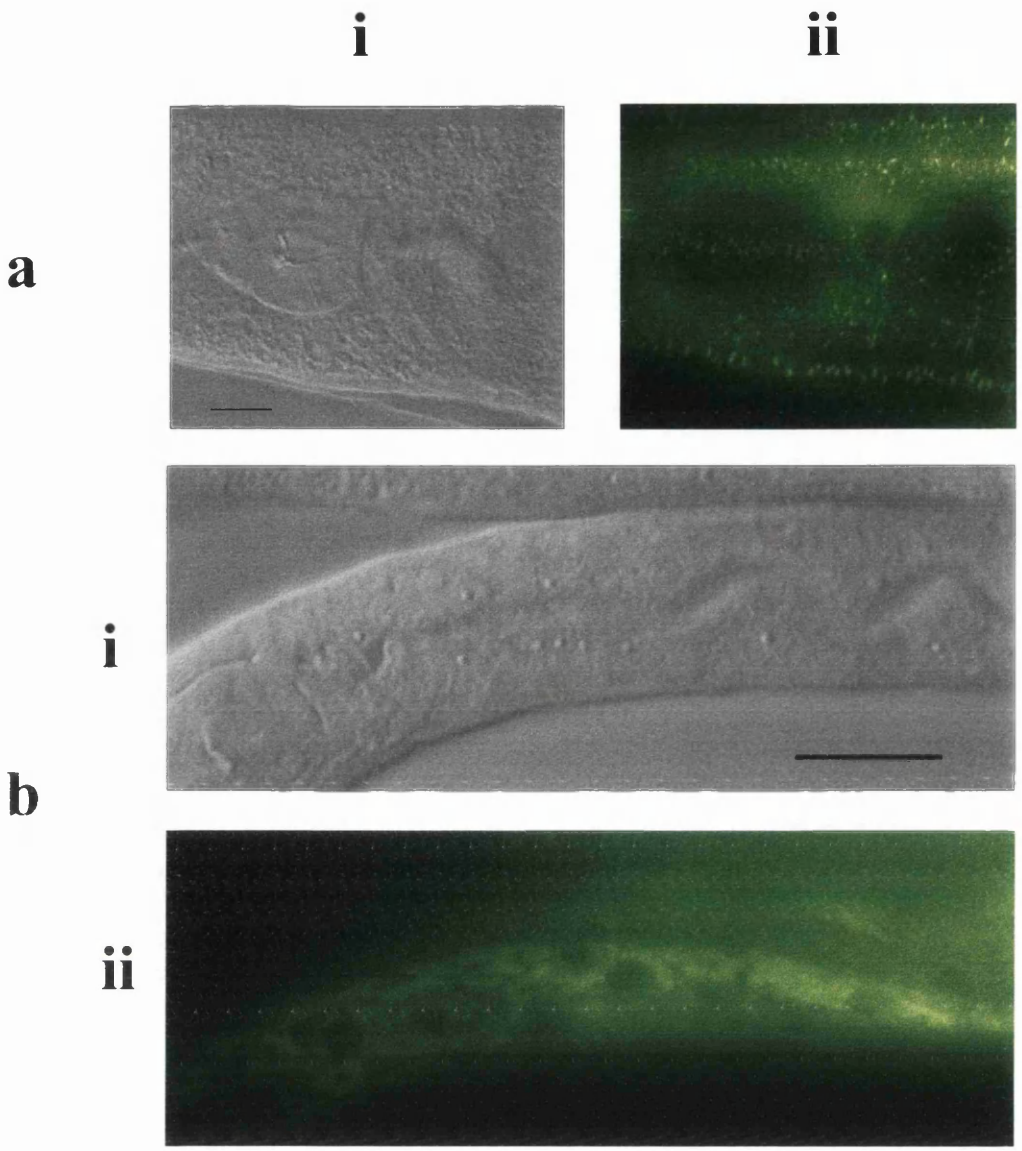

Figure 3.18

Postembryonic localisation of DPY-7 in *dpy-7(e88)* mutants

a Adult *dpy-7(e88)* homozygote

i) DIC image

ii) DPY7-5a staining showing the speckled pattern of extracellular DPY-7 secretion clearly different to the wild type pattern (Figure 3.16).

b Homozygous *dpy-7(e88)* larva

i) DIC image

ii) DPY7-5a staining showing intracellular localisation of DPY-7 postembryonically. This can be seen clearer in *dpy7(e88)* homozygotes due to the reduction in extracellular staining.

Scale bars are 10μm.

3.7. Spatial localisation of DPY-7 collagen in mosaic *dpy-7(e88)* mutants carrying a wild type *dpy-7* transgene

In order to measure the difference in secreted DPY-7 staining observed between animals with and without wild type DPY-7 more directly, I stained a mixed population of larvae from an unstable line of *dpy-7(e88)* homozygotes which carried a wild type copy of the *dpy-7* gene as a transgenic array. Transformed lines containing unstable transgenic arrays are commonly used in *C.elegans* to generate somatic mosaics where some cells of an individual animal are genotypically mutant and others are genotypically wild type (Herman, 1995). There was a high proportion of array loss in this line and consequentially *dpy-7(e88)* mosaics should be produced. Since the *dpy-7(e88)* mutation was not dominant, the presence of the mutant DPY-7 collagen in the strains also carrying a wild type copy of the *dpy-7* gene should not interfere with the function of wild type DPY-7. I found that the results obtained by staining these larvae on the same slide was consistent with the DPY7-5a pattern already seen as some larvae exhibited a wild type pattern of secreted DPY-7 while others showed the speckled appearance (Figure 3.19a). I co-stained with the anti-LIN-26 polyclonal antibody to check that all animals examined had been fixed and permeabilised properly (Figure 3.19b). Since I was not using another marker of array presence or absence, I could not say which animals on the slide carried the array and which did not, but the results coincided with the differences seen between wild type and *dpy-7(e88)* larvae and so suggested that the animals which stained normally contained the array while animals showing a speckled staining appearance had lost the array.

I also looked for the presence of mosaic animals in which some hypodermal cells showed a normal pattern of DPY-7 secretion and others did not. This was problematical as hypodermal cells are mostly multinucleate syncytia. Syncytia make mosaic analysis difficult as one wild type nuclei in a multinucleate cell will result in the production of wild type collagen which will be secreted normally. However, there are several tri-, bi- and mononucleate hypodermal cells at hatch which secrete DPY-7: hyp1-hyp5,hyp8-hyp11 and the ventral P cells, and so the absence of the wild type transgene would be detected in these cells. Hyp1-hyp5 are present in the head and hyp8-hyp11 in the tail, which are regions where it is more difficult to see local differences in staining due to the closer proximity of the annulae and the smaller cells.

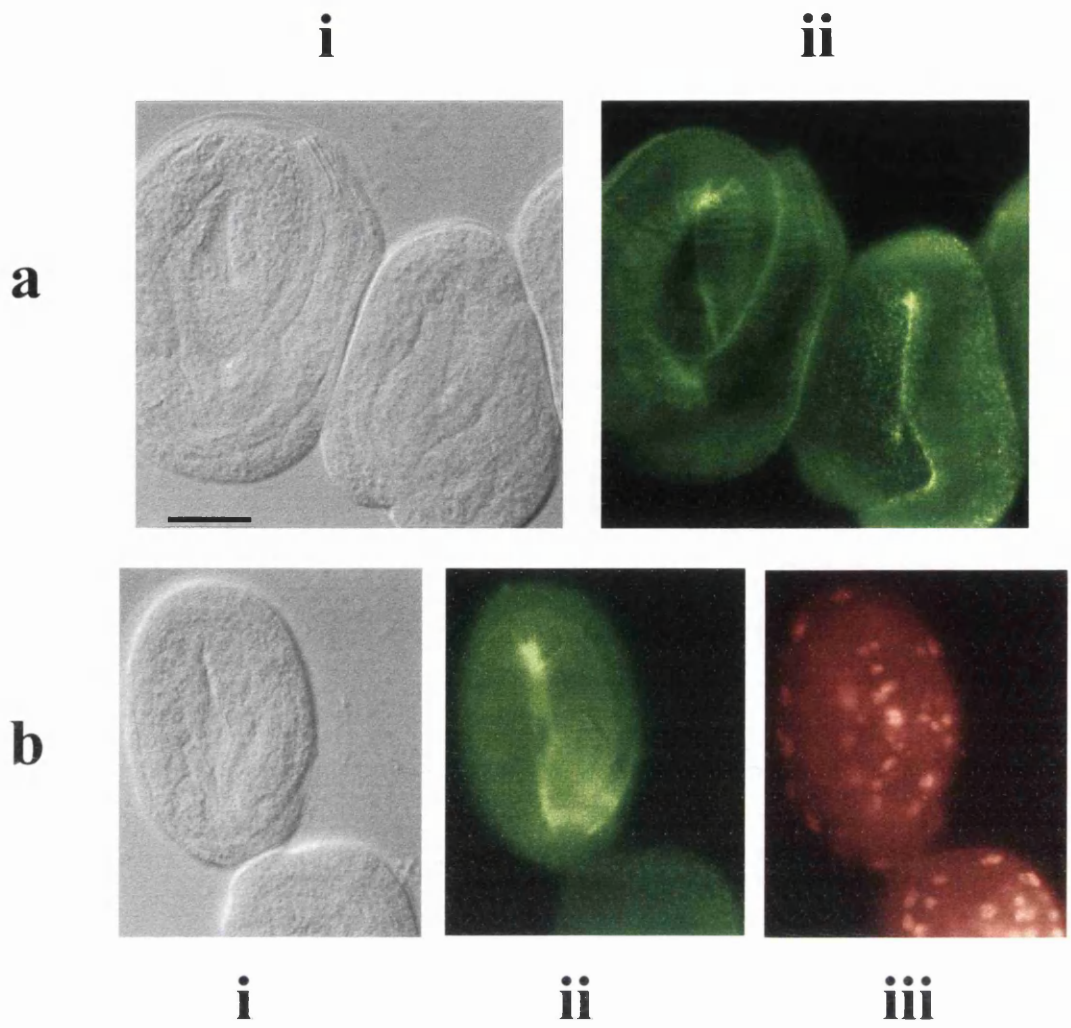

Figure 3.19

Extracellular localisation of DPY-7 in mosaic *dpy-7(e88)* embryos carrying a transgene which contains the wild type copy of *dpy-7*

Embryos are in various orientations with lateral views showing in the images

a DPY7-5a staining of mosaic 3-fold embryos

i DIC image

ii DPY7-5a staining showing wild type-like staining in the embryo on the left and *dpy-7(e88)*-like staining in the embryo on the right.

b DPY7-5a and anti-LIN-26 staining of mosaic 3-fold embryos

i DIC image

ii DPY7-5a staining

iii anti-LIN-26 staining

The embryo to the base of the image has a very speckled DPY7-5a extracellular staining pattern although the wild type anti-LIN-26 staining pattern shows that the embryo has been permeabilised.

The scale bar in **a** is 10μm and refers only to image **a**.

The P cells are in two rows just ventral to the seam cells at hatch but during the L1 stage the nucleus of each P cell enters the ventral cord and the cells rotate to form a single row (Podbilewicz and White, 1994). A large number of larva were observed from this transgenic *dpy-7(e88)* line but no mosaicism was observed.

3.8. DPY7-5a staining pattern and annulae spacing in *dpy-13(e458)* mutants

In order to check that the altered DPY7-5a extracellular staining seen in *dpy-7(e88)* mutants was not simply due to dumpyness, larvae and adults homozygous for *dpy-13(e458)* were stained with the DPY7-5a monoclonal antibody. *dpy-13* encodes another cuticular collagen and the *dpy-13(e458)* allele is a 673bp deletion which is considered to be a null allele of *dpy-13* (ACeDB). Costa *et al.*,1997 have shown that the pattern of actin filament bundles in the hypodermal cells is coincident with the furrows in the secreted cuticle between the annular peaks. They have suggested that it is the presence of the membrane associated actin filaments at each stage in the life cycle that creates the furrowed pattern of the cuticle. Because the shape change seen in *dpy-13(e458)* homozygotes is a result of an abnormal cuticle rather than a hypodermal defect, the number of annulae in these mutants, visualised with DPY7-5a, should be equal to the number of annulae in wild type animals. Consequentially, the adult pattern of DPY7-5a should show a decreased spacing between annular rings in *dpy-13(e458)* hermaphrodites compared to wild type as the overall body length is reduced.

dpy-13(e458) homozygotes show an embryonic DPY7-5a staining pattern which appears to be equivalent to the wild type pattern (Figure 3.20). The switch from intracellular to extracellular staining occurs at the same stage as in wild type embryos and the annular spacing also appears equivalent at this stage. These results show that the absence of a wild type amount of DPY-7 collagen becoming incorporated into the cuticle is not a general aspect of the dumpy phenotype. At later postembryonic stages the DPY7-5a pattern shows bright staining circumferential rings coincident with the annular ridges as in wild type. However, these annular ridges appear to be much closer together than in the equivalent wild type stage and this is especially evident in the adult stage when *dpy-13(e458)* mutants have an annular spacing of almost half the distance of wild type adults (Figure 3.21 and Table 3.2). These results suggest that the number of annulae is indeed equivalent in wild type animals and the much shorter *dpy-13(e458)*

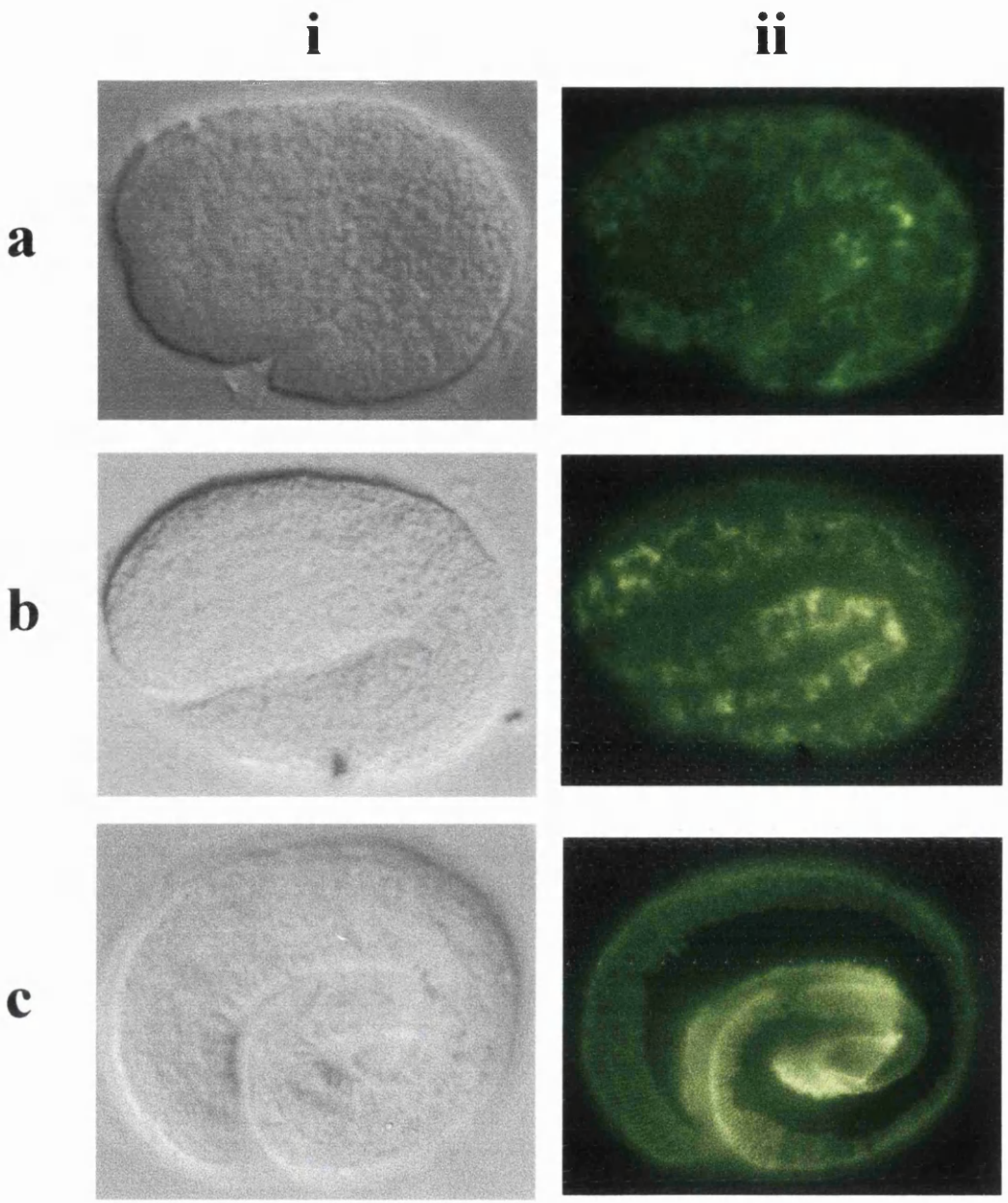

Figure 3.20

Localisation of DPY-7 in homozygous *dpy-13(e458)* embryos

In all cases image **i** is a DIC image and **ii** shows DPY7-5a staining. Both intracellular and extracellular staining appears as wild type embryos (see Figure 3.10). All embryos are positioned with the anterior to the left and the dorsal region to the top of the page.

a Lateral view of a *dpy-13(e458)* 1.5-fold stage embryo

b Lateral view of a *dpy-13(e458)* 2-fold stage embryo

c Lateral view of a *dpy-13(e458)* 3-fold stage embryo

Figure 3.21

Difference in the distance between annular ridges in *dpy-13(e458)* homozygote and wild type old adult hermaphrodites

Alae are indicated with arrows in all the images. Images to the left are DIC images and those to the right show DPY7-5a staining

a DPY7-5a staining in a section of a *dpy-13(e458)* homozygote old adult hermaphrodite

b DPY7-5a staining in a section of a wild type old adult hermaphrodite

Scale bars are 10μm

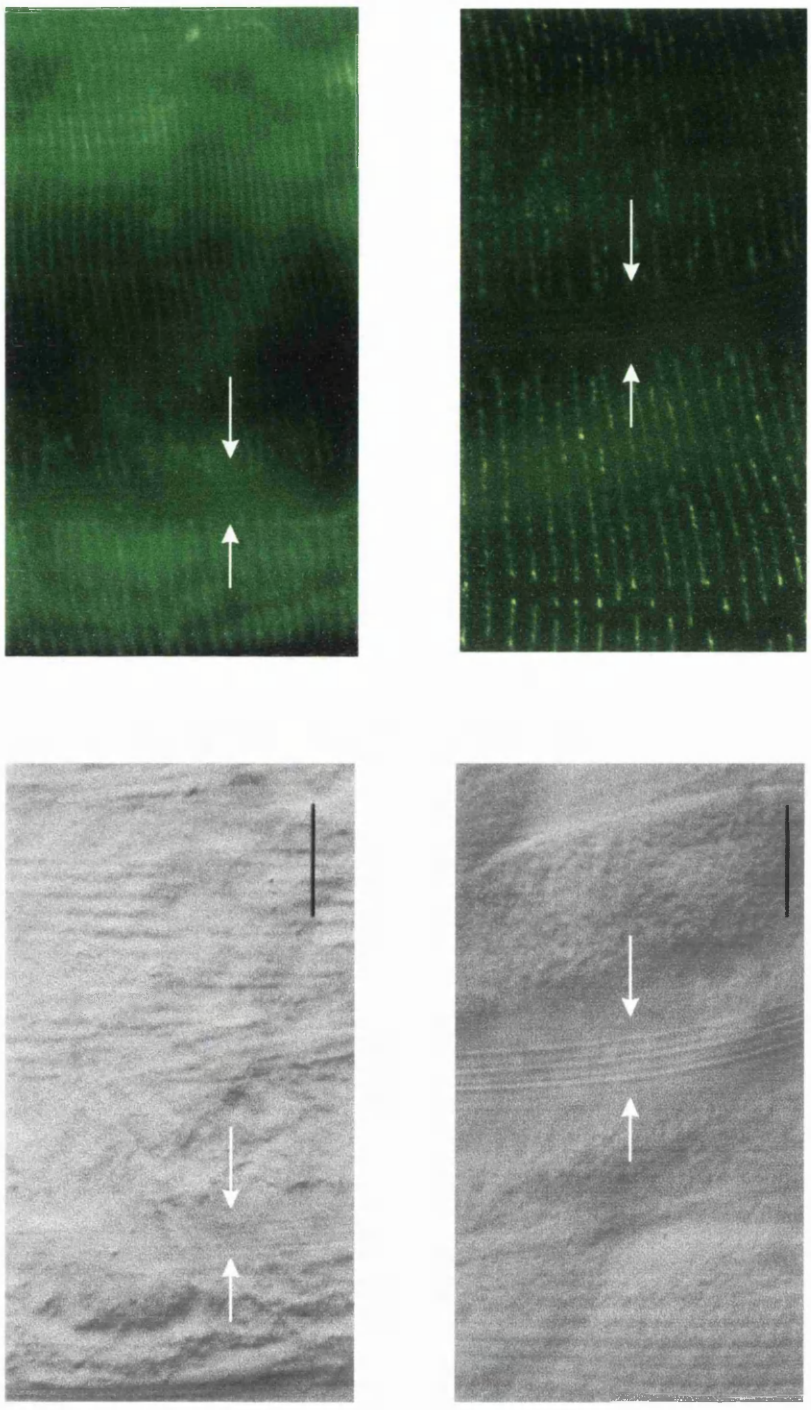
a
b

homozygotes indicating that the actin filaments in the hypodermis are not affected by the collagen mutation and in turn they appear to have no have no influence on this postembryonic defect in body length.

3.9. Discussion

The spatial and temporal expression of many cuticular collagen genes have been examined extensively and the subsequent results show an high level of complexity in the control of cuticle formation. In order to elucidate some of the components of this process, it is valuable to follow the synthesis of the encoded collagens and their localisation in the secreted cuticle. This will not only provide further information on any particular collagen, but may also help in understanding the overall structure of the secreted cuticle at each stage of the life cycle. We have developed a monoclonal antibody against the non-conserved carboxy domain of the DPY-7 cuticular collagen and the pattern of localisation observed at different stages has strengthened previous ideas about synthesis and secretion and provided new information about cuticle organisation. This antibody was shown to be specific to the DPY-7 collagen by its complete absence in *dpy-7(qm63)* mutants which are homozygous for a 6.6kb deletion at the *dpy-7* locus.

DPY7-5a is first seen at the early comma stage of embryonic development and is localised to the cytoplasm of hypodermal cells until the end of embryonic elongation (the 3-fold stage) when it is present extracellularly in circumferential bands corresponding to the cuticular annulae. DPY7-5a staining can be seen within the lateral seam cells before cuticle secretion but is apparently absent above the seam cells once the staining switches to an extracellular location. The extracellular staining of DPY7-5a is seen throughout post embryonic development, although intracellular staining is much more difficult to detect in these stages due to the overlying cuticle. In all stages, the bright bands of DPY7-5a staining correspond to the ridges of the annulae running circumferentially around the surface of the worm and I will henceforth refer to these fluorescent bands as annulae. The extracellular DPY7-5a staining is absent above the seam cells only when the special cuticular structures known as alae are present, in L1 and adult stages. In L2-L4 stages, the DPY7-5a staining extends over the boundaries of the seam cells, as visualised by MH27, and almost interdigitates with annulae crossing

the other side of the seam. It therefore appears that it is the presence of the alae and not the presence of the seam cells per se which prevents DPY7-5a staining, and thus either DPY-7 localisation or the detection of DPY-7 localisation, above the seam cells. Costa *et al.* (1997) reported that annulae were not present above the seam cells as the aligned microfilaments in the seam are not associated with the cell surface and therefore do not pattern the cuticle. It is interesting, therefore, that in postembryonic stages without alae, DPY7-5a staining is seen above the seam in a continuation of the bright bands coinciding with the annulae of the dorsal and ventral surfaces.

The fact that DPY7-5a staining showed a pattern coincident with annulae ridges, and that damaged cuticles showed that DPY7-5a stained material did seem to be in threads rather than sheets suggests two things. Firstly, since the external cortical layer is the only layer of the cuticle to be patterned into annular furrows and ridges, it seems likely that the DPY-7 collagen is present in the cortical layer of the cuticle. Secondly, the staining pattern suggests that DPY-7 collagen is not present evenly throughout a layer of the cuticle but is possibly localised to structures within the annular ridges.

The staining pattern of DPY7-5a was examined in a glycine substitution DPY-7 mutant carrying the mutation *dpy-7(e88).* The embryonic intracellular staining is indistinguishable between wild type embryos and *dpy-7(e88)* homozygotes. However, at the switch from intracellular to extracellular localisation, homozygous *dpy-7(e88)* embryos show a quantitatively different staining pattern with a speckled surface appearance rather than the bright circumferential bands normally seen. This speckled extracellular staining is seen throughout postembryonic development also. Intracellular staining is present during each larval stage as normal. Although a greatly reduced secreted staining pattern is seen in these mutants, the intracellular staining disappears at the same time as in wild type. These results agree with the idea that the mutant collagens are mostly prevented from being incorporated into the cuticle in glycine substitution mutants although it would appear that more mutant collagen is secreted than previously thought and therefore this could possibly be a factor in the phenotype produced (Johnstone, 1994; Kramer, 1997). The absence of intracellular staining after the normal intracellular to extracellular switch also seems to indicate that the mutant collagen synthesised within hypodermal cells is mostly degraded quite efficiently once the cuticle is secreted and there is no evidence that mutant collagens are retained within the cells. These results may indicate a mechanism in hypodermal cells which results in

the swift degradation and removal of unsecreted mutant collagens from the cell. This would prevent disruption of the synthesis or function of other proteins in hypodermal cells as is thought to happen in muscle cells due to a build up of non-secreted type IV basement membrane collagens (Gupta *et al.*, 1997). A 'clean-up' mechanism such as this would not be surprising in a group of cells which synthesised a cuticle at five separate stages during the life cycle especially when collagens are synthesised in temporal waves during each larval stage (Johnstone and Barry, 1996). With such a high turnover of wild type collagens, a clean-up process would be a means of preventing untrimerised collagen chains from one wave of synthesis from trimerising with different collagen chains from the next wave of synthesis, potentially disrupting cuticle formation.

When observing the DPY7-5a staining pattern in *dpy-7(e88)* transformed homozygotes carrying the wild type *dpy-7* gene in an unstable extracellular array, no animals showing mosaic staining were found. This may simply have been due to not finding any animals which had lost the array in nuclei present in mononucleate cells or in all the nuclei of a multinucleate cell. Since most of the hypodermis consists of multinucleate syncytia this is certainly a possibility. However there is also a chance that an animal showing mosaic staining was not found because of the nature of DPY-7 secretion. If there is a mechanism whereby DPY-7 can move across the cell surface during cuticle formation then it could possibly travel to, and be incorporated into the cuticle above, the surfaces of cells which do not secrete it directly. Because of this, cells which had lost the wild type *dpy-7* array may still have DPY-7 incorporated into the cuticle above them and no interruption to the extracellular DPY7-5a staining pattern would be seen.

The clear embryonic and postembryonic DPY7-5a staining pattern of *dpy-13(e458)* homozygotes shows that the greatly reduced incorporation of DPY-7 into the secreted cuticle is not an aspect of all dumpy mutants. *dpy-13(e458)* homozygotes are as short as *dpy-7(e88)* homozygotes yet show an apparently wild type DPY7-5a staining pattern. The only observable difference is that the annular ridges stained by the DPY7-5a antibody in *dpy-13(e458)* homozygotes are almost twice as close together than in wild type animals of the same stage. Actin microfilament alignment in hypodermal cells should be independent of collagen synthesis and therefore the number of annulae in a dumpy animal, homozygous for a collagen mutation, should be equivalent to the

number of annulae in a wild type animal of the same stage. As dumpy adults are much shorter than wild type adults, it follows that the spacing between the annular ridges should be less in dumpy adults.

The staining pattern of a DPY-7 cuticular collagen-specific monoclonal antibody has been characterised and has elucidated several previously held ideas about cuticle secretion and patterning. The beginning of antibody staining in the embryo mirrors the onset of collagen gene expression previously shown from other studies as does the switch of the staining pattern from an intracellular to an extracellular location (Johnstone and Barry, 1996; Gilleard *et al.*, 1997). The noticeable reduction of secreted DPY-7 when there is a Gly-X-Y glycine substitution in the collagen is consistent with the previous idea that certain mutant collagens could not assemble normally and therefore would not be secreted as wild type collagens (Johnstone *et al.*, 1992; Johnstone, 1994; Kramer, 1997). However as some mutant collagen is secreted, this may have an effect on the phenotype produced rather than the phenotype resulting simply from the absence of wild type collagen in the cuticle (Johnstone *et al.*, 1992; Levy *et al.*, 1993). The DPY7-5a staining pattern shows that the distance between annular ridges in *dpy-13(e458)* mutants is around 50% less than the spacing in wild type. This suggests that there are an equivalent number of annulae in the wild type and *dpy-13(e458)* mutants indicating that the annulae do indeed appear to originate from a non-cuticle component such as the actin microfilaments suggested by Costa *et al.* (1997). The production of an antibody specific to a cuticular collagen has been shown to be a very useful tool, in examining cuticle synthesis and secretion in wild type animals and when investigating the cause of mutant phenotypes due to alterations in the collagen. Observations of the staining pattern of a cuticular collagen in mutants of other collagens expressed at the same time during each developmental stage may uncover previously unknown interactions at different stages of cuticle formation such as the trimerisation of collagen chains and may help to explain the reason for these temporal waves of collagen expression.

Chapter 4

Characterisation of a zygotic embryonic lethal mutation, *w4*

4.1. Introduction

4.1.1. Zygotic lethal screens used to generate mutants defective in embryonic elongation

During *C.elegans* development, embryonic transcription begins as early as the 4 cell stage for some genes although components from maternally expressed genes appear to be sufficient to allow normal embryonic development until around the 26 cell stage when gastrulation begins (Edgar *et al.*, 1994; Powell-Coffman *et al.*, 1996). In embryos where zygotic transcription is blocked by the inhibition of RNA polymerase II activity, embryos continue cell division until around the 100 cell stage when they arrest although development after the 26 cell stage is not as wild type (Powell-Coffman *et al.*, 1996). It seems therefore that early events in the *C.elegans* embryo are controlled by maternal factors while later events rely on the transcription of zygotic genes for their control and execution. I was interested in the processes of body shape change (elongation) and body shape maintenance in the *C.elegans* embryo, driven by the hypodermis, which occurs from mid- to late-embryogenesis after cell division has been completed, producing 558 cells (Wood, 1988). I therefore concentrated on finding zygotic lethal mutants which had apparently completed cell division and gastrulation but were defective in enclosure of the hypodermis, elongation, and/or cuticle synthesis and secretion. I focused on embryonic lethal mutants because shape change is a vital process in development and thus morphogenetic defects usually result in embryonic arrest. Several mid- to late-zygotic lethal mutants were generated in a mutant screen performed by J.Rothman and were kindly given to us as gifts. The screen identified late embryonic zygotic lethal mutants with a view to isolating genes involved in hypodermal or cuticular defects.

4.1.2. Enclosure of the hypodermis in the *C.elegans* embryo

4.1.2.1. The process of enclosure in wild type embryos

The hypodermal cells arise on the dorsal surface of the embryo and organise into a monolayer of six rows, and before elongation can occur, this sheet of cells must first migrate laterally around the embryo and meet at the ventral midline in a process known as enclosure. Initially, a quartet of hypodermal cells, known as the leading cells, from the two outer rows of hypodermal cells migrate around the embryo bilaterally, two on each side, using the underlying neuroblasts as the substratum (Williams-Masson *et al.*, 1997). There is no evidence for the presence of a basement membrane at this stage. The two anterior leading cells migrate by extending actin-rich filopodia across the substratum towards the ventral midline while the two posterior leading cells extend actin-rich filopodia which connect to the anterior leading cells. It appears that the two anterior most leading cells migrate actively and the two posterior leading cells migrate partially by adherence to the anterior cells. The other marginal cells may be pulled around the embryo due to the tension set up by the leading cell migration. When the leading cells meet at the ventral midline they form adherens junctions and eventually fuse. Experiments with cell inactivation or the inhibition of actin function indicate that the leading cells are necessary for the initiation of enclosure as are the actin filaments in the filopodia. However, the leading cells from only one side of the embryo are sufficient to complete enclosure apparently normally as they have the ability to migrate past the ventral midline and form proper adherens junctions with their contralateral inactivated neighbour.

The second process of enclosure occurs at the ventral midline when the hypodermal cells from the anterior and posterior meet in a circular 'pocket'. These cells are known as the ventral pocket cells and appear to close in a purse string manner similar to that employed in *Drosophila* dorsal enclosure or the healing of small wounds (Martin and Lewis, 1992; Young *et al.*, 1993). The pocket cells form tight lateral junctions and there is a thick actin cable running around the apical surface of all these cells even without the presence of apical adherens junctions (Williams-Masson *et al.*, 1997). It is thought that the contraction of these cells is actin mediated as the inhibition of actin function at this stage also causes retraction of the hypodermis. After the

circular gap is closed in this way, the cells form adherens junctions with their contralateral neighbours at the ventral midline and ventral enclosure is complete. Hypodermal cells also enclose separately in a more anterior region but the processes involved in this anterior enclosure have not been reported.

4.1.2.2. Genes involved in *C.elegans* ventral enclosure

Although the hypodermal leading cells migrate over the underlying neuronal precursors and the hypodermal filopodia seam to follow grooves between these neuronal cells, ablation of individual or small groups of neuronal precursors does not appear to prevent normal enclosure (Williams-Masson *et al.*, 1997). However, mutants of the *vab-1* gene which is expressed only in neuronal precursor cells at the time of enclosure, show variable defects in hypodermal enclosure with the leading cells in some mutants migrating too far towards the anterior (George *et al.*, 1998). *vab-1* encodes an Ephrin (Eph) receptor tyrosine kinase and appears to have both kinase dependent and kinase independent functions as none of the *vab-1* alleles with alterations in the kinase domain cause complete loss of *vab-1* function. Modulation of cell shape change and adhesion are common features of Eph-mediated signalling in vertebrates (Holder and Klein, 1999). It is possible that in wild type *C.elegans* embryos, VAB-1 could function by sending inhibitory signals from the neuronal precursors to the leading cells which stops them migrating too far to the anterior and in the mutants this inhibitory signal is blocked (George *et al.*, 1998). Another idea which may act in tandem to the inhibitory signal, is that disruption to the neuronal precursors seen in some *vab-1* mutants where the ventral cleft is not closed normally, may inhibit the migration of hypodermal cells as there is an abnormal substratum. The ablation experiments carried out by Williams-Masson *et al.* (1997) suggested that specific neuronal precursors were not necessary for normal enclosure, however, studies on *vab-1* seem to indicate that a properly organised neuronal precursor layer with normal VAB-1 function does seem to be necessary for normal hypodermal enclosure (George *et al.*, 1998). A further morphogenetic defect is seen in many *vab-1* mutant alleles which enclose normally and elongate but have deformed head and tail regions. The number of hypodermal cells in these regions appear normal and so the defects seen must be as a result of abnormal morphogenesis of these regions after the time of enclosure.

Other genes which have recently been implicated with a possible role in hypodermal enclosure are *hmr-1, hmp-1* and *hmp-2, C.elegans* homologues of cadherin, α-catenin and β-catenin respectively (Costa *et al.*, 1998). 98% of *hmr-1* homozygotes arrest with abnormal enclosure and embryos that are deficient in both maternal and zygotic *hmp-1* or *hmp-2* also fail to enclose. HMR-1, HMP-1 and HMP-2 are all absent from, or at very low levels in, the leading edge of enclosing hypodermal cells. Instead it is thought that these proteins may function at the time the cells meet and form adherens junctions at the ventral midline. Although it has been shown that these proteins are not required to form general adherens junctions between adjacent cells in *C.elegans*, they appear to have a function in stabilising contacts and increasing adhesion between contralateral pairs of hypodermal cells during the final stages of ventral enclosure.

mup-4 is a gene essential for the hypodermal functions of morphogenesis and the maintenance of body wall muscle position and two classes of *mup-4* homozygote mutant phenotypes result in arrest at the precomma or 2-fold stage with abnormal enclosure of the hypodermis (Gatewood and Bucher, 1997). In the more severe precomma arrest, the hypodermis appears to be arranged into clumps rather than rows and only extends over small areas of the embryo surface while in the 2-fold arrest embryos, hypodermal cells are abnormally shaped and there are hypodermal lesions on the dorsal surface through which internal cells are exuded. This may indicate a defect in the integrity or adhesion properties of the hypodermal sheet.

Mutations in another gene, *pha-4,* which encodes a transcription factor homologous to the Fork head protein in *Drosophila* and HNF-3 in mammals, prevent the formation of a pharynx and also show defects in hypodermal enclosure (Mango *et al.*, 1994a; Horner *et al.*, 1998; Kalb *et al.*, 1998). *pha-4* is present in all cells of the pharynx from the earliest stages and acts as an 'organ identity factor'. It is unknown whether there is a direct requirement for *pha-4* during hypodermal migration or whether incomplete enclosure is an indirect consequence of the absence of a pharynx. As one of the pharyngeal precursors from the AB lineage is switched from an hypodermal to a pharyngeal cell fate by the MS founder cell, the absence of *pha-4* may prevent this switch and produce extra hypodermal cells which could result in morphogenetic abnormalities (Hutter and Schnabel, 1994; Mello *et al.*, 1994). Certain mutant alleles of another gene, *glp-1,* which encodes a member of the Notch family of transmembrane receptors, also result in a percentage of embryos undergoing incomplete hypodermal

enclosure (Priess *et al.*, 1987). *glp-1* is also involved in the pharyngeal inductive switch in the AB lineage and mutants show supernumerary hypodermal cells resulting in morphogenetic defects.

4.1.2.3. Mechanisms of epiboly and wound healing in other systems

The spreading, or epiboly, of epithelial sheets is seen in many other developmental systems. It occurs during the embryogenesis of many organisms when epidermal sheets originate at a small area on one side of the embryo and subsequently migrate around the embryo enclosing it completely, and also during wound healing when epidermal cells bordering the wound move into the area left uncovered and reseal it. The epithelial sheets have an advancing margin, known as the free edge and various mechanisms are utilised in the movement of the epidermal cells at this free edge. In certain systems, actin-rich lamellipodia are extended from the marginal cells across their substrate and the cells migrate, pulling the submarginal cells with them. This is seen in the healing of large wounds in cell monolayers where the border cells subsequently migrate into the wound to seal the epithelial gap (McCormack *et al.*, 1992; Nusrat *et al.*, 1992). It is also seen during epiboly of the outer layer of the chick blastoderm when a small group of free edge cells adhere strongly to the vitelline membrane, which is the substratum that they move along, and extend actin-rich lamellipodia which pull the submarginal cells behind them (Downie and Pegrum, 1971). The epiboly of the blastoderm in several other vertebrates does not appear to follow the same mechanisms. Epiboly in teleost fish comprises the movement of the enveloping layer (EVL) of the blastoderm, and the deep cells of the blastoderm, over the yolk cell. The EVL travels with the yolk syncytial layer (YSL) around the embryos of *Fundulus heteroclitus* and the zebrafish (*Danio rerio)* and due to the tight junctions between these two layers, the ability of the YSL to complete epiboly independently of the EVL and the organisation of microtubules in the YSL, it has been suggested that the EVL is passively towed around the embryo by the underlying YSL (Trinkaus, 1951; Betchaku and Trinkaus, 1978; Strähle and Jesuthasan, 1993). The migration of the YSL is thought to be driven by microtubule motors and is halted when microtubule function is inhibited (Betchaku and Trinkaus, 1978; Strähle and Jesuthasan, 1993; Solnica-Krezel and Driever, 1994). However, there are constant orderly cell rearrangements in the cells of the EVL free

edge in response to changes in the size of the spherical embryo in *Fundulus* (Keller and Trinkaus, 1987) and it has also been postulated separately that the EVL can move independently of the YSL in *Danio* (Solnica-Krezel and Driever, 1994) and that a possible contraction at the blastoderm marginal cells after the equator can aid blastoderm closure (Strähle and Jesuthasan, 1993).

Other developmental systems seem to use a mechanism of contraction at the free cell margin to close the final epithelial breach. Honey bee epiboly occurs by blebbing of the free edge cells of the spreading preserosal epithelium which do not adhere to any substratum (Fleig and Sander, 1988). This migration appears to be driven by the rearrangement and flattening of cells at the free edge rather than active migration and when the free edges almost meet, the final circular opening closes by contraction. Actin-driven contraction has been seen to function in the closure of small wounds in both chick epidermis and a cultured human intestinal cell line (Martin and Lewis, 1992; Bement *et al.*, 1993). Also, in the dorsal closure of the Drosophila epidermis, a contractile 'purse string' mechanism is utilised to close the gap in the epithelium (Young *et al.*, 1993). Actin and Myosin co-localise at the leading edge of the epidermis and homozygous *zip* mutants, which have mutations in the non-muscle myosin heavy chain, fail to undergo normal dorsal closure.

4.2. Phenotypic Characterisation of *w4* homozygotes

Of the mutants received from J.Rothman, four were selected for initial study, and from this group, one mutant with the allelic designation *w4* was chosen for characterisation. *w4* was selected for study due to several features implicating hypodermal or cuticular abnormalities. The mutant did not elongate past 2-fold, although a percentage of embryos hatched and arrested as lumpy-dumpy L1 larvae. There were also visible structures in the cuticle, the lateral ridges, or alae, which showed abnormalities, and most of the unhatched arrested embryos were ruptured at the ventral posterior surface.

In order to characterise the phenotype of the *w4* mutation, both Nomarski optics and fluorescence microscopy were used. Because of the transparent nature of the *C.elegans* embryo, much tissue detail can be seen using Nomarski microscopy alone, although in situ detection of subtle defects in structure can be visualised using

antibodies against specific molecules and labelling with fluorescent secondary antibodies.

4.2.1. General characteristics of *w4* homozygote mutants

Using Nomarski, also known as differential interference contrast (DIC), microscopy, it can be seen that *w4* embryos range from very abnormal arrested embryos at around the 2-fold stage of elongation which are quite wide and lumpy with a ruptured ventral posterior region, to lumpy-dumpy larvae which usually have a detached buccal cavity (Figure 4.1ai,bi). The mutant strain was outcrossed at least three times before a phenotypical characterisation was undertaken and all *w4* mutants studied were the *w4*/*w4* homozygote progeny of *w4*/+ heterozygote hermaphrodites. The percentage of L1 death compared with embryonic death varies widely in each brood raised at 20°C, from 0% to 53%, with an average of 25.70±2.77% (st.dev.=15.9, n=33 broods). The raw data is shown on Appendix 4.1. Despite the wide variation in the percentage of L1 death per brood, the mean percentage determined from pooling the individual progeny from all these broods together is very similar 28.63% (n=2961 progeny). The homozygote *w4* mutants will henceforth be referred to as either 'unhatched' or 'hatched'.

The hatched mutants die within around a couple of days without growing larger, presumably due to starvation as most have a detached and fused buccal cavity and therefore cannot feed (Figure 4.1ci). They seem to move relatively well and there is definite pharyngeal pumping although the contractions are not regular and seem to occur in groups. The pharynx may not contract for several minutes and then it will contract around 10 or more times in a row within 10-30 seconds. These hatched mutants also have clear alae along each lateral surface although these alae are often abnormally branched towards the anterior at regions where the larvae are very flaccid and have a slack shape with dorsal and ventral bulges (Figure 4.1ei).

Most homozygotes arrest as unhatched 1.5- to 2-fold stage embryos with a ruptured ventral posterior region, although the severity of the rupture varies between arrested mutants. The buccal cavities are usually detached and most unhatched mutants

Figure 4.1

DIC (Nomarski) images showing the terminal arrest phenotypes of *w4* homozygous mutants, fully elongated wild type embryos, and wild type L1 larvae.

Mutants are shown on the left column (**i**), wild type embryos and larvae on the right column(**ii**). In all images, the anterior is to the left and the dorsal region is to the top.

a **i** Unhatched *w4* homozyogte

ii 3-fold, fully elongated wild type embryo

b **i** Hatched *w4* homozygote with an arrow pointing to the gut autofluorescence

ii Hatched L1 wild type larva

c **i** The anterior of an hatched *w4* homozygote with an arrow indicating the detached buccal cavity

ii The anterior of a wild type L1 larva with an arrow indicating the normal attached buccal cavity

d **i** An unhatched *w4* homozygote with arrowheads indicating the position of the four regions of the pharynx: the procorpus, metacorpus, isthmus, and terminal bulb. An arrow points to the gut autofluorescence.

ii A wild type 3-fold embryo with arrowheads indicating the position of the four regions of the normal pharynx. It can be seen that the mutant pharynx is much shorter with the four regions positioned much closer together.

e **i** A section of an hatched *w4* homozygote with an arrow indicating branched alae.

ii A section of a wild type L1 larva with an arrow indicating normal alae.

All scale bars are 10μm

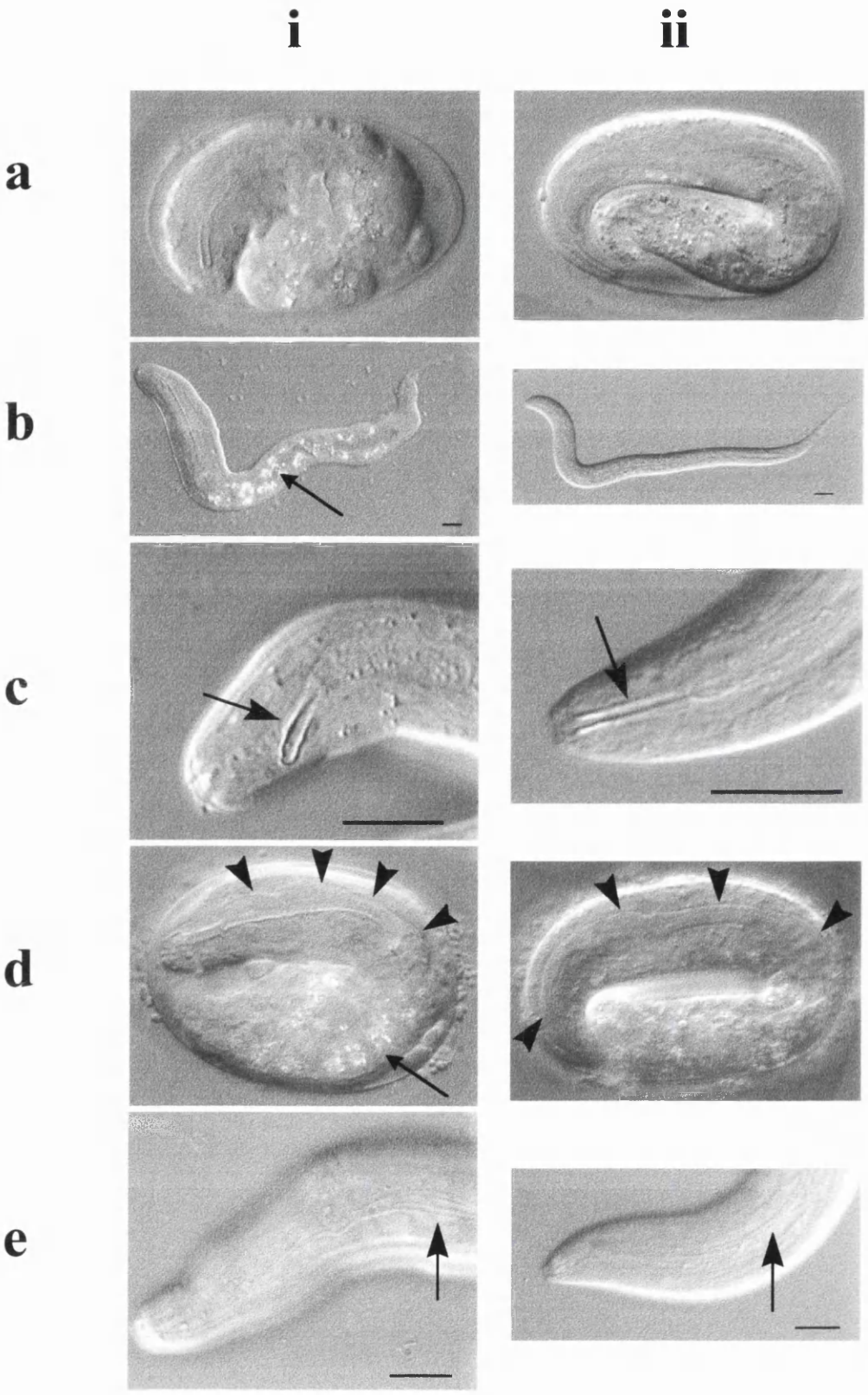
i
ii
a
b
c
d
e

appear wide and lumpy at the anterior and amorphous towards the posterior (Figure 4.1ai). No alae are visible inside the eggshell but a cuticle can be seen covering the area where the body shape is intact i.e. the non ruptured region. Internal cells of the embryo burst out from the ruptured region and lie loose within the eggshell outside the embryo. Some embryos are very disrupted and very little evidence of intact body shape can be seen. Although the pharynx is well developed in unhatched mutants (Figure 4.1di), I have not observed pharyngeal contractions.

I have looked at mutants maintained at 16°C, 20°C and 25°C and have seen no reproducible difference in the percentage of hatched versus unhatched death or in the terminal phenotypes of each class. Unhatched mutants at each temperature are shown in Figure 4.2. However, one *w4* homozygote which hatched and developed at 13°C (due to a faulty incubator) was viable and produced 100% dead progeny (Appendix 4.1). This points to a possible maternal component, although the conditions were not within normal temperature limits for *C.elegans* and no other evidence of a maternal element has been observed under normal conditions.

From time course microscopy observations, it seems that embryogenesis proceeds normally to around the 1.5-fold stage and then, while wild type embryos elongate further, *w4* embryos begin to rupture at the ventral surface towards the posterior of the embryo (Figure 4.3a). Elongation decreases significantly and the mutant embryos continue growing much more slowly until around 2-fold while further tissue is exuded from the ventral surface(Figure 4.3b). This can also be seen in a mixed embryo population of developing mutant embryos. If a selection of embryos are viewed at different stages of development, estimated by the development of the pharynx and buccal cavity, some are at an early stage of tissue differentiation and are already exuding tissue from their lower ventral surface. Later mutant embryos with a fully developed pharynx are much more severely ruptured, possibly as a result of attempted elongation pushing cells through a break in the hypodermis. The lower ventral surface is the site of ventral enclosure within the developing *C.elegans* embryo.

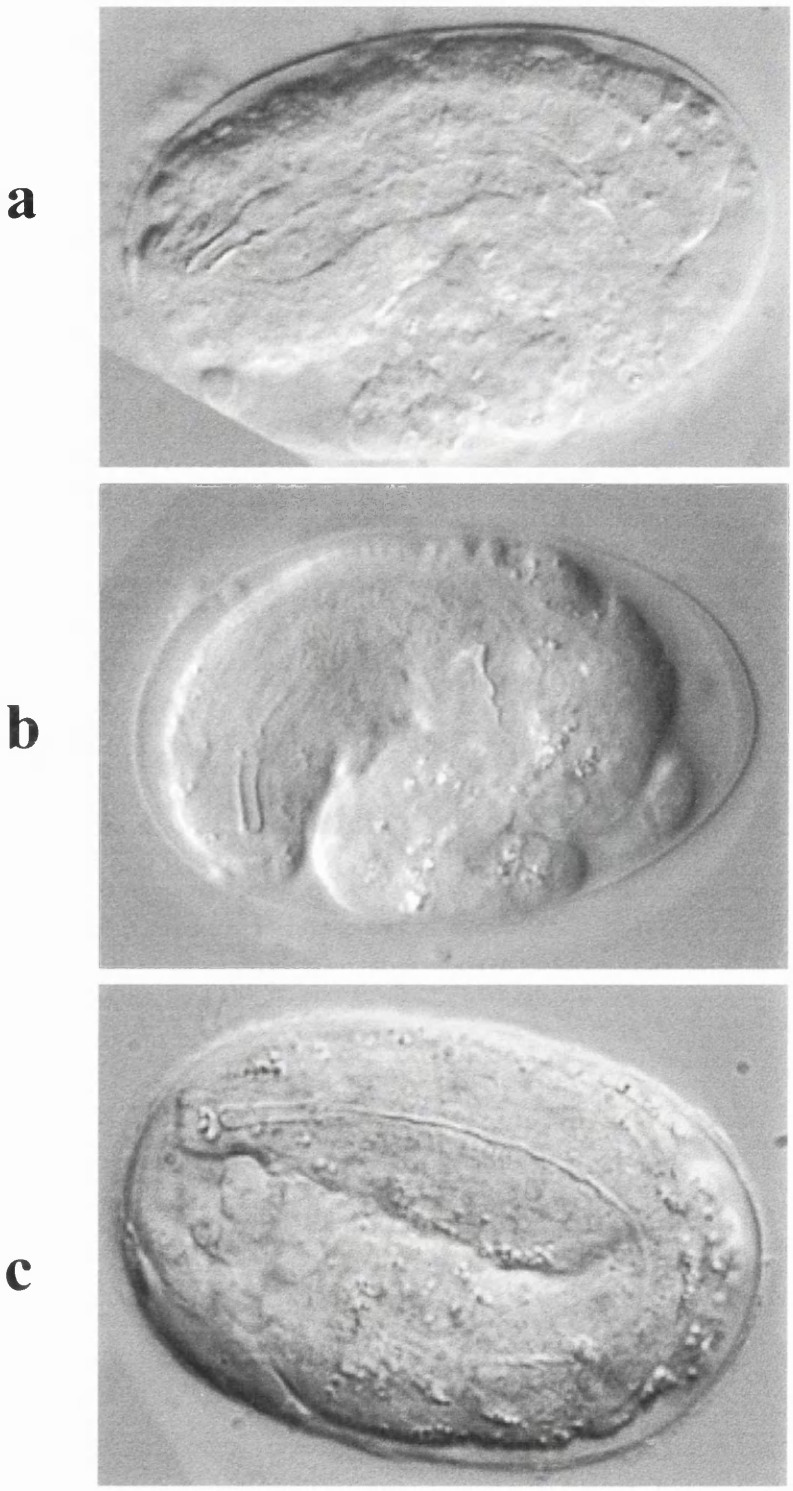

Figure 4.2

DIC images showing terminal arrest phenotypes of unhatched *w4* homozygotes at various temperatures.

In all images, the anterior is to the left and the dorsal region is to the top.

a 16°C

b 20°C

c 25°C

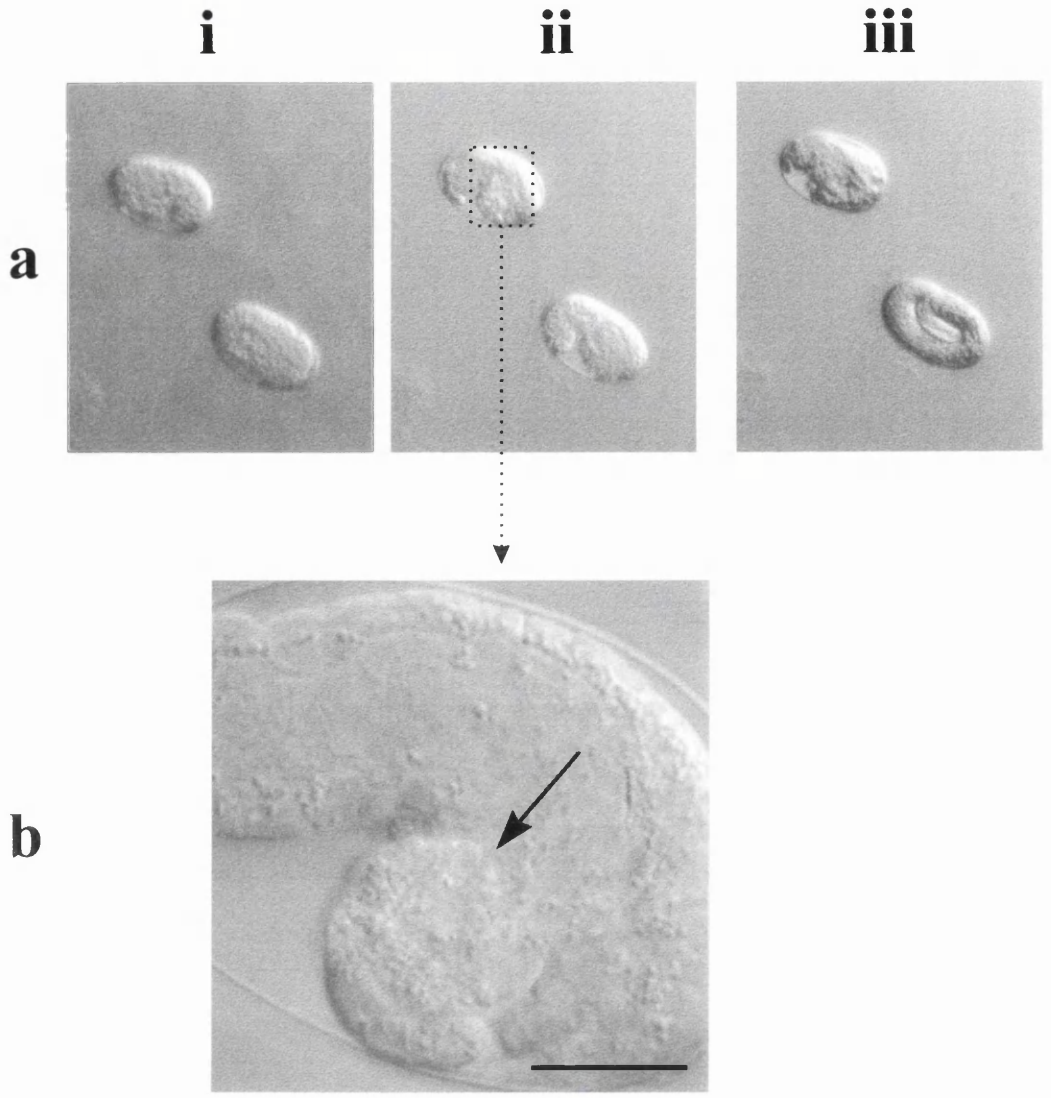

Figure 4.3

DIC images showing ventral rupture of unhatched *w4* homozygotes at various stages during development

a *w4* homozygote (upper embryo) and wild type (lower embryo) at various stages of development. *w4* mutant is shown with anterior to the left and dorsal region to the top, wild type embryos is shown with the anterior towards the bottom left corner and dorsal region to the top right corner of the image.

i *w4* embryo is at comma stage, wild type embryo is at precomma stage

ii *w4* embryo is rupturing at the ventral surface, wild type embryo is at 1.5-fold stage

iii *w4* embryo is very ruptured and deformed while the wild type embryo has elongated completely to the 3-fold stage.

b Magnification of the area denoted by a box in **aii** showing the rupture at the ventral surface of the *w4* mutant. Arrow points to the site of rupture.

Scale bar is 10μm

4.2.2. Specific characterisation of tissues and structures within *w4* homozygote mutants.

I used fluorescence microscopy to study tissues within the mutant embryos. The most obvious markers to test were hypodermal and cuticle specific reagents as the hypodermis drives and maintains shape change (Priess and Hirsh, 1986; Costa et al, 1998). Different components of the body wall and pharyngeal muscle, and the connections of muscle to the hypodermis including basement membrane components were also visualised. Another tissue that undergoes shape change and development during this time in morphogenesis is the pharynx which was observed using several tissue-specific antibodies. In all cases, the markers used showed patterns equivalent to wild type patterns in hatched mutants and so only images of unhatched mutants will be shown in this section.

4.2.2.1. Hypodermis

MH27 is a widely used monoclonal antibody which recognises a protein within adherens junctions, both between adjacent hypodermal cells and within the intestine (Priess and Hirsh, 1986, Waterston, 1988). The staining pattern of the monoclonal MH27 antibody during embryogenesis has been extensively characterised and every individual hypodermal cell fusion has been followed (Podbilewicz and White, 1994). In *w4* mutants, the MH27 pattern indicates that the correct number of terminal hypodermal cells are present although in unhatched mutants, intestinal staining extends past the intact edge of the embryo right through the exuded tissue at the site of rupture, while hypodermal staining ceases at the edge of the embryo (Figure 4.4 and Figure 4.11b). This leads strongly to the idea of incomplete enclosure of the hypodermis at the lower ventral region of the embryo, at least in unhatched mutants. Another defect leading to rupture would be the presence of a weak cuticle at a specific region of the embryo. If this was the case the embryo should elongate normally to 3-fold and then collapse back as the defective cuticle is secreted. This phenotype is seen in certain *sqt-3* alleles which have a mutant *col-1* gene and secrete an abnormal cuticle (Priess and Hirsh, 1986; van der Keyl *et al.*, 1994).

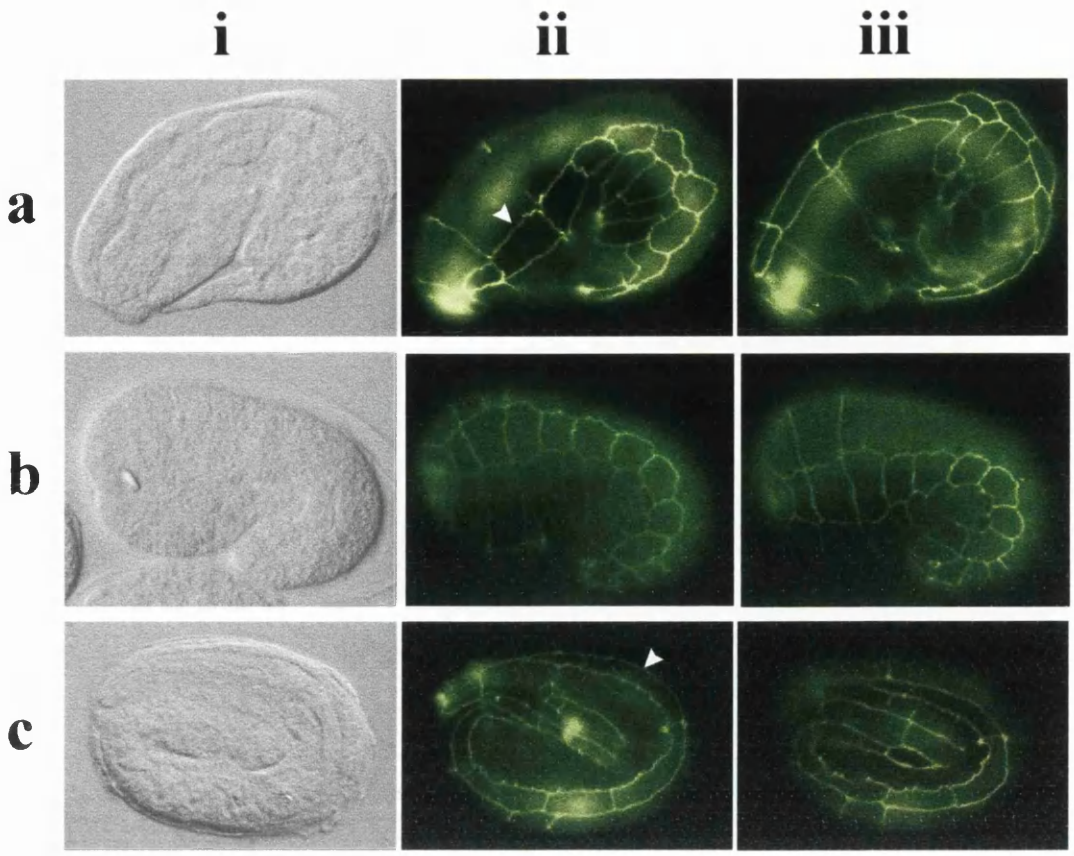

Figure 4.4

Hypodermal cell shapes and positions in *w4* unhatched embryos and wild type embryos.

Embryos were stained with the monoclonal antibody MH27 to visualise the adherens junctions between hypodermal cells. In all images, the anterior is to the left and the dorsal region is to the top. A lateral seam cell is indicated with an arrowhead in image **ii** of all embryos. DIC images are shown in column **i.**

a Unhatched *w4* homozygote

ii and **iii** MH27 staining showing lateral views of the hypodermis. The hypodermal cells appear to be of approximately wild type shape and position although they are not as elongated as a wild type 3-fold embryo due to the overall body elongation defect.

b 1.5-fold wild type embryo

ii and **iii** MH27 staining showing lateral views of the hypodermis

c 3-fold wild type embryo

ii and **iii** MH27 staining showing lateral views of the hypodermis

The nuclear protein LIN-26 is expressed in all hypodermal cells of *C.elegans* and is required for their development (Labouesse *et al.*, 1996). The polyclonal anti-LIN-26 antibody which recognises the LIN-26 protein can be used in conjunction with MH27 to look for specific defects such as abnormal fusion patterns. Although I did not have the equipment necessary to count the number of hypodermal nuclei accurately in the mutant embryos, it could be seen that the seam and P-cells were mononucleate and that the other hypodermal syncytia were multinucleate (data not shown). This indicates that basic fusions have occurred normally within the hypodermis during *w4* embryogenesis although minor abnormalities would not have been detected and I cannot say definitely whether all hypodermal nuclei were present.

4.2.2.2. Cuticle

To examine the synthesis and secretion of the cuticle I used the DPY7-5a monoclonal antibody which recognises the cuticular collagen DPY7. DPY7 is one of the proteins which make up the structural framework of the *C.elegans* cuticle. In both unhatched and hatched *w4* mutants, the antibody clearly shows that the cuticle has been secreted on the surface of the embryo (Figure 4.5). This is evident from the alae on hatched mutants. However, their lumpy-dumpy shape may indicate a cuticular defect which is unseen in the ruptured unhatched embryos or may reflect other hypodermal abnormalities. Again, it can be clearly seen that the DPY7-5a staining extends in the unhatched embryos only as far as the body remains intact. Where tissues have been exuded from the body, there is no DPY7-5a staining. The presence of extracellular DPY7-5a staining is an indication of terminal hypodermal differentiation, at least with respect to cuticle formation, as cuticle secretion is the final role of the hypodermis during embryogenesis.

4.2.2.3. Muscle

DM5.6 is a monoclonal antibody which recognises a component of the body wall muscle myosin heavy chain, myosin A (Figure 4.6)(Miller *et al.*, 1983; Hresko *et al.*, 1994; Moerman *et al.*, 1996). I used this antibody to identify body wall muscle cells in order to observe sarcomere organisation in this mutant. Myosin staining in wild type

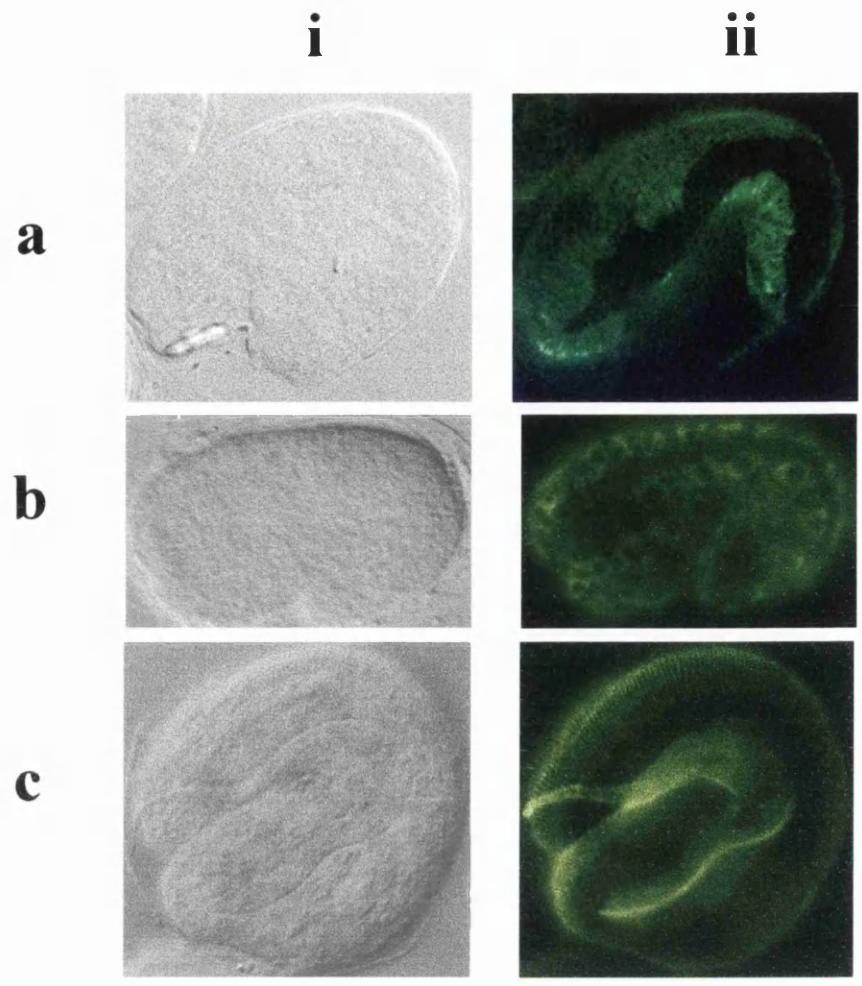

Figure 4.5

The localisation of a cuticular collagen, DPY-7 in *w4* unhatched mutants and wild type embryos indicating presence or absence of a secreted cuticle.

Embryos were stained with the monoclonal antibody DPY7-5a which visualises the carboxy terminus of the DPY-7 collagen. Only one side view of each embryo is shown. In all images the anterior is to the left and in images **a** and **b** the dorsal region is to the top. DIC images are shown in column **i**.

a Unhatched *w4* mutant

ii DPY7-5a staining of one lateral view of mutant **a** showing the extracellular localisation of the antibody indicating that a cuticle has been secreted.

b 1.5 fold stage wild type embryo

ii DPY7- 5a staining of one side view of the embryo showing internal localisation of DPY-7

c 3 fold wild type embryo

ii DPY7-5a staining of one side view of the embryo showing the extracellular localisation of DPY-7 indicating that a cuticle has been secreted

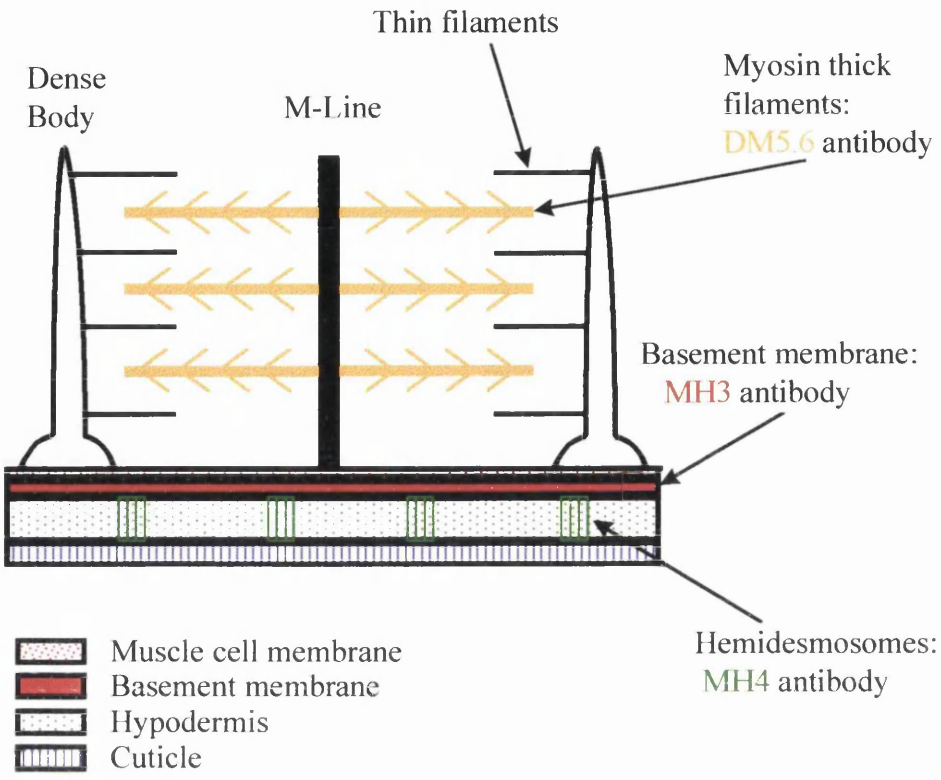

Figure 4.6

Schematic model of a *C.elegans* body wall muscle sarcomere showing the localisation of antibodies: MH3, MH4 and DM5.6

Thin filaments are anchored to dense bodies and, at the other end, overlap with thick filaments. The alignment of thick filaments is maintained by the M-Line components. Contractile force is generated by myosin heads which pull on adjacent thin filaments, bringing the dense bodies closer together. This contractile force is transferred to the outside through the basement membrane and hemidesmosome attachments to the cuticle. DM5.6 is a monoclonal antibody which recognises myosin A in the centre of the thick filaments. MH3 recognises a protein, Perlecan, in the basement membrane. MH4 recognises a component of the hemidesmosome intermediate filaments.

(Adapted from Hresko *et al.*, 1994)

embryos is tightly arranged in four longitudinal rows along the developing embryo (Figure 4.7b). *w4* embryos appear to have the four muscle quadrants which are stained with the DM5.6 monoclonal antibody. The staining is usually very regular in mutant embryos within the intact body region but staining is absent outside the site of rupture (Figure 4.7a). Irregular staining could reflect some defect in muscle-hypodermis attachment which would definitely occur at a site where enclosure is incomplete.

4.2.2.4. Muscle-hypodermis attachments and basement membrane

MH4 is a monoclonal antibody which recognises areas of the hypodermis associated with the attachment of the underlying body wall muscle cells, called intermediate filaments within structures called known as hemidesmosomes. It also stains areas of the pharynx, the excretory cell, and the amphid sensory neurons (Figure 4.6)(Francis and Waterston, 1991; Hresko *et al.*, 1994). In mutant embryos, MH4 is clearly present in the correct positions, although hypodermal staining is less clear than in 3-fold wild type embryos and staining does not extend past the intact body surface at the edge of posterior rupture (Figure 4.8). At the site of rupture, staining is more disorganised and diffuse. Elsewhere, it looks as if the hemidesmosomes are present in the correct positions within the hypodermis and consequently the underlying muscles seem to be in the correct position also.

The monoclonal antibody MH3 recognises several isoforms of the basement membrane protein UNC-52, a homologue of vertebrate perlecan, which has a primary function in anchoring the muscle myofilament lattice (Figure 4.6)(Francis and Waterston, 1991). It is present at both muscle:muscle and muscle:hypodermal cell junctions. In unhatched *w4* homozygote embryos, MH3 is present and appears to lie in the correct positions where the body is intact (Figure 4.9a). Outside this area, where the embryos have ruptured, staining is again irregular and diffuse and does not extend past the site of rupture. This corresponds to the MH4 data and the position of DM5.6 sarcomere staining.

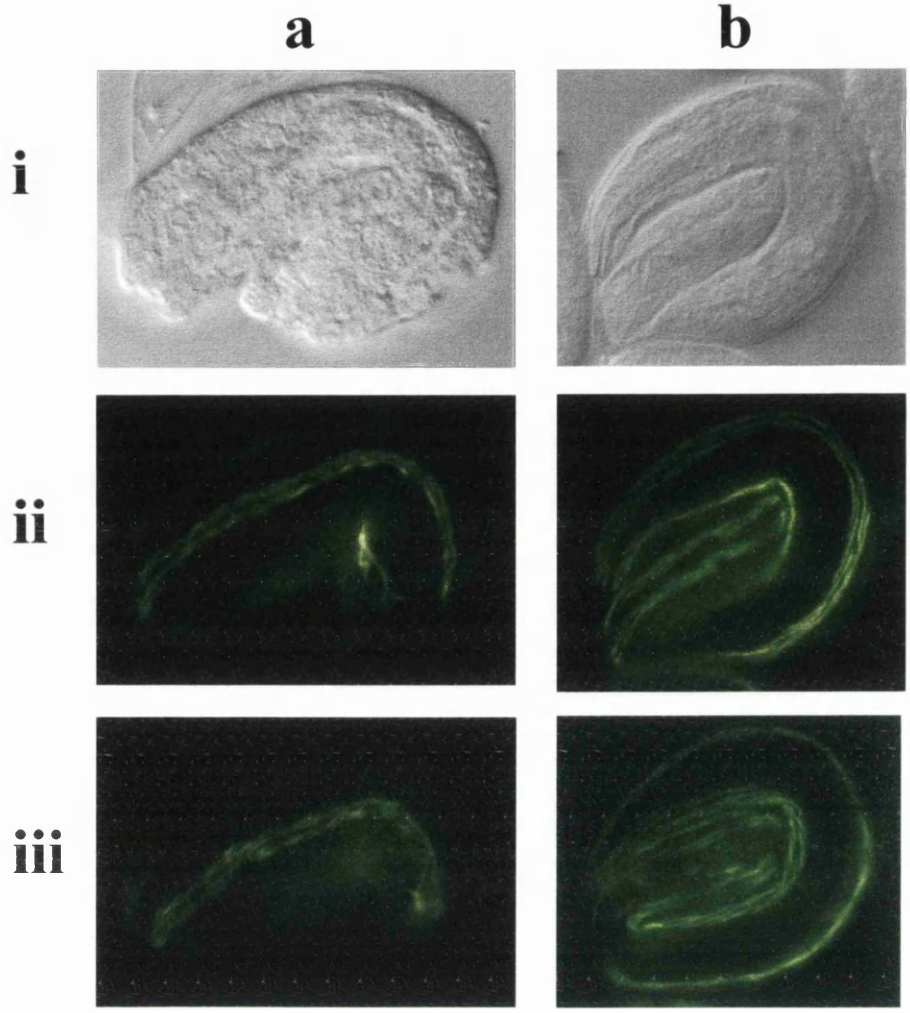

Figure 4.7

Position of muscle sarcomeres in *w4* unhatched mutants and wild type embryos

Embryos were stained with the monoclonal antibody DM5.6 to visualise myosin A within the muscle sarcomeres. In both images, the anterior is to the left and in image **a** the dorsal region is to the top of the image.

a unhatched *w4* mutant

i DIC image

ii and **iii** DM5.6 staining showing different views of the mutant embryo muscle sarcomeres. Sarcomeres appear to be organised in an approximately wild type manner.

b 3-fold wild type embryo

i DIC image

ii and **iii** DM5.6 staining showing two views of the embryo muscle sarcomeres

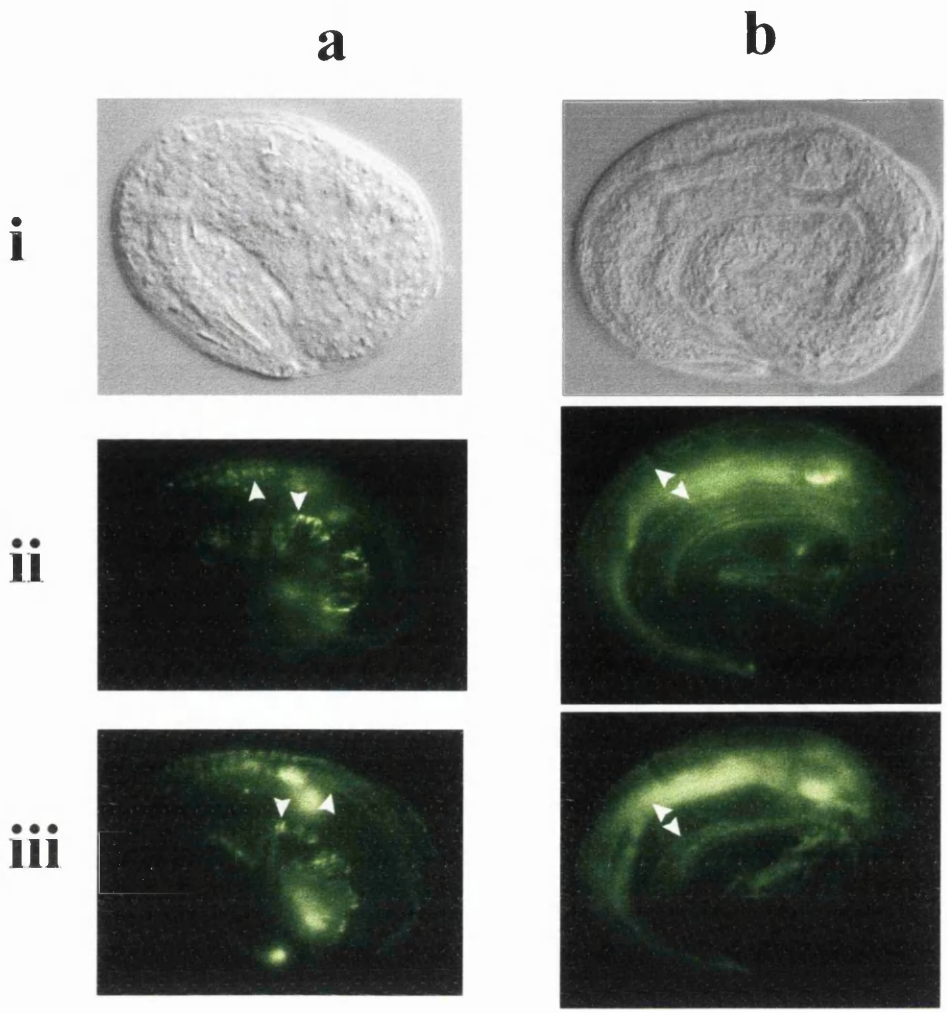

Figure 4.8

Association of the hypodermis and underlying muscle in *w4* unhatched mutants and wild type embryos

Embryos were stained with the monoclonal antibody MH4 which recognises intermediate filaments, part of the hemidesmosomes, present in hypodermal cells overlying muscle sarcomeres. Bands of MH4 staining are denoted with arrowheads on the images. Both embryos are positioned with the anterior curving down to the bottom centre of the image. MH4 also stains the pharynx, the secretory cell, and several sensory neurons which can be seen on more internal focal planes. DIC images are shown in row **i**.

a unhatched *w4* mutant

ii and **iii** MH4 staining showing hemidesmosome positions at two lateral views of the mutant embryo. The MH4 staining pattern in *w4* mutants appears equivalent to the wild type staining pattern.

b 3-fold wild type embryo

ii and **iii** MH4 staining showing normal hemidesmosome positions at two lateral views of the wild type embryo.

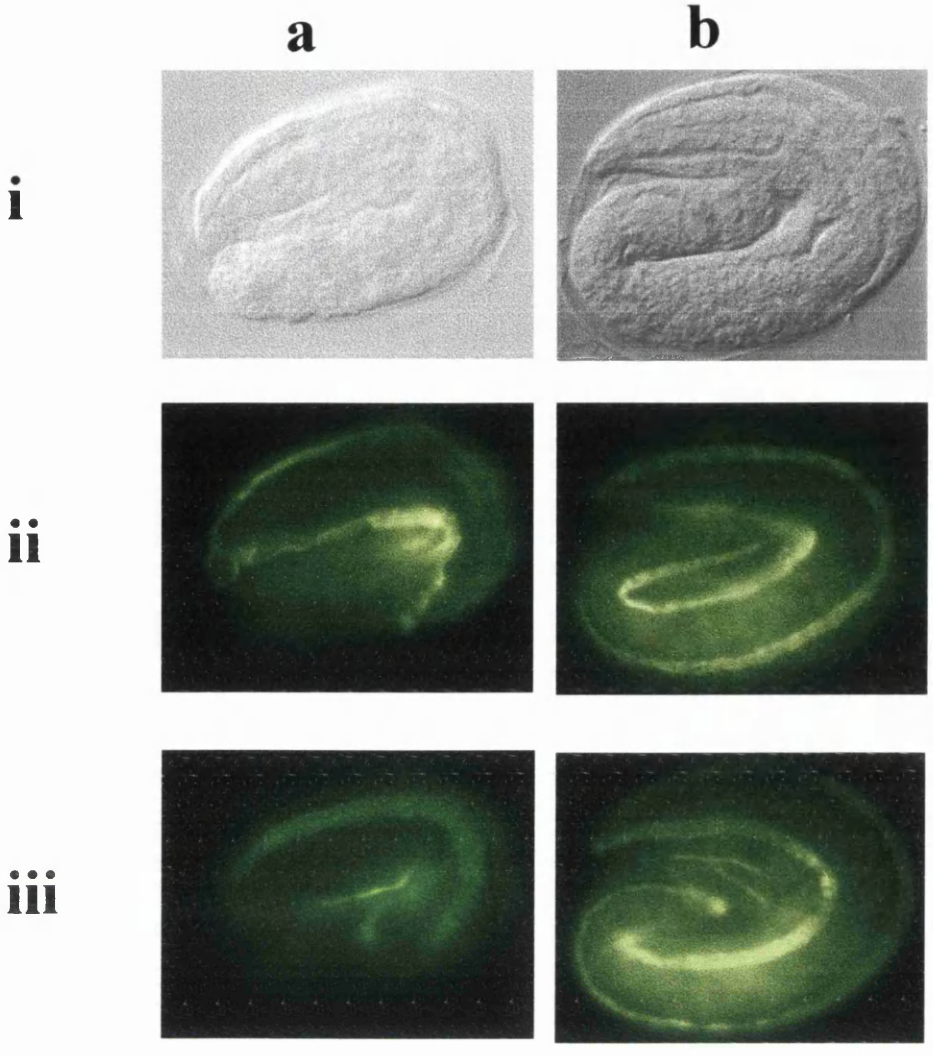

Figure 4.9

Positions of muscle:muscle and muscle:hypodermis junctions in *w4* unhatched mutants and wild type embryos

Embryos were stained with the monoclonal antibody MH3 which recognises several isoforms of the protein UNC-52 present in the basement membrane between adjacent muscle cells and muscle:hypodermal cells. In all images the anterior is to the left and the dorsal region is to the top and right.

a *w4* unhatched mutant

i DIC image

ii and **iii** MH3 staining pattern at the two sides of the mutant embryo.

b 3-fold wild type embryo

i DIC image

ii and **iii** MH3 staining pattern at two sides of the wild type embryo.

4.2.2.5. Pharynx and intestine

The monoclonal antibody 3NB12 stains a subset of pharyngeal muscles (from 6 hours of development) and shows clearly the differentiation and morphogenesis of the pharynx in wild type embryos (Okomoto and Thomson, 1985; Priess and Thomson, 1987; Mango *et al.*, 1994a). MH27 and MH4 also stain specific areas of the marginal cells in the terminally differentiated pharynx. In unhatched mutants, all antibody staining showed that the pharynx is differentiated fully but is shorter than wild type probably due to the shorter body length and internal rupture (Figure 4.10a,c,e). Together, 3NB12, MH27 and MH4 stain muscle, adherens junctions, and hemidesmosomes respectively within the pharynx and so it seems that apart from some shortening resulting from a detached buccal cavity, several representative cell types within the pharynx are present as normal.

MH27 staining also showed that intestinal adherens junctions appear normal in *w4* mutants (Figure 4.10c). The refractile gut granules of the intestine can also be seen clearly in Figure 4.1bi and di.

4.3. Mapping

As a first step towards cloning the wild type copy of the *w4* allele, I mapped the mutant allele using classical genetic methods. Initially the chromosome assignment cross was performed using a triply mutant strain and then the mutant allele was positioned relative to other genes on that chromosome using a variety of two- and three-factor crosses. Whilst three-factor crosses are used to order the genes, two-factor crosses are more important in calculating the distance of the mutant allele from a marker gene. Because of this, it is important to perform two-factor crosses with marker genes that have been accurately mapped or cloned. A big factor in mapping an allele is the marker genes that are chosen to map it and how accurately these have previously been positioned on the genetic map. The area of study, the right arm of chromosome I, turned out to be very sparse in good marker genes and, at the time of characterising this mutant, had many gaps in the physical sequence. The genes used as markers in the mapping of *w4* were *dpy-5(e61)* position 0.00±0.008 on chromosome I, *unc-75(e950)* position 9.48±0.077 (chromosome I) and *unc-101(m1)* position 13.30±0.196

Figure 4.10.

Pharynx and intestine position and shape in *w4* unhatched mutants and 3-fold wild type embryos.

Embryos were stained with the monoclonal antibodies 3NB12, MH4 and MH27 (see text for details). DIC images are in the left column (**i**) and UV images showing antibody staining are shown in the column to the right (**ii**). In all images the anterior is towards the left and in images of mutant embryos (**a, c,** and **e**) the dorsal region is to the top. In all images, arrowheads denote the four main regions of the pharynx as in Figure 4.1d.

a *w4* unhatched mutant

ii 3NB12 staining of the mutant embryo showing the position of pharyngeal muscles which appears to show differentiation equivalent to wild type but much less elongation of the pharynx.

b 3-fold wild type embryo

ii 3NB12 staining of the 3-fold embryo showing the normal position of pharyngeal muscles.

c *w4* unhatched mutant

ii MH27 staining of the mutant embryo showing the position of pharyngeal and intestinal adherens junctions which again appears differentiated as wild type but shows much shorter structures.

d 3-fold wild type embryo

ii MH27 staining of the 3-fold embryo showing the normal position of pharyngeal and intestinal adherens junctions.

e *w4* unhatched mutant

ii MH4 staining showing the position of intermediate filaments within the marginal cells of the mutant embryo pharynx. Again these structures appear differentiated as wild type but are not as elongated.

f 3-fold wild type embryo

ii MH4 staining of the 3-fold embryo showing the normal position of intermediate filaments within the marginal cells of the mutant embryo pharynx.

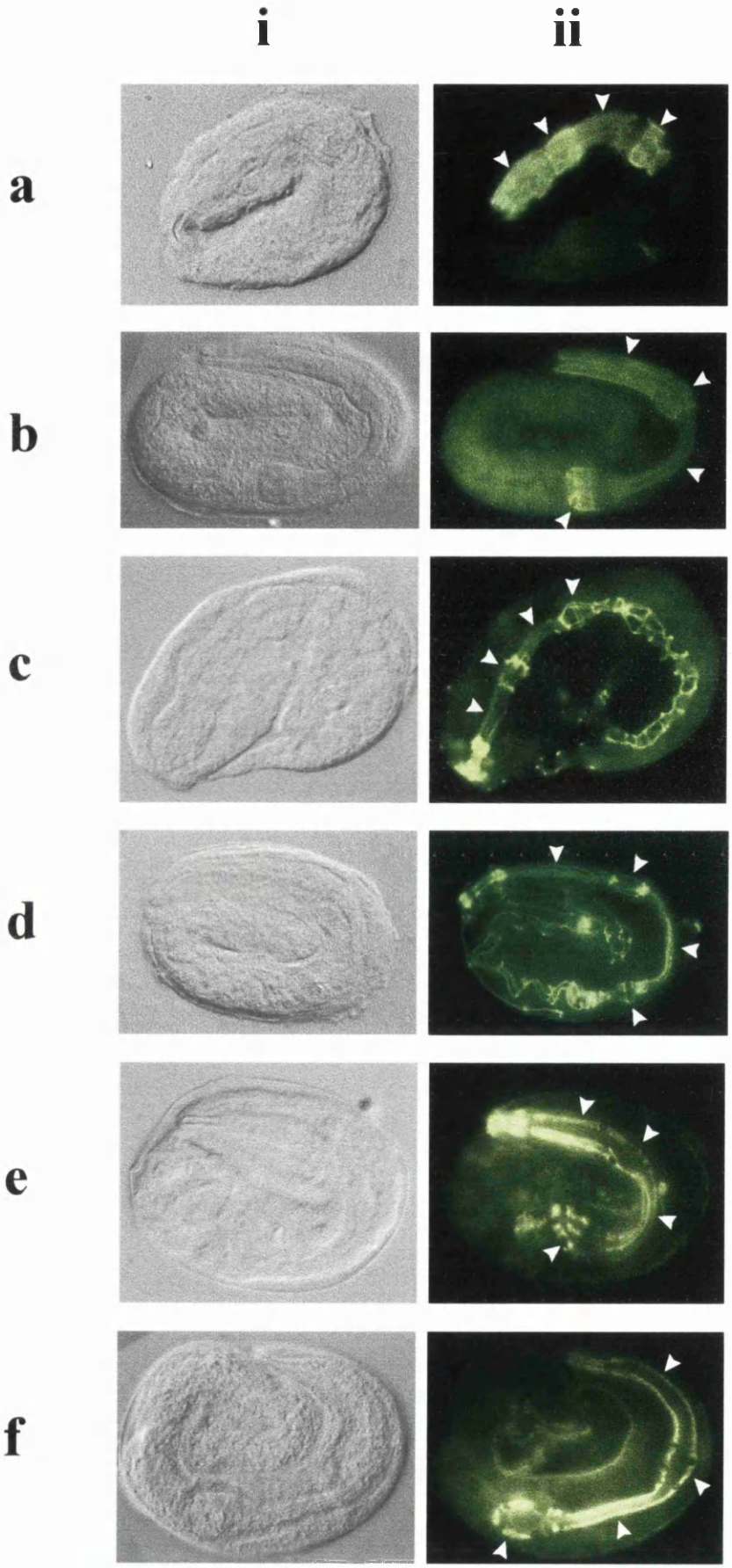
i
ii
a
b
c
d
e
f

(chromosome I). *dpy-5(e61)* is a strong dumpy, *unc-75(e950)* is sluggish, short and coils if touched on the anterior tip of the head, but moves forward well, and *unc-101(m1)* resembles *unc-75(e950)* but is also slightly egg-laying defective (Egl) and moves less well. A problem with comparing results from crosses in which strong dumpys are scored with crosses in which Uncs are scored, is that the dumpy phenotype is much more obvious and will be scored more easily. Care must be taken in interpreting the results as mis-scoring of Uncs, especially less strong Uncs, may occur and this may effect the map distance calculated.

4.3.1. MT465 Chromosomal Assignment Cross

I crossed the heterozygote mutant strain carrying the *w4* mutation with N2 males to produce male F1s carrying the mutation. These F1 males were then mated with hermaphrodites of the MT465 strain which are homozygous for three recessive mutant marker genes: *dpy-5(e61)* I, *bli-2(e768)*II, and *unc-32(e189)* III. I scored the F1 generation of this cross (which were phenotypically wild type) for segregation of lethal mutants. All of these F1s were heterozygous for each of the three marker genes and approximately 50% carried the *w4* mutation and so it was evident that *w4* did not lie on the X chromosome. If *w4* did lie on X, hemizygous males which have only one X chromosome would be lethal and therefore the mutant allele could not be passed on to the next generation via males. I selected recombinant Dpy-non-Unc-non-Bli, Unc-non-Dpy-non-Bli, and Bli-non-Dpy-non-Unc F2 progeny from the F1 hermaphrodites carrying *w4* and scored the progeny of each of these classes for the number of F2s carrying the *w4* mutation. If *w4* is unlinked to the marker gene then approximately $^2/_3$ of the animals should segregate *w4* lethality (12 out of 18 animals). Results are shown in Table 4.1 and raw data in Appendix 4.2.. There is a significant deviation from the expected ratio in the dumpy recombinants which indicates that *w4* is linked to *dpy-5(e61)* on chromosome I ($p<0.001$, χ^2 test, 1df, n=18).

Table 4.1

Mapping data from MT465 Chromosomal Assignment Cross

Recombinant type	adults carrying *w4* allele	adults not carrying *w4* allele	Total number of adults
Bli-non-Dpy-non Unc	16	2	18
Unc-non-Dpy-non-Bli	14	4	18
Dpy-non-Bli-non-Unc	2	16	18

4.3.2. *dpy-5(e61)/dpy-5(e61)w4* two-factor cross

I used the *dpy-5(e61)* homozygote/ *w4* heterozygote (*dpy-5(e61)+/dpy-5(e61) w4*) mutants obtained from the MT465 cross to perform a *cis* two-factor self-cross. This cross should give the frequency of recombination between *w4* and *dpy-5(e61)*. I crossed these *dpy-5(e61)+/dpy-5(e61)w4* hermaphrodites with N2 males, picked F1 hermaphrodites clonally and allowed them to self before removing the parent. I scored the number of dumpy recombinant, phenotypically wild type, and total number of progeny of the F1s that carried the *w4* mutation, transferring the parent hermaphrodites several times so that the entire progeny was scored. The results are shown in Table 4.2. In order to measure the recombination distance between *dpy-5(e61)* and *w4*, I used a formula which allows for the production of recombinant classes of progeny and also takes into account that certain classes of progeny may be subviable (see section 2.11.3.2 for full derivation). Because both *w4* and *dpy-5(e61),w4* homozygotes are lethal, the recombination frequency was calculated using only the numbers of viable dumpy and phenotypically wild type progeny. The formula used was:

$$\frac{A}{(A+W)} = \frac{(2p-p^2)}{3}$$ (Sulston and Hodgkin, 1988).

Where A= number of viable *dpy-5(e61)* homozygote progeny, W= number of wild type progeny and p= the recombination frequency.

The mean value of p=0.099±0.00527 (n=3 broods). Therefore, the best estimate of *w4* position from *dpy-5(e61)* is 9.9map units, which corresponds to position ± 9.9±0.527 on chromosome I.

Table 4.2

Mapping data from *dpy-5(e61)/dpy-5(e61)w4* two-factor cross

Brood number	dead progeny	*dpy-5(e61)* recombinants	wild-type progeny	p
1	56	12	206	0.086
2	43	15	203	0.109
3	54	15	220	0.101

4.3.3. *dpy-5(e61)unc-101(m1)/w4* three-factor cross

In order to decide whether *w4* mapped to the left or right arm of chromosome I, I carried out a three factor cross using *dpy-5(e61)* and *unc-101(m1)* as marker mutations. *dpy-5(e61)unc-101(m1)* homozygotes were crossed with *w4* heterozygote males and the F1 hermaphrodites were allowed to self. From F1 broods carrying the *w4* mutation (parental genotype: *dpy-5(e61)+unc-101(m1)/+w4+*), Dpy-non-Unc and Unc-non-Dpy recombinant hermaphrodites were picked out clonally and allowed to self. The progeny of these hermaphrodites were scored for the presence (indicated by 25% death) or absence of the *w4* mutation. The results are shown in Table 4.3 and the raw data can be found in Appendix 4.3. These results indicated that the *w4* locus lies between *dpy-5(e61)* and *unc-101(m1)* at a ratio of 50:28. *unc-101(m1)* is at position 13.3 on chromosome I and so this would place *w4* at around position 8.5, slightly closer to *dpy-5(e61)* than the two-factor cross predicted. However, three-factor crosses are not as accurate as two-factor crosses and are of use in predicting position relative to other genes rather than actual distance from a marker gene. So the most valuable information gained from this cross was that the *w4* locus lies on the right arm of chromosome I, between *dpy-5(e61)* and *unc-101(m1)*.

Table 4.3

***dpy-5(e61)unc-101(m1)/w4* three-factor cross**

The table below shows the number of recombinant Dpy-non-Unc and Unc-non-Dpy F2 hermaphrodites carrying the *w4* mutation

Recombinant phenotype	carrying *w4* mutation	not carrying *w4* mutation	total number of recombinants
Dpy-non-Unc recombinants	30 (*dpy-5(e61)+ unc-101(m1)/ dpy-5(e61)w4+)*	13 (*dpy-5(e61)unc-101(m1)/ dpy-5(e61)+*)	43
Unc-non-Dpy recombinants	15 (*dpy-5(e61)+ unc-101(m1)/+ w4unc-101(m1)*)	20 (*dpy-5(e61)unc-101(m1)/+ unc-101(m1)*)	35

4.3.4. *dpy-5(e61)unc-75(e950)/w4* three-factor cross

From previous data, it would seem that the *w4* locus is situated to the right of, and is very closely linked to *unc-75(e950)* which has a genetic map position of 9.48±0.077. A three-factor cross between *dpy-5(e61),unc-75(e950)* homozygotes and *w4* heterozygotes was carried out in the same way as the three-factor cross described above. The results are shown in Table 4.4. This cross positioned *w4* between *dpy-5(e61)* and *unc-75(e950)* with the ratio 20:7, giving the *w4* allele an approximate position of 7. Again this differs from the *dpy-5(e61)* two-factor cross data but it coincides with the positioning of *w4* relative to the marker genes. The distance of *w4* from *dpy-5(e61)* may have been over-estimated from the previous two-factor cross.

Table 4.4

***dpy-5(e61)unc-75(e950)/w4* three-factor cross**

The table below shows the number of Dpy-non-Unc and Unc-non-Dpy recombinant F2s which carry the *w4* mutant allele:

Recombinant phenotype	carrying *w4* mutation	not carrying *w4* mutation	total number of recombinants
Dpy-non-Uncs	9 (*dpy-5(e61)+ unc-75(e950)/ dpy-5(e61)w4+*)	3 (*dpy-5(e61)unc-75(e950)/ dpy-5(e61)+*)	12
Unc-non-Dpys	4 (*dpy-5(e61)+ unc-75(e950)/+ w4unc-75(e950)*)	11 (*dpy-5(e61)unc-75(e950)/+ unc-75(e950)*)	15

4.3.5. *spe-9(hc88)/w4 unc-75(e950)* two-factor cross

A second two-factor cross was performed to measure the distance of *w4* from *unc-75(e950)*. This was scored in a slightly different way to the *dpy-5(e61)* two-factor cross as there was a third mutation, *spe-9(hc88)*, present in the mapping strain, although it was not used as a marker mutation. This strain [+ *spe-9(hc88)+/w4+unc-75(e950)*] was constructed as a balanced strain which enforces maintenance of heterozygotes as *spe-9(hc88)* homozygotes are sterile, and *w4,unc-75(e950)* homozygotes are lethal. In addition, *spe-9(hc88)* and *unc-75(e950)* are at positions 9.41±0.779 and 9.48±0.077 respectively, only 0.07 map units apart on chromosome I, therefore there is a very low recombination frequency between these two loci. I carried out the two-factor cross using essentially the same steps as before although the initial outcross was not necessary as the balanced strain was already heterozygous for both *unc-75(e950)* and *w4*. + *spe-9(hc88)+/w4+ unc-75(e950)* hermaphrodites were allowed to self and the entire brood was scored for uncoordinated (Unc) recombinants and *w4* death (Table 4.5).

Table 4.5

***spe-9(hc88)/w4 unc-75(e950)* two-factor cross**

Brood number	dead progeny	Unc progeny	total number of progeny	p
1	47	2	181	0.022
2	24	4	125	0.064
3	23	1	99	0.020
4	50	5	181	0.055
5	42	3	173	0.035
6	31	2	157	0.025
7	36	2	161	0.025
8	36	2	166	0.024
9	68	2	256	0.016
10	42	4	214	0.037
11	44	3	231	0.036
12	48	3	231	0.026
13	41	1	192	0.010
14	38	4	158	0.051

This time I could not calculate the recombination frequency, p, using the equation $(2p-p^2)/3=(A/A+W)$ because of the *spe-9(hc88)* mutation in the *unc-75(e950)/w4* heterozygote parent. The sterile *spe-9(hc88)* homozygotes could not be separated easily from the wild type progeny (W). Instead, p was calculated using the equation:

$$p = \frac{\text{Uncs present x2 (recombinant Unc chromosomes)}}{\text{total expected Unc chromosomes (if unlinked)}}$$

The number of viable Unc recombinants are multiplied by two because half of the recombinant *unc-75(e950)* chromosomes will pair with *spe-9(hc88)* and remain unseen. The results are shown in Table 4.5. The mean value of p= 0.032±0.004 (n=14 broods). These results place the *w4* locus further left (at around 6.2 on the right arm of Chromosome I). There is a high range of p values and *unc-75(e950)* homozygotes are more easily mis-scored than *dpy-5(e61)* homozygotes due to their ability to move forward well, which may render this p value less accurate than the value from *dpy-5(e61)*. Also, the method for working out the recombination frequency in this cross is

more simplified than before because of the *spe-9(hc88)* homozygotes among the wild type progeny. Therefore the *dpy-5(e61)+/+w4* two-factor cross is probably still more accurate for the map position of the *w4* allele although there may be errors in both methods of calculating p.

To conclude, the mapping data all agrees on an area within chromosome I but the absolute position appears to vary between crosses. The *dpy-5(e61)+/+w4* two-factor cross gives a value of 9.9±0.527 although other positional information obtained suggests that *w4* is closer to *dpy-5(e61)* and between *dpy-5(e61)* and *unc-75(e950)*. It is still possible that *w4* is a small deletion and this would result in inconsistent recombination frequencies when mapping the locus. Further map data could be obtained using STS mapping (Williams, 1992; section 5.3.2) when more mapped Tc1 sites are available on chromosome I.

4.4. Attempt to clone the wild type copy of the *w4* mutant gene

4.4.1. Background of DNA transformation

The *C.elegans* physical map is represented by overlapping cosmid, lambda and yeast artificial chromosome (YAC) clones covering almost the entire genome. It is also well aligned with the genetic map using genetically mapped sequences of cloned genes and as the sequencing project nears completion, the accuracy of the alignment continues to increase. Newly characterised genes that have been mapped finely to an area of the genome will be contained within cosmid or other clone sequences covering that region. An extremely useful tool available when working with *C.elegans* is the ability to generate transgenic strains (Fire *et al.*, 1986; Mello *et al.*, 1991). This can be achieved by injecting DNA molecules into hermaphrodite gonads as these molecules can recombine and be inherited as transgenic arrays in a small fraction of the progeny of the injected worms (Mello *et al.*, 1991). In each of these transgenic lines, the extrachromosomal array will be transmitted at a certain frequency, specific to each line, and so the proportion of transformed animals can be estimated at every generation. In order to clone a gene, it is possible to inject worms homozygous for a mutation with cosmids covering the region of the genome to which the mutant gene has been mapped. The wild type copy of the gene will often rescue the mutant phenotype when present as

part of an extrachromosomal array and so the gene can be identified from the rescuing cosmid or cosmids. When the mutation under study is lethal, balanced heterozygotes can be injected and the transformed homozygous descendants examined. It is known that homologous recombination is important for driving transgenic array assembly (Mello *et al.*, 1991) and so when searching for a gene in a certain region, it is the usual practice to inject groups of overlapping cosmids from this region which have shared areas of homology. This also increases the likelihood of rescue as some genes may traverse two cosmids. Each transformed line containing a transgenic array has a characteristic frequency of array transmission from generation to generation. In order to follow the transmission of arrays between generations, plasmid containing a dominant mutation resulting in a clear visible phenotype is injected with the test DNA molecules. I used the semi-dominant mutation *rol-6(su1006)* contained in the plasmid pRF4 (Mello *et al.*, 1991) which results in a helically twisted cuticle causing transformed animals to move in an obvious circular manner. Because DNA molecules have been shown to recombine when injected together, it is assumed that animals carrying the marker plasmid also carry the test DNA molecules on the same array (Mello *et al.*1991), . To ensure that the effect of all injected DNA has been studied, several lines should be examined from each set of injections as all test DNA molecules may not be present in all arrays.

4.4.2. Attempted rescue of the *w4* mutant phenotype

In an attempt to clone the *w4* gene, I determined whether cosmid(s) from the region to which *w4* was mapped could rescue the mutant phenotype. I first constructed a balanced strain which would show an obvious change in phenotype if rescue occurred. The previously mentioned strain, *spe-9(hc88)/w4 unc-75(e950),* is well balanced as *spe-9(hc88)* homozygotes are sterile and *w4unc-75(e950)* homozygotes arrest as embryos. The strain is therefore maintained by the natural selection of heterozygotes. There will be recombination events between *w4* and *unc-75(e950)* but the strain was scored for the presence of around 25% steriles and a very small number of recombinant Uncs at each generation. Recombination resulting in an *unc-75(e950)/w4spe-9(hc88)* genotype was easily detected if the ratio of Uncs increased to around 25% and there were very few

spe-9(hc88) homozygotes. If the *w4* phenotype was rescued, there would be an increase in Uncs to a percentage equivalent to the transgene array transmission frequency which is estimated from the proportion of rolling animals (Rollers) in each generation of a transmitting line. Conversely, these rescued Uncs (*w4unc-75(e950)/w4unc-75(e950)* [rescuing array]) would segregate dead embryos with the *w4* phenotype at an equivalent proportion to the loss of the rescuing array. If the increased proportion of Uncs was due to recombination rather than rescue, then unc homozygotes would segregate 25% death (*w4unc-75(e950)/unc-75(e950)*) or, on rare occasions, no death (*unc-75(e950)/unc-75(e950)*). Another indication of rescue rather than recombination is to check the extra Uncs to see if they are rollers or non rollers - this can be seen in Uncs from the twisting of their cuticle. If the extra Uncs are rescued *w4* death then they should all be rollers.

I injected 93 adult hermaphrodites from the balanced strain with a purified mix of nine cosmids from the region of chromosome I to which *w4* was mapped (Figure 4.11) along with pRF4 containing the marker mutation *rol-6(su1006)* and a plasmid, pTAG, to aid recombination between non-overlapping cosmids (see section 2.14.1). This was necessary as there were gaps between some of the injected cosmids where overlapping clones were not available. 68 F1 rollers were obtained from the injections and these were plated out in groups of 2. I obtained 5 transmitting lines from these F1s and F2 rollers were plated out clonally in order to score the phenotypes of the progeny (Table 4.6). All the F2 rollers plated out from 4 of the lines were sterile. This was completely unexpected and is statistically different from the expected ratio of 25% ($p<0.001, \chi^2$ test, 1d.f, n=73). However, one of the transmitting lines was fertile and was scored for the different phenotypes (Appendix 4.4). The line had a transmission frequency of around 13% (n=1131) and showed no evidence of rescue, with a mean of 2.67±0.78 % Uncs per brood (n=32 broods).

Table 4.6 Transmitting lines of w4 cosmid injections

Line	number of F2 Rollers plated out	F2 progeny phenotype
1	25	F2s all sterile
2	11	same proportions of different phenotypes as untransformed lines (Appendix 4.4)
3	25	F2s all sterile
4	13	F2s all sterile
5	20	F2s all sterile

Figure 4.11

Schematic diagram showing relative positions of cosmids which were injected in an attempt to rescue the *w4* mutant phenotype

A section of the physical map of the right arm of Chromosome I is shown with relative positions of the injected cosmids. Parallel vertical lines indicate breaks in the physical map which have not yet been sequenced. The nearest cloned genes are shown with their genetic map positions for reference. At the time of injections, the section indicated with a star was not present in the AceDB physical map (Thierry-Meig and Durbin, unpublished software) and so it was thought that W02B9 was the next cosmid to F28D9 available in the physical map. The cosmids shown are not to scale although overlaps are indicated by overlapping lines. Cosmids T02A8 and AA2 have not been sequenced completely to date and so their actual size is unknown.

Right arm of
Chromosome I

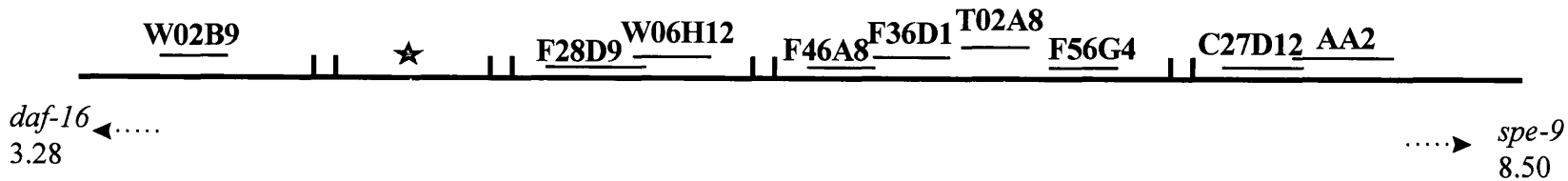

A problem with interpreting this is that a negative result may arise for many reasons and is not very informative. It does not indicate conclusively that the cosmid containing the wild type *w4* gene was not present in the mix although this would be one reason for a negative result. Some of the injected cosmids contained deletions undetected at the time of injections as the full sequence data for the cosmids under study was not available and so the restriction digest patterns could not be accurately analysed. At the time of writing, 3 of the cosmids: T02A8, AA2 and C17D12 still had unfinished sequences. Also, I do not know whether all cosmids were present in the transmitting array, in fact a low transmission frequency often indicates a small array size. Since the concentration of some of the cosmids may not have been accurate due to incorrect OD readings at low concentrations, I cannot be certain that equivalent amounts of each was added to the mix and if there was a large variation among concentrations, this may also result in some cosmids not forming part of the array. Another possible reason for a negative result is that there were many gaps in this region of the cosmid map at the time of injecting and the wild type *w4* gene may have been present within a gap, or traverse an injected cosmid and a gap, or indeed, traverse an injected cosmid and an overlapping cosmid not in the same mix. Further lines from the same mix and other overlapping cosmids from the same region would obviously have to be injected before any conclusions about rescue could be drawn.

A high incidence of sterile F2s could be explained if recombination had occurred at an early stage in the injection process and if the injected cosmids did rescue *w4*. Injection tends to give all-or-nothing results and quite often most of the transgenic lines are obtained from a very small number of injected animals. The injected adults were progeny of a correctly scored adult so a small proportion of these will be *unc-75(e950)/spe-9(hc88)w4* recombinants, and if a few recombinant adults were injected well and gave a high proportion of transmitting F1s, this would cause further selection for recombinants. The phenotypes were not scored again until the F2 progeny (F3 generation). However, even if these lines were recombinant and rescued, this does not explain why all F2 rollers were sterile.

In conclusion, the wide region that the gene was mapped to due to the lack of marker genes, the many gaps present in the physical map at the time of attempted rescue, and possible recombination events made results difficult to interpret. Therefore

I decided to terminate the characterisation of this mutant and attempt to characterise other mutant alleles which lie in better regions of the genome.

4.2.5. Discussion

w4 homozygotes arrest either as embryos with a ruptured ventral posterior surface or lumpy-dumpy L1s with a detached buccal cavity. Looking at markers for many tissue types, it can be seen that the homozygous L1s and the intact regions of arrested embryos have relatively normal muscle, basement membrane, hypodermal fusions, muscle-hypodermal connections, and also secrete a cuticle. The most likely cause of the homozygous embryonic phenotype is a failure of hypodermal cells to enclose normally at the posterior ventral surface. This results in internal tissues being squeezed out through the hypodermal 'hole' as elongation contractions occur in the hypodermis.

Both hypodermal enclosure and elongation are disrupted when actin filament function is inhibited (Priess and Hirsh, 1986; Williams-Masson *et al.*, 1997) which indicates that genes in the same pathway are controlling both processes. This may explain the percentage of lumpy-dumpy L1 homozygotes of *w4*. It is possible that there are hypodermal defects present other than that of abnormal enclosure which would not be noticed when examining the more severe phenotype. The L1s clearly do not elongate normally and have bulges on the dorsal and ventral sides. This, coupled with abnormally branched alae and a detached pharynx strongly points to a further defect in hypodermal function. MH27 shows that fusions appear normal but other aspects of elongation i.e. the actin cytoskeleton may not be.

The *hmr-1* mutant phenotype described in the introduction shares several aspects with the *w4* mutant phenotype. Most *hmr-1* or *w4* homozygotes arrest without elongating normally and with a substantial rupture of their internal organs. In *hmr-1*, and the progeny of viable Hmp mutants, hypodermal cells fail to enclose at the anterior region of the ventral surface and may also have small enclosure defects at the posterior ventral surface also. *w4* unhatched homozygotes appear to be predominantly defective in posterior ventral enclosure although very occasionally a *w4* homozygote is seen with a ruptured anterior. Interestingly, *hmr-1* maps to the same region of chromosome I as *w4* and is rescued by the cosmid W02B9 which was one of the cosmids I injected in my

attempt at cosmid rescue. Due to the similarity in the phenotypes and map positions, It is possible that *w4* is an allele of *hmr-1*. It would be interesting to attempt cosmid rescue with W02B9 to test this idea, or look at complementation with another *hmr-1* allele.

w4 produces an interesting phenotype connected with aspects of hypodermal development such as enclosure and elongation. When more sequence data is made available it would be beneficial to the understanding of these processes to clone this gene and examine the role of the encoded protein.

Chapter 5

Characterisation of a deficiency, *ijDf2*

5.1. Introduction

5.1.1. Genetic mutant screens

ijDf2 and *ijDf1* (see next chapter) are mutants that were obtained by Ethyl methanesulphonate (EMS) mutagenesis of a stable transgenic *C.elegans* strain, IA023 (I.Johnstone, pers.comm.). IA023 contains an integrated copy of a *dpy-7* promoter::GFP transgene. As discussed in chapter 3, *dpy-7* is a cuticular collagen gene which is expressed specifically in the hypodermis and therefore the GFP expression pattern in IA023 was used to facilitate the identification of mutants with hypodermal defects. As *dpy-7* is normally expressed at the beginning of elongation, the *dpy-7*::GFP expression pattern indicates the developmental maturity of the hypodermis. The GFP expression pattern also allows a rapid estimation of the stage of mutant embryo elongation using a dissecting microscope with a UV source, prior to selecting mutants for more detailed phenotypic characterisation. Both *ijDf2* and *ijDf1* were selected for study as they expressed *dpy-7*::GFP but failed to elongate normally.

5.1.2. Gastrulation in *C.elegans*

Gastrulation is the process whereby descendants of the founder blastomeres E, MS, AB and P_2 (C, D and P_4) migrate towards the centre of the embryo allowing novel cell contacts which are important for the specification of cell fates. Without normal gastrulation, later developmental processes including enclosure of hypodermal cells (see section 4.1.2) and morphogenesis are blocked although gastrulation failure itself does not prevent individual tissues from differentiating to their terminal states (Knight and Wood, 1998). Gastrulation in *C.elegans* has been described in wild type embryos using Nomarski microscopy to follow the movements of individual cells. Several different mutants have been discovered which disrupt gastrulation and these, together with laser ablation studies, have aided in the understanding of many essential requirements of this process. However, there are still many aspects of *C.elegans* gastrulation, including its

control, which are not understood and it is hoped that the isolation of further gastrulation-defective mutants and information from other organisms will increase the body of knowledge about this process.

5.1.2.1. Cell movements and divisions before and during gastrulation in *C.elegans*

The E blastomere is one of the descendants of the EMS founder cell and generates only intestine, resulting in a total of 20 gut cells in the adult (Sulston *et al.*, 1983). Between the 8 and 15 cell stages of development, E divides generating two daughter cells, Ea, to the anterior and Ep, to the posterior. These cells are present on the ventral surface and contact the vitelline membrane which surrounds the embryo within the eggshell. At around the 24 cell stage of development, a basic blastocoele is formed in the centre of the embryo and at the 26 cell stage, gastrulation is initiated by the movement of Ea and Ep away from the vitelline membrane towards the blastocoele. The migration of Ea and Ep towards the centre of the embryo creates a fissure, known as the ventral cleft, through which other cells subsequently migrate. At the end of their migration, around the 44 cell stage, Ea and Ep divide once in a left/right orientation and afterwards continue to divide further until a rudimentary gut is formed at the 180 cell stage. P_4 is the next cell after Ea and Ep to migrate through the ventral cleft and 4 granddaughters of MS follow from an anterior position. At around the 100 cell stage, the ventral cleft widens and myoblasts derived from the C and D founder cells enter from the posterior. After this, AB derived pharyngeal precursors enter the ventral cleft from the anterior and the cleft closes. Internal cell movements continue as the myoblasts are positioned between the gut and the hypodermis and eventually the gut and pharyngeal precursors lie in a central tube surrounded by MS-, C- and D-derived myoblasts.

5.1.2.2. Mutants showing specific defects in gastrulation

Maternal effect mutations in any of the genes *gad-1*, *emb-5*, *emb-13, emb-16*, *emb-23* or *emb-31* cause failure of either the initiation or the later stages of gastrulation (Knight and Wood, 1998; Denich *et al.*, 1984; Nishiwaki *et al.*, 1993). In all of the mutants, the Ea and Ep divisions occur prematurely and often in an anterior/posterior

rather than the normal left/right orientation. In the temperature sensitive mutation *gad-1*, this premature division results in a complete lack of gastrulation movements and this suggests that the control of cell cycle timing and spindle orientation in the E lineage at this stage may be important for normal gastrulation (Knight and Wood, 1998). *gad*-1 encodes a protein which has a series of WD repeats similar to G_β proteins. G-protein signalling is one of several mechanisms controlling spindle orientation, and mutations in the *gbp-1* gene, which encodes the G_β subunit in *C.elegans*, result in randomised spindle orientations in early embryos (Zwaal *et al.*, 1996). Of the *emb* genes, the only one to be molecularly characterised to date, *emb-5,* has been shown to encode a protein similar to the STP6 protein of *Saccharomyces cerevisiae* which is thought to regulate transcription by controlling chromatin assembly (Nishiwaki *et al.*, 1993). It has previously been shown that inhibition of RNA polymerase II using RNA interference also causes premature Ea and Ep divisions and prevents gastrulation initiation (Powell-Coffman *et al.*, 1996). This would suggest that one or more zygotically transcribed genes are essential for the initiation of gastrulation and that these are regulated by the maternal-effect genes described here. There are several zygotically transcribed genes, *end-1* and *rrs-1*, which result in gastrulation defects although they do not block its initiation and so it appears that there remains a zygotically transcribed gene or genes involved in the initiation of gastrulation as yet undiscovered (Ferguson *et al.*, 1996; Zhu *et al.*, 1997).

5.1.2.3. The involvement of cell adhesion in gastrulation

It has been proposed that Ea and Ep initiate their inward movements by reducing adhesive contacts with neighbouring cells (Junkersdorf and Schierenberg, 1992). Although none of the genes already known to affect gastrulation have been shown to encode proteins involved in adhesion, it seems likely that cell adhesion would play a role in this stage of gastrulation. In *Drosophila,* gastrulation also involves the inward movements of mesoderm and endoderm precursors although there are two regions of invagination, the ventral furrow through which mesodermal precursors invaginate, and the posterior midgut invagination through which endodermal precursors invaginate (Sweeton *et al.*, 1991). Another difference to *C.elegans* gastrulation is that the invaginating cells in *Drosophila* undergo shape changes although those in *C.elegans* do not (Sweeton *et al.*, 1991; Oda *et al.*, 1998). In *Drosophila*, the *D*E-cadherin-catenin

system which comprises *D*E-cadherin, Armadillo (β-catenin), and *D*α-catenin, is involved in cell shape changes, motility and adhesion in the invaginating mesoderm via changes in localisation and adherens junction formation within the cells (Oda *et al.*, 1998). However, while genes encoding homologues of α-catenin, Armadillo and classical cadherin in *C.elegans*, *hmp-1, hmp-2* and *hmr-1* respectively, are involved in cell shape change during morphogenesis, they do not appear to be required for general cell adhesion, polarity or the formation of adherens junctions (Costa *et al.*, 1998). Mutants of these genes show no gastrulation defects and phenotype is only observed in later stages of embryogenesis. These results would seem to suggest that if there are cell adhesion processes acting during *C.elegans* gastrulation to enable the migration of cells, then they involve different components to the cadherin-catenin systems seen in other species during embryonic development.

5.1.3. Hypodermal enclosure

After gastrulation is completed, hypodermal cells, which arise on the dorsal surface of the embryo migrate laterally and eventually meet and fuse at the ventral midline, completely encasing the embryo in an outer monolayer of hypodermis (Sulston *et al.*, 1983). Hypodermal enclosure and its role in subsequent morphogenetic processes mediated by the hypodermis is discussed in detail in section 4.1.2.

5.2. Phenotypic characterisation

ijDf2 was outcrossed four times before phenotypic characterisation was attempted and all mutant embryos described are *ijDf2* homozygous progeny of an *ijDf2* heterozygote mother. At 20°C, 100% of *ijDf2* homozygotes arrest as unhatched embryos with a complete absence of elongation (Figure 5.1a). They have a lumpy shape and do not appear to secrete a cuticle which was initially thought to be a possible cause of the phenotype seen. However, the phenotype manifests itself much earlier than the time of cuticle secretion (see below). No difference was seen in the phenotype at 16°C or 25°C (Figure 5.1b,c) and no maternal effect was observed. From time-course studies, the embryo develops as normal apparently until just prior to the precomma stage of development (Figure 5.2a). Then, as wild type embryos develop to the

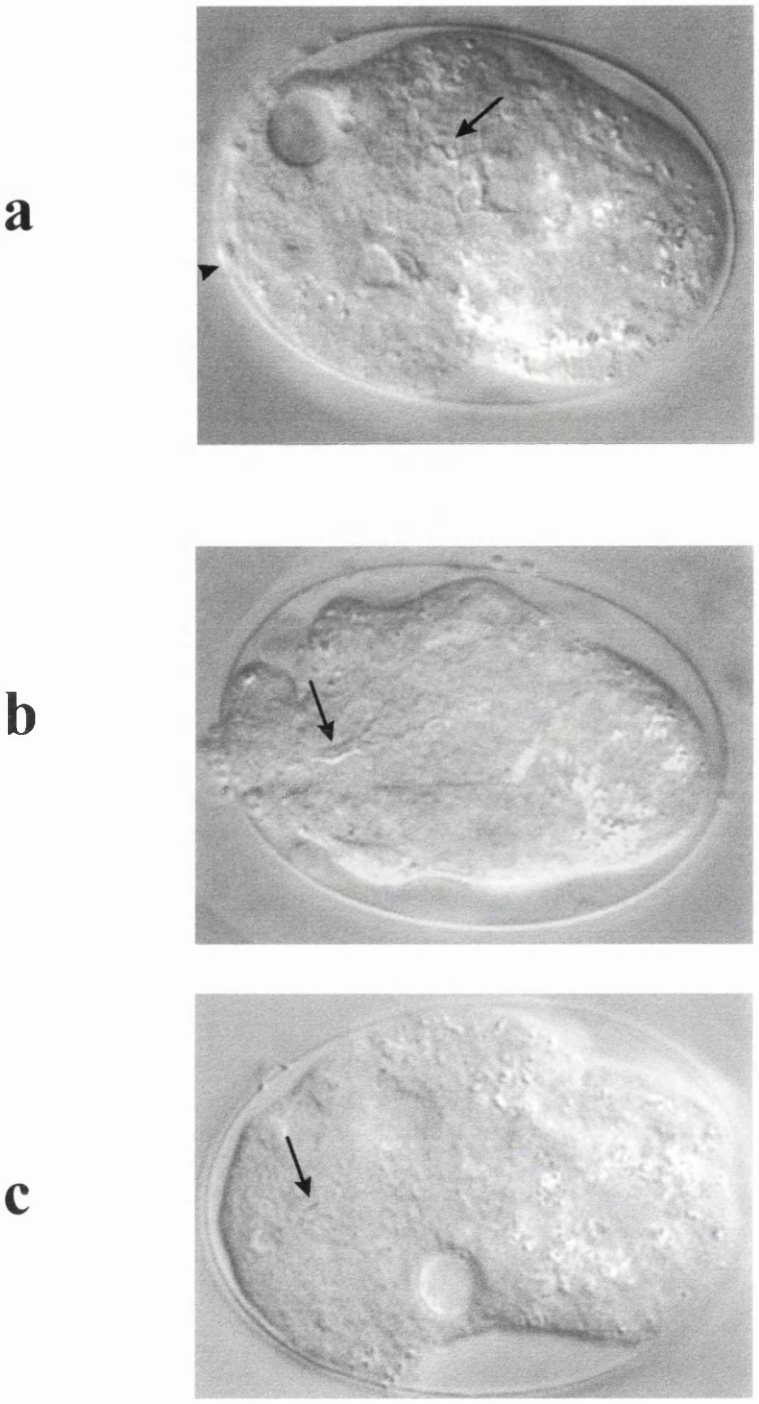

Figure 5.1

DIC images of *ijDf2* homozygote terminal arrest phenotypes at various different temperatures.

The anterior of all images is to the left. Arrows point to the buccal cavity in all images

a 20°C arrest. The arrowhead indicates the maternal pole cell

b 16°C arrest.

c 25°C arrest.

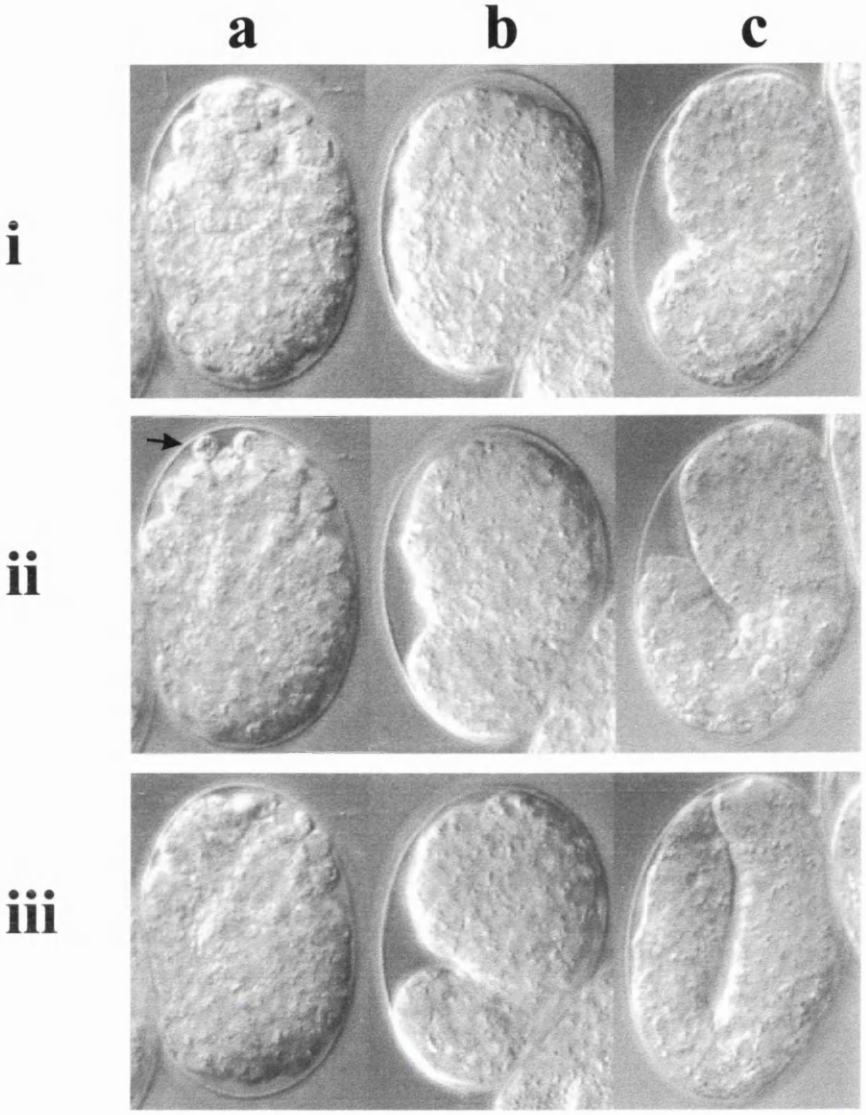

Figure 5.2

DIC images of *ijDf2* homozygote and wild type embryos during development

All embryos are positioned with the anterior to the top of the image and embryos **b** and **c** have the dorsal region to the right of the image. Images **b** and **c** are wild type embryos and image **a** is an *ijDf2* homozygote which is approximately the same age as the wild type embryo in image **b**.

i Embryos **a** and **b** are at the precomma stage of development while embryo **c** is at the comma stage

ii 60 mins after **i.** Note the loose cells in mutant embryo **a** indicated with an arrow. Embryo **a** has not elongated at all while embryo **b** has progressed to the comma stage.

iii 95 mins after **i.** Embryo **b** has reached the 1.5-fold stage while embryo **a** still has not begun morphogenesis and the shape of the mutant embryo has become more irregular.

comma and 1.5-fold stages, *ijDf2* mutant embryos begin showing an irregular outline with surface cells rounding up and not forming tight boundaries with neighbour cells (Figure 5.2b). Wild type embryos then elongate rapidly while the mutant embryos develop into a much more amorphous shape without elongating at all (Figure 5.2c). Most of the *ijDf2* embryos observed showed some rupture or 'oozing' of cells into the eggshell cavity and they remained flaccid and lumpy until the end of embryogenesis. These observations ruled out the absence of a cuticle as the cause of the observed phenotype as the initial defect was seen long before the time of normal cuticle secretion.

Very few tissues or structures can be distinguished within the *ijDf2* mutant embryos using DIC microscopy. In most embryos, the central canal of the pharynx can be seen running through the anterior midsection of the embryo and occasionally the buccal cavity can be seen (Figure 5.1 arrows). However, a recognisably normal pharyngeal structure appears to be completely absent. I found it impossible to orientate the dorsal and ventral surfaces of the mutants, and was only able to distinguish between anterior and posterior by assuming the position of the underdeveloped pharynx was towards the anterior and that gut autofluorescence was towards the posterior. The mutant embryos show irregular muscle twitching although there are no large scale movements.

Because of the lack of information from DIC observations, I used several reagents to view different structures and tissues. Terminal markers of muscle, basement membrane, muscle-hypodermis attachments as well as several pharyngeal components and markers of hypodermal and cuticle development were used to determine aspects of the *ijDf2* phenotype. In a mutant with such an abnormal end phenotype, the terminal pattern of marker reagents may be misleading and possibly the more important information to be obtained from these markers is the presence or absence of a specific expression pattern, tissue, or structure. Antibody staining, or GFP expression, patterns would be very informative at the time when the phenotypic defect is first manifested. Unfortunately, at the precomma stage of development most of the hypodermal and other marker antibodies I used have very faint patterns which are difficult to interpret. Also, it is very difficult to detect mutant embryos at an early stage in a mixed slide of wild type and mutant embryos after the antibody staining process.

5.2.1. Hypodermis

MH27 is a monoclonal antibody which recognises a protein component of the adherens junctions between the apical surfaces of hypodermal cells and within the intestine (Priess and Hirsh, 1986; Waterston, 1988). In *ijDf2* mutants the hypodermal cell boundaries are completely disorganised compared to wild type embryos (Figure 5.3a-c). There are clusters of very small cells and larger areas without internal boundaries which probably correspond to the seam and P mononucleate cells compared to the large multinucleate syncytia of hyp7. In order to examine whether the large blank areas were regions lacking hypodermal cells, or whether they were large hypodermal syncytia, I co-stained with the anti-LIN-26 polyclonal antibody which recognises LIN-26, a nuclear protein present in all hypodermal cells (Labouesse *et al.*, 1996). The co-staining indicated that hypodermal cells did cover the surface of *ijDf2* homozygotes and that both syncytia and mononucleate cells are present (Figure 5.3d). It is difficult to determine whether they are in the right positions relative to one another as the embryo is so amorphous. There are clusters of mononucleate cells, presumably the lateral seam and P cells, although they do not appear to lie in the same positions in each mutant although this may be due to stained embryos lying in various different orientations. Wild type embryos tend to lie on their lateral sides during elongation as the shape of the embryo promotes this orientation. *ijDf2* embryos do not have the dorsal bend seen in early wild type embryos and so there is no constraint against lying on the dorsal or ventral sides. Because the hypodermis is so disorganised and the embryos are orientated in different positions, it was difficult to observe the number of mononucleate cells present and the numbers of nuclei in the syncytia. There are large syncytia present with many nuclei present and smaller cells just with 2 or 3 nuclei. However, the overall number of hypodermal cells (multinucleate and mononucleate) was determined for 5 embryos and appears to be well below the normal number of 43, possibly indicating hyperfusion of cells (Table 5.1).

Figure 5.3

Hypodermal cell shapes and positions in *ijDf2* homozygotes and wild type embryos

Embryos were stained with the monoclonal antibody MH27 to visualise the adherens junctions between hypodermal cells (images **a-e**) and the polyclonal antibody anti-LIN-26 to visualise hypodermal cell nuclei (images **d** and **e**). wild type embryos are positioned with the anterior to the left and the dorsal surface to the top of the image. *ijDf2* homozygotes are positioned with the anterior either to the right or left although the actual orientation could not be determined. DIC images are shown in column **i** and antibody staining of the two lateral sides of the embryo is shown in columns **ii** and **iii**.

a *ijDf2* homozygote stained with MH27 showing very disorganised hypodermal cells.

b wild type embryo at the 1.5-fold stage stained with MH27

c wild type embryo at the 3-fold stage stained with MH27

d *ijDf2* homozygote stained with MH27 and anti-LIN-26 showing the presence of mononucleate (arrow) and multinucleate (arrowhead) hypodermal cells

e wild type embryo at the comma stage stained with MH27 and anti-LIN-26. Hypodermal cells have not fused into syncytia at this stage.

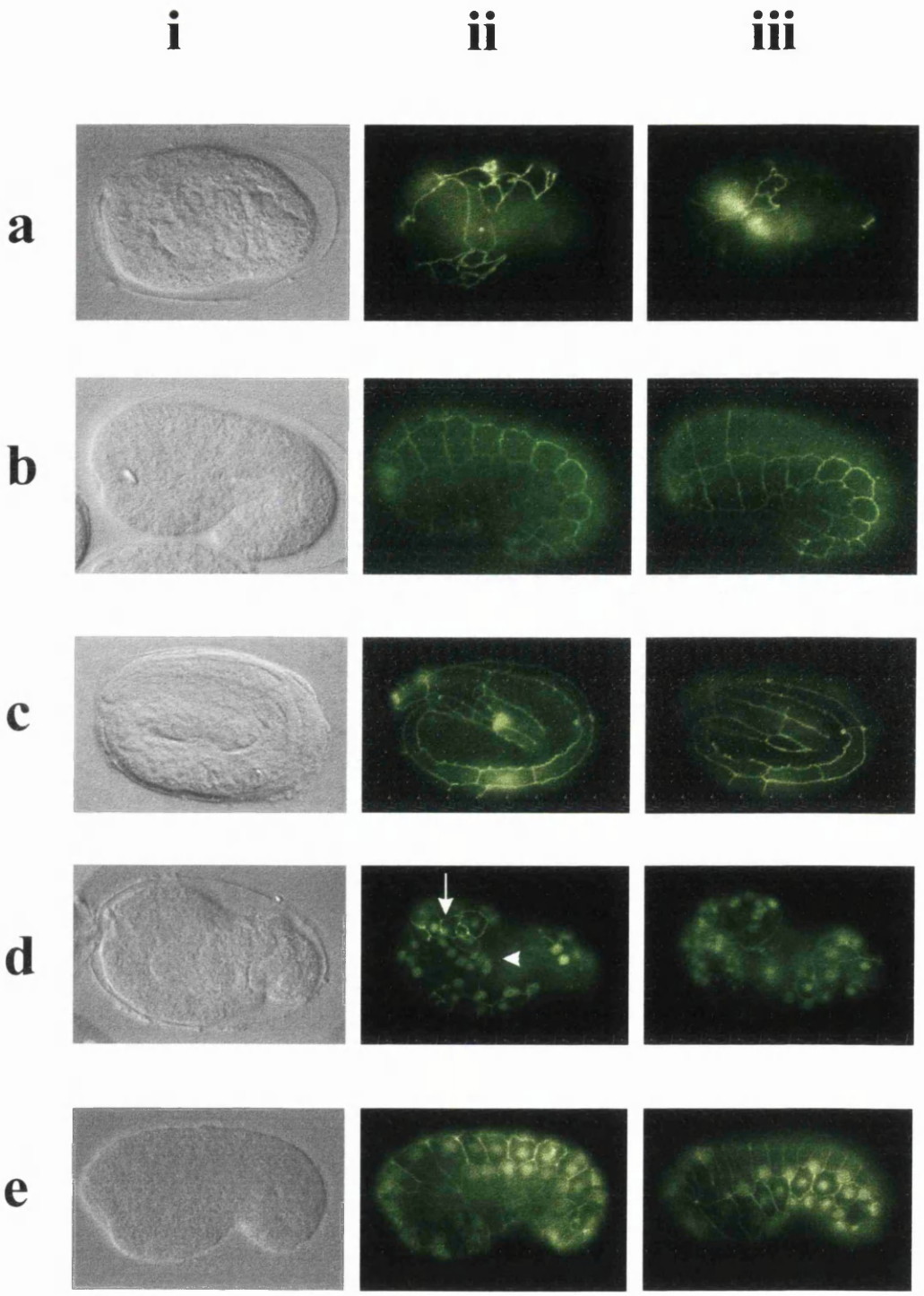
i
ii
iii
a
b
c
d
e

Table 5.1

Total number of hypodermal cells in five different *ijDf2* homozygote embryos

ijDf2 homozygous embryo	Total number of hypodermal cells	Comments
A	27	Some cells were much smaller than normal seam or P cells
B	31	
C	36	Some cells were much smaller than normal seam or P cells
D	23	
E	30	

5.2.2. Cuticle

The expression patterns of two cuticular collagens were visualised by crossing the *ijDf2* mutant strain into two stains containing an integrated copy of either a *col-12* promoter::GFP (IA022) or a *dpy-7* promoter::GFP (IA105) transgene. These collagens, *dpy-7* and *col-12* are two of the structural proteins which form the cuticle and are synthesised within hypodermal cells. *dpy-7* expression begins in wild type embryos at around the comma stage (Johnstone and Barry, 1996). Conversely, *col-12* is among the last group of collagens to be expressed and normal expression is not seen until after the *C.elegans* embryo has completed elongation. The constructs used were nuclear localised for easier examination of the pattern, although the nuclear localisation is much clearer with the *dpy-7* construct.

ijDf2 homozygotes express both *dpy-7* and *col-12* collagen::GFP reporter transgenes although the *col-12* expression pattern is irregular (Figure 5.4). A striking difference is that the terminal pattern of the *dpy-7*::GFP reporter construct shows a clear pattern of hypodermal cells which does not vary widely between embryos (Figure 5.4a) but the *col-12*::GFP reporter construct is only present in several areas of each embryo and the pattern is not consistent between embryos (Figure 5.4c). The *dpy-7*::GFP reporter construct expression pattern also shows clearly that hypodermal nuclei are present over all of the embryo surface. The presence of *col-12*::GFP reporter construct expression indicates that at least some hypodermal cells have developed to a

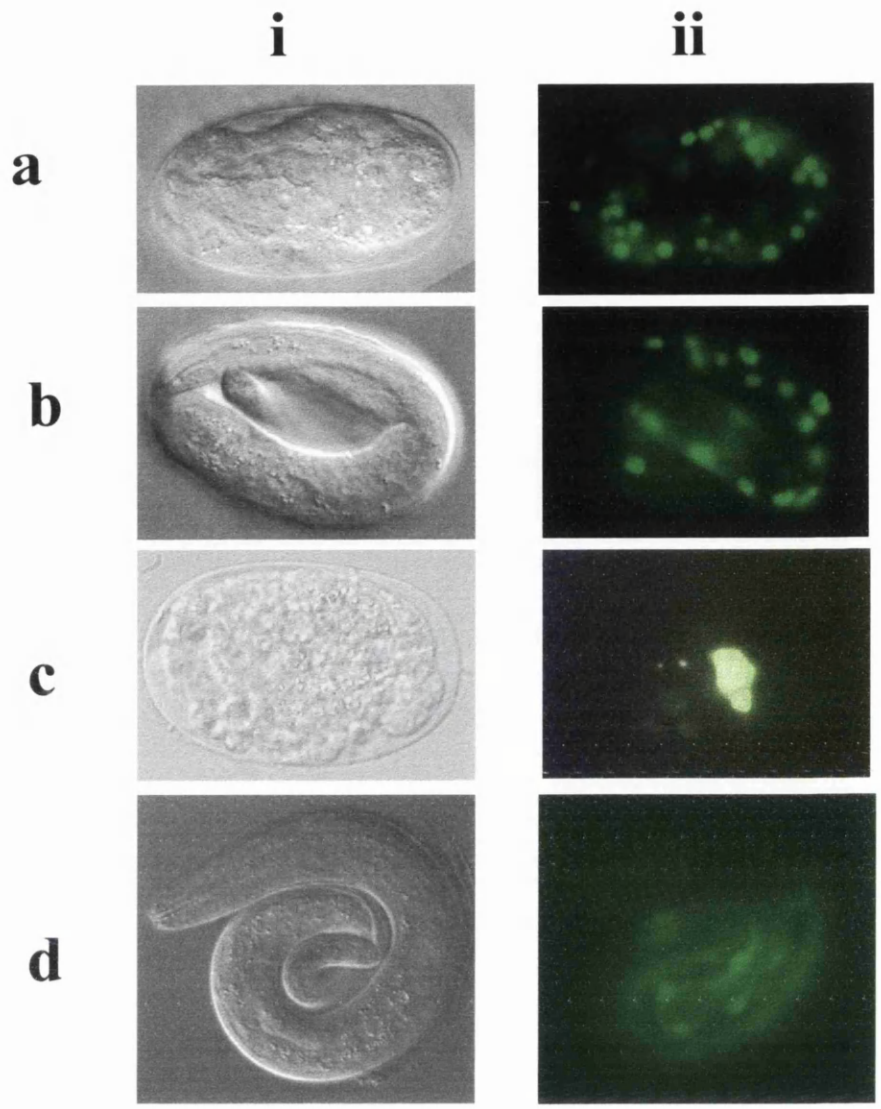

Figure 5.4

Expression of cuticular collagen::GFP constructs in the hypodermis of *ijDf2* homozygotes and wild type 3-fold stage embryos

All embryos are positioned with the anterior to the left of the image. DIC images are shown in column **i** and UV images showing collagen::GFP expression are shown in column **ii**.

a *ijDf2* homozygote showing the expression of a *dpy-7*::GFP nuclear localised transgene

b wild type 3-fold stage embryo showing *dpy-7*::GFP expression

c *ijDf2* homozygote showing the expression of a nuclear localised *col-12*::GFP transgene

d wild type 3-fold stage embryo showing *col-12*::GFP expression. This transgenic line had a very weak expression pattern so the expression shown is faint.

terminal stage with respect to collagen synthesis. However, the localised regions of *col-12*::GFP reporter construct expression are very different to normal and may indicate some abnormality in hypodermal function at this time.

The monoclonal antibody DPY7-5a, which recognises the carboxy terminal of the cuticular collagen DPY-7 (Chapter 3), was used to test for the presence of a cuticle with anti-LIN-26 antibody used as a marker of proper permeabilisation and fixing (Figure 5.5). No secreted cuticle was observed in the majority of *ijDf2* homozygotes although in rare cases there are very small patches of staining at the surface. In wild type embryos, intracellular staining of DPY-7 is much fainter than secreted DPY-7 staining but this did not appear to be present within *ijDf2* homozygotes at all. The very patchy staining on mutant embryo surfaces is apparently artefactural as it was only seen on a small number of specimens, and so it could be concluded that DPY-7 was not produced in these mutants which would be surprising as the GFP reporter construct shows that *dpy-7* is transcribed. Another possibility is that DPY-7 is produced within the hypodermal cells but is not secreted normally resulting in subsequent rapid degradation of the intracellular collagens and therefore a complete, or near complete, absence of DPY7-5a staining. As it is almost impossible to distinguish fixed early *ijDf2* embryos, at the time when DPY-7 should be present intracellularly, from precomma stage wild type embryos, it would be very difficult to test whether DPY-7 is indeed synthesised within hypodermal cells but not secreted.

5.2.3. Muscle

DM5.6 is a monoclonal antibody which recognises a component of the body wall muscle myosin heavy chain- myosin A (Miller *et al.*, 1983; Hresko *et al.*, 1994 and Moerman *et al.*, 1996). Clear DM5.6 staining is present in *ijDf2* mutant embryos and the pattern is completely irregular, although there appears to be a general organisation into sarcomeres in some *ijDf2* homozygotes (Figure 5.6). In other *ijDf2* mutant embryos, the bright DM5.6 staining branches throughout the entire embryo. It is evident from the pattern, however, that the muscle is positioned internally and so the cells have migrated inward at some point during development.

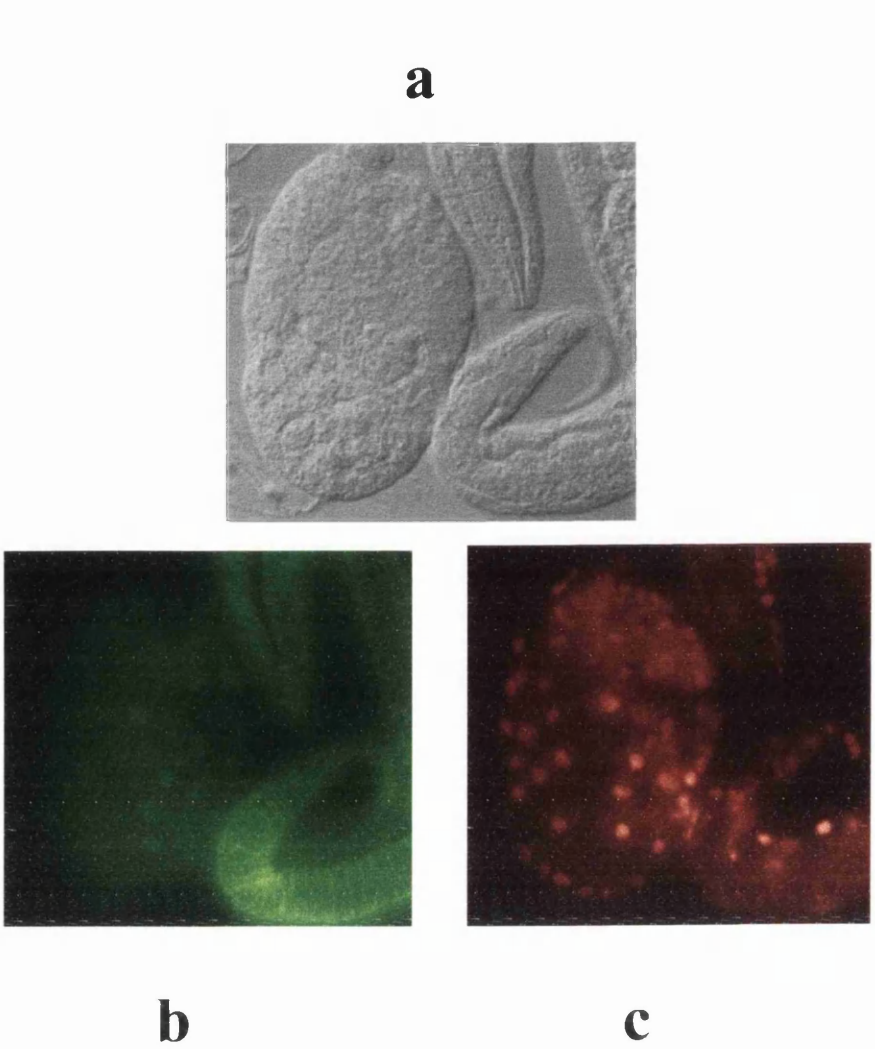

Figure 5.5

Localisation of a cuticular collagen, DPY-7, in *ijDf2* homozygotes and wild type 3-fold stage embryos indicating the presence or absence of a cuticle

Embryos were stained with the monoclonal DPY7-5a antibody and the polyclonal anti-LIN-26 antibody. Only one side view of the embryos is shown. The anterior of the *ijDf2* homozygous embryo (on the left) is towards the top of the image and the anterior of the wild type 3-fold embryo (on the right) is facing downwards at the centre of the image.

a DIC image

b DPY7-5a staining showing a secreted cuticle on the wild type 3-fold stage embryo to the right but shows no staining above background in the *ijDf2* embryo indicating that no DPY-7 protein is present. Faint green spots are the bleed through from the anti-LIN-26 nuclei staining.

c anti-LIN-26 staining showing that both embryos are sufficiently fixed and permeabilised

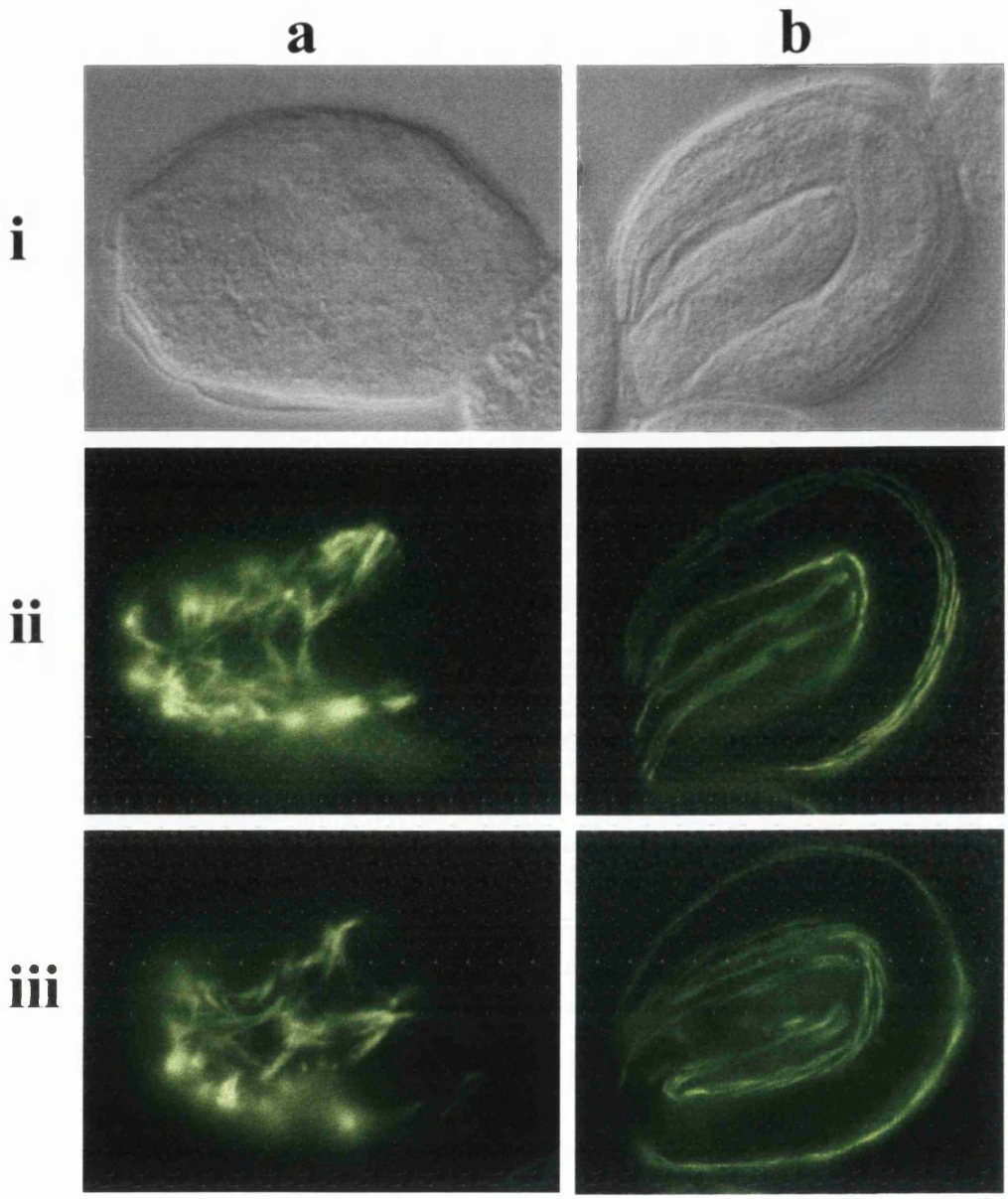

Figure 5.6

Position of muscle sarcomeres in *ijDf2* homozygotes and wild type embryos

Embryos were stained with the monoclonal antibody DM5.6 to visualise myosin A within the muscle sarcomeres. The embryo in column **b** is positioned with the anterior to the left of the image. The anterior of the embryo in column **a** is either to the right or left but the actual orientation could not be determined. DIC images are shown in row **i** and DM5.6 staining of the two lateral views of the embryo muscle sarcomeres is shown in rows **ii** and **iii**.

a *ijDf2* homozygote showing very disorganised muscle sarcomeres

b wild type 3-fold stage embryo showing the wild type position of the muscle sarcomeres

5.2.4. Muscle-hypodermis attachments and basement membrane

MH4 is a monoclonal antibody which recognises areas of the hypodermis (intermediate filaments) which are associated with underlying body wall muscle cells and also recognises regions of the pharynx, the excretory cell, and amphid sensory neurons (Francis and Waterston, 1991). In *ijDf2* mutants, MH4 staining is clearly present with a completely irregular staining pattern (Figure 5.7a). Hypodermal and pharyngeal staining could be distinguished although both staining patterns were completely incomparable to the wild type patterns (Figure 5.7b and Figure 5.9e). Hypodermal staining was not organised into bands but was widespread and in some cases radiated out from dark patches. It looked threadlike in appearance.

MH3 is a monoclonal antibody which recognises several isoforms of the basement membrane component UNC-52, a homologue of perlecan (Francis and Waterston, 1991). It is present in the junctions between muscle cells and between muscle:hypodermis connections. Again, MH3 is present in *ijDf2* embryos showing a pattern completely divergent to the wild type pattern (Figure. 5.8). Despite the disorganised pattern, there seems to be some organisation of muscle into separate sarcomeres as in wild type. Perlecan is required in wild type animals for sarcomere organisation and attachment of muscle cells (Moerman *et al.*, 1996). MH3 staining appears more organised than the MH4 pattern which is surprising as MH3 indicates junctions between muscle and hypodermal cells and MH4 is usually present in hypodermal cells overlying muscle cells. Because of this the patterns produced by the two antibodies should be quite similar. The more organised MH3 pattern may be due to muscle:muscle junctions as it follows the DM5.6 staining pattern much more closely. A very disorganised MH4 pattern could arise from a completely disorganised hypodermis although it has been shown previously that when body muscle cell precursors are ablated, the hypodermal cells that would have been in contact with them do not show MH4 staining, and so the pattern does seem to be dependent on underlying muscle cells (Hresko *et al.*, 1994).

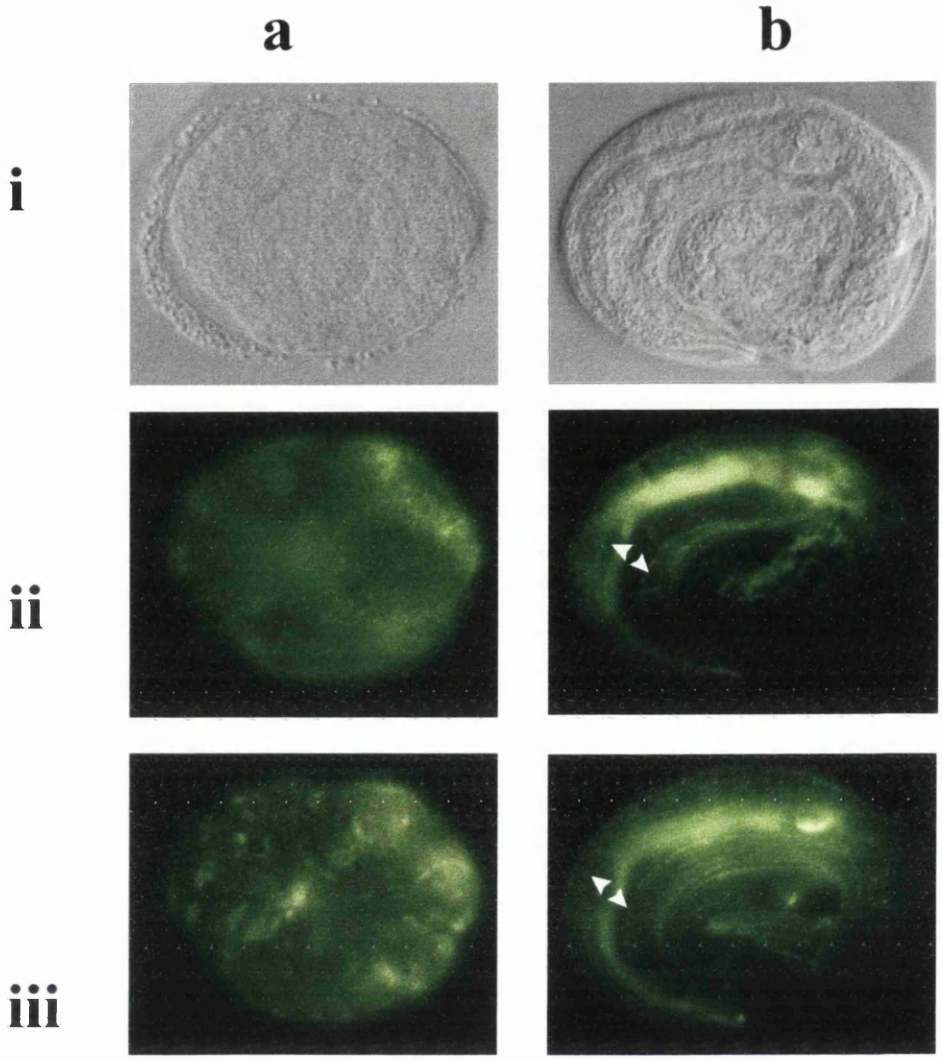

Figure 5.7

Association of the hypodermis and underlying muscle in *ijDf2* homozygotes and wild type embryos

Embryos were stained with the monoclonal antibody MH4 which recognises intermediate filaments, part of the hemidesmosomes in hypodermal cells overlying the muscle sarcomeres. The embryo in **b** is positioned with the anterior curving down to the bottom centre of the image and facing right. The embryo in **a** is positioned with the anterior facing either right or left but the actual orientation could not be determined. DIC images are shown in row **i** and MH4 staining of two lateral views is shown in rows **ii** and **iii**.

a *ijDf2* homozygote showing a very disorganised pattern of MH4 staining

b wild type 3-fold embryo showing the normal organisation of MH4 in the hypodermis. Bands of hypodermal staining are indicated using arrowheads.

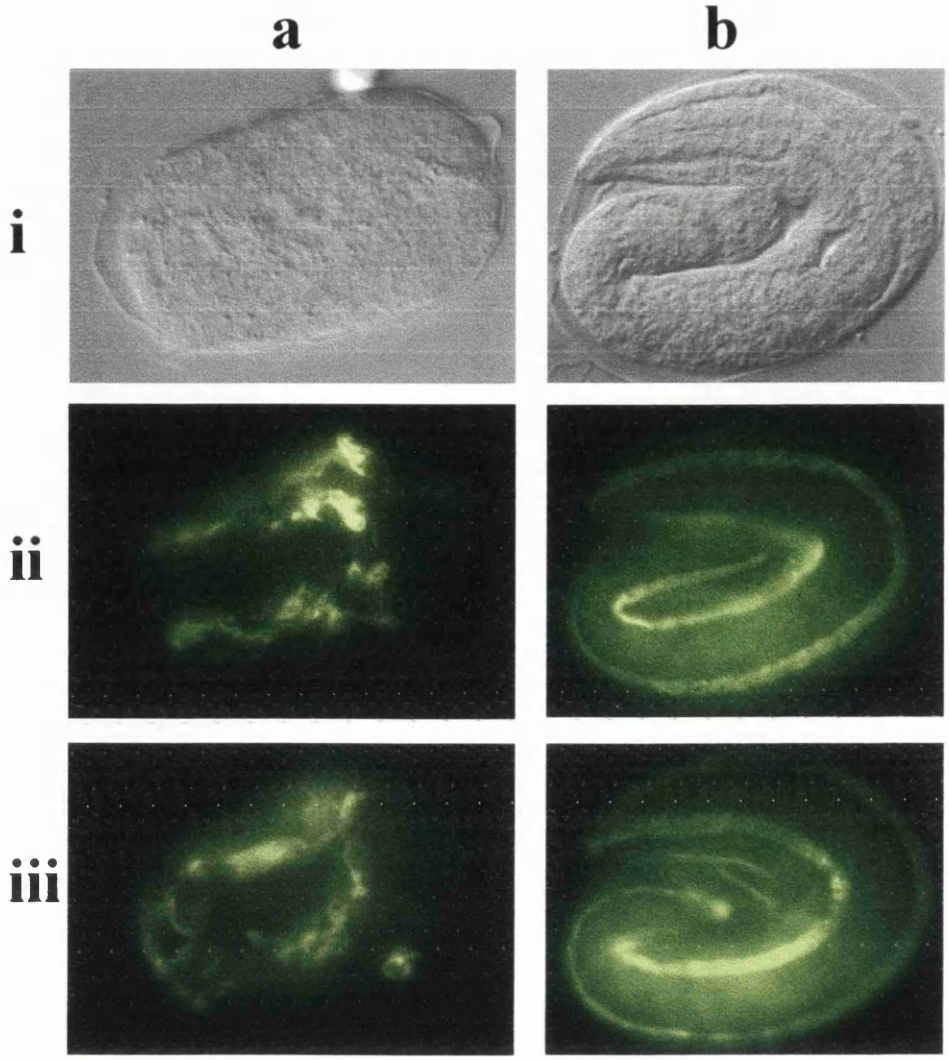

Figure 5.8

Positions of muscle:muscle and muscle:hypodermis junctions in *ijDf2* homozygotes and wild type embryos

Embryos were stained with the monoclonal antibody, MH3, which recognises several isoforms of the protein UNC-52 present in the basement membrane between adjacent muscle cells and between muscle cells and the hypodermis. In image **b** the anterior of the embryo is to the left. In image **a**, the anterior of the embryo is facing towards either the left or the right but the actual orientation of the embryo could not be determined. DIC images are shown in row **i** and antibody staining is shown in rows **ii** and **iii**.

a *ijDf2* homozygote showing a completely disorganised MH3 staining pattern

b wild type 3-fold stage embryo showing the normal MH3 pattern

5.2.5. Pharynx and intestine

The monoclonal antibody 3NB12 was used to detect pharyngeal muscle precursors and other structures were visualised by MH27 (adherens junctions) and MH4 (filaments in marginal cells). Pharyngeal muscle cell precursors were present, but showed neither elongation nor differentiation of the pharynx (Figure 5.9a,b). The staining was present internally in the mid region of the embryo. Adherens junctions could also be seen in this area, although again were distinct from wild type patterns (Figure 5.9c,d). As mentioned above, MH4 staining was present but it did not show any structures comparable to a wild type pharynx (Figure 5.9e,f). Internal MH4 staining was different in nature to the threadlike hypodermal staining seen and was completely diffuse. It seemed to be of a more disorganised nature than either 3NB12 or MH27 staining of the pharynx.

Gut autofluorescence could be seen in *ijDf2* embryos towards the mid posterior and adherens junctions were present between intestinal cells indicated by MH27 staining (Figures 5.9c, 5.10).

5.3. Mapping

ijDf2 was mapped using various different methods. Initially, before I realised that the mutation was the result of a deficiency, classical genetic methods were used to map this lesion. I also used the PCR-based method involving polymorphisms in the genome known as Sequence-Tagged Sites (STS). This enables a gene to be mapped finely by carrying out one or two simple crosses and then testing the progeny for the presence or absence of these polymorphisms (Williams, 1992 and materials and methods section). STS mapping is explained in more detail below.

After several lines of evidence indicated, unexpectedly, that *ijDf2* was a deficiency, a molecular approach was used to determine the position of the end points on the physical map. As has been mentioned, the genome of *C.elegans* is represented by overlapping clones including cosmids which comprise the physical map. In order to position a deficiency in the physical map as well as the genetic map, these maps must be aligned by equating the genetic map positions of previously cloned genes and the physical location of the cosmid sequences they are contained within. I tested for

Figure 5.9

Pharynx and intestine position and shape in *ijDf2* homozygotes and 3-fold wild type embryos.

Embryos were stained with the monoclonal antibodies 3NB12, MH4 and MH27 (see text for details). DIC images are in the left column (**i**) and UV images showing antibody staining are shown in the column to the right (**ii**). In images except **b**, the anterior is towards the left. In image **b,** the anterior is facing to the right. In all images except images **a** and **e**, arrowheads denote the four main regions of the pharynx. In images **a** and **e**, the main regions of the pharynx cannot be distinguished and so an arrow indicates the entire pharyngeal structure.

a *ijDf2* homozygote

ii 3NB12 staining of the mutant embryo showing the position of pharyngeal muscles which indicates a completely underdeveloped and unelongated pharynx.

b 3-fold wild type embryo

ii 3NB12 staining of the 3-fold embryo showing the normal position of pharyngeal muscles.

c *ijDf2* homozygote

ii MH27 staining of the mutant embryo showing the position of pharyngeal and intestinal adherens junctions which appear to be differentiated into four main regions but are still very abnormal and unelongated. The intestine is much shorter than normal.

d 3-fold wild type embryo

ii MH27 staining of the 3-fold embryo showing the normal position of pharyngeal and intestinal adherens junctions. Intestinal adherens junctions are indicated with an arrow.

e *ijDf2* homozygote

ii MH4 staining showing the position of intermediate filaments within the marginal cells of the mutant embryo pharynx. These structures appear completely disorganised and are not differentiated into a recognisable pharynx.

f 3-fold wild type embryo

ii MH4 staining of the 3-fold embryo showing the normal position of intermediate filaments within the marginal cells of the mutant embryo pharynx.

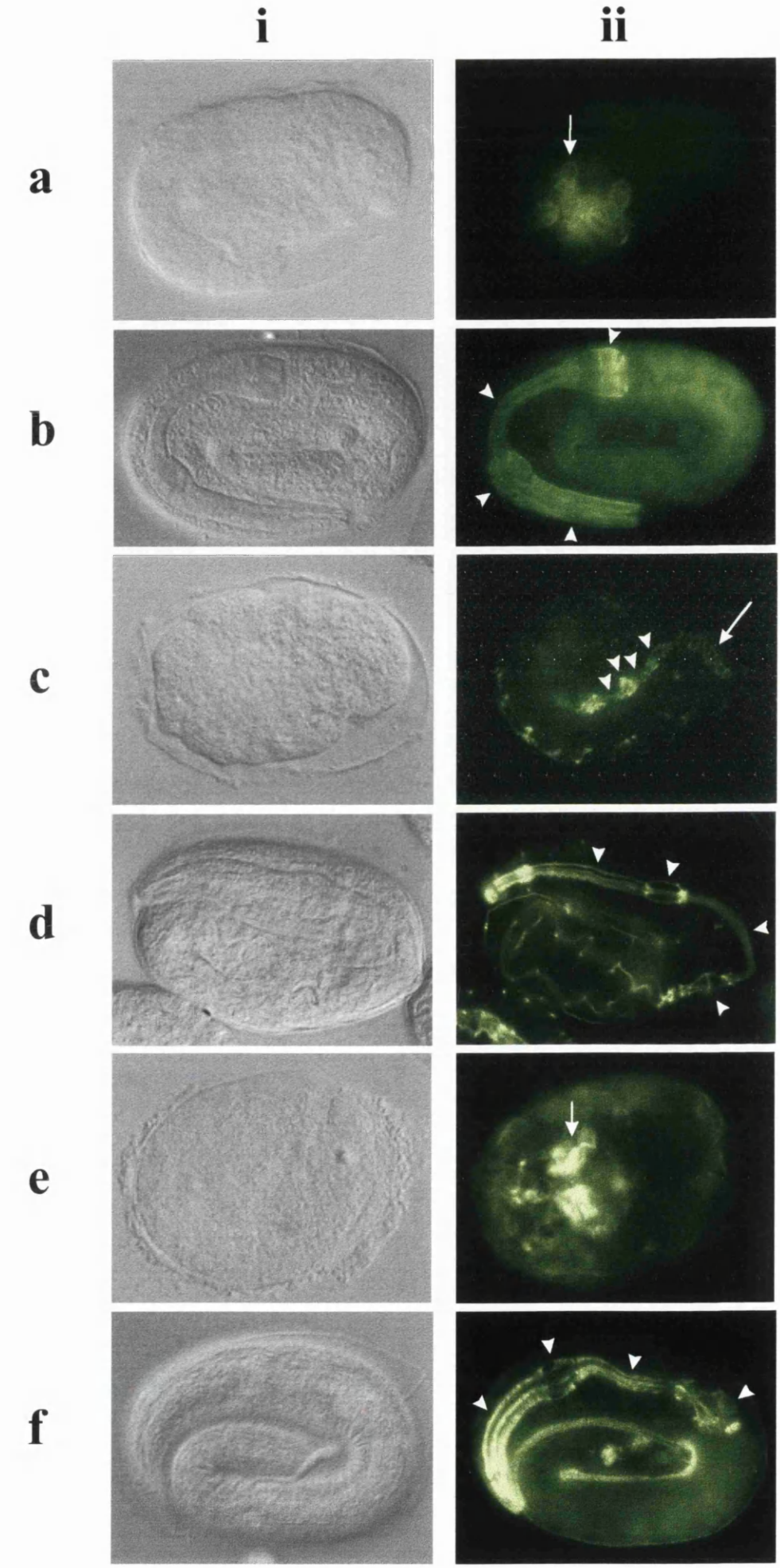
i
ii
a
b
c
d
e
f

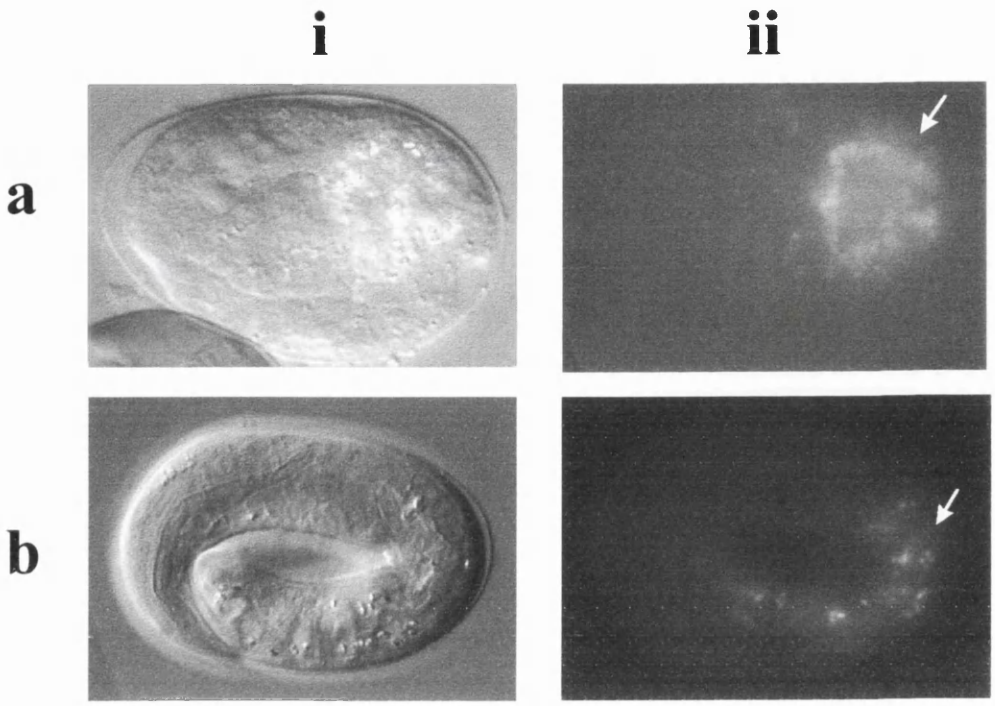

Figure 5.10

Position of the intestine in *ijDf2* homozygotes and wild type embryos as indicated by gut granule autofluorescence.

DIC images are shown in column **i** and UV images showing gut autofluorescence in column **ii**. Embryos are positioned with the anterior to the left of the image. An arrow points to the gut autofluorescence in each embryo.

a *ijDf2* homozygote
The intestine position is towards the posterior in the correct area of the embryo. Autofluoresence appears to be brighter than in the wild type, probably because the intestine is restricted to a much smaller space in the unelongated mutant.

b wild type 3-fold stage embryo showing the normal position of the intestine.

the presence or absence of various cosmid sequence markers (CSM) corresponding to the region of the deficiency in *ijDf2* homozygote embryos. A PCR-based method was used with primers specific to a small region of each cosmid sequence, the CSM, using sequences from cloned genes where available. The molecular extent of the deficiency were mapped in this way. An overlapping deficiency was mapped and characterised in a similar manner. This deficiency, *sDf30*, also results in embryonic arrest when homozygous but the embryos have a more elongated terminal phenotype, arresting at around the 2-fold stage. From these results, I focused on a region deleted by *ijDf2* but not *sDf30*. The deletion of this region is what appears to cause the earlier defect seen in *ijDf2* homozygotes and is therefore likely to contain a gene or genes involved with events prior to, or at the initiation of, elongation.

5.3.1. Chromosomal assignment - classical genetic mapping

A classical genetic cross was first used to map the *ijDf2* mutation to a chromosome. Males carrying the *ijDf2* deficiency were crossed into the triply mutant strain MT465 (*dpy-5 (e61)*I; *bli-2(e768)*II; *unc-32(e189)* III). Approximately 50% of outcrossed F1 animals, heterozygous for each marker gene, carried *ijDf2* and this transmission of the deficiency via males, which posses only one X chromosome, indicated that it was not linked to the X chromosome. F2 Recombinants were picked as in section 4.3.1, and scored for the presence or absence of *ijDf2* death among the progeny (Table 5.2).

Table 5.2

Percentage of F2 recombinant animals from the MT465 mapping cross carrying the *ijDf2* mutation.

Recombinant phenotype	carrying *ijDf2* mutation	not carrying *ijDf2* mutation	Total number of recombinants	Percentage carrying *ijDf2*
Unc-non-Dpy-non-Bli	20	16	36	56
Bli-non-Dpy-non-Unc	5	3	8	62
Dpy-non-Unc-non-Bli	12	3	15	80

If the mutation is unlinked to the marker gene then $^2/_3$ of recombinants will be carriers of *ijDf2*. None of the results above are significantly different from this expected ratio, although the numbers of blister recombinants are very small and the result could be misleading. There was therefore no evidence for linkage of *ijDf2* to chromosomes I, II, or III.

5.3.2. Chromosome assignment - STS mapping

Further chromosomal assignment mapping, and finer mapping was done using Sequence-Tagged Site (STS) mapping (Williams et al, 1992). The principle of STS mapping is that the presence or absence of polymorphisms at specific chromosomal locations in different strains can be detected using PCR assays. The polymorphisms are therefore being utilised as genetic markers. The strain carrying the mutation to be mapped is crossed into a strain carrying multiple STS markers at specific sites and the DNA from the outcrossed progeny is scored for their presence or absence. The observed 'phenotype' in this cross are bands on a gel and so large numbers of mutant progeny can be tested from a single cross and the mutant gene finely mapped.

STS mapping in *C.elegans* utilises copies of the transposable element, Tc1 which is easily identified and is present in a widely different copy number in the two major *C.elegans* strains: Bristol and Bergerac (Williams, 1995). The Bergerac strain has around 500 or more copies of Tc1 while the Bristol strain, the strain used universally as the wild type, has only around 30 copies (Brenner, 1974). These cloned Tc1 polymorphisms can used as genetic STS markers as they can be amplified easily using PCR with primers specific to each site. Therefore, by performing one cross between a Bristol strain (containing the mutation to be mapped) and a Bergerac strain (carrying Tc1 genetic markers present at sites specific to the Bergerac strain), F2 progeny exhibiting the mutant phenotype under examination can be tested for recombination by looking for the presence or absence of the STS markers. If the mutation is tightly linked to an STS, it should rarely, or never, recombine with the mutant chromosome and so should never be detected in F2 animals homozygous for the mutation. The Bergerac strain used most commonly for STS mapping is RW7000 (Williams, 1992). RW7000 is a mutator strain with active germline Tc1 transposition and because of this spontaneous mutations can occur at a relatively high rate (Moerman

and Waterston, 1984). A spontaneous lethal mutation may result in dead RW7000 embryos which will be positive for all STS markers tested (Williams, 1995). This can lead to confusing results and must always be kept in mind when mapping lethal mutations.

A chromosome carrying *ijDf2* was crossed into an RW7000 strain and the outcrossed F1 hermaphrodites were allowed to self. *ijDf2* homozygote embryos produced in the F2 generation were picked, lysed and tested for the presence or absence of STS markers. I used primers specific to each site and internal to the Tc1 polymorphism to amplify bands of certain sizes which could be determined from a gel (see section 2.12)(Williams, 1992). A specimen gel is shown in Figure 5.11b. If the mutation is unlinked to a chromosome then the STS marker chosen for that chromosome should be present in 75% of arrested embryos because it behaves as a dominant marker. The more tightly linked a mutation is to an STS marker, the fewer *ijDf2* homozygote embryos will carry the marker. The results for the chromosomal assignment PCR are shown in Table 5.3 and Appendix 5.2a.

From these results it was clear that *ijDf2* was linked to Chromosome V and was probably very close to the bp1 marker.

Table 5.3

STS Chromosomal assignment cross

Chromosome	STS marker	No. of embryos with marker	Total no. of animals tested	Percentage of animals with marker
I	hP4	32	47	68
II	maP1	33	47	70
III	mgP21	34	47	72
IV	sP4	35	47	74
V	bP1	1*	47	2

*The number of bP1 bands may have been underestimated - see appendix 5.2.

Figure 5.11

STS mapping of Deficiency *ijDf2* on chromosome V.

a Positions of STS markers and several genes on the physical and genetic maps of chromosome V (Williams et al., 1992). The physical map is shown on the top with the genetic map underneath.

b Representative gel showing positions of STS markers from the right of chromosome V. Lanes 1,3,4, and 5 contain DNA from *ijDf2* homozygote embryos while Lane 2 is a control containing DNA from an RW7000 embryo. STS markers are scored as present for each embryo if a band of the correct size is present:
Lane 1 - markers stP128, stP6, stP105, stP108 and bP1 are present
Lane 2 - control, contains all markers
Lane 3 - markers stP128, stP6, stP105 and stP108 are present
Lane 4 - markers stP128, stP105 and stP108 are present
Lane 5 - markers stP128 and stP105 are present

c

i Proposed recombination events between the RW7000 chromosome V (top line) and the *ijDf2* chromosome V (bottom line) which produces the classes A-F:
class A (n=5 mutant embryos), class B (n=15), class C (n=7), class D (n=9), class E(n=5) and class F(n=1). This places *ijDf2* in a position between stP3 and bP1.
ii Proposed recombination events between the RW7000 chromosome V (top line) and the *ijDf2* chromosome V (bottom line) in pools of 10 embryos which produces classes A-G: class A (n=5 embryo pools), class B (n=3), class C (n=8), class D (n=2), class E (n=4), class F (n=2) and class G (n=6). This accounts for more rare recombination events and places *ijDf2* between stP3 and stP23.

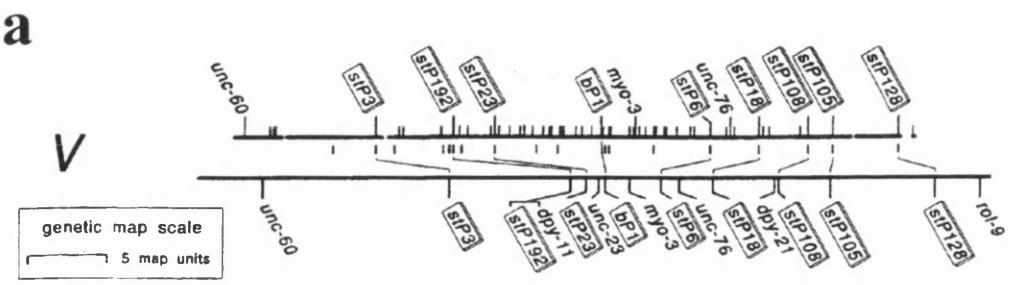
a
V
genetic map scale
5 map units
unc-60
stP3
stP192
stP23
bP1
myo-3
stP6
unc-76
stP18
stP108
stP105
stP128
dpy-11
unc-23
dpy-21
rol-9

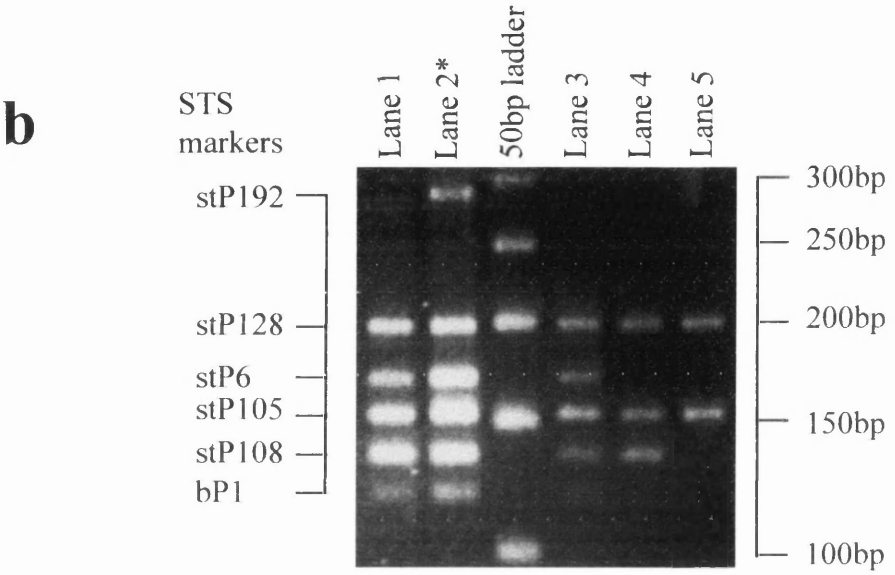
b
STS markers
Lane 1
Lane 2*
50bp ladder
Lane 3
Lane 4
Lane 5
stP192
stP128
stP6
stP105
stP108
bP1
300bp
250bp
200bp
150bp
100bp

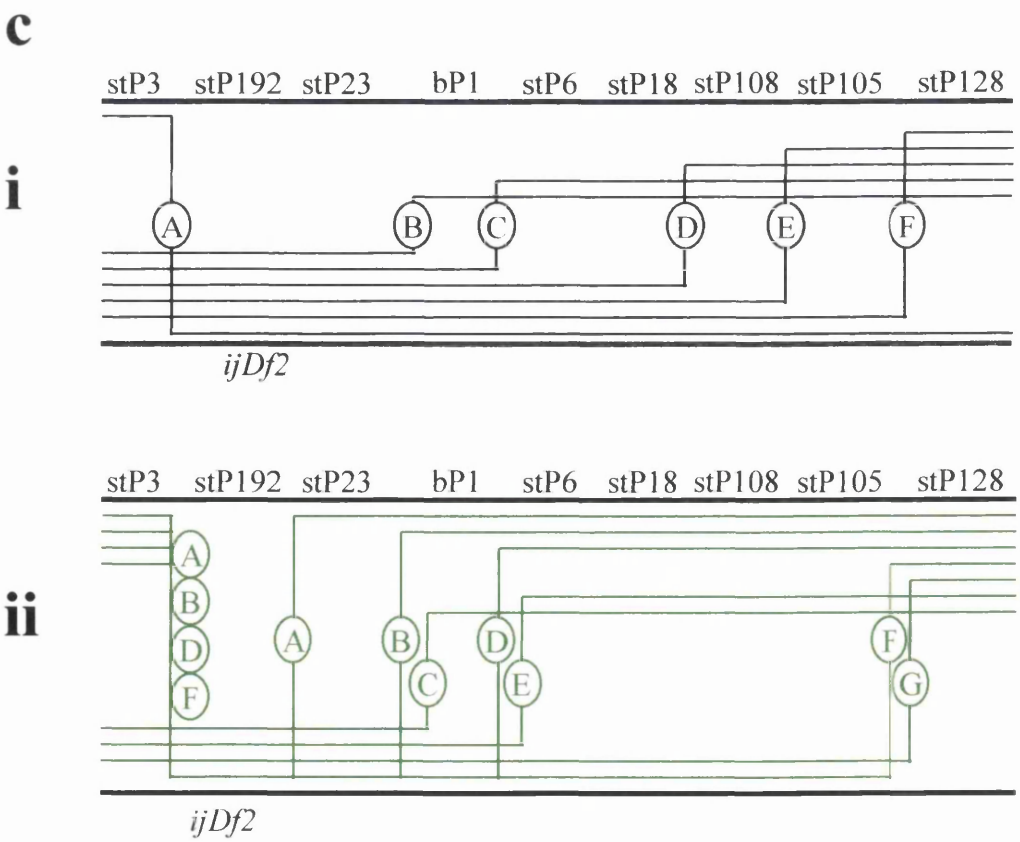
c
i
stP3
stP192
stP23
bP1
stP6
stP18
stP108
stP105
stP128
A
B
C
D
E
F
ijDf2
ii
A
B
D
F
A
B
C
D
E
F
G
ijDf2

5.3.3. Fine mapping of *ijDf2* - STS mapping

The *ijDf2* chromosome was crossed into the RW7000 strain and F2 embryos homozygous for *ijDf2* were lysed in the same way as for the chromosome assignment mapping. I used a set of 9 STS markers from chromosome V to map *ijDf2* more finely (Figure 5.11a; Williams, 1992). Two groups of markers were tested separately, one group corresponding to the left of chromosome V and another group corresponding to the right of chromosome V. Results are shown in representative gel, Figure 5.11b, Appendices 5.2b-d and Figure 5.11c. From the results I concluded that *ijDf2* was tightly linked to stP192 and stp23.

5.3.4. Complementation test

I crossed *ijDf2* heterozygotes with *dpy-11*/+ males in order to map *ijDf2* more finely and test for complementation with *dpy-11*. *dpy-11* maps to position 0 on Chromosome V, very close to stP192 (-0.01±0.11). I found that around 25% of F1 males and hermaphrodites were dumpy (47/213) which indicated that *ijDf2* was either allelic to *dpy-11* or was a deficiency which deletes *dpy-11*, the latter proving to be the case.

5.3.5. Deficiency end-point mapping

To confirm that *ijDf2* was indeed a deficiency, I designed primers specific to a small region of the genomic sequence contained in cosmid clones F44C4, which contains stP192 and K04A8 (Figure 5.12a) in order to use a PCR-based approach to test for their presence or absence on a gel. I will use the term cosmid sequence marker (CSM) to denote this amplified region from the genomic sequence contained within each cosmid clone tested. Genomic DNA from wild type and mutant embryos was obtained in the same way as for STS mapping (see section 2.12). Both CSMs were present in wild type controls but absent in *ijDf2* homozygous embryos (Figure 5.12b) and so it was obvious that certain sequences are deleted in *ijDf2* homozygotes. I had already mapped *ijDf2* to a region of the genetic map but in order to obtain information about genes deleted by

Figure 5.12

Physical mapping of *ijDf2* using Cosmid Sequence Markers (CSMs)

a Schematic map of the centre of Chromosome V showing the positions of cosmids used to map deficiency *ijDf2* relative to one another on the physical map. CSMs K04A8 and F44C4 were the first markers tested and are highlighted in red. Two of the STS polymorphisms are shown with their positions on the genetic map in map units.

b Gels showing DNA amplified from *ijDf2* homozygote and wild type embryos. Each band represents a CSM from the cosmid named on the gel. Lanes containing DNA from *ijDf2* homozygote embryos are marked with asterisks, all other lanes represent wild type embryos.

The DNA marker used is 50bp ladder (Gibco) and representative bands are marked with arrows. The marker bands are all 50bp apart.

a

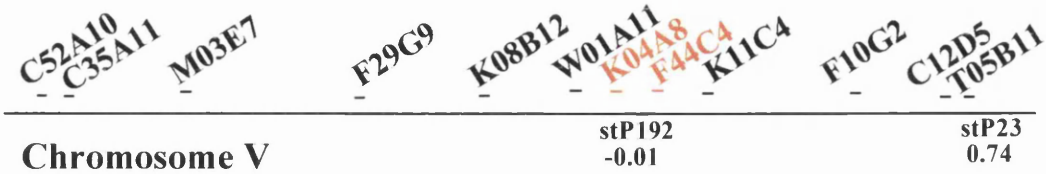
C52A10
C35A11
M03E7
F29G9
K08B12
W01A11
K04A8
F44C4
K11C4
F10G2
C12D5
T05B11
Chromosome V
stP192
-0.01
stP23
0.74

b

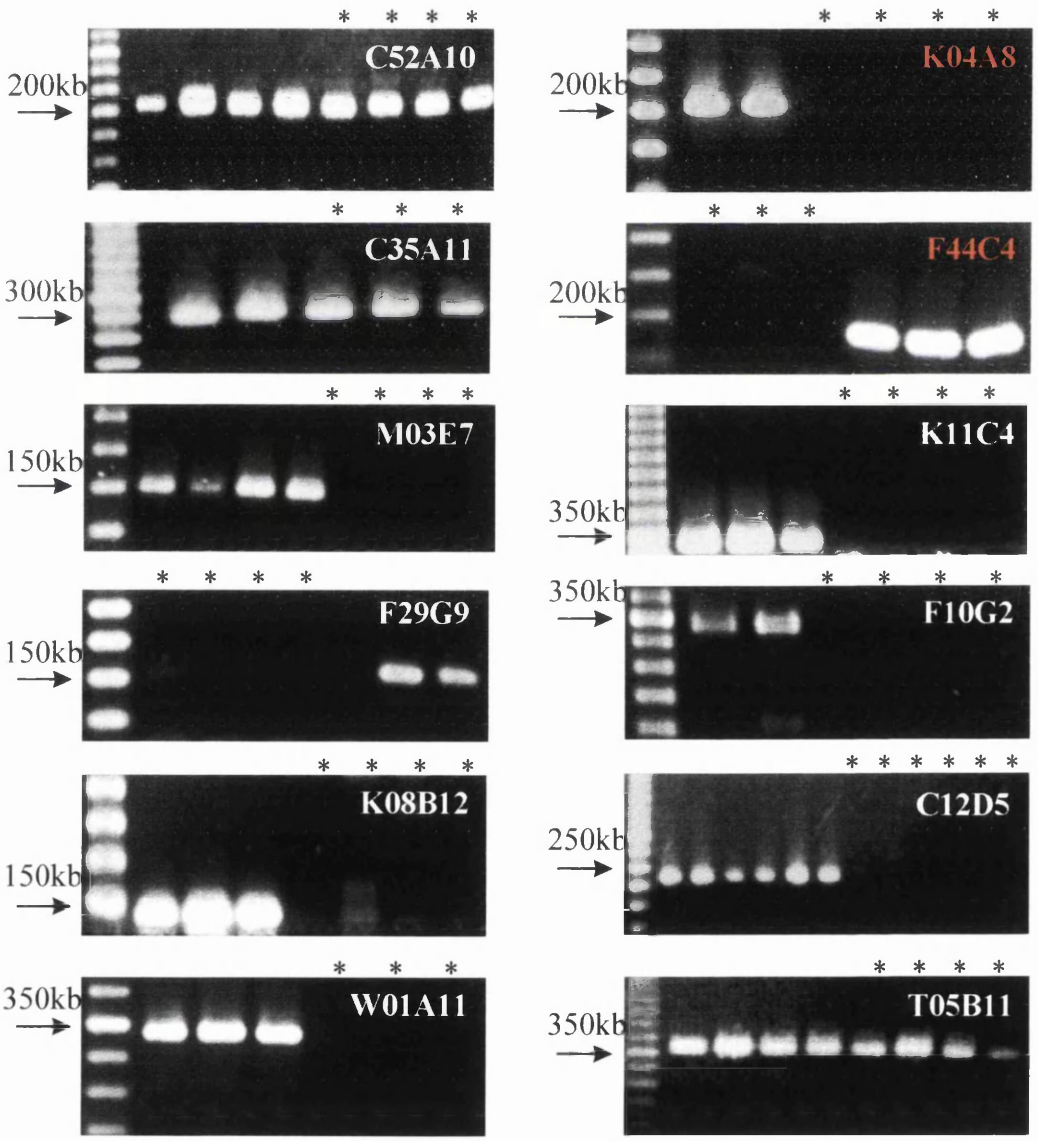
C52A10
200kb
K04A8
200kb
C35A11
300kb
F44C4
200kb
M03E7
150kb
K11C4
350kb
F29G9
150kb
F10G2
350kb
K08B12
150kb
C12D5
250kb
W01A11
350kb
T05B11
350kb

ijDf2 I used this CSM molecular approach to estimate the molecular extent of the deficiency. Primers were designed similarly towards other cosmid sequences in this region and *ijDf2* homozygote embryos were lysed again tested for the presence or absence of these CSMs using PCR. All results are shown on Figure 5.12. One of the main problems encountered when testing for presence or absence of CSMs was that, when the primers were very effective, faint bands could be seen in *ijDf2* embryos while very bright bands were amplified in N2 embryos. Since control CSMs from different chromosomes showed equivalent bands in N2 and *ijDf2* homozygote embryos, and certain other primer pairs that worked less well came up clearly in N2 and not at all in *ijDf2* homozygotes, I propose that primer pairs which worked very effectively can amplify DNA from pole cells within *ijDf2* homozygote embryos. Pole cells are seen in terminal arrest *ijDf2* embryos (Figure 5.1a) and in wild type embryos at the three fold stage and so it is possible that a very sensitive PCR system could detect DNA from these cells in mutant embryos. However, there was a clear difference between the faint bands amplified from the deficiency homozygotes and the bands from wild type embryos, and also between CSMs that were known to be present or absent in the deficiency embryos because of data from cloned genes. Positive and negative controls were used along with test cosmids for each individual embryo, as the DNA was divided among several reactions (see section 2.13). The results showed that *ijDf2* comprises a large deficiency which deletes around 2.16Mb of the genome. The approximate left end point of the deficiency lies between cosmids M03E7 and C35A11 and the approximate right end point lies between C12D5 and T05B11. Aligning these end points with the genetic map proved to be difficult as there are few cloned genes in this region. The right end point is near the polymorphism stP23 which has a position of 0.7 on the genetic map. The left end point, however, is not near any cloned genes, but the next polymorphism much further to the left, eP74, has a position of -2.46 on the genetic map of Chromosome V. An overlapping deficiency was characterised and similarly mapped in order to narrow down the deleted region which results in the amorphous, unelongated phenotype of *ijDf2*.

5.4. Characterisation of an overlapping deficiency, *sDf30*

5.4 1. Phenotypic characterisation of *sDf30*

sDf30 is a deficiency which is predicted to significantly overlap *ijDf2* from genetic data (Rosenbluth et al, 1985). The genetic data predict the *sDf30* endpoints as -0.89 and 0.68 (Rosenbluth et al, 1985; ACeDB). The *sDf30* deficiency was outcrossed from the balanced strain once, and further outcrossed twice before any observations were made. I have found that animals homozygous for the *sDf30* deficiency arrest as embryos with a terminal elongation of 1.5 to 2-fold and all appear to have a large indentation at the site of the buccal capsule (Figure 5.13). I carried out a time course of the embryonic development of *sDf30* homozygotes using Nomarski optics and found that development was relatively normal until comma stage and then the mutant embryos began to grow at a slower rate and exhibit abnormal morphology. Many elongated to 2-fold or over but then slowly regressed to a terminal phenotype of around 1.5-fold. I saw no evidence of embryos rupturing or loose cells within the egg which indicates that hypodermal cells seem to have enclosed the embryo sufficiently. The regression of the homozygote embryos to a 1.5-fold stage may have been due to the secretion of an inadequate cuticle. Because of the difference in phenotype between *sDf30* and *ijDf2*, I mapped the end points of the *sDf30* deficiency to narrow down the region deleted by *ijDf2* alone which must contain genes involved in the initiation of elongation or earlier.

5.4.2. Physical Mapping of *sDf30* end-points

The end points of the *sDf30* deficiency were physically mapped using the CSM approach in the same way as the *ijDf2* deficiency. The presence and absence of the test CSMs in *sDf30* homozygotes is shown in Figure 5.14. The molecular overlap of the two deficiencies is shown in Figure 5.15. It can be seen that *sDf30* almost completely overlaps *ijDf2* but there is a region to the right of the *ijDf2* deficiency which is deleted by it alone and possibly also a region to the left of the deficiency between the last two CSMs tested. Because *ijDf2* homozygotes show defects from an earlier stage in embryogenesis than *sDf30* homozygotes, a gene or genes involved in processes prior to,

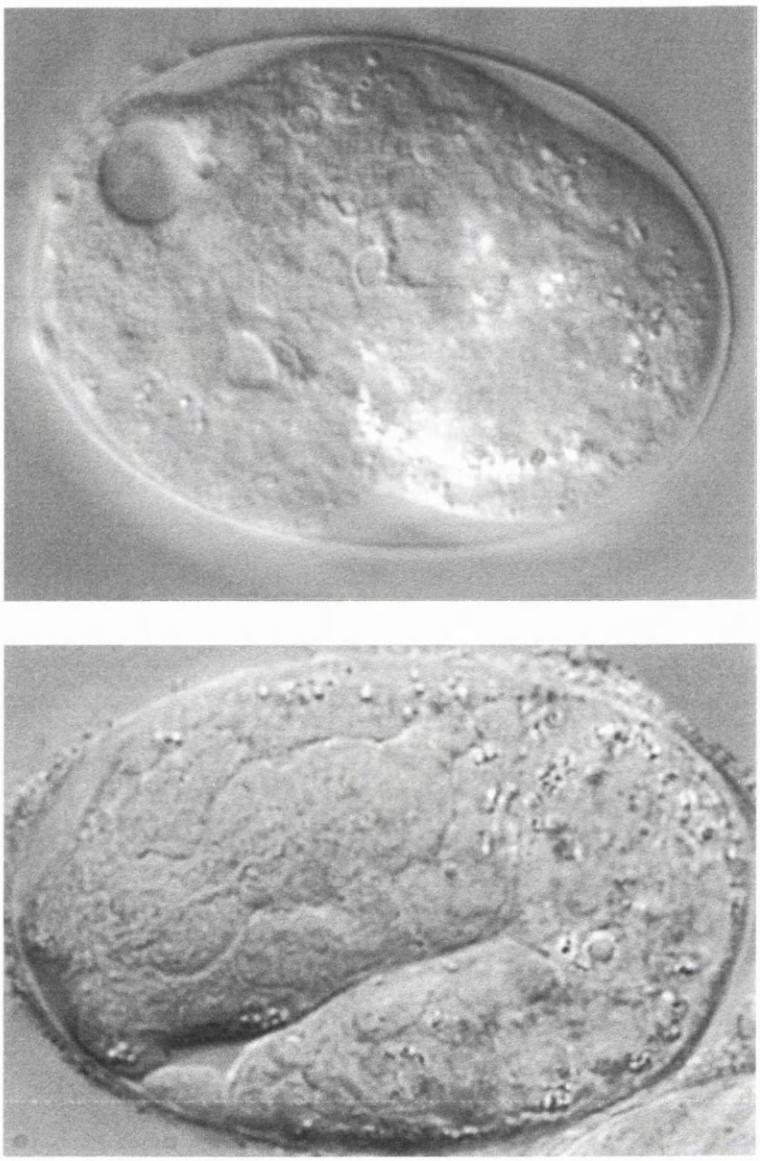

Figure 5.13

DIC images of mutants homozygous for deficiencies *ijDf2* or *sDf30*

Both embryos are positioned with the anterior to the left and the embryo in image **b** also has the dorsal surface to the top of the image.

a *ijDf2* homozygote which arrests without any elongation.

b *sDf30* homozygote which arrests at around the 2-fold stage of elongation

Figure 5.14

Physical mapping of *sDf30* using Cosmid Sequence Markers (CSMs)

a Schematic map of the centre of Chromosome V showing the positions of cosmids used to map deficiency *sDf30* relative to one another on the physical map. Two of the STS polymorphisms are shown with their positions on the genetic map in map units.

b Gels showing DNA amplified from *sDf30* and wild type embryos. Each band represents a CSM from the cosmid named on the gel.
Lanes containing DNA from *sDf30* homozygote embryos are marked with asterisks, all other lanes represent wild type embryos.

The ladder used is 50bp ladder (Gibco) and representative bands are marked with arrows. The marker bands are all 50bp apart.

a

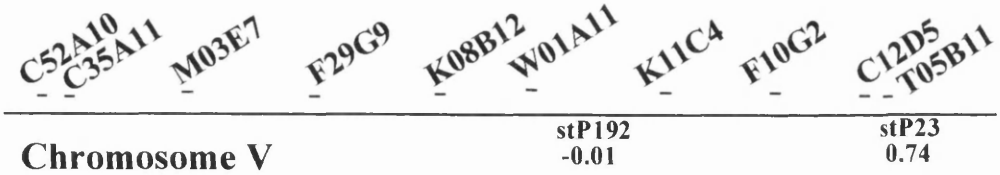
C52A10
C35A11
M03E7
F29G9
K08B12
W01A11
K11C4
F10G2
C12D5
T05B11
Chromosome V
stP192
-0.01
stP23
0.74

b

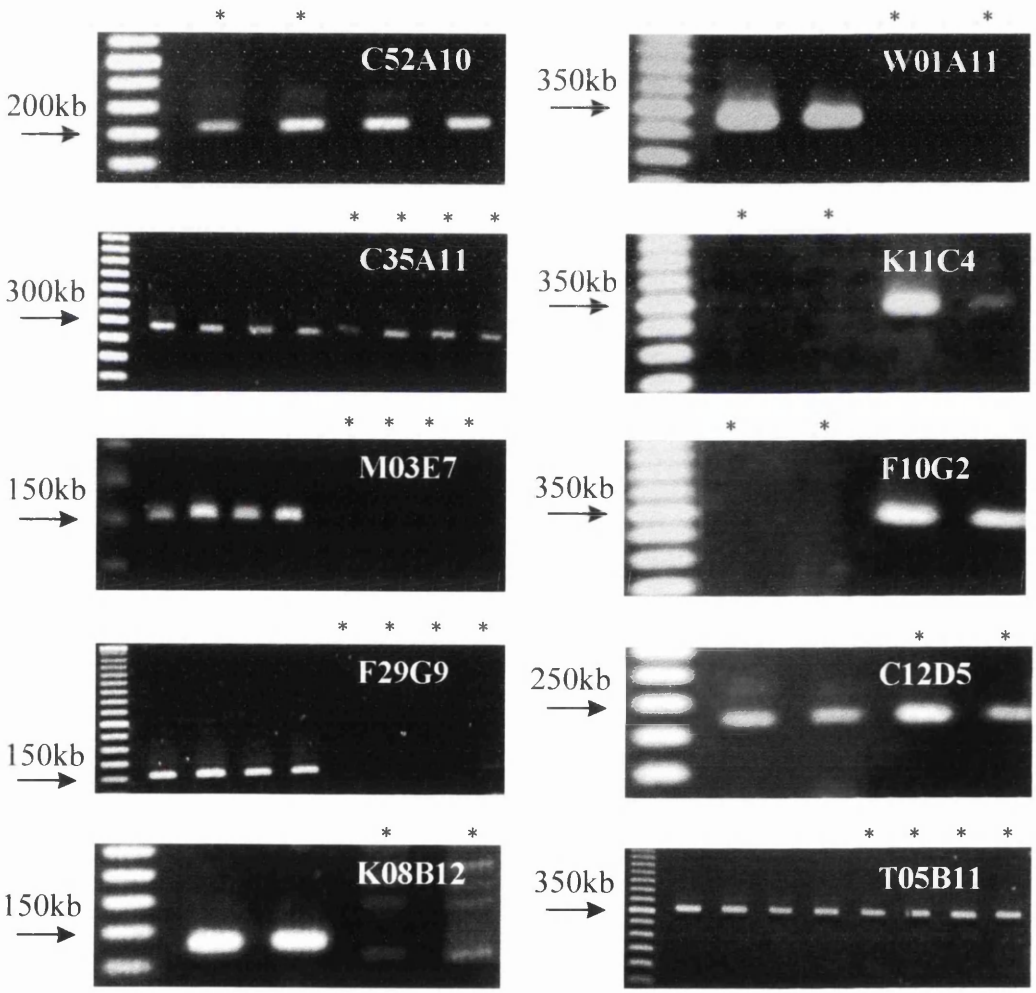
C52A10
200kb
W01A11
350kb
C35A11
300kb
K11C4
350kb
M03E7
150kb
F10G2
350kb
F29G9
150kb
C12D5
250kb
K08B12
150kb
T05B11
350kb

Figure 5.15

Comparison of deficiencies *ijDf2* and *sDf30* in the centre of chromosome V

Representative cloned genes or polymorphisms are shown to indicate the approximate position in map units of the deficiencies on the genetic map. There are no cloned genes or polymorphisms to the left of *gad-1* within the deficiencies, however the left point of sDf30 has been quoted as -0.9 from genetic data. The dashed areas of the deficiencies are regions between the last deleted cosmid and the first undeleted cosmid. The deficiency endpoint lies somewhere within this region.

Chromosome V (centre)

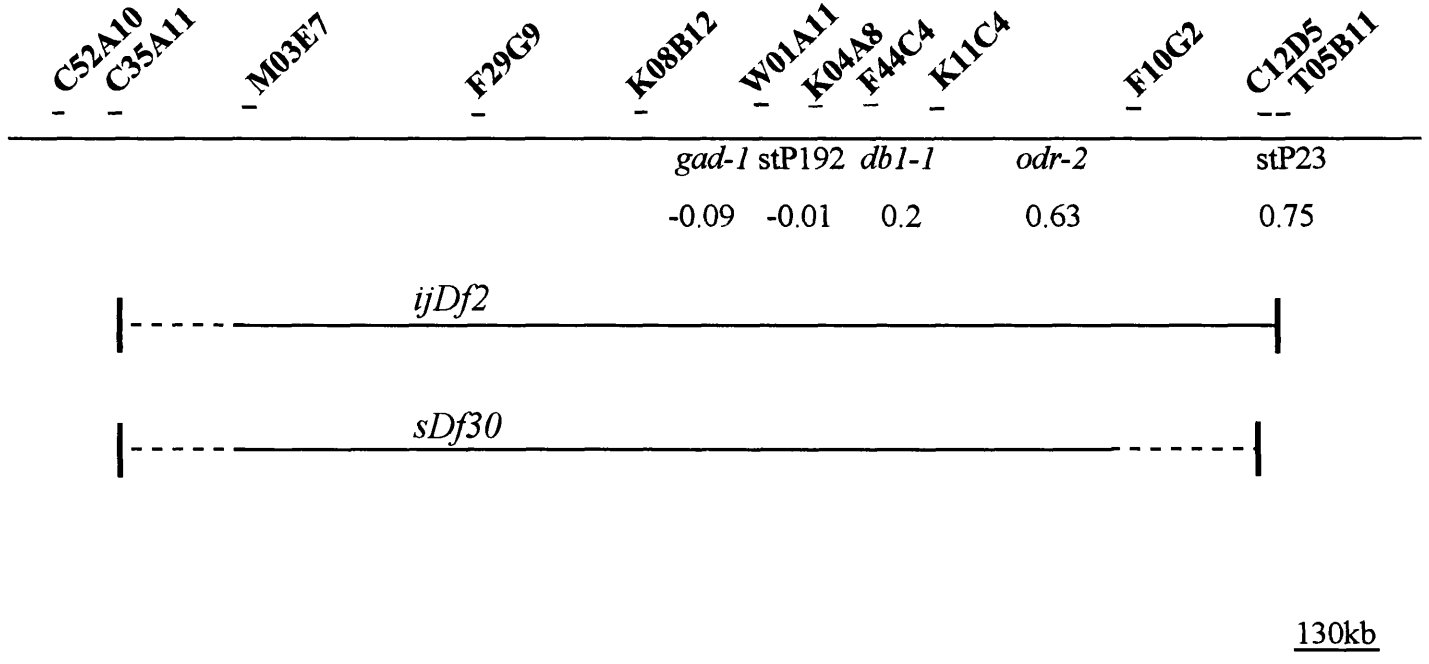

or at the beginning of, elongation may therefore be present within these regions of the genome. Because the approximate left end points of both deficiencies are relatively close, it is possible to use genetic map information from *sDf30* to infer an approximate map position for *ijDf2* also. The left end point of *sDf30* is cited as -0.89 (ACeDB) which agrees with the left end point of *ijDf2* being much further right than eP74 (-2.46).

5.5. Discussion

ijDf2 is a deficiency around 2.2Mb in size, deleting cosmids from between C35A11 and M03E7 to the left, to between C12D5 and T05B11 to the right. This corresponds to the genetic map of chromosome V from a left end position of approximately -0.9 to a right end position of approximately 0.7 map units. Animals homozygous for this deficiency arrest as embryos, showing abnormalities as early as 270 mins post fertilisation, before the precomma stage of development. Very high magnification studies of early development were not carried out and so abnormalities in cell movements before this time may not have been detected. Although there is no body morphogenesis, markers of muscle, basement membranes and hemidesmosomes are present. However, the pattern of all of these is very abnormal. The hypodermis is also present around the entire embryo with an approximately normal number of nuclei although there appears to be a smaller number of hypodermal cells than normal indicating possible hyperfusion of cells. The embryos express both *dpy-7* and *col-12* collagen::GFP reporter transgenes in the hypodermis which indicates that the hypodermis is developmentally mature with respect to collagen synthesis as it is executing certain aspects of a terminal fate. The *ijDf2* homozygotes do not secrete a cuticle incorporating DPY-7, however, and there is no evidence of intracellular DPY-7 staining. Intestinal and pharyngeal cells are also present but in a very underdeveloped form. Most of the embryos show some rupture with loose cells present within the cavity between the embryo and the eggshell.

These embryos share several phenotypic aspects with gastrulation defective mutants. They show abnormalities prior to the comma stage of development, the gut is positioned towards the posterior and the end phenotype is a misshapen ball even though many tissues have developed to their terminal stage (Bucher and Seydoux, 1994; Knight and Wood, 1998). However, in mutant embryos which fail to gastrulate normally, the

gut primordia and founder cells of other tissues fail to migrate inwards and instead develop at the surface of the embryo, whereas in *ijDf2* homozygotes the underdeveloped gut and pharynx seem to be positioned towards the centre of the embryo and muscle is also present internally. This is an interesting phenotype as there is a complete failure to elongate even though the hypodermis is present around the entire embryo and expresses collagen genes which are normally expressed at the very end of embryogenesis. The organisation of the hypodermal cells is very abnormal, as is the organisation of body wall muscle cells and the attachments between the two tissues. A possible explanation for the phenotype is that some aspect of cell adhesion has been disrupted which would account for the early defects seen at around 4½ hours post fertilisation when cells appear to be less tightly packed around the edges and resemble a cluster of grapes. Hypodermal boundaries are also completely disorganised within the embryo which would be another indication of subnormal cell adhesion, but there are multinucleate as well as mononucleate cells so hypodermal cell fusion is occurring. In fact, there appear to be fewer hypodermal cells than normal which would indicate hyperfusion. As previously mentioned, elongation does not normally begin as an active process until the comma stage when the hypodermal cells have completely enclosed the embryo which could suggest that the phenotype in *ijDf2* shows a pre-elongation defect. However, if the dorsal hypodermal cells do not interdigitate normally then the embryo will not form this characteristic shape and it may be that earlier abnormalities in the positioning or interactions between hypodermal cells are preventing *ijDf2* mutant embryos from elongating. This could result from a possible cell adhesion defect. It is also an interesting point that hypodermal cells express cuticular collagen genes that are normally produced at the beginning (*dpy-7*) and end (*col-12*) of elongation when the organisation of these cells relative to one another appears to be so disorganised. However, there is no evidence for the presence of these collagens either within cells or secreted as a cuticle. It is possible that such a disorganised hypodermis may produce collagens intracellularly but be unable to secrete them, leading to their degradation within the cells as is thought to happen with unsecreted mutant collagens (see chapter 3). Because every structure or tissue type seems to be affected to some extent, the phenotype does appear to be a general abnormality. A cell adhesion defect would affect not only the hypodermis, but any cell type that relies on cell-cell interactions for some or all of its development. This would include all the tissues and structures visualised in

the phenotypic characterisation and could have effects as early as late gastrulation when adhesion between cells is an essential precursor to embryogenesis and would disrupt processes such as enclosure which relies both on correct termination of gastrulation and the adhesion of hypodermal cells migrating around the embryo (Williams-Masson *et al.*, 1997; George *et al.*, 1998).

From comparison with the *sDf30* deficiency it is clear that *ijDf2* deletes one or more genes which when present allow the embryo to elongate to 1.5- or 2-fold. *sDf30* does not seem to show the irregular cell contacts or rupture phenotypes seen in *ijDf2* and so, if a gene involved in cell adhesion is deleted in *ijDf2* homozygotes, it would presumably be present in *sDf30* homozygotes. As can be seen from Figure. 5.15, *sDf30* is almost completely contained within *ijDf2* although the left end-points of both deficiencies have not been mapped more finely. Both delete M03E7 and do not delete C35A11, so there is a region of 200Kb within which the endpoints of both deficiencies lie. The right end of *ijDf2* extends beyond *sDf30* to the interval between C12D5 and T05B11 (a distance of 37Kb) while *sDf30* ends between F10G2 and C12D5 (323Kb apart). Further endpoint mapping and an attempt at cloning the genes involved in this elongation defect was not carried out because of the complexity of the phenotype and the lack of any other deficiency overlapping the regions which *sDf30* did not delete. As mentioned above, it is likely that the phenotype seen in *ijDf2* is due to the deletion of a gene or genes involved in a general role in embryogenesis, possibly cell adhesion. There may or may not also be another gene deleted which is specifically involved in the onset of morphogenesis as the correction of a cell adhesion defect alone may be enough to allow elongation to a certain stage. Although normal cell adhesion is vital in the process of morphogenesis, a gene controlling general cell adhesion would not be specifically involved in elongation and so may not facilitate the understanding of elongation as much as other more related genes. Another very important point is that, in this region of the genome, there is a large cluster of essential genes and so reducing the deleted genes to a subset which are involved in gastrulation, cell adhesion, or morphogenesis may be extremely difficult.

The study of deficiencies can uncover relationships between genes that would otherwise go unnoticed and may be a more valuable tool than is currently thought, although with very large deficiencies, so many genes may be knocked out and the phenotype produced may be a combinatorial affect of this large scale knock-out.

Discovering which deleted genes are responsible for the observed phenotype and which are non-essential or give no observed phenotype can be examined by RNAi, for example, and may reveal redundancies and pathway similarities previously unknown. If more time was available, it is possible that the *ijDf2* deficiency could unearth developmental genes that are important in the initiation or execution of morphogenesis.

Chapter 6
Characterisation of a deficiency, *ijDf1*

6.1. Introduction

6.1.1. Elongation of the *C.elegans* embryo

Contraction of the hypodermal actin cytoskeleton is thought to drive the cell shape changes involved in the elongation of the *C.elegans* embryo (Priess and Hirsh, 1986). Actin microfilaments and microtubules in the hypodermal cytoplasm form a meshwork which is not oriented in any direction until ventral enclosure and dorsal intercalation are complete or nearing completion (Williams-Masson *et al.*, 1998). Microtubules appear to begin aligning circumferentially in the hypodermis at the final stages of ventral enclosure and actin microfilament bundles become circumferentially oriented shortly after this. Microtubules and actin microfilament bundles are aligned parallel in the apical region of the dorsal and ventral hypodermis. However, in the lateral hypodermis, microtubules do not become circumferentially oriented but instead remain in a complex network throughout the cytoplasm (Priess and Hirsh, 1986). Actin microfilament bundles do align circumferentially in the lateral hypodermal cells as well as in the dorsal and ventral hypodermis, although the microfilaments in the dorsal and ventral hypodermis appear to be closely associated with the plasma membrane while the lateral microfilaments are not (Costa *et al.*, 1997). Actin microfilament bundles also seem to be anchored to the adherens junctions at either side of the hypodermal cell they traverse while microtubules appear to terminate before these junctions (Priess and Hirsh, 1986; Costa *et al.*, 1998). Studies using actin and microtubule inhibitors, cytochalasin D and nocodazole respectively, showed that actin microfilaments are essential for the initiation and maintenance of elongation until the embryo is fully elongated and while microtubules are not essential for elongation, they are necessary for the normal elongation process (Priess and Hirsh, 1986). Embryos that had been treated with a microtubule inhibitor continued to elongate but did not elongate fully and developed many surface abnormalities. Priess and Hirsh (1986) proposed that the actin microfilament bundles were contractile and that their apical contraction caused an asymmetrical change in the shape of the hypodermal cells. They suggested that this

shape change creates pressure on the internal cells of the embryo and ultimately results in elongation. The idea that actin microfilaments are contractile is further strengthened by observations on mutant embryos homozygous for *hmp-1* or *hmp-2*, which encode homologues of α-and β-catenin respectively, in which the actin microfilaments detach from the adherens junctions at either side of the dorsal hypodermal cells (Costa *et al.*, 1998). The detached actin microfilaments become shorter and thicker indicating that they are contractile. The mechanism of actin microfilament bundle contraction has not been elucidated although observations of other contractile systems and evidence from several elongation defective mutants suggest that there is a myosin component involved (Ridley and Hall, 1992; Allen and Walsh, 1994; Wissmann *et al.*, 1997). The change of hypodermal cell shape can be seen clearly during elongation using an antibody, MH27, which recognises a component of adherens junctions in hypodermal cells (Priess and Hirsh, 1986; Waterston, 1988). There is also an obvious pressure exerted on the internal cells of the embryo during elongation as seen in mutant embryos which do not enclose completely and in embryos which have lesions created in the hypodermis by a laser microbeam (Priess and Hirsh, 1986; Costa *et al.*, 1998; Chapter 4). Prior to elongation, no cells are exuded from the embryo. However, after the onset of elongation, internal cells squeeze through any openings in the hypodermal sheet and the embryos rupture. The internal pressure which creates this rupturing, is prevented by treatment with cytochalasin D which interferes with actin filaments (Priess and Hirsh, 1986). This evidence indicates that the actin microfilaments produce the internal pressure observed.

The microtubules are thought to provide a relatively rigid support to the hypodermal cells which helps to distribute the mechanical stresses produced from microfilament contraction (Priess and Hirsh, 1986). It can be seen that the circumferential margins of the lateral hypodermal cells, which do not possess circumferentially oriented microtubules, decrease much more in width than the dorsal and ventral hypodermal cells with their microtubule support. Another feature of the embryo which is thought to play a part in elongation is the hypodermal sheath. This sheath has not been extensively characterised but is an extracellular layer which is secreted over the surface of the hypodermis prior to elongation and eventually forms the outer cortical layer of the first secreted cuticle at the end of elongation (Priess and Hirsh, 1986; Costa *et al.*, 1997). When lesions were produced in this sheath during elongation using trypsin, embryos ceased elongating normally and developed abnormal

constrictions on the surface (Priess and Hirsh, 1986). These constrictions are thought to be due to microfilament contraction as they did not develop in the presence of cytochalasin D. It is thought that the sheath could play a role in transmitting the mechanical stress from microfilament contraction longitudinally across the embryo during elongation and thus provide an additional support for the hypodermal cells (Priess and Hirsh, 1986).

6.1.2. Pharyngeal development during embryonic elongation

Another structure which undergoes elongation and differentiation during embryogenesis is the pharynx which is discussed in more detail in section 1.7.5.5. Although it has been shown that the embryo can elongate in the absence of a pharynx, pharyngeal and body shape morphological defects often occur together (Schnabel and Schnabel, 1990; Mango *et al.*,1994a; Wissmann *et al.*, 1997; McKeown *et al.*,1998). The active process of body morphogenesis may also pull the pharynx out into its elongated shape and so animals which are defective in elongation may consequently have much shorter pharynxes. Conversely, an absent or abnormal pharynx may lead indirectly to morphogenetic defects even when hypodermal cells seem normal, as the pharynx normally fills the anterior third of the developing embryo (Schnabel and Schnabel, 1990).

In this chapter I will describe the characterisation of the *ijDf1* deficiency which has defects primarily in body morphogenesis but also shows abnormal pharyngeal development. It was generated as described in section 5.1.1.

6.2. Phenotypic characterisation of *ijDf1*

A strain heterozygous for the *ijDf1* deficiency was outcrossed four times before phenotypic observations were made. *ijDf1* heterozygotes are healthy, fertile animals and all embryos studied were *ijDf1* homozygotes segregated from an hermaphrodite heterozygous for *ijDf1*. *ijDf1* homozygotes are embryonic lethals which arrest at the 1.5-fold stage of elongation. While this is a very uniform arrest, there are two main classes of shape which are commonly seen (Figure 6.1a and b). The percentage of total

Figure 6.1

DIC images showing terminal arrest phenotypes of *ijDf1* homozygous mutants

All embryos in **a** are orientated with the anterior to the left and the dorsal region to the top of the page. In **b** the embryo anterior is facing to the left at the top centre of the image and in **c** and **d** the anterior is curving around the bottom left of the image with the dorsal surface to the top and right.

a *ijDf1* 1.5-fold homozygotes

i Usual terminal phenotype of *ijDf1* homozygotes

ii Variations of the usual terminal phenotype showing a mutant with a kinked anterior (top) with an arrow pointing to the anterior tip, and a mutant with a more uneven outline (bottom) with a very pointed tail indicated with an arrow.

b *ijDf1* 1.5-fold 'Long posterior' homozygote

The buccal cavity is indicated with an arrow.

c 3-fold wild type embryo

The buccal cavity is indicated with an arrow.

d *ijDf1* 1.5-fold homozygote showing the shortened pharynx.

The grinder and the anterior basement membrane are indicated by arrowheads but the four main regions can not be seen distinctly. This is typical for most *ijDf1* homozygotes where the pharynx is visible

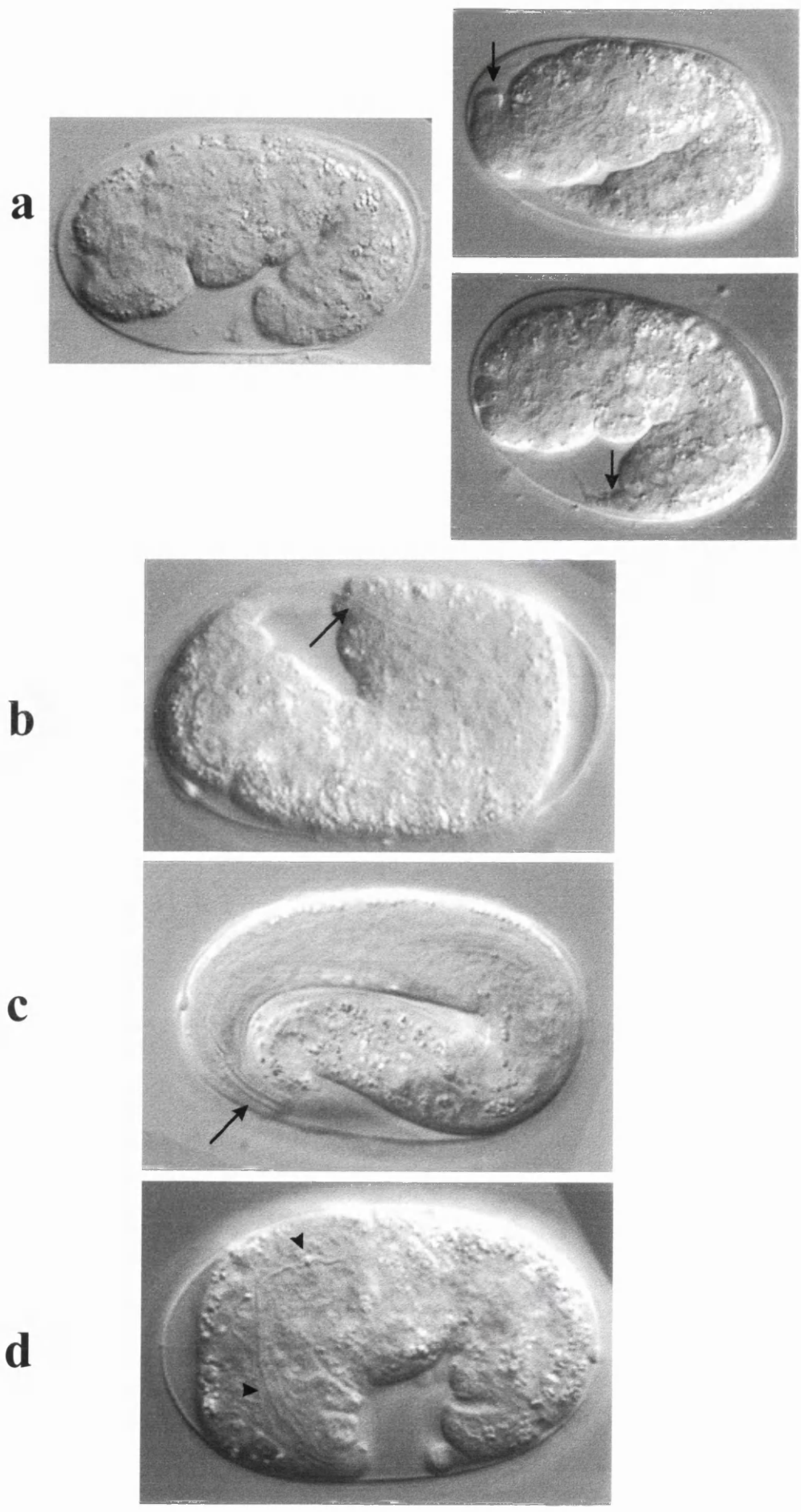
i
ii
a
b
c
d

ijDf1 homozygotes made up by each of these phenotypic variations is shown on Table 6.1.

Table 6.1

Phenotypic variations in body shape among *ijDf1* homozygotes

Phenotype name	Distinguishing phenotypic features	Percentage of total *ijDf1* homozygotes (n=291)
1.5-fold (Figure 6.1a)	Arrest at 1.5-fold. Relatively smooth outline although a proportion have a 'kinked' anterior or a more irregular outline with a very pointed tail. A small number of embryos arrest slightly longer, some getting to around 1.75 fold.	88
Long posterior (Figure 6.1b)	Arrests at around 1.5-1.75 fold stage of elongation but anterior is very short while posterior is much more elongated than normal 1.5-fold phenotype and curls around the anterior.	12

Both these phenotypes were seen at terminal arrest and subsequent phenotypic characterisation showed that all observations and antibody staining patterns were very similar for both phenotype classes. Because of this, I will only give detailed descriptions of the 1.5-fold embryo phenotype. From DIC microscopy, the buccal cavity is seen in some mutant embryos (Figure 6.1b arrow), and a very underdeveloped pharynx is also apparent in most embryos which does not appear to pump (Figure 6.1d). From time-course observations, *ijDf1* homozygote embryos appear to reach the comma stage of development at an equivalent time to wild type embryos but they then elongate very slowly only to 1.5 or 1.75 fold while wild type embryos rapidly elongate to the full length in just over 2 hours. There is no evidence of rupture or loose cells within the mutant eggshells and so it appears that hypodermal cells have enclosed the embryo normally. These embryos show defects only after the active process of elongation has

been initiated and therefore there is evidence to suggest that genes involved in the active process of elongation have been deleted by the *ijDf1* deficiency. Movement is seen in *ijDf1* homozygotes although it is often 'jerky' with the mutant embryos constantly twitching. No clear differences in either of the terminal phenotypes of the *ijDf1* homozygotes were observed at 16°C, 20°C or 25°C (Figure 6.2).

In order to examine the mutant embryos in more detail, I used fluorescent markers of several tissues and structures including the hypodermis, cuticle, muscle, muscle hypodermis attachments, basement membrane, pharynx and intestine.

6.2.1. Hypodermis

Hypodermal cells are joined at their apical junctions by specialised adherens junctions and the monoclonal antibody MH27 recognises a protein component of these junctions (Priess and Hirsh, 1986; Waterston, 1988). In *ijDf1* homozygote embryos, the MH27 pattern is very similar to the wild type embryo pattern at the same stage of elongation (Figure 6.3a,b). Normally large numbers of hypodermal cells fuse in wild type embryos between the 1.5-fold stage and the 3-fold stages (Podbilewicz and White 1994). Some *ijDf1* homozygous embryos arrest without completing these fusions indicating that the hypodermis has not reached its terminal stage of development (Figure 6.3a, arrow).

Observations of the pattern of the hypodermal nuclear protein, LIN-26 using the anti-LIN-26 polyclonal antibody, indicate that there are an approximately wid type number and position of hypodermal nuclei in *ijDf1* homozygotes (Labouesse *et al.*, 1996). Co-staining with anti-LIN-26 polyclonal, and MH27 monoclonal antibodies shows that the mutant hypodermal nuclei appear to be in relatively wild type positions, and this can be shown most clearly by comparisons with a wild type embryo at the 1.5-fold stage of elongation (Figure 6.4).

6.2.2. Cuticle

Cuticular collagens that are synthesised by hypodermal cells are expressed in temporally distinct waves throughout elongation starting with the expression of *dpy-7* at the comma stage of development and ending with the expression of *col-12* after

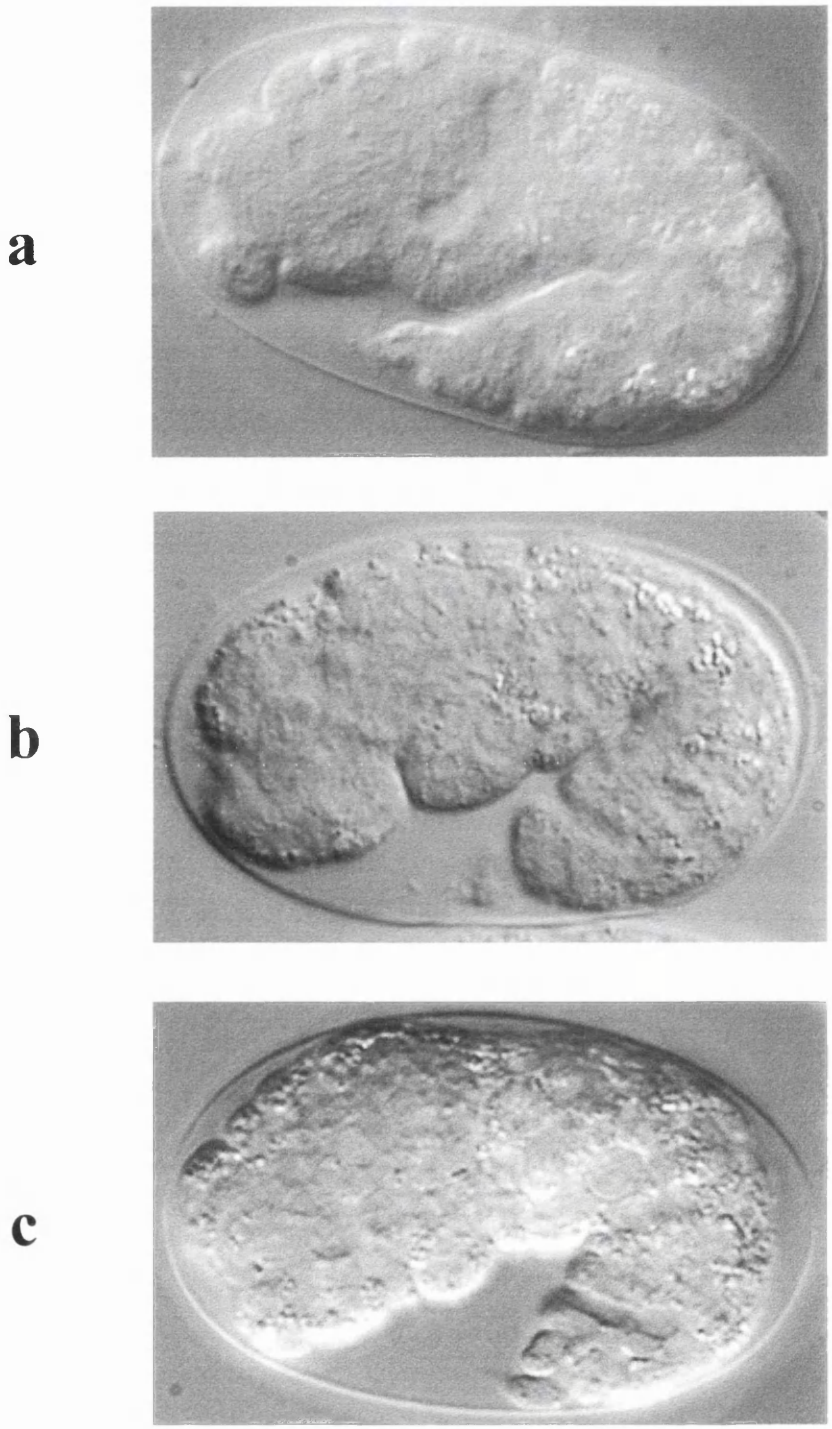

Figure 6.2

DIC images showing terminal arrest phenotypes of *ijDf1* homozygotes at various temperatures

a 16°C

b 20°C

c 25°C

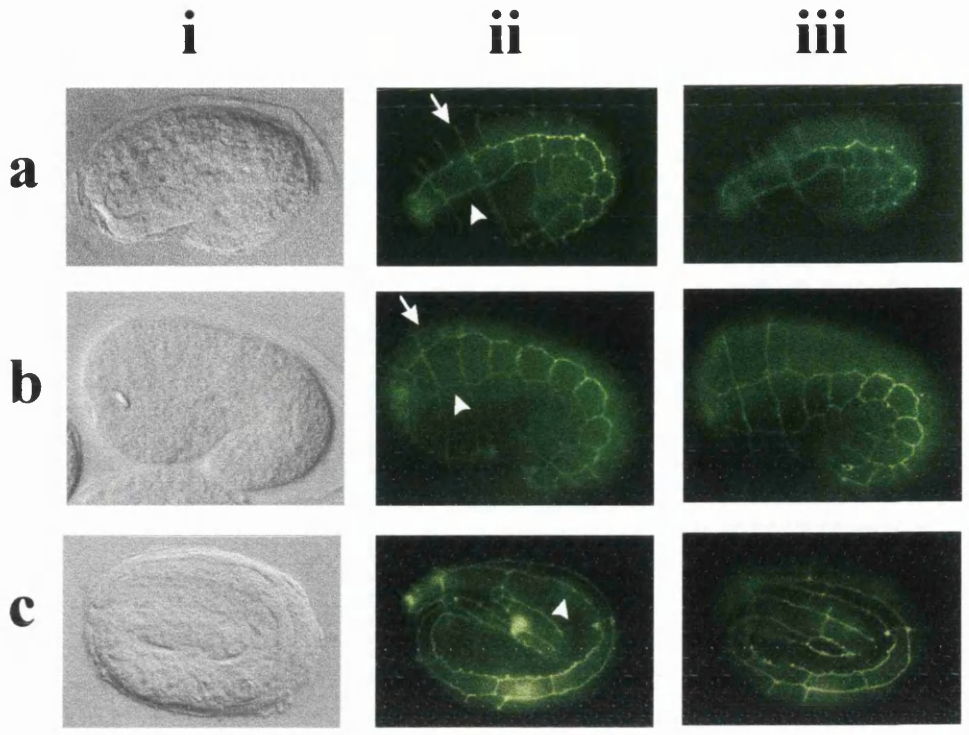

Figure 6.3

Hypodermal cell shapes and positions in *ijDf1* mutant embryos and wild type embryos

Embryos were stained with the monoclonal antibody MH27 to visualise the adherens junctions between hypodermal cells. In all images, the anterior is to the left and the dorsal region is to the top. DIC images are shown in column **i**. A seam cell is indicated with an arrowhead in image **ii** of all embryos.

a *ijDf1* homozygote

ii and **iii** MH27 staining showing lateral views of the hypodermis. The hypodermal cells appear to be of approximately wild type shape and position although they are not as elongated as a wild type 3-fold embryo and fewer hypodermal fusions have occurred in the dorsal region of the embryo as shown by extra hypodermal cell boundaries (indicated with an arrow in images **aii** and **bii**).

b 1.5-fold wild type embryo

ii and **iii** MH27 staining showing lateral views of the hypodermis

c 3-fold wild type embryo

ii and **iii** MH27 staining showing lateral views of the hypodermis

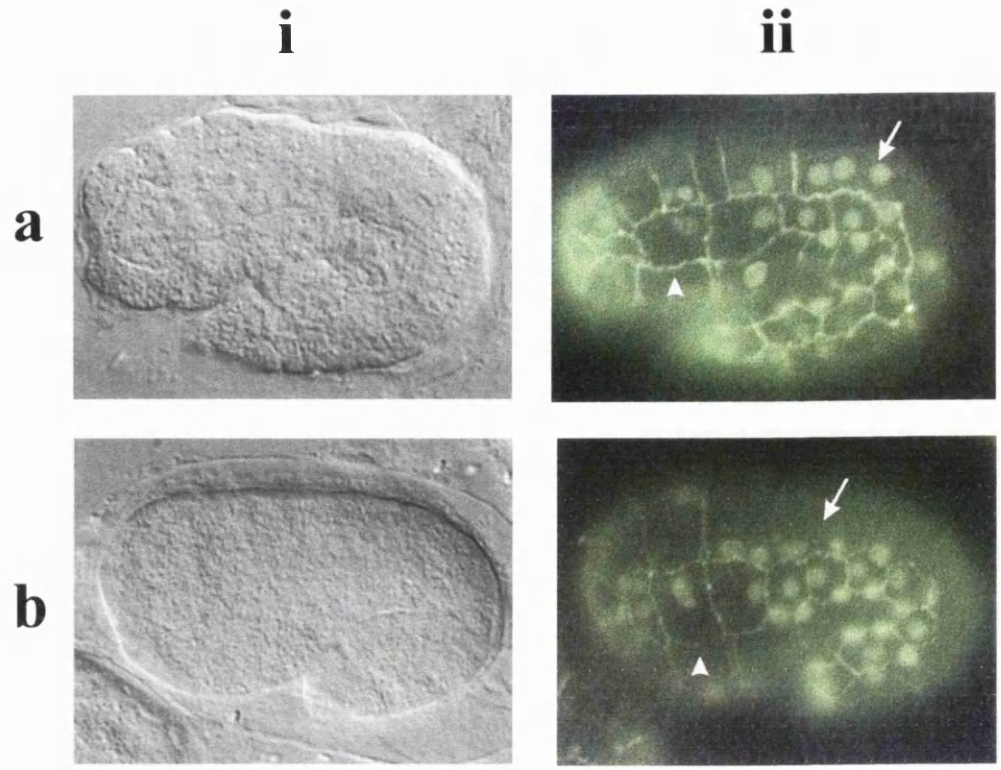

Figure 6.4

Position of hypodermal nuclei in *ijDf1* mutant embryos and 1.5-fold wild type embryos

Embryos were stained with the monoclonal antibody MH27 and the polyclonal antibody anti-LIN-26 which recognise hypodermal cell boundaries and hypodermal nuclei respectively. Column **i** shows DIC images and column **ii** shows MH27 and anti-LIN-26 staining. All embryos are positioned with the anterior to the left and the dorsal region to the top of the page.

a *ijDf1* homozygote showing that the seam cells are mononucleate as expected (one is indicated by an arrowhead) and that dorsal hypodermal cells are mostly multinucleate syncytia (indicated by an arrow). Hypodermal nuclei seem to be in approximately wild type positions.

b 1.5-fold stage wild type embryos showing the normal positions of the hypodermal cells and nuclei. A mononucleate seam cell is indicated with an arrowhead and a multinucleate dorsal hypodermal cell with an arrow as in **a**.

elongation has been completed (Johnstone and Barry, 1996). Because of this, the expression patterns of constructs consisting of collagen promoters fused to GFP within mutant embryos provide temporal markers of the stage of hypodermal development with respect to cuticle synthesis. *ijDf1* homozygotes express both *dpy-7* and *col-12*::GFP reporter constructs (Figure 6.5a,c). The intensity of *col-12*::GFP transgene expression in *ijDf1* is equivalent to the transgene expression in wild type embryos although the expression pattern did not appear as uniform as wild type. The expression of this transgene was very faint in wild type as well as *ijDf1* homozygote embryos in all lines obtained from injecting the pMW0003 *col-12*::GFP construct (Figure 6.5d). Because *col-12* is expressed after elongation and just prior to cuticle secretion and hatching in wild type embryos, the expression of the *col-12*::GFP transgene in *ijDf1* homozygote embryos suggests that hypodermal cells have reached the terminal stage of development regarding the synthesis of cuticular collagens (Johnstone and Barry, 1996).

To determine whether *ijDf1* homozygote embryos actually secreted a cuticle, I used a monoclonal antibody, DPY7-5a, described in chapter 3, which recognises the carboxy terminus of the DPY-7 cuticular collagen. A cuticle is clearly secreted in *ijDf1* embryos and it has the same pattern as secreted wild type cuticle seen in embryos at the end of elongation (Figure 6.5e,f). The circumferentially orientated furrows, or annulae of the cuticle are much closer together than wild type which would be expected from an unelongated embryo, and this makes the antibody appear much brighter in mutants than in wild type. Costa *et al.*,1997 suggest that the pattern of the annulae, or furrows, seen in the cuticle coincides with the pattern of actin filament bundles in the underlying hypodermis. The presence of these parallel furrows in *ijDf1* homozygotes, albeit much more closely packed together than in elongated wild type embryos, suggests that at some stage during embryogenesis, actin fibres in the hypodermis of these mutant embryos become circumferentially orientated as in normally elongating embryos prior to elongation.

6.2.3. Muscle

Myosin A is a component of body wall muscle which is recognised by the monoclonal antibody DM5.6 (Miller *et al.*, 1983; Hresko *et al.*, 1994; Moerman *et al.*, 1996). The overall pattern of DM5.6 staining in *ijDf1* homozygotes is the same as wild

Figure 6.5

Expression of cuticular collagen:: GFP constructs in the hypodermis and localisation of the cuticular collagen, DPY-7, in *ijDf1* homozygotes and wild type embryos

Column **i** shows DIC images while column **ii** shows UV images of collagen::GFP transgene expression (**a-d**) or DPY7-5a antibody staining (**e, f**). The monoclonal antibody, DPY7-5a, recognises the cuticular collagen DPY-7. In all images, except image **f**, the anterior of the embryos is to the left and in images **a, c** and **e** the dorsal region of the embryos is towards the top of the page.

a *ijDf1* homozygote

ii *dpy-7*::GFP transgene expression in the mutant embryo.
This shows that the transgene is clearly expressed in the mutant embryo although mutant embryos at the terminal phenotype often showed a diffuse transgene expression in the hypodermis.

b 3-fold wild type embryo

ii Normal pattern of the *dpy-7*::GFP nuclear localised transgene expression in the 3-fold wild type embryo

c *ijDf1* homozygote

ii *col-12*::GFP nuclear localised transgene expression in the mutant embryo.
The expression of this particular *col-12* GFP transgene in the lines observed was faint in mutant and wild type embryos. It can be seen that the *col-12*::GFP transgene is expressed in mutant embryos

d 3-fold wild type embryo

ii Normal pattern of the *col-12*::GFP nuclear localised transgene expression in the 3-fold wild type embryo although this was very faint in the lines observed.

e *ijDf1* homozygote

ii Staining pattern of the monoclonal antibody, DPY7-5a in the mutant which shows an extracellular localisation indicating that a cuticle has been secreted.

f 3-fold wild type embryo

ii Normal extracellular localisation of the DPY7-5a antibody in a 3-fold wild type embryo showing a secreted cuticle

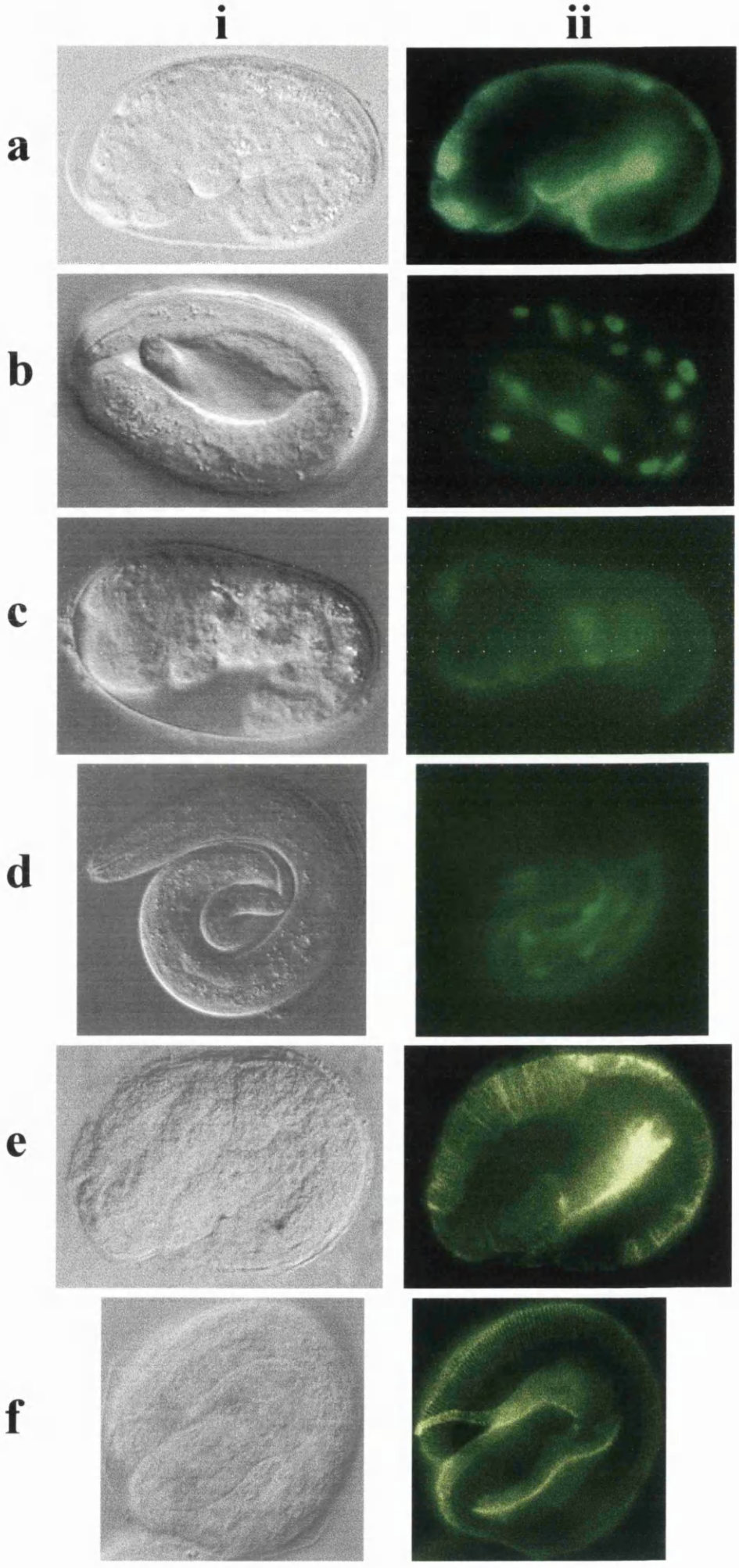
i
ii
a
b
c
d
e
f

type embryos showing four regions of sarcomere staining in parallel rows (Figure 6.6). However, the fine structure of these sarcomeres seems to be slightly more disorganised in *ijDf1* mutants compared to wild type embryos, appearing more branched and diffuse (Figure 6.6a). This may reflect a real difference of muscle organisation in *ijDf1* mutants or it may be a result of abnormalities in other associated tissues. It is also possible that the unelongated phenotype of *ijDf1* embryos results in slight changes in the pattern of these tissues as they are present in a much shorter space than normal.

6.2.4. Muscle-hypodermis attachments and basement membrane

UNC-52 is a component of the basement membrane between the hypodermis and body wall muscle (Rogalski *et al.* ,1993). It is a homologue of perlecan and functions to organise muscle sarcomeres and anchor myofilaments to the cuticle through the hypodermal cells (Moerman *et al.*, 1996). Several of the isoforms of this protein are recognised by the monoclonal antibody MH3 which indicates both muscle:hypodermis and muscle:muscle boundaries(Francis and Waterston, 1991). The MH3 pattern in *ijDf1* homozygotes is organised essentially as wild type (Figure 6.7).

Hemidesmosomes are regions of the hypodermis associated with the attachment of underlying body wall muscle. A component of hemidesmosomes, the intermediate filaments, are recognised by a monoclonal antibody, MH4, which also recognises regions of the pharynx, the excretory cell, and amphid sensory neurons (Francis and Waterston, 1991). In *ijDf1* homozygote embryos, there is MH4 staining in the pharynx, excretory cell, and amphid sensory neurons but no staining at all apparent in the hypodermis (Figures 6.8 and 6.9e). It has been found that hypodermal cells under which the body wall muscle has been ablated do not show MH4 staining (Hresko *et al.*, 1994). However, in *ijDf1* homozygotes there is both muscle staining and staining of the basement membrane at muscle:muscle, and/or muscle:hypodermal junctions. Muscle attachment is normally mediated by a region of the basement membrane and the hemidesmosomes (Hresko *et al.*, 1994). It is possible that a component of the intermediate filaments in the hypodermis recognised by MH4 is encoded by a gene which is deleted by *ijDf1*.

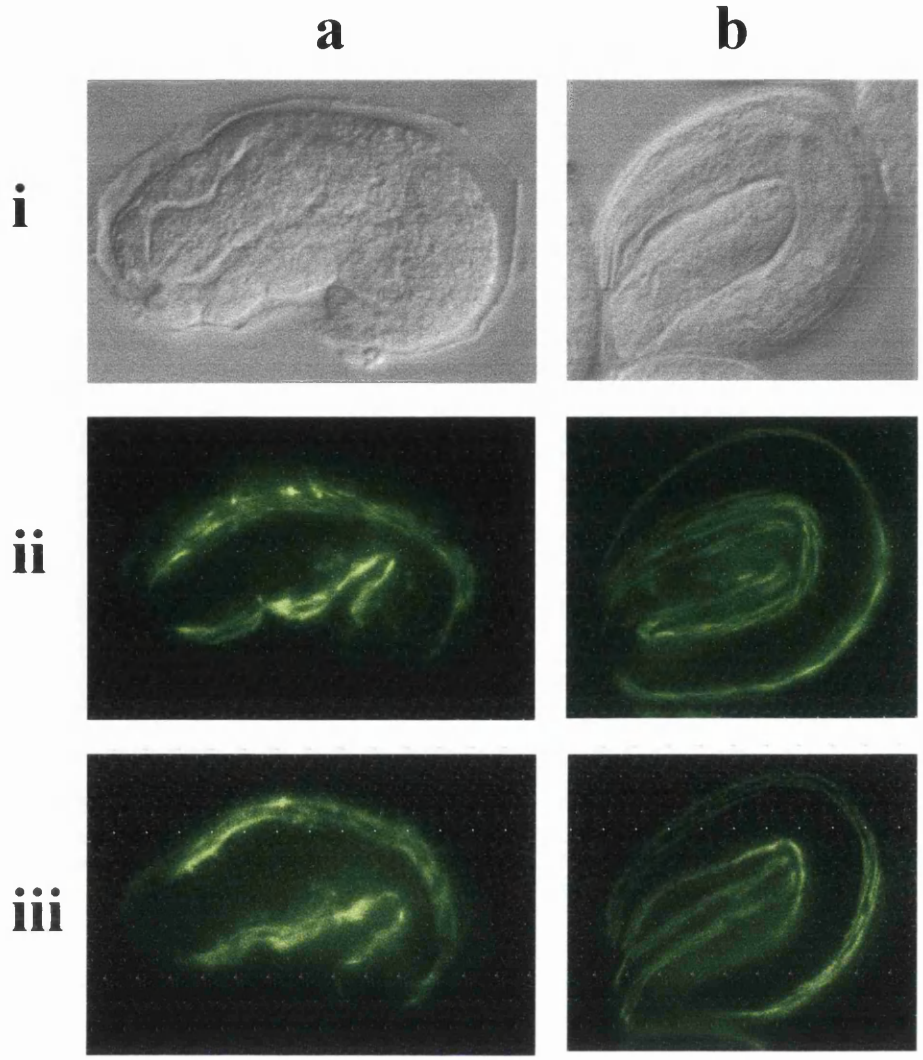

Figure 6.6

Position of muscle sarcomeres in *ijDf1* mutants and wild type embryos

Embryos were stained with the monoclonal antibody DM5.6 to visualise myosin A within the muscle sarcomeres. In both images, the anterior is to the left and in image **a** the dorsal region is to the top of the image. DIC images are shown in row **i**.

a *ijDf1* homozygous mutant

ii and **iii** DM5.6 staining showing different views of the mutant embryo muscle sarcomeres. Sarcomeres appear to be organised in an approximately wild type manner.

b 3-fold wild type embryo

ii and **iii** DM5.6 staining of the 3-fold embryo showing two views of the normal positions of the muscle sarcomeres.

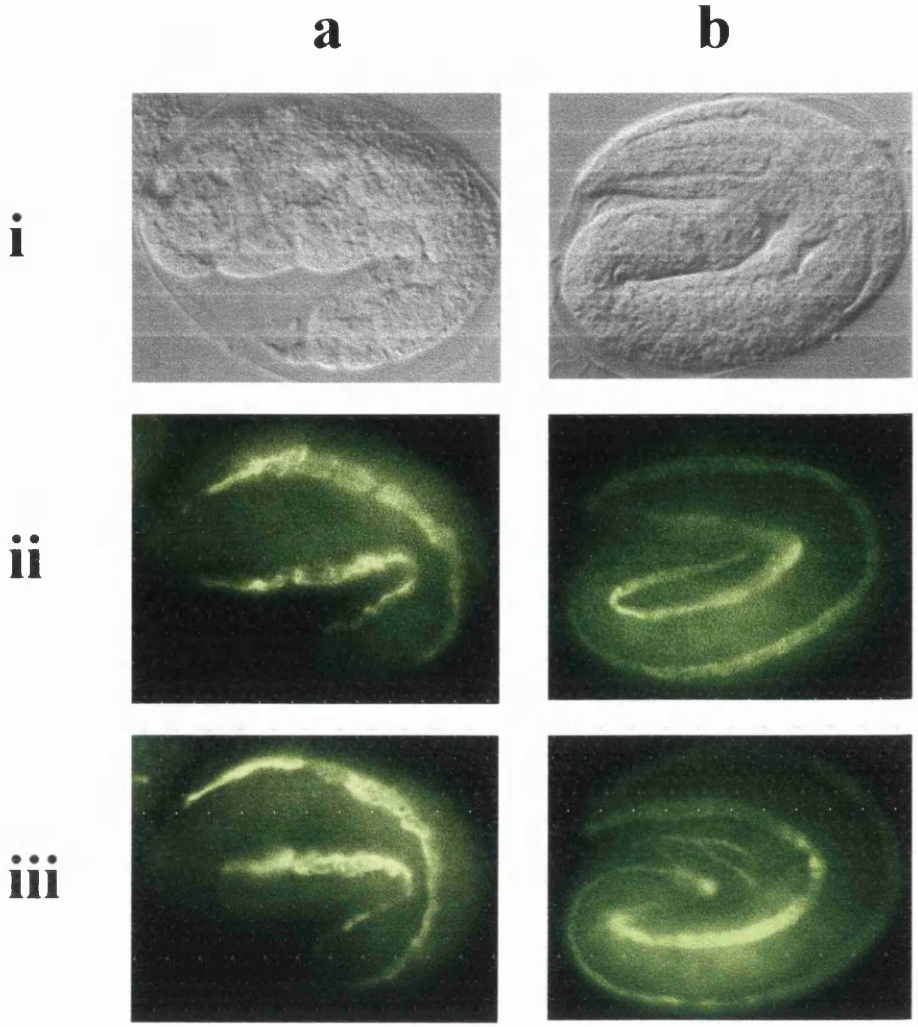

Figure 6.7

Positions of muscle:muscle and muscle:hypodermis junctions in *ijDf1* homozygous mutants and wild type embryos

Embryos were stained with the monoclonal antibody MH3 which recognises several isoforms of the protein UNC-52 present in the basement membrane between adjacent muscle cells and muscle:hypodermal cells. In all images the anterior is to the left and the dorsal region is to the top and right. DIC images are shown in row **i**.

a *ijDf1* homozygous mutant

ii and **iii** MH3 staining pattern at the two sides of the mutant embryo. MH3 staining is equivalent to the wild type pattern.

b 3-fold wild type embryo

ii and **iii** Normal MH3 staining pattern at two sides of the wild type embryo.

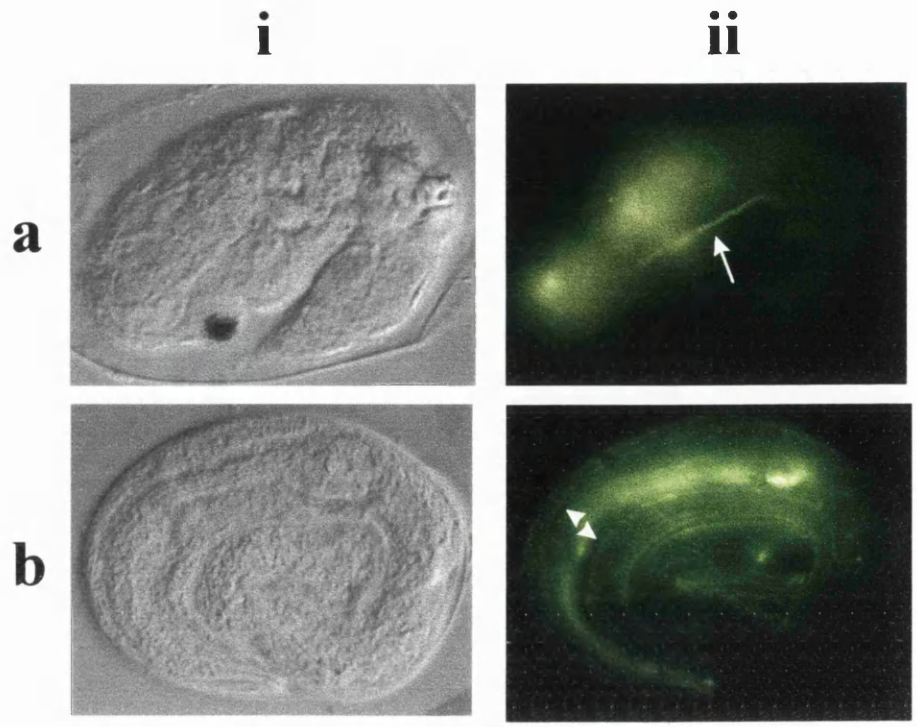

Figure 6.8

Association of the hypodermis and underlying muscle in *ijDf1* mutants and wild type embryos

Embryos were stained with the monoclonal antibody MH4 which recognises intermediate filaments, part of the hemidesmosomes, present in hypodermal cells overlying muscle sarcomeres. Bands of MH4 staining are denoted with arrowheads on image **bii**. The *ijDf1* embryo in **a** is positioned with the anterior to the left of the image and the dorsal region to top of the image. The wild type embryo in **b** is positioned with the anterior towards the bottom centre of the image. MH4 also stains regions of the pharynx which can be seen on a more internal focal plane. DIC images are shown in column **i**.

a unhatched *w4* mutant

ii and **iii** MH4 staining showing the absence of intermediate filaments in the hypodermis of the mutant embryo. MH4 staining of a sensory neuron can be seen and is indicated with an arrow.

b 3-fold wild type embryo

i and ii MH4 staining showing normal hemidesmosome positions at one side of the wild type embryo.

6.2.5. Pharynx and intestine

The pharynx is a structure made up of many cell types including muscle, epithelial and nerve cells. The main regions of the wild type pharynx are shown in Figure 1.4c. In order to examine the pharynx, I used the monoclonal antibodies, 3NB12, which recognises pharyngeal muscle precursor cells, MH27, which recognises adherens junctions within the pharynx and intestine, and MH4, which recognises intermediate filaments in pharyngeal epithelial cells in regions adjacent to pharyngeal muscle cells (Priess and Hirsh, 1986; Waterston, 1988; Francis and Waterston, 1991; Hresko *et al.*, 1994; Mango *et al.*, 1994a). The pharynx of *ijDf1* embryos has not elongated to the terminal pharyngeal length, possibly as a result of the much shortened body, and staining of some cell types that make up the pharynx indicate that it is underdeveloped (Figure 6.9a,c,e). The 3NB12 pattern appears shorter and less differentiated than a wild type pharynx at the 3-fold stage of development which indicates that the pharyngeal muscles are more underdeveloped than in the fully elongated wild type embryo (Figure 6.9a,b) . The MH27 staining pattern also shows the pharynx to be shorter than a 3-fold stage embryo but otherwise appears to show differentiation into the four main regions (Figure 6.9c,d). The MH4 staining pattern looks shorter and possibly less differentiated than in a 3-fold stage embryo (Figure 6.9e,f). It is possible that the apparent defects seen in these different pharyngeal tissue groups is due mostly to the unelongated body of the mutant embryos causing the pharynx to occupy a much shorter space and therefore appear abnormal.

Gut autofluorescence is present approximately in the correct position and is equivalent to a wild type embryo at the same stage of elongation (Figure 6.10). From MH27 staining, intestinal adherens junctions also appear to be intact and in approximately the correct position. Compared to wild type embryos, they are possibly closer to the pattern of fully elongated embryos rather than 1.5-fold elongated wild type embryos (Figure 6.9g-l). This may suggest that unlike the pharynx, the intestine has reached a further stage of development possibly even developing to completion.

Figure 6.9

Pharynx and intestine position and shape in *ijDf1* homozygote mutants and 3-fold wild type embryos.

Embryos were stained with the monoclonal antibodies 3NB12, MH4 and MH27 (see text for details). DIC images are in the left column (**i**) and UV images showing antibody staining are shown in the column to the right (**ii**). In all images except image **f** the anterior is towards the left and in images of mutant embryos (**a, c,** and **e**) the dorsal region is to the top. In image **f** the anterior is curving down to the bottom centre of the image pointing to the right. In all images, arrowheads denote the four main regions of the pharynx.

a *ijDf1* homozygote mutant

ii 3NB12 staining of the mutant embryo showing the position of pharyngeal muscles which appears to show less differentiation and elongation of the pharynx compared to wild type.

b 3-fold wild type embryo

ii 3NB12 staining of the 3-fold embryo showing the normal position of pharyngeal muscles.

c *ijDf1* homozygote mutant

ii MH27 staining of the mutant embryo showing the position of pharyngeal and intestinal adherens junctions which appears differentiated as wild type but shows much shorter structures.

d 3-fold wild type embryo

ii MH27 staining of the 3-fold embryo showing the normal position of pharyngeal and intestinal adherens junctions.

e *ijDf1* homozygote mutant

ii MH4 staining showing the position of intermediate filaments within the marginal cells of the mutant embryo pharynx. These structures appear possibly less developed than in the wild type and are not as elongated.

f 3-fold wild type embryo

ii MH4 staining of the 3-fold embryo showing the normal position of intermediate filaments within the marginal cells of the mutant embryo pharynx.

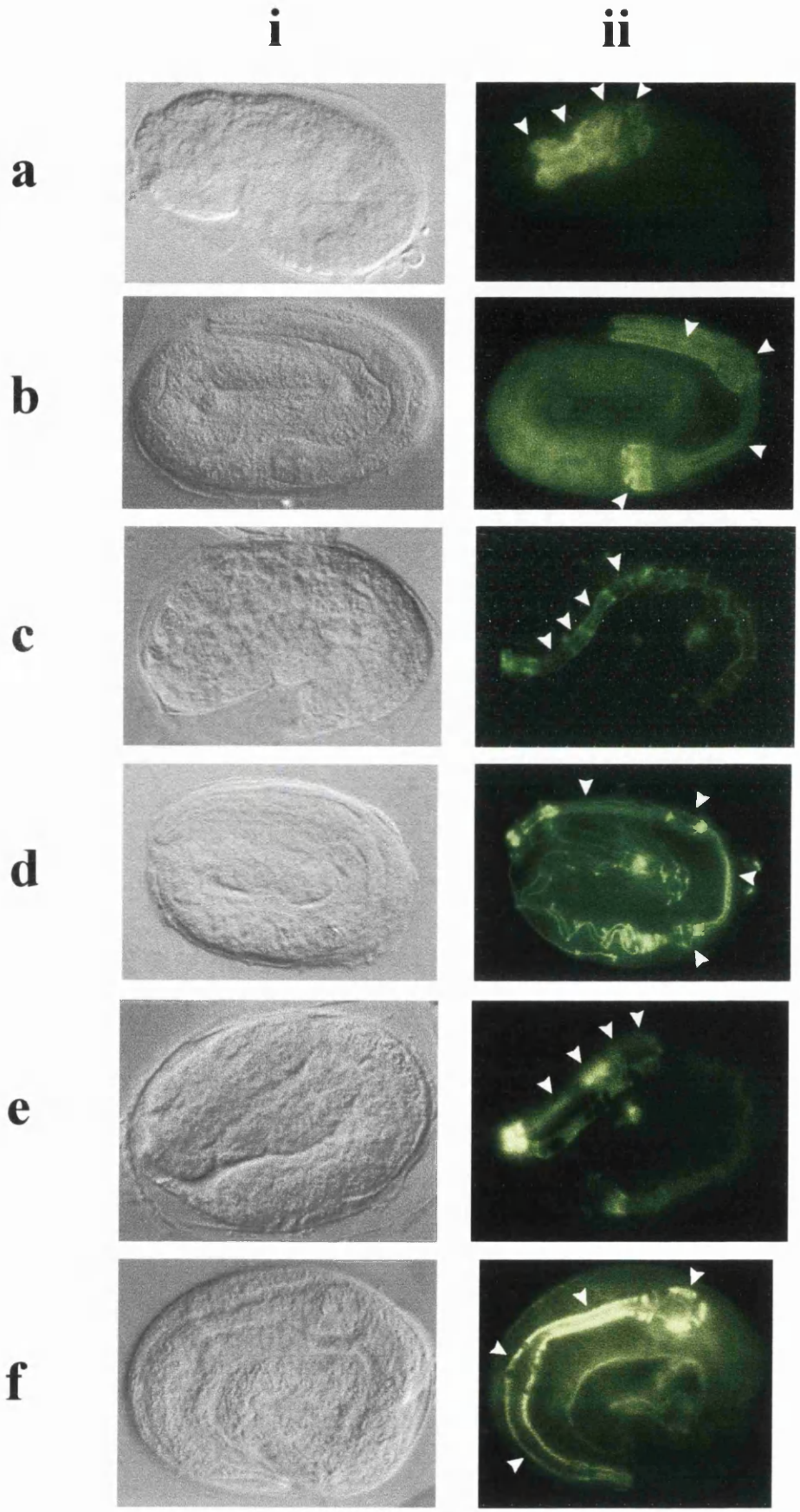
i
ii
a
b
c
d
e
f

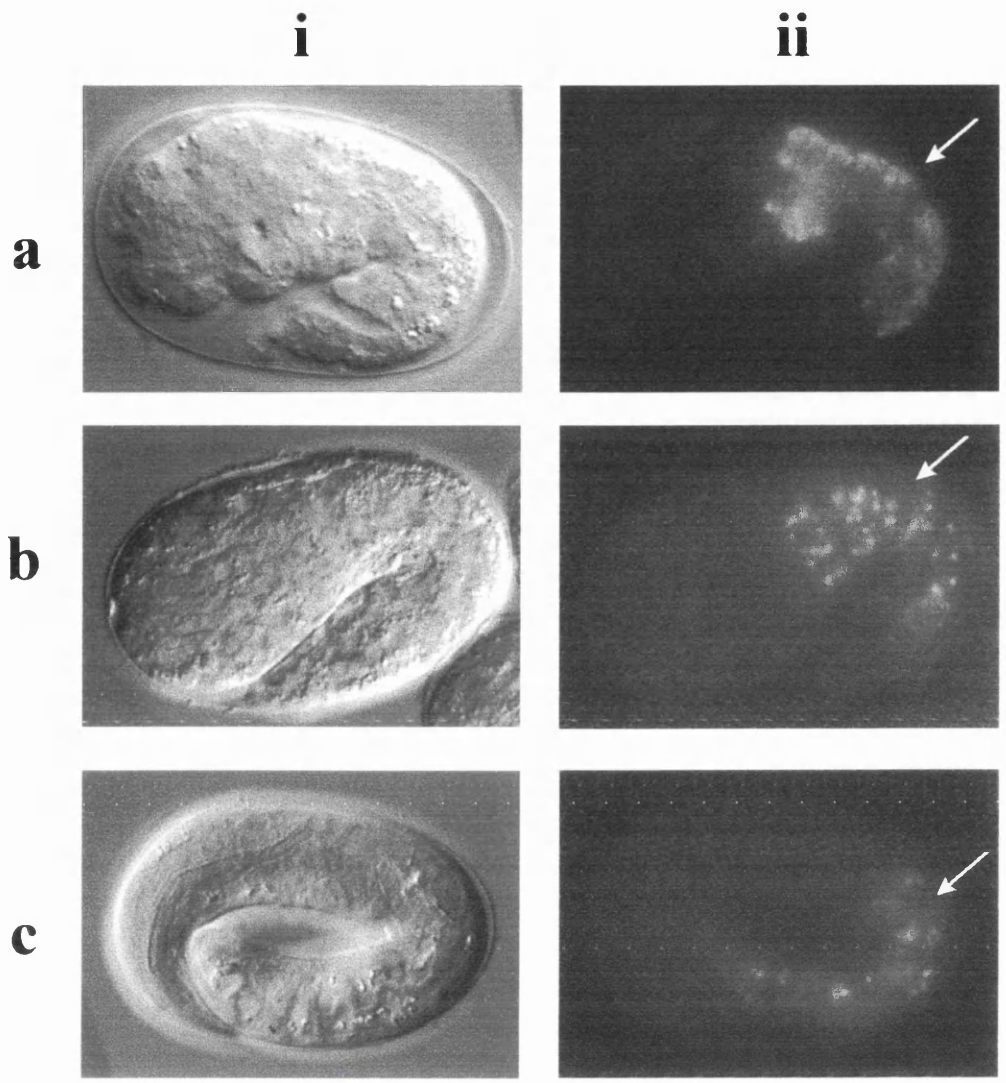

Figure 6.10

Position of the intestine in *ijDf1* homozygote mutants and wild type embryos as indicated by gut granule autofluorescence

DIC images are shown in column **i** and UV images showing gut autofluorescence in column **ii**. Embryos in all images are shown with the anterior to the left and the dorsal region to the top and right of the image. An arrow points to the gut autofluorescence in each embryo

a *ijDf1* homozygote mutant embryo

The gut autofluorescence appears as wild type. It appears slightly brighter than a 3-fold wild type embryo which is probably due to the shortened overall body length.

b 1.5-fold stage wild type embryo

c 3-fold stage wild type embryo

6.3. Mapping

I mapped *ijDf1* using a mixture of classical genetic crosses, the sequence-tagged site (STS) PCR-based method explained in section 5.3.2, complementation tests, and the cosmid sequence marker (CSM) method explained in section 5.3.5.

6.3.1. Chromosomal assignment

Hermaphrodites heterozygous for the *ijDf1* deficiency were crossed with wild type males and the resulting F1 males were crossed into several mapping strains. The F2 outcrossed hermaphrodites never contained *ijDf1* and since it could not be transferred through males, I deduced that the mutation was most likely linked to the X chromosome. Males contain only one X chromosome whereas hermaphrodites have two, therefore a male carrying an embryonic lethal allele on the X chromosome will arrest as an embryo.

6.3.2. Fine mapping of *ijDf1* - STS mapping

The principles of STS mapping are explained in section 5.3.2. The same Bergerac strain, RW7000, containing Tc1 markers at specific sites (the STS markers), was used in the crosses, although the initial crosses had to be carried out in a different way as the mutation was linked to the X chromosome. Firstly, RW7000 hermaphrodites were crossed with wild type males and the resulting F1 males, all carrying the maternal RW7000 X chromosome, were crossed into hermaphrodites heterozygous for *ijDf1*. The outcrossed hermaphrodites from this cross, all carried one RW7000 X chromosome and 50% of them carried the *ijDf1* deficiency X chromosome. These hermaphrodites were allowed to self and the resulting *ijDf1* homozygous embryos were lysed and tested for the presence or absence of the STS markers using PCR. I used 6 STS markers from the X chromosome to map *ijDf1* (Figure 6.11a, Appendix 6.2; Williams *et al.*, 1992). A representative gel showing the marker bands is shown in Figure 6.11b and the full results are given in Appendix 6.2 and Figure 6.11c. The results showed that *ijDf1* lies to the far right of the X chromosome, to the right of stP72. As explained in section 5.3.2,

Figure 6.11

STS mapping of Deficiency *ijDf1* on the X chromosome.

a Positions of STS markers and several genes on the physical and genetic maps of the X chromosome (Williams et al., 1992). The physical map is shown on the top and genetic map underneath.

b Representative gel showing positions of STS markers from the right of chromosome V. Lanes 1-15 contain DNA from *ijDf1* homozygote embryos except Lane 7 which is a control containing DNA from an RW7000 embryo. Lanes 9-11 and Lane 14 are either failed reactions or contain none of the STS markers. STS markers are scored as present for each embryo if a band of the correct size is present:
Lane 1 - markers stP33, stP40, stP41 and stP129 are present
Lane 2 - markers stP33, stP40 and stP41 are present
Lane 3 - markers stP40, stP41, stP129 and stP72 are present
Lane 4 - markers stP40 and stP41 are present
Lane 5 - markers stP40 and stP41 are present
Lane 6 - markers stP40 and stP41 are present
Lane 7 - control, all markers are present
Lane 8 - markers stP33, stP40, stP41, stP129 and stP72 are present
Lane 12 - markers stP33, stP40 and stP41 are present
Lane 13 - markers stP40 and stP41 are present
Lane 15 - markers stP33, stP40 and stP41 are present

c Proposed recombination events between the RW7000 X chromosome (top line) and the *ijDf1* X chromosome (bottom line) which produces the classes A-E:
class A (n=30 mutant embryos), class B (n=45), class C (n=28), class D (n=17) and class E(n=4). This places *ijDf1* in a position to the right of stP72 as shown on the bottom chromosome.

a

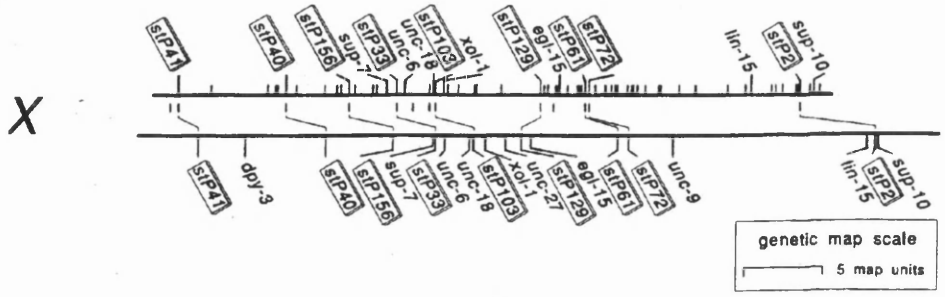
X
stP41
stP40
stP156
sup-7
stP33
unc-6
unc-18
stP103
xol-1
stP129
egl-15
stP61
stP72
lin-15
stP2
sup-10
dpy-9
unc-9
unc-27
genetic map scale
5 map units

b

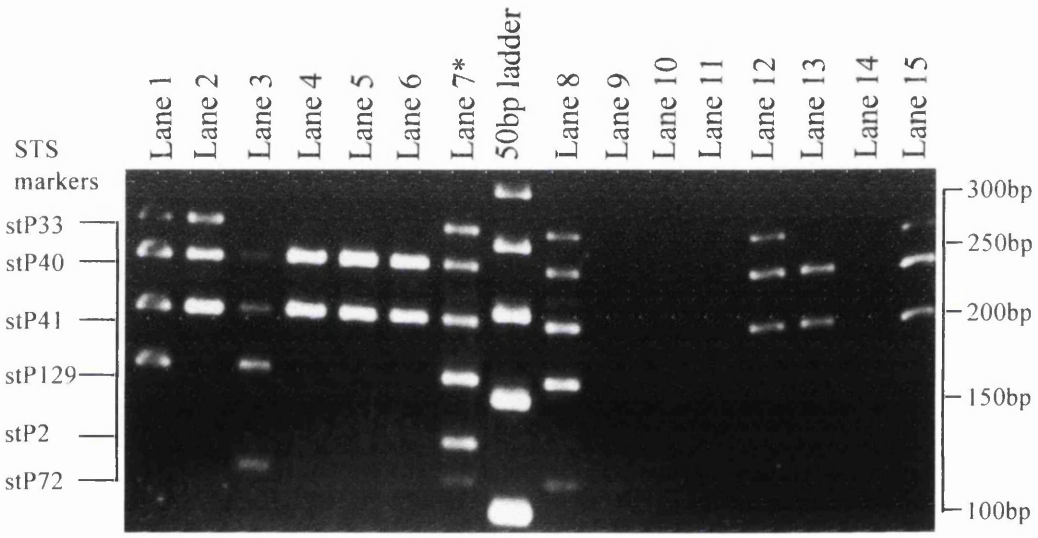
Lane 1
Lane 2
Lane 3
Lane 4
Lane 5
Lane 6
Lane 7*
50bp ladder
Lane 8
Lane 9
Lane 10
Lane 11
Lane 12
Lane 13
Lane 14
Lane 15
STS markers
stP33
stP40
stP41
stP129
stP2
stP72
300bp
250bp
200bp
150bp
100bp

c

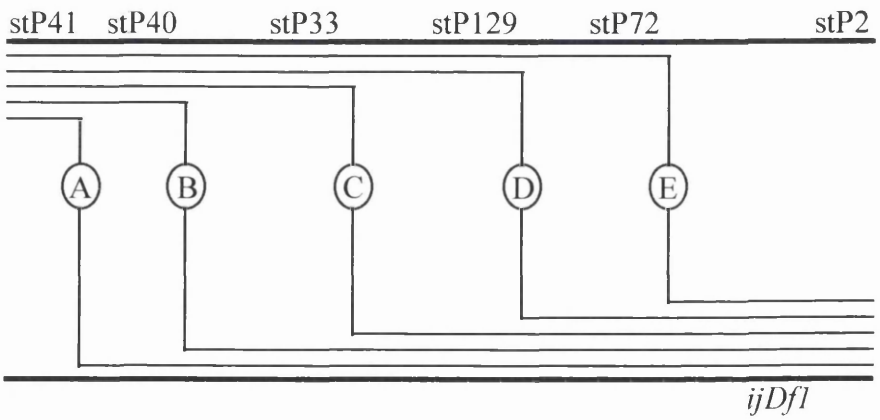
stP41
stP40
stP33
stP129
stP72
stP2
A
B
C
D
E
ijDf1

spontaneous lethal mutations may result from Tc1 insertion in the RW7000 strain leading to arrested embryos testing positive for all STS markers (Williams, 1995).

6.3.4. Complementation tests

ijDf1 was crossed into strains carrying marker genes in this region of the X chromosome in order to map the mutation more finely. Crossing with a strain carrying *lin-15(n309)* at position 22.30 on X and separately with a strain, SP219 carrying *unc-3(e151)* at 18.56 on X gave non-complementation. Hermaphrodites homozygous for the recessive temperature-sensitive allele, *lin-15* show a multivulva (Muv) phenotype and hemizygous males can only mate at the permissive temperature of 15°C. After mating had occurred at 15°C between males hemizygous for *lin-15* and hermaphrodites heterozygous for *ijDf1*, the worms were moved to 25°C and I observed that around 50% of F1 hermaphrodites showed the Muv phenotype. 14 Muv and 14 non-Muv F1s were left to self separately at 25°C and while all the Muv hermaphrodites carried *ijDf1*, none of the non-Muv hermaphrodites did. Similarly, I crossed males hemizygous for *unc-3(e151)*, and carrying the *mnDp1* duplication (X;V) which covers *unc-3* to allow mating, with hermaphrodites heterozygous for *ijDf1*. Around 25% of F1 hermaphrodites were Unc as 50% of all F1s would be carrying the *mnDp1* duplication, and after cloning out 15 Unc and non-Unc F1s it was found that all the Unc F1s carried *ijDf1* while none of the non-Unc F1s did. It was concluded that *ijDf1* must be a deficiency which deletes both *unc-3* and *lin-15* and the region between these genes.

6.3.5. Deficiency physical end-point mapping

In order to investigate the extent of the deficiency, I tested *ijDf1* homozygote genomic DNA for the presence or absence of cosmid sequence markers (CSMs) from this region of the X chromosome. As before, primers were designed specific to a region of the genomic sequence contained in each cosmid clone tested and the presence or absence of a particular band on a gel indicated if the cosmid sequence had been deleted or not. I had the same problem as that mentioned in section 5.3.5 when executing this method. Several primer pairs worked very effectively on wild type embryos and gave much fainter bands within *ijDf1* homozygote embryos. This was seen with several

CSMs corresponding to the region close to and between the genes *unc-3* and *lin-15* which were already known to be deleted in *ijDf1* from the complementation tests. As mentioned in section 5.3.5, I propose that primer pairs that worked very effectively can amplify DNA from polar bodies within *ijDf1* homozygote embryos which can be seen clearly at terminal arrest (Figure 6.13a, arrowhead). It was difficult to get PCR conditions optimum for each primer set so that bands were seen from zygotic genomic DNA only. However, each PCR was repeated at least four times and the end point results obtained were reproducible. Results are shown in Figure 6.12. The end point mapping showed that the *ijDf1* deficiency deletes around 1.6Mb, stretching from between cosmids F54E4 to F42D1 (around 125Kb apart) on the left to between cosmids F52E10 and C11G6 (around 34Kb apart) on the right. These approximate end points correspond to a region of the genetic map between position 18 and 23.5 on the X chromosome, a distance of approximately 5.5 map units.

6.4. Characterisation of overlapping deficiencies, *mnDf17* and *mnDf43*

This region of the genetic map is well characterised and there are many deficiencies which have been genetically mapped using information about genes which they do or do not delete. Several of these deficiencies overlap *ijDf1* and after preliminary characterisation of their phenotypes, two were selected with a view to identifying a region of the genome deleted by *ijDf1* which is involved in the elongation process.

6.4.1. Phenotypic characterisation of *mnDf17* and *mnDf43*

These deficiencies, *mnDf17* and *mnDf43* appeared to overlap *ijDf1* significantly using the genetic data available (Meneely and Herman, 1981; ACeDB). Embryos homozygous for *mnDf17* arrest at an equivalent stage of elongation to *ijDf1* homozygotes with quite a similar phenotype (Figure 6.13b). In contrast, embryos homozygous for *mnDf43* appear to elongate much further, to originally around 2.5 fold, but they retract to just over 2-fold and there are loose cells and areas of rupture within the eggshell (Figure.6.13c). These embryos have a more elongated pharynx than the *ijDf1* pharynx which also appears possibly more differentiated from DIC microscopy.

Figure 6.12

Physical mapping of the *ijDf1* deficiency using Cosmid Sequence Markers (CSMs)

a Schematic diagram representing the mapped region of the X chromosome showing the positions of cosmids from the region of the deficiency relative to one another and corresponding cloned genes with their positions on the genetic map (where known) in map units. Cosmids used in ijDf1 mapping are shown in green.

b Gels showing the presence or absence of each CSM used in mapping. Lanes containing DNA amplified from *ijDf1* homozygote embryos are marked with an asterisk, all other lanes contain DNA from wild type embryos.

The DNA marker used was 50bp ladder (Gibco) and a representative marker band is noted in each gel picture. Each of the bands is 50bp apart.

a

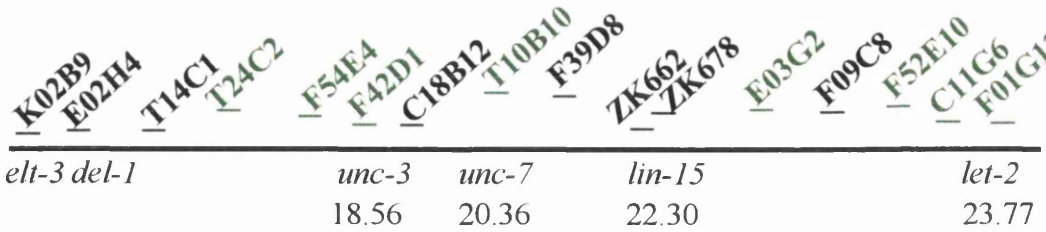
K02B9
E02H4
T14C1
T24C2
F54E4
F42D1
C18B12
T10B10
F39D8
ZK662
ZK678
E03G2
F09C8
F52E10
C11G6
F01G12
elt-3 del-1
unc-3
unc-7
lin-15
let-2
18.56
20.36
22.30
23.77

b

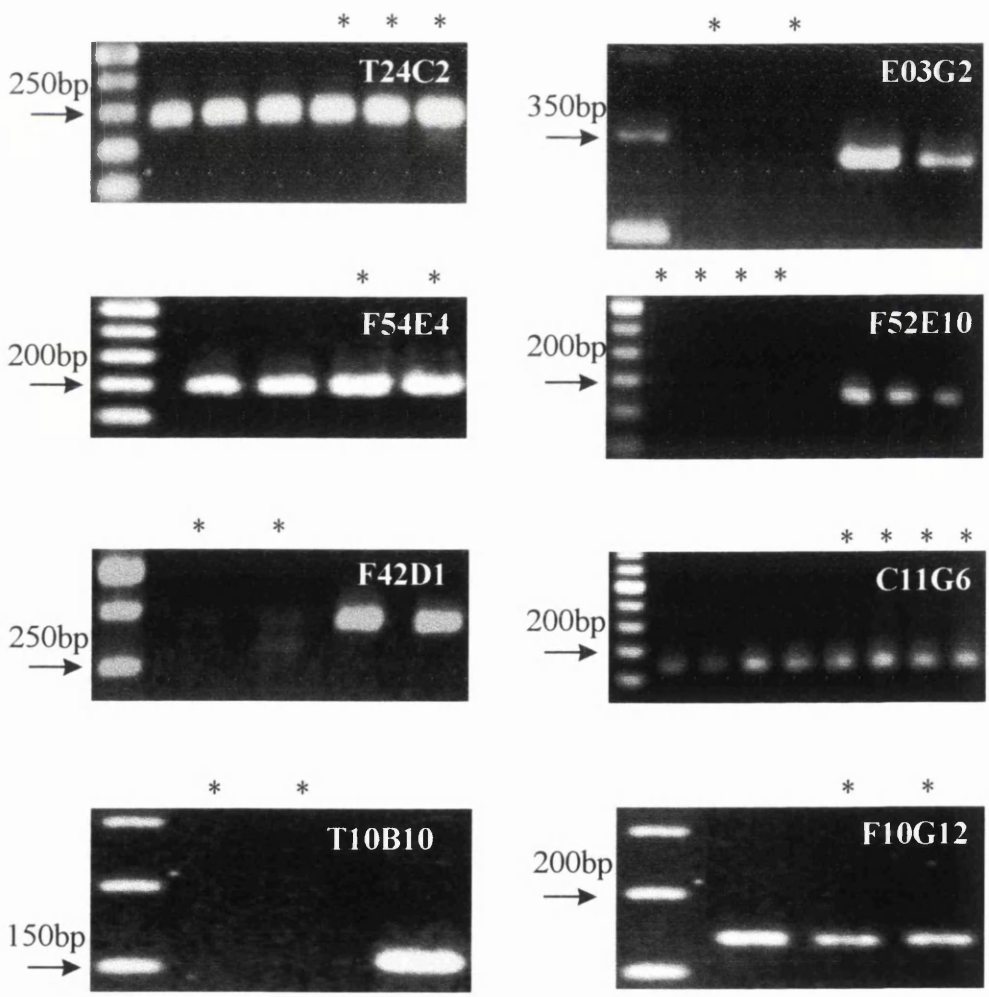
T24C2
250bp
E03G2
350bp
F54E4
200bp
F52E10
200bp
F42D1
250bp
C11G6
200bp
T10B10
150bp
F10G12
200bp

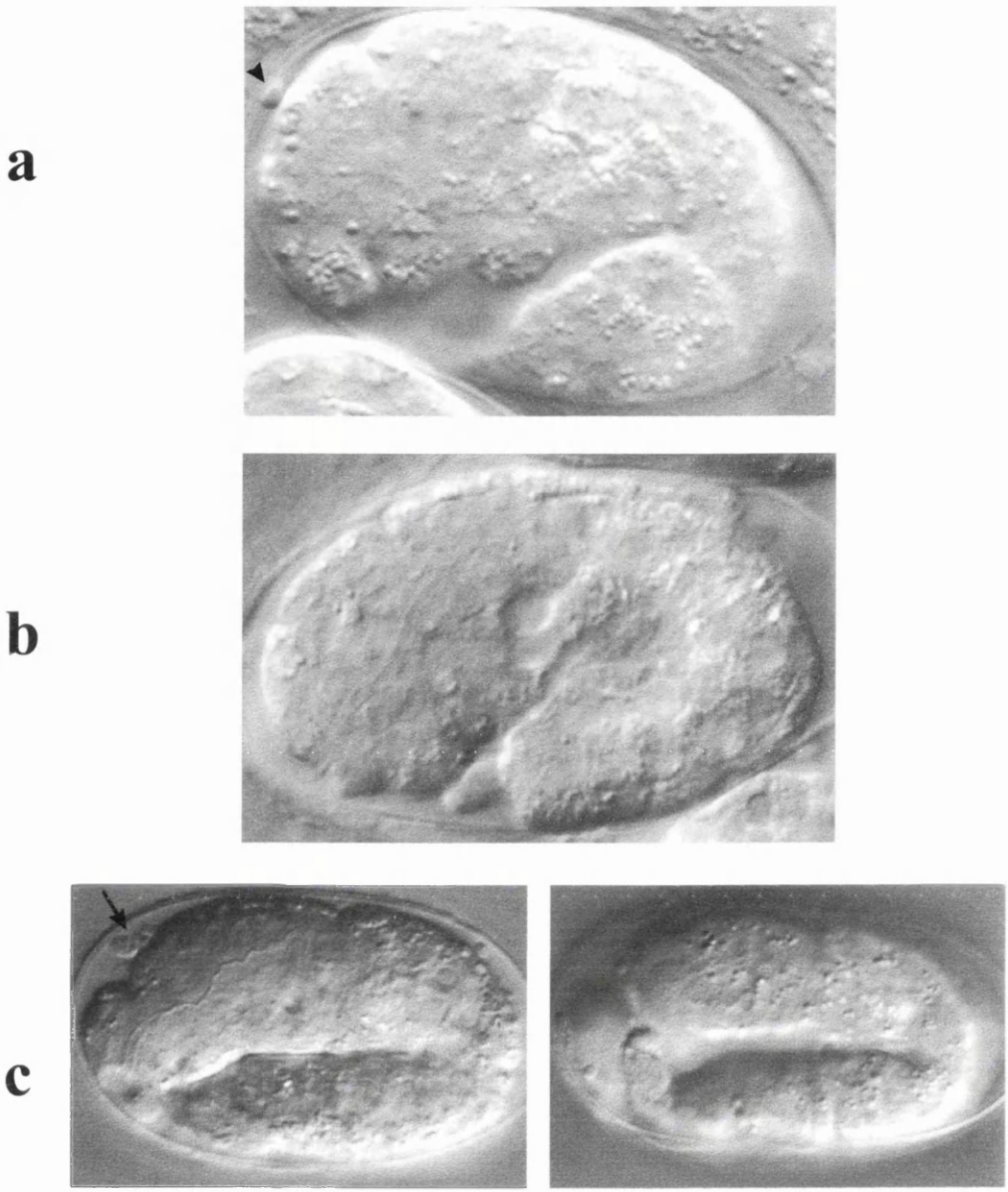

Figure 6.13

DIC images of the arrest phenotypes of mutants homozygous for deficiencies *ijDf1*, *mnDf17* or *mnDf43*

All embryos are positioned with the anterior to the left and dorsal regions to the top of the image.

a *ijDf1* homozygote which arrests at the 1.5-fold stage. An arrow indicates the position of the maternal pole cell.

b *mnDf17* homozygote which arrests at around the 1.5- to 1.75-fold stage

c *mnDf43* homozygote which arrests at just over the 2-fold stage. An arrow points to loose cells floating outside the embryo within the eggshell.

The rupture could be caused by abnormal enclosure of the hypodermis, abnormal hypodermal cell junctions or the secretion of an abnormal cuticle which has weak areas. This would result in tissue bursting through the regions with abnormal hypodermal coverage or cuticle and a retraction of embryo length. Because both of these deficiencies overlap *ijDf1*, it seems possible that the same deleted region is responsible for the severe elongation defect seen in *ijDf1* and *mnDf17* embryos. This region would not be deleted by *mnDf43* allowing embryos homozygous for this deficiency to elongate much further, although *mnDf43* appears to also delete a gene involved in either enclosure of the embryo or cuticle secretion which may or may not be deleted in *mnDf17* and *ijDf1*. *mnDf43* appears to have a better developed pharynx than *mnDf17* or *ijDf1* although this may be due to the increased length of *mnDf43* homozygotes. The important aspect of the *mnDf43* phenotype is that embryos homozygous for the deficiency can elongate significantly over 2-fold even if they subsequently rupture or retract, while in *mnDf17* and *ijDf1*, the embryos never elongate past 1.5- to 1.75-fold. Because *ijDf1* and *mnDf17* homozygote embryos arrest at an equivalent stage of elongation while *mnDf43* homozygotes have the ability to elongate past 2-fold, it is likely that there is a gene or genes involved in elongation deleted by both *ijDf1* and *mnDf17* but not by *mnDf43*. In order to locate the region of the genome where this gene or genes could lie, I mapped the end points of these deficiencies on the physical map using the CSM method as before.

6.4.2. Physical mapping of *mnDf17* and *mnDf43* endpoints

Available genetic map data for *mnDf17* and *mnDf43* from complementation tests with strains carrying point mutations in cloned genes, indicate that *mnDf17* extends from around 15.44 to 22.48 on X and *mnDf43* extends from 15.44 to 21.53 on X (ACeDB). Both deficiencies delete *let-4* (17.44) and not *unc-84* (13.44) to the left, but their left end-points have not been further defined. The right end points on the genetic map are between *let-10* (22.46) and *let-14* (22.49) for *mnDf17*, and between *exc-1* (21.24) and *dyn-1* (21.39) for *mnDf43*. In order to compare the molecular extent of these deficiencies with *ijDf1*, I had to physically map them using the same method. The presence or absence of the CSMs used to physically map these deficiencies is shown in Figures 6.14 and 6.15. From this end point mapping, it became clear that there was a

Figure 6.14

Physical mapping of the *mnDf17* deficiency using Cosmid Sequence Markers (CSMs)

a Schematic representation of the region of the X chromosome to which the deficiency maps. Positions of cosmids relative to one another on the physical map are shown above and cloned genes from the genetic map are shown below the chromosome line with their approximate positions (where known) in map units. Cosmids highlighted in green are those used in the end-point mapping of *mnDf17*.

b Gels showing the presence or absence of CSMs used to map *mnDf17* in mutant and wild type embryos. Lanes containing DNA amplified from *mnDf17* homozygote embryos are denoted with an asterisk and all other lanes contain DNA from wild type embryos.

The marker used was 50bp ladder (Gibco) and a representative marker band is indicated in each gel picture. Each of the bands is 50bp apart.

a

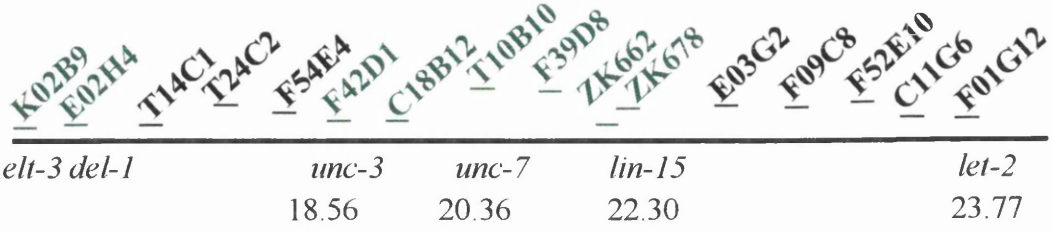
K02B9
E02H4
T14C1
T24C2
F54E4
F42D1
C18B12
T10B10
F39D8
ZK662
ZK678
E03G2
F09C8
F52E10
C11G6
F01G12
elt-3 del-1
unc-3
18.56
unc-7
20.36
lin-15
22.30
let-2
23.77

b

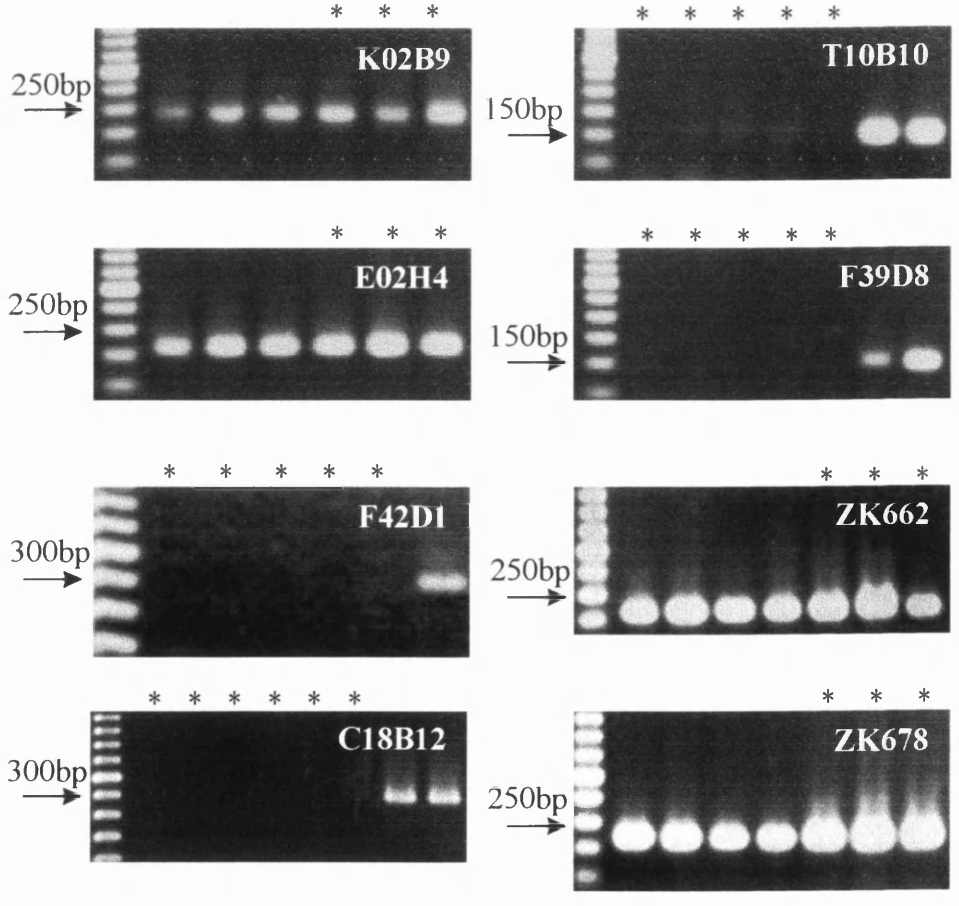
K02B9
250bp
T10B10
150bp
E02H4
250bp
F39D8
150bp
F42D1
300bp
ZK662
250bp
C18B12
300bp
ZK678
250bp

Figure 6.15

Physical mapping of the *mnDf43* deficiency using Cosmid Sequence Markers (CSMs)

a Schematic representation of the region of the X chromosome to which the deficiency maps. Positions of cosmids relative to one another on the physical map are shown above and cloned genes from the genetic map are shown below the chromosome line with their approximate positions (where known) in map units. Cosmids highlighted in green are those used in the end-point mapping of *mnDf43*.

b Gels showing the presence or absence of CSMs used to map *mnDf43* in mutant and wild type embryos. Lanes containing DNA amplified from *mnDf43* homozygote embryos are denoted with an asterisk and all other lanes contain DNA from wild type embryos.

The marker used was 50bp ladder (Gibco) and a representative marker band is indicated in each gel picture. Each of the bands is 50bp apart.

a

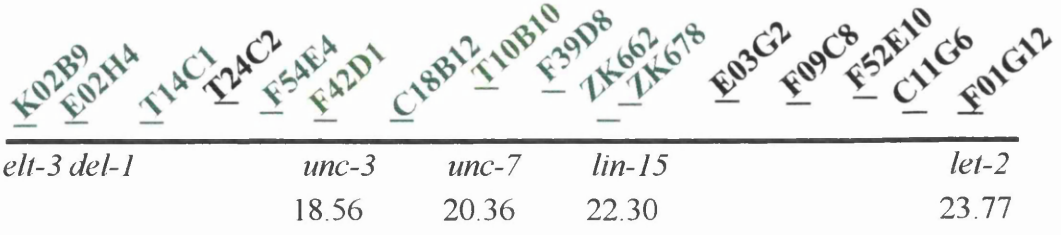

elt-3 del-1	*unc-3*	*unc-7*	*lin-15*	*let-2*
	18.56	20.36	22.30	23.77

b

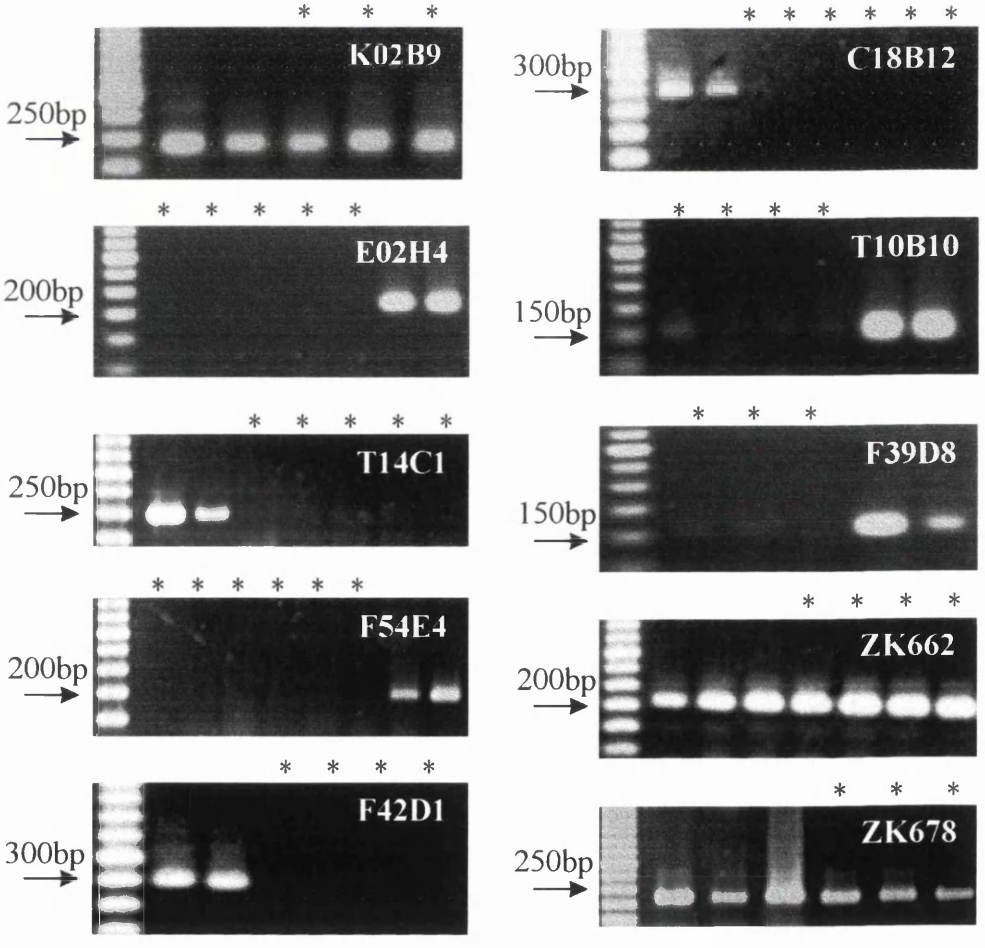

possible region deleted by *ijDf1* which is also deleted by *mnDf17* and not *mnDf43* between the CSMs for F39D8 and ZK662 and this is supported by the genetic data. The molecular overlaps of all three deficiencies are shown in Figure 6.16. *mnDf43*, which is around 1.8Mb in length, deletes an area further left than *mnDf17* (1.4Mb long) or *ijDf1*. This region may contain the gene or genes, which when deleted result in the rupture seen in many *mnDf43* homozygotes. To the right of the deficiencies, *mnDf43* and *mnDf17* delete the F39D8 CSM and not the ZK662 CSM while both CSMs are deleted in *ijDf1*. This area is indicated by arrows in Figure 6.16. The genetic data shown above indicates that *mnDf17* extends further right in this region than *mnDf43* and so this is an ideal region in which to search for the gene or genes which when deleted result in the 1.5-fold arrest, but when present allow elongation past 2-fold. The next step was to attempt to rescue the early elongation defect seen in *ijDf1* by injecting genomic DNA from this region and clone the gene or genes involved.

6.5. Cosmid rescue of the early elongation defect in *ijDf1*

Overlapping cosmid, lambda and yeast artificial chromosome (YAC) clones are represented in the *C.elegans* physical map and cover the entire genome, with the exception of a few very small gaps (The *C.elegans* sequencing Consortium, 1998). The X chromosome has excellent alignment between the genetic and physical maps due to the high proportion of cloned genes and the alignment is increasing further as more genes are investigated. The ability of injected DNA molecules to recombine and form heritable extrachromosomal transgenic arrays within *C.elegans* hermaphrodites constitutes a valuable tool which enables the study of mutations and cloning of genes (Fire *et al.*, 1986; Mello *et al.*, 1991). DNA transformation is discussed in more detail in section 4.4.1.

In the case of *ijDf1*, I did not expect to achieve complete rescue of the mutant phenotype. *ijDf1* is a large deficiency deleting many genes and it is probable that a number of these are essential. By injecting cosmids from the region between F39D8 and ZK662, I was adding back a small proportion of wild type genes into animals homozygous for a large deficiency and so I was simply looking for transformed homozygotes of *ijDf1* which arrested at a much later stage of elongation, possibly equivalent to the elongation phenotype seen in *mnDf43*. For simplicity, I will refer to a

Figure 6.16

Schematic diagram showing the overlaps of the deficiencies *ijDf1*, *mnDf17* and *mnDf43* on the right arm of the X chromosome

Cosmid positions are drawn relative to one another although these are not to scale, and cloned genes are also shown with their positions on the genetic map in map units as reference points. Solid black lines indicate areas that deficiencies delete with dashed black lines representing the region from the last absent CSM to the first present CSM where the endpoints have not been more finely mapped. The area of the genome between the red arrows possibly contains a region which is deleted by *mnDf17* and *ijDf1* but not *mnDf43*. Because of the different phenotypes of embryos homozygous for each deficiency, a gene or genes involved in early elongation may be present within this region. The region denoted by the green star may contain the gene which, when deleted in *mnDf43* results in hypodermal rupture. The scale bar refers to the lines indicating the extent of the deficiencies and not to the cosmids.

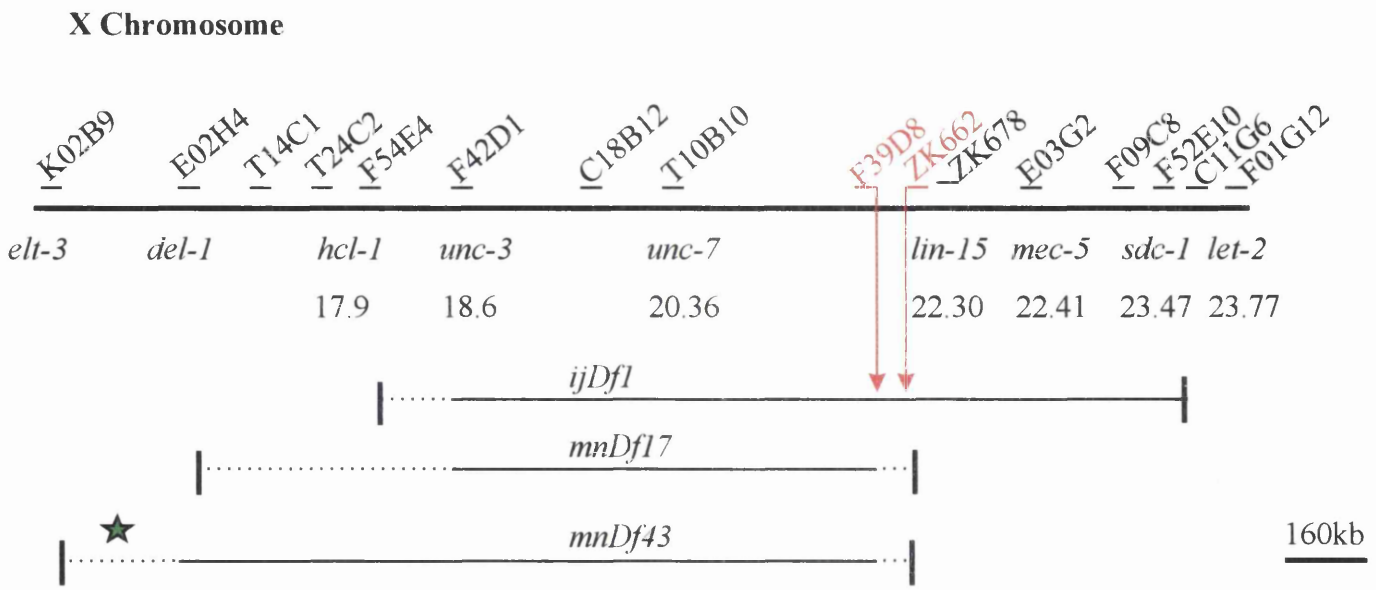
X Chromosome
K02B9
E02H4
T14C1
T24C2
F54E4
F42D1
C18B12
T10B10
F39D8
ZK662
ZK678
E03G2
F09C8
F52E10
C11G6
F01G12
elt-3
del-1
hcl-1
unc-3
unc-7
lin-15
mec-5
sdc-1
let-2
17.9
18.6
20.36
22.30
22.41
23.47
23.77
ijDf1
mnDf17
mnDf43
160kb

quantitative increase in the degree of elongation at arrest as rescue. Because I was looking for differences between transformed and non-transformed arrested embryos, I needed to inject a marker visible in embryos along with the cosmid and pRF4 (containing the *rol-6(su1006)* mutation) DNA. I selected the plasmid pMW0002, containing the promoter region of the collagen gene, *dpy-7* fused to, and in frame with, the GFP gene (I.Johnstone, pers.comm.). This plasmid did not interfere with embryogenesis when injected alone and it was known that *dpy-7* was expressed in *ijDf1* homozygotes (see section 6.2.2). When viewed under UV light, embryos containing the pMW0002 marker plasmid fluoresce and so they can be distinguished readily from embryos which do not contain the plasmid. Both pMW0002 and pRF4 were included as markers in all the injection mixes described below.

6.5.1. Rescue achieved with groups of cosmids

Initially, while mapping of the deficiencies *mnDf17* and *mnDf43* was in progress, I injected 15 overlapping cosmids (Figure 6.17a) between the genes *unc-7* (position 20.36) and *lin-15* (position 22.30) into hermaphrodites of a partially balanced strain with the genotype *+,ijDf1/unc-84,+*. Two lines were obtained from these injections and both showed rescue of the early elongation phenotype (Figure 6.18a and Table 6.2). This rescue phenotype showed elongation to over the 2-fold stage with no apparent rupturing of tissues and usually quite a narrow anterior. The pharyngeal grinder was also generally more conspicuous with the entire pharynx appearing much more similar to a wild type pharynx. By this stage of the rescue experiments, I had mapped the end-points of *mnDf17* and *mnDf43* further right and so it reduced the number of cosmids in the target region to 11, C11G10-C02D4 on the left being placed outside the region of interest. Two subgroups of 6 overlapping cosmids from within these 11 cosmids were then injected (Figure 6.17b,c). The cosmids from F59D12 to C02C6 were positioned as Figure 6.17b at the time of injections but more recently their positions have been amended to the order in 6.17c. These subgroups were towards the right of the 15 cosmid group as mapping by this stage had uncovered the region from F39D8 to ZK662 as being important. Only one line was obtained from each subgroup and while the subgroup to the 'left' of the region, from C33A11 to H08J19, gave no rescue, the subgroup to the 'right' of the region, from F59D12 to C02C6 gave rescue

Figure 6.17

Schematic diagram showing groups of cosmids used in rescue injections of *ijDf1*

a Original group of 15 overlapping cosmids on the X chromosome with approximate position of cloned genes on the genetic map in map units. Double lines represent gaps in the physical map. The cosmids highlighted in red in Figure 6.16 are also highlighted in red here for position reference. The distance from C11G10 to ZK678 is approximately 670kb.

b, c Subgroups of 6 cosmids representing the 'left' and 'right' of the area. Cosmids in blue were present in the 'left' group only, cosmids in pink were present in the right group only, and cosmids in purple were present in both groups. **b** shows the positions of the cosmids as they were placed at the time of injections and **c** shows the revised positions of the cosmids at the time of writing. Double lines represent gaps in the physical map. The distance between cosmids C33A11 and ZK678 is approximately 470kb.

a

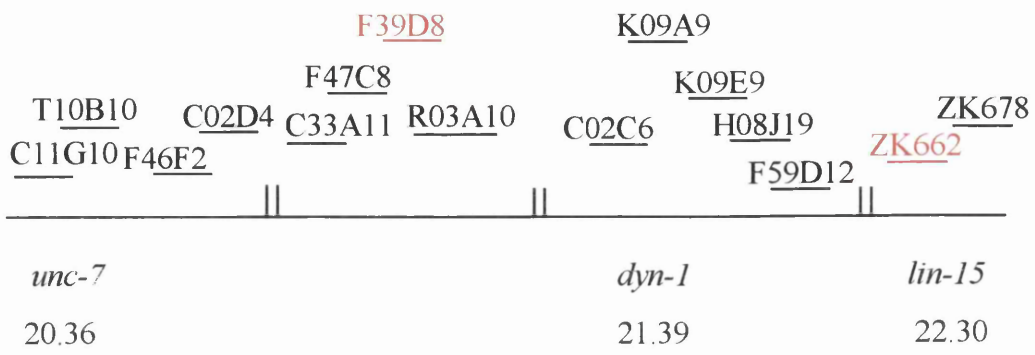
F39D8
K09A9
F47C8
K09E9
T10B10
C02D4
C33A11
R03A10
C02C6
H08J19
ZK678
C11G10
F46F2
ZK662
F59D12
unc-7
dyn-1
lin-15
20.36
21.39
22.30

b

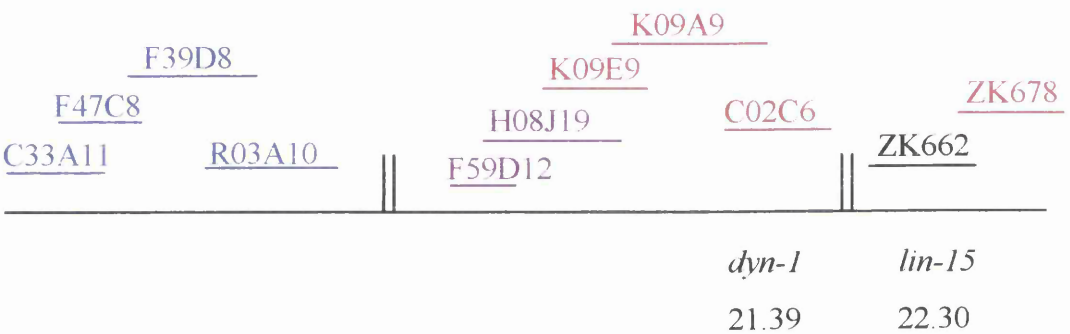
K09A9
F39D8
K09E9
ZK678
F47C8
H08J19
C02C6
C33A11
R03A10
ZK662
F59D12
dyn-1
lin-15
21.39
22.30

c

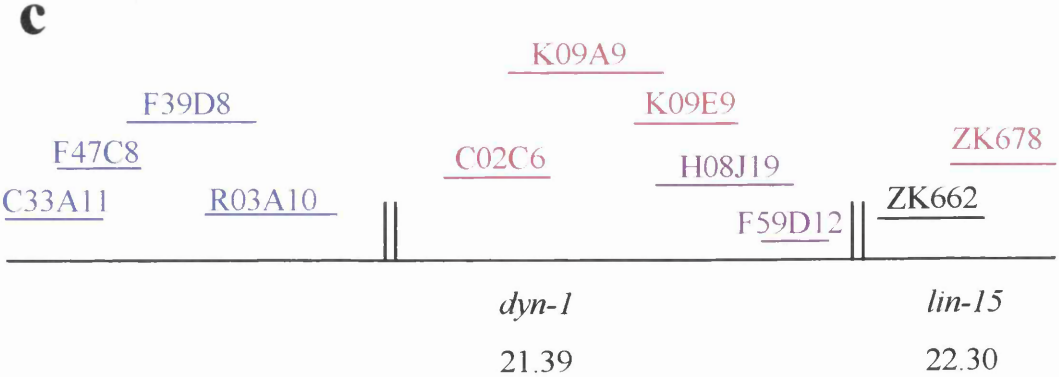
K09A9
F39D8
K09E9
ZK678
F47C8
C02C6
H08J19
C33A11
R03A10
ZK662
F59D12
dyn-1
lin-15
21.39
22.30

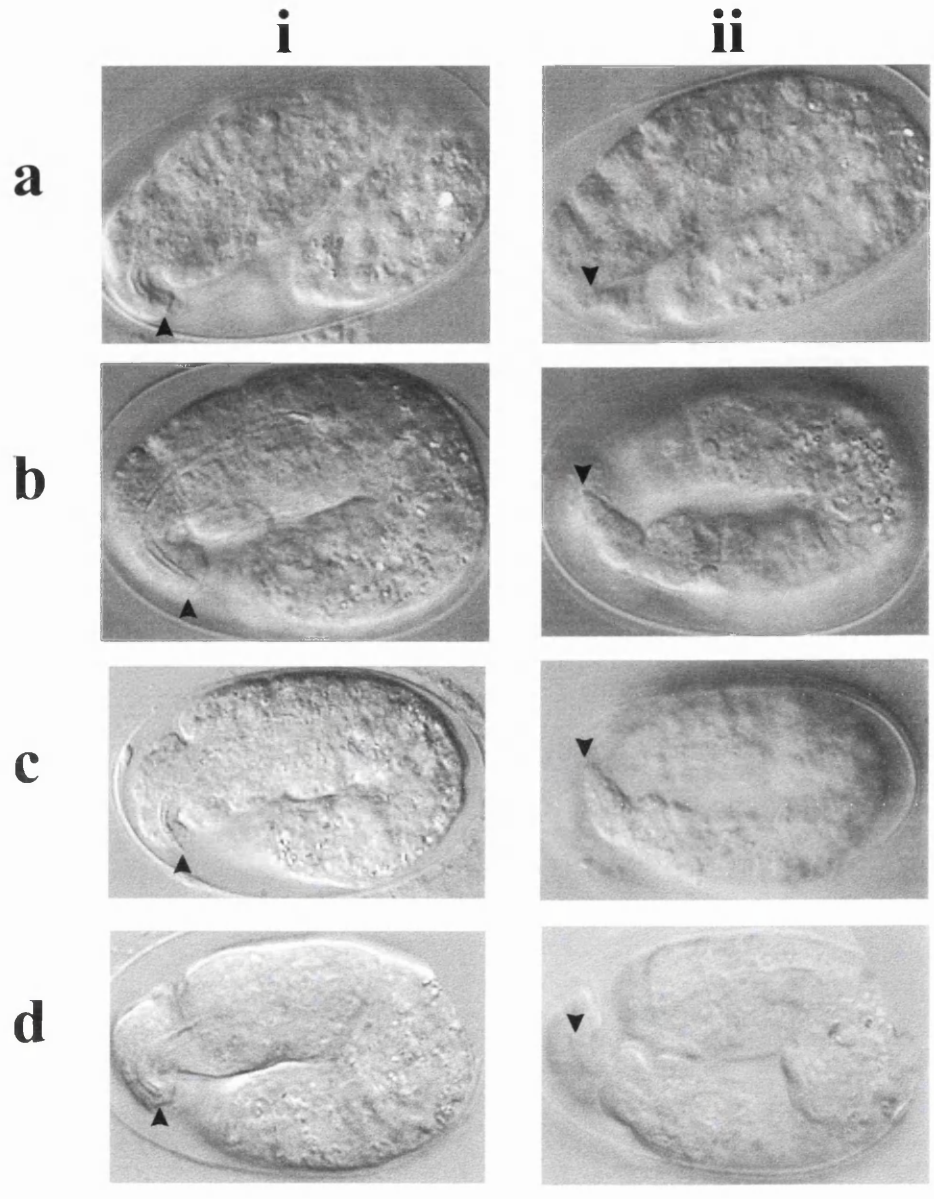

Figure 6.18

DIC images showing rescue phenotypes of *ijDf1* homozygous mutants transformed with various combinations of cosmids

All embryos are positioned with the anterior to the left and the dorsal region to the top of the image. Column **i** shows the anteriors of the embryos while column **ii** shows the posteriors. In all images of column **i,** the anterior tip of the head is indicated with an arrowhead and in all images of column **ii**, the posterior tip of the tail is indicated with an arrowhead.

a 15 cosmid rescue

b 6 cosmid rescue

c Ambiguous phenotype of some of the embryos from the K09A9 10ng injections

d 5 cosmid rescue (as **b** but without K09A9)

equivalent to that obtained with the 15 cosmid injections (Figure 6.18b). As these subgroups were formed at the time when the cosmid positions were shown as Figure 6.17b, they were thought to contain 6 overlapping cosmids, except for the group to the right which also included ZK678 by mistake. These results coincided with the physical and genetic mapping data that the area of interest is to the right of F39D8.

Table 6.2 Rescue achieved with groups of cosmids and single cosmids

Injected cosmids	Number of lines	Number of lines showing rescue
15 cosmid group (see section 6.5.1)	2	2/2
6 cosmid group L (see section 6.5.1)	1	0/1
6 cosmid group R (see section 6.5.1)	1	1/1
F29D12	2	0/2
H08J19	6	0/6
K09E9 (10ng/µl)	2	0/2
K09E9 (5ng/µl)	2	0/2
K09A9 (10ng/µl)	2	?/2 [1]
K09A9 (5ng/µl)	11	0/11
C02C6	4	0/4
ZK678 [2]	3	0/3
5 cosmid group (see section 6.5.1)	1	1/1
K09E9 plus K09A9	3	0/3? [3]
K09A9 plus C02C6	7	7/7 [4]
K09E9 plus C02C6	5	5/5

[1] These lines gave a variable phenotype: some transformed embryos were as *ijDf1* homozygotes, some were over 2-fold and a small proportion had narrow anteriors. Overall, rescue was not observed in any way comparable to rescue with 15 cosmids

[2] ZK678 was added as a mistake to the 6R group of cosmids and so was subsequently tested alone to make sure it was not contributing to the rescue seen.

[3] Around half the transformed embryos were as *ijDf1* 1.75fold embryos but none had narrow anteriors. They did not look like the rescued phenotype.

[4] There were occasional 1.5-fold transformed embryos with much narrower anteriors than *ijDf1* homozygotes

6.5.2. Single cosmid injections from within the rescuing groups

I subsequently began injecting each cosmid singly (at a concentration of 10ng/µl) from the rescuing group of 6 cosmids (shown in pink and purple in Figure 6.17b,c). The cosmids that had been included in both mixes were also tested as they may not have been present in the non-rescuing line from the 'left' group of cosmids. From this point on, *ijDf1*/+ hermaphrodites were used for injections as there was too much recombination in the +,*ijDf1/unc-84*,+ strain to make its use beneficial. None of these cosmids rescued alone although I obtained ambiguous results from K09A9 with some of the transformed embryos resembling rescue (Figure 6.18d, Table 6.2). K09A9 was injected singly again at a concentration of 5ng/µl as this was the concentration of each of the cosmids in the rescuing group of 6. At this concentration, K09A9 showed no rescue and so the ambiguous effects seen with this cosmid seem to be concentration dependent. In the rescue seen with other groups of cosmids, all transformed embryos showed the rescue phenotype. This result indicated that the rescue seen in the original group of 6 cosmids was not due to K09A9 alone. To further test the effect of the K09A9 cosmid, I injected a mix of all of the cosmids in the original rescuing group of 6, except K09A9. Interestingly, this group of 5 cosmids rescued the phenotype as before (Figure 6.18d and Table 6.2).

6.5.3. Rescue achieved with two groups of two cosmids

Because none of the cosmids in this mix rescued the phenotype when they were injected alone, either the gene causing rescue in the mix was present across two cosmids, or there was more than one gene contributing to the rescue seen. Groups of two overlapping cosmids were injected from the original rescuing group of 6 starting from the left of the 5 overlapping cosmids: C02C6, K09A9, K09E9, H08J19, and F59D12 (new amended positions). The first group injected: C02C6 and K09A9 did rescue the phenotype as completely as the group of 6 (Figure 6.19a; Table 6.2). Injecting K09A9 along with K09E9 the cosmid which overlaps it on the right gave no rescue. From information available with the sequence data, there is only one gene spanning the intersection of the genomic sequences contained within cosmids K09A9 (accession number Z79601) and C02C6 (accession number Z79596), *dyn-1*, but as this

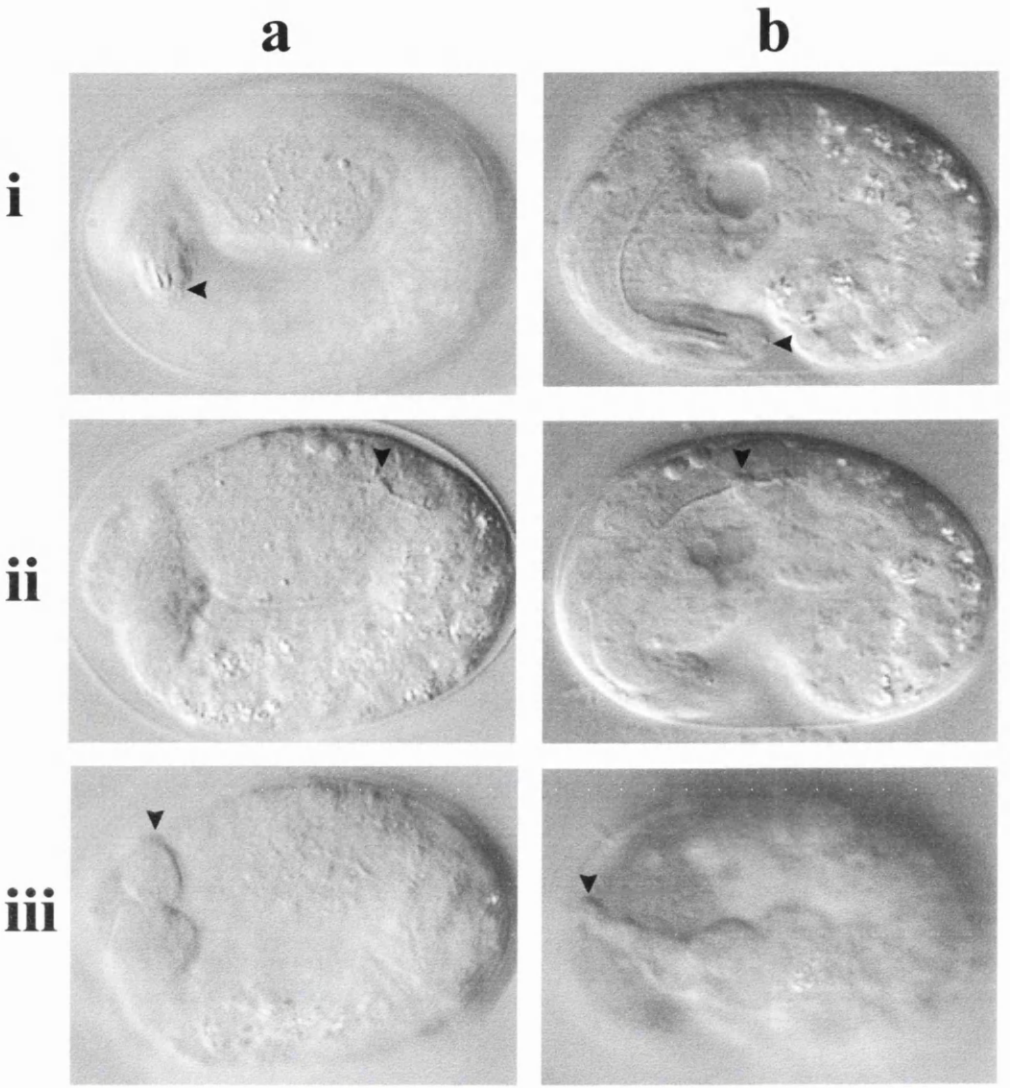

Figure 6.19

DIC images showing rescue phenotypes of *ijDf1* homozygous mutants transformed with cosmid C02C6 plus either cosmid K09A9 or K09E9

The embryo in **a** is positioned with the anterior facing downwards at the left of the image and the dorsal surface to the top and right of the image. The embryo in **b** is positioned with the anterior facing right at the bottom left of the image and the dorsal surface towards the top of the image. Arrowheads point to the anterior tip of the head in **i,** the pharyngeal grinder in **ii**, and the posterior tip of the tail in **iii**.

a Rescue achieved with cosmids C02C6 and K09A9

b Rescue achieved with cosmids C02C6 and K09E9

was contained in its entirety in C02C6 alone, it did not seem to be a good candidate for rescue on its own. This suggested that the rescue seen may have been due to two or more genes in C02C6 and K09A9. Information available with the sequence data of K09A9 and K09E9 (accession number Z79602) also predicts two genes, K09A9.1 and K09A9.2, contained entirely within the overlap of genomic sequences contained within these cosmids and although the above results show that they do not rescue on their own, it seemed possible that either of them in conjunction with C02C6 may achieve rescue. Because of this, I looked at the effect of injecting C02C6 along with K09E9 and found that this combination did indeed give rescue (Figure 6.19b; Table 6.2). However, this result did not remove the possibility that there may be a separate gene contained within K09A9 and K09E9 which gives rescue in conjunction with a gene in C02C6. In order to investigate whether the genes in the K09A9/K09E9 genomic sequence overlap were contributing to rescue, and if so, which of them were involved, I cloned the genes separately into plasmids to inject along with C02C6 without the rest of the genomic sequences within the K09A9 or K09E9 cosmids.

6.6. Cloning and injection of genes in the overlap of cosmids K09A9 and K09E9

The predicted genes, K09A9.1 and K09A9.2, were subcloned from K09A9 into pBluescript SK- to form the plasmids pKA1 and pKA2. pKA1 contains a 4.7kb *Pvu*II-*Kpn*I fragment of K09A9 containing the predicted gene K09A9.1 (3.3kb) along with 0.8kb upstream and 0.6kb downstream flanking sequence and pKA2 contains a 4.5kb *Bam*HI-*Xho*I fragment of K09A9 containing the predicted gene K09A9.2 (1.3kb) along with 0.9kb upstream and 2.3kb downstream flanking sequence (Figure 6.20). The diagnostic digests for pKA1 and pKA2 are shown in Figure 6.21. The pKA1 and pKA2 digests appear to show the correct positions of bands although there was a dip in the gel which made size comparisons more difficult. Lanes 5 and 6 are shown as additional size markers (see Figure 6.21 legend). In order to ensure that the correct fragment was cloned for both pKA1 and pKA2, I tested the plasmids with primers specific to K09A9.1 and K09A9.2 respectively (Table 2viii, primers K09A9.1-T3 and -T7, K09A9.2-T3 and -T7; Figure 6.22). From the PCR it is clear that the correct predicted gene is present in both plasmids and in the case of K09A9.1, the primers amplified the entire sequence of the predicted gene (Table 2viii, primers K09A9.2-T3 and T7).

Figure 6.20

Subcloning of genes K09A9.1 and K09A9.2 from genomic sequence contained within the cosmid K09A9

a A representation of the *C.elegans* Genomic DNA contained within the cosmid K09A9 showing the GENEFINDER predicted genes, K09A9.1-K09A9.6. K09A9.1 and K09A9.2 are shown as blue arrows and the other genes are shown as orange arrows. Restriction sites used to cleave the gene-containing sequence from the genomic DNA are shown in purple. K09A9.1 was cut out using *Kpn*I and *Pvu*II restriction enzymes resulting in a 4.7kb fragment shown below the K09A9 genomic map. K09A9.2 was cut out using *Bam*HI and *Xho*I restriction enzymes resulting in a 4.5kb fragment shown below the K09A9 genomic map.

b Plasmid pKA1 consisting of a pBluescript SK- backbone (purple) and the 4.7kb insert (grey) containing predicted gene K09A9.1 (blue arrow) as detailed in **a**. Cloning sites are shown in purple. pBluescript SK- was cut with *Kpn*I and *Eco*RV as there are two *Pvu*II sites in pBluescript SK-, both outwith the polylinker (see section 2.16.1.1).

c Plasmid pKA2 consisting of a pBluescript SK- backbone (purple) and the 4.5kb insert (grey) containing predicted gene K09A9.2 (blue arrow) as detailed in **a**. Cloning sites are shown in purple.

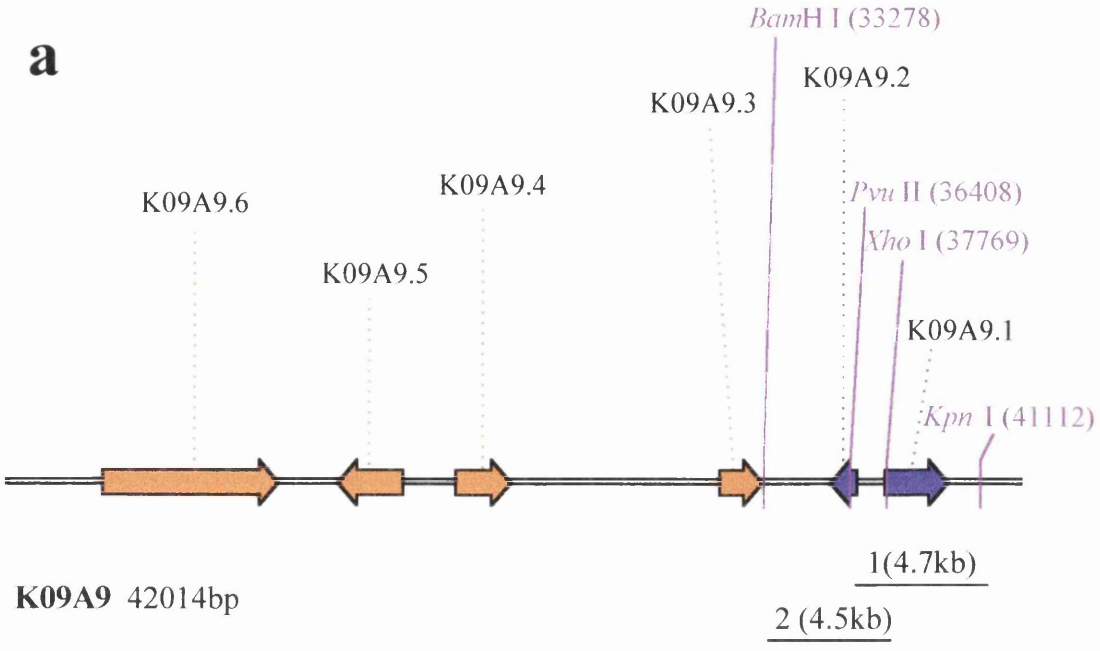
a
BamH I (33278)
K09A9.2
K09A9.3
K09A9.6
K09A9.4
Pvu II (36408)
Xho I (37769)
K09A9.5
K09A9.1
Kpn I (41112)
1(4.7kb)
K09A9 42014bp
2 (4.5kb)

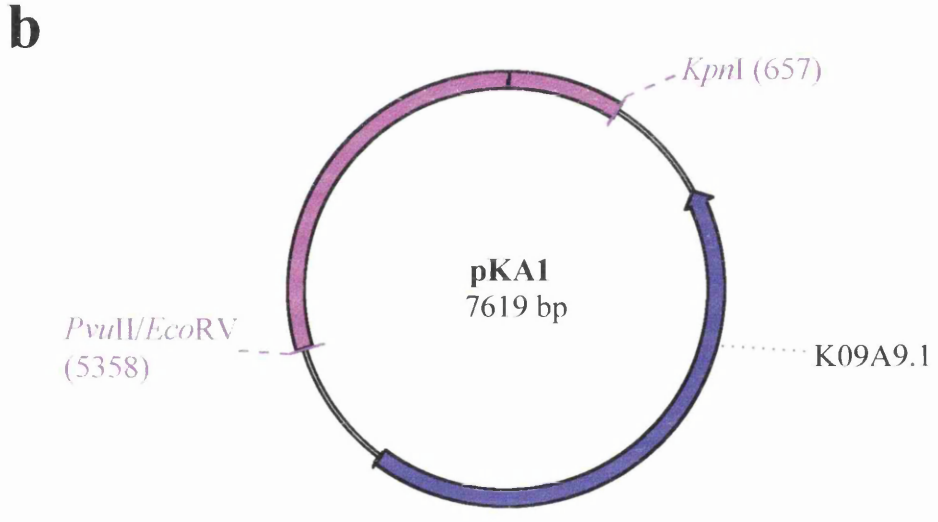
b
KpnI (657)
pKA1
7619 bp
PvuII/EcoRV
(5358)
K09A9.1

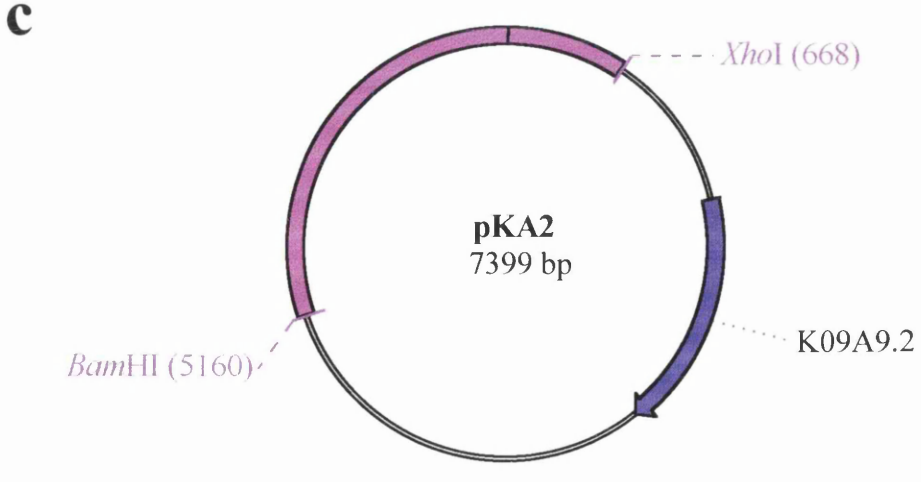
c
XhoI (668)
pKA2
7399 bp
BamHI (5160)
K09A9.2

Figure 6.21

Restriction maps and diagnostic digests of plasmids pKA1 and pKA2

a pKA1 restriction map

b pKA2 restriction map

purple shading: vector DNA (pBluescript SK-)

grey shading: *C.elegans* genomic DNA

blue arrows: Coding sequence of gene K09A9.1 or K09A9.2

The plasmids have been linearised and positions of restriction sites are in base pairs from the origin of the pBluescript SK- plasmid as given in the published sequence (accession number: X52324).

c Gel showing diagnostic restriction digests for pKA1 and pKA2.

Lanes 5 and 6 are included as size markers

*Sal*I digest of pKA1 - 7.62kb band

*Xho*I digest of pKA1 - bands of 950bp and 6.67kb

*Pvu*II digest of pKA2 - bands of 842bp, 1.50, 2.51 and 2.54kb

*Xba*I digest of pKA2 - bands of 844bp and 6.56kb

Lane5: bands of 3.8 and 6.8kb

Lane6: bands of 4.4 and 6.4kb

1kb ladder band sizes are given to the right of the gel in kb. The gel dips on the right hand side so the 1kb ladder bands at the left do not match up exactly with those on the right. The contrast was enhanced for bands under 1kb in size to enable them to be seen more clearly.

All bands were as expected for plasmid digests.

a **pKA1**

7619 bp

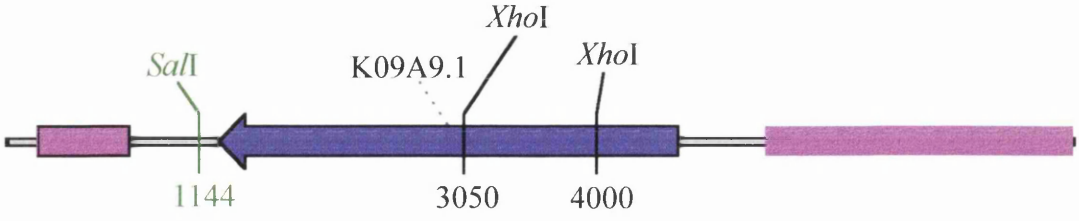

b **pKA2**

7399 bp

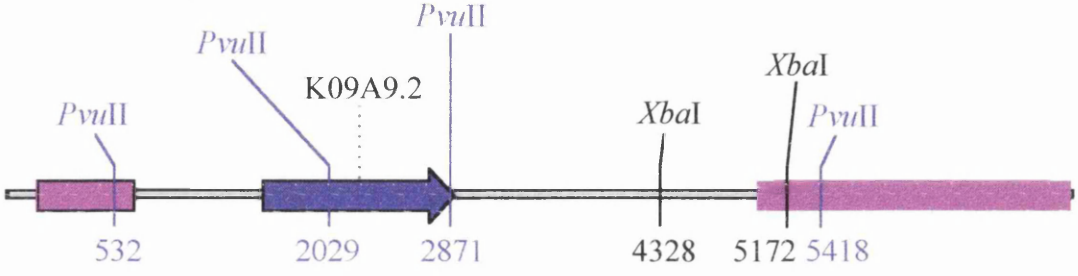

c

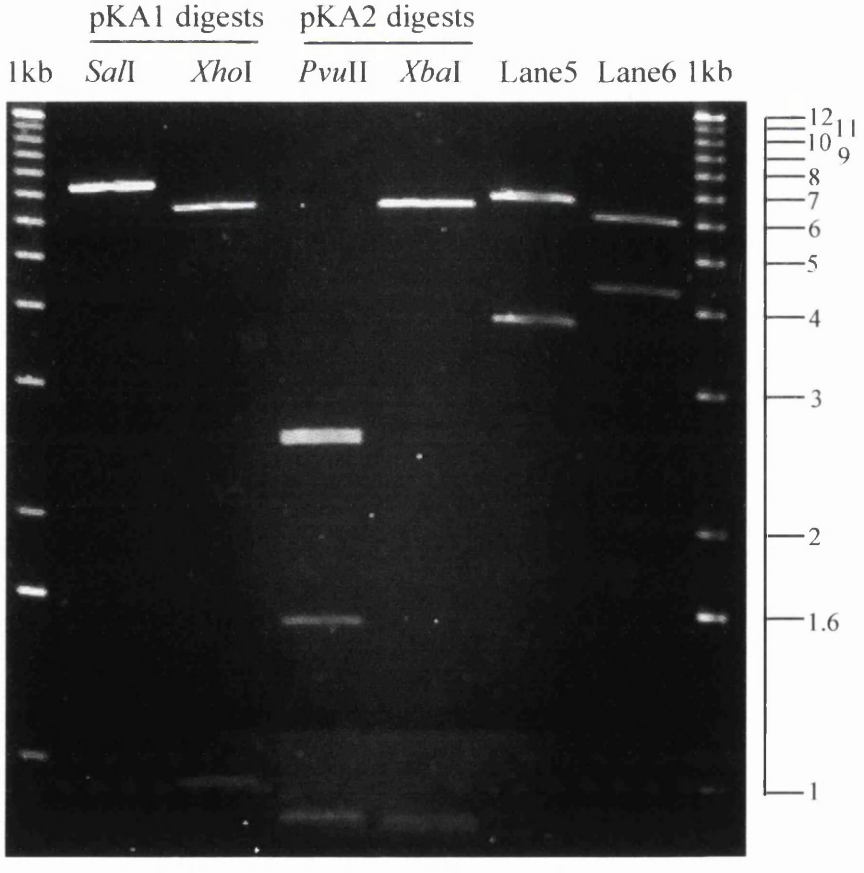

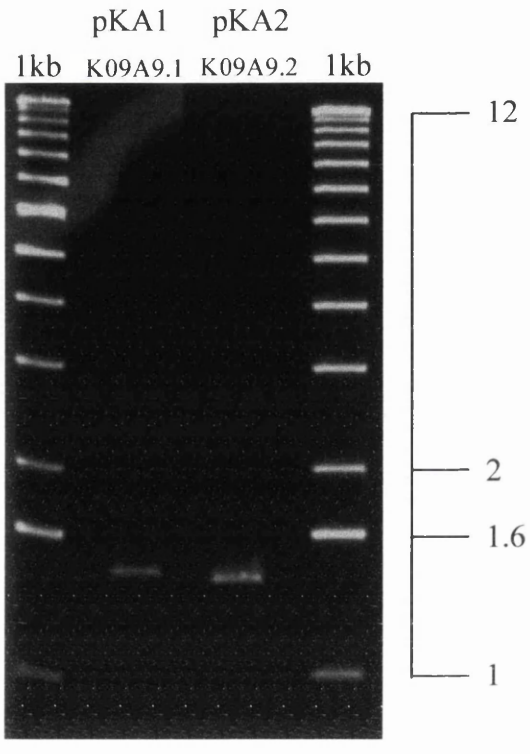

Figure 6.22
Gel showing the presence of coding sequences from predicted genes K09A9.1 and K09A9.2 in plasmids pKA1 and pKA2

The K09A9.1 lane contains a 1.45kb fragment of the coding sequence of the predicted gene K09A9.1 amplified from the plasmid pKA1. The K09A9.2 lane contains the entire coding sequence of the predicted gene K09A9.2 (1.38kb) amplified from the plasmid pKA2.

This shows the presence of each gene in the correct plasmid.

Sample marker bands from 1kb ladder are shown to the right of the gel in kb. Above the 2kb band, all subsequent higher bands differ by 1kb in size up to the largest band of 12kb which is shown.

ijDf1/+ hermaphrodites were injected with a mix containing pKA1, pKA2 and C02C6 as well as the marker plasmids. The subclones were injected at a concentration of 1ng/µl as previous injections at a higher concentration had yielded many F1 transformants but no lines which is an indication that one or more of the plasmids are toxic at a high copy number. C02C6 was injected at a concentration of 5ng/µl. The results are shown in Table 6.3. This combination of DNA molecules did not give rescue which was a surprising result that suggested rescue was due to a different gene in each of K09A9 and K09E9 after all. However, non-rescue can be due to many factors. Even though an upstream region of 769bp and 908bp were included for K09A9.1 and K09A9.2 respectively (see Figures 6.20 and 6.21), this may not be enough to include the entire promoter sequence. It is possible that the promoter for each predicted gene lies within the coding region of the other although this may be unlikely. If this was the problem, however, the entire promoter regions for each gene could be restored when the two predicted genes were injected together as they may recombine in the region of overlap. The GENEFINDER program is used by the *C.elegans* sequencing consortium to predict genes and these predictions are often inaccurate. If the 5′ ends of these genes were actually further upstream than predicted, then even less of the upstream flanking sequence would be present in the subclone plasmids. To check whether it was the overlap contributing to rescue or another gene in each cosmid, I subcloned the entire overlap region and, the genes contained in the non-overlap region of the K09E9 cosmid.

Table 6.3

Rescue obtained from injection of the C02C6 cosmid plus regions of the K09A9 and K09E9 cosmids

Injected cosmids, plasmids and deleted cosmids	Number of lines	Number of lines showing rescue
pKA1,pKA2,C02C6	6	0/6
pKEO and C02C6	10	4/10
pKENO and C02C6	3	possibly 2/3 (see text)

6.7. Subcloning and injecting the overlap and non-overlap regions of K09E9

The overlap and non-overlap regions were subcloned in a different way to the predicted genes K09A9.1 and K09A9.2. I chose restriction enzymes to cut out the regions of the genomic DNA that were unwanted and re-ligated the remaining genomic DNA, complete with the original cosmid backbone, Lorist B. Unfortunately, careful examination of initial digests of K09E9 and K09A9 indicated that large areas of the genomic sequence contained in these cosmids were deleted. I had previously been preparing cosmid DNA from at least two colonies and comparing the restriction digest patterns as an assay for intact cosmids. However, when I examined the cosmids I had used in the rescue injections accurately, many of them had deletions which had not been noticed before. I was unaware of the extent of cosmid deletions and in consequence, it is possible that some cosmids may have failed to rescue due to the presence of these deletions. The implications of the K09A9 and K09E9 deleted regions on previous results is discussed in section 6.8. I subsequently received an undeleted version of the K09E9 cosmid and used this for further subcloning. pKEO contained the K09E9 Lorist B backbone and genomic sequence specific to the region in the K09A9/K09E9 overlap. It was constructed by deleting a 29kb region between *Avr*II sites from 8312bp to 37447bp (Figure 6.23a) and re-ligating the remainder of the cosmid, forming a subclone of 10.2kb containing the genes K09A9.1 and K09A9.2, plus the Lorist B backbone (Figure 6.23b). pKENO contained the K09E9 Lorist B backbone and genomic sequence specific to the region of K09E9 not contained in the K09A9/K09E9 overlap. It was formed by deleting a region from *Bam*HI at 478bp to *Pme*I at 6992bp containing genes K09A9.1 and K09A9.2 (Figure 6.23a) and blunt-end ligating the remainder of the genomic DNA, forming a subclone of 32.7kb plus the Lorist B backbone (Figure 6.23c). Diagnostic digests of these subclones are shown in Figure 6.24.

ijDf1/+ hermaphrodites were injected with DNA mixes containing either pKEO or pKENO plus the C02C6 cosmid. Results are shown in Table 6.3. 4 out of 10 lines from the C02C6 plus pKEO injections did indeed result in rescue as complete as with the initial cosmid group (Figure 6.25a,b) but the other 6 lines showed no rescue at all. The most likely explanation for this is that the 4 rescuing lines contained both cosmids but the other lines only contained one, or neither of them and therefore did not give rescue. When C02C6 and pKENO were injected together, however, two of the lines

Figure 6.23

Subcloning of 'overlap' and 'non-overlap' genomic sequences from within the cosmid K09E9

a Schematic diagram of the *C.elegans* genomic DNA contained within the cosmid K09E9 showing the GENEFINDER predicted genes: K09A9.1 and K09A9.2 present within the K09A9/K09E9 overlap genomic sequence (blue arrows), and K09E9.1-K09E9.3 present within the K09E9 non-overlap genomic sequence (green arrows). The restriction sites used in creating the subclones are shown. *Avr*II was used to cut out the non-overlap genomic sequence of K09E9 so that only the overlap sequence and the vector backbone (shown in purple in **b** and **c**) remained after re-ligation. *Pme*I and *Bam*HI were used to cut the overlap sequences from the K09E9 cosmid so that only the non-overlap sequence remained along with the vector backbone.

b Plasmid pKEO showing the Lorist B vector backbone in purple, genomic sequence in grey and the genes present in the K09A9/K09E9 overlap as blue arrows. The site of *Avr*II re-ligation is shown.

c Plasmid pKENO showing the Lorist B vector backbone in purple, genomic sequence in grey and the genes present in the K09E9 non-overlap genomic sequence as green arrows. The site of the *Pme*I/*Bam*HI ligation is shown.

a

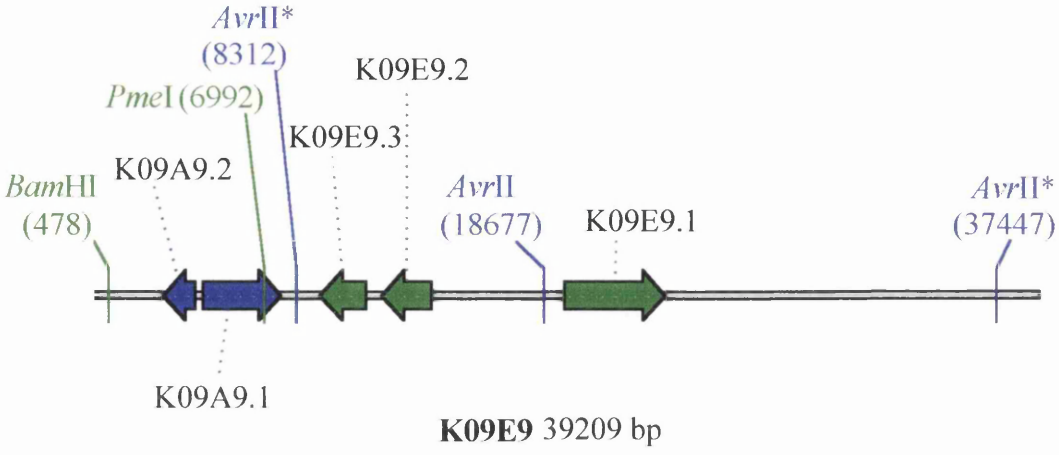
AvrII*
(8312)
PmeI (6992)
K09E9.2
K09E9.3
K09A9.2
BamHI
(478)
AvrII
(18677)
K09E9.1
AvrII*
(37447)
K09A9.1
K09E9 39209 bp

b

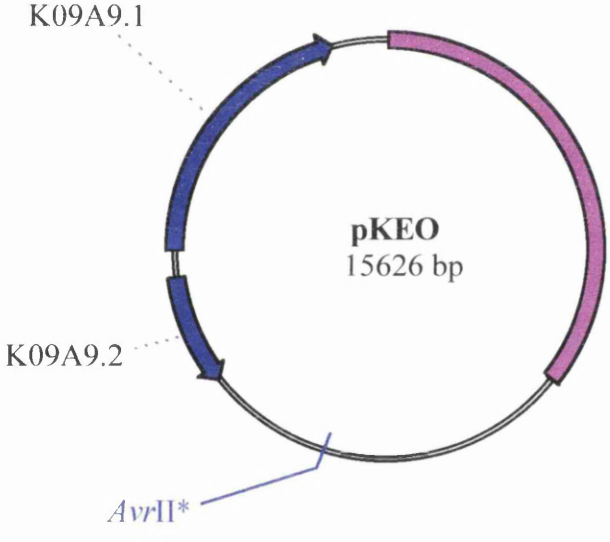
K09A9.1
pKEO
15626 bp
K09A9.2
AvrII*

c

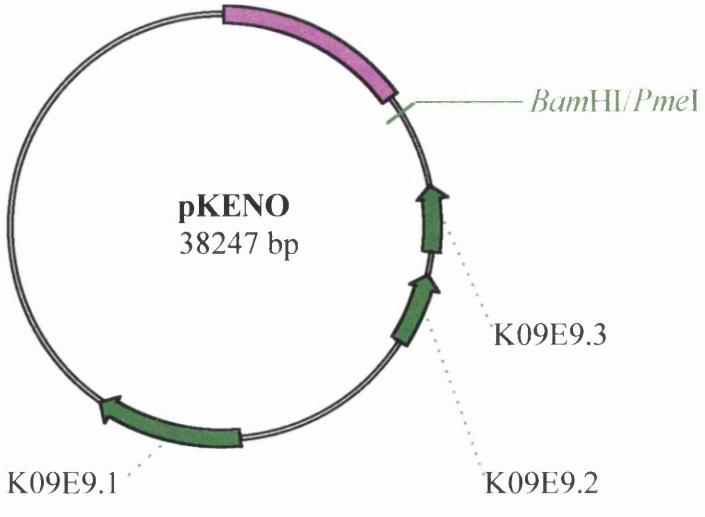
BamHI/PmeI
pKENO
38247 bp
K09E9.3
K09E9.1
K09E9.2

Figure 6.24

Restriction map and diagnostic digests of deleted cosmids pKEO and pKENO

a pKEO restriction map

b pKENO restriction map

purple shading: vector DNA (Lorist B)

grey shading: *C.elegans* genomic DNA

blue arrows: predicted genes K09A9.1 and K09A9.2

green arrows: predicted genes K09E9.1-K09E9.3

The deleted cosmids have been linearised and positions of restriction sites are in base pairs from the origin of the Lorist B vector as given in the published sequence (accession number: X98613) added to the deleted genomic DNA contained within the K09E9 cosmid from the origin stated in the published sequence (accession number: Z79602).

c **Gels showing diagnostic restriction digests for pKEO and pKENO**

i pKEO diagnostic digests:

*Xho*I digest of pKEO - 3 bands of 950bp, 3.9kb and 10.7kb.

*Sal*I digest of pKEO - 2 bands of 6.3 and 9.3kb.

ii pKENO diagnostic digests:

*Eco*RI digest of pKENO - showing 8 bands of 1.2, 1.4, 2.3, 3.1, 3.7, 4.9, 10.2, and 10.8kb. Not shown are lower bands of 302 and 196bp as these were very faint and diffuse.

*Bgl*II digest of pKENO - showing 8 bands of 650bp, 968bp, 1.7, 2.1, 2.3, 3, 5.9, and 21kb. Not shown is a band of 61bp which could not be seen on the gel.

1kb ladder band sizes are given to the left of the pKEO gel in kb and selected bands are indicated to the left of the pKENO gels in **ii**.

All bands were as expected for the plasmid digests.

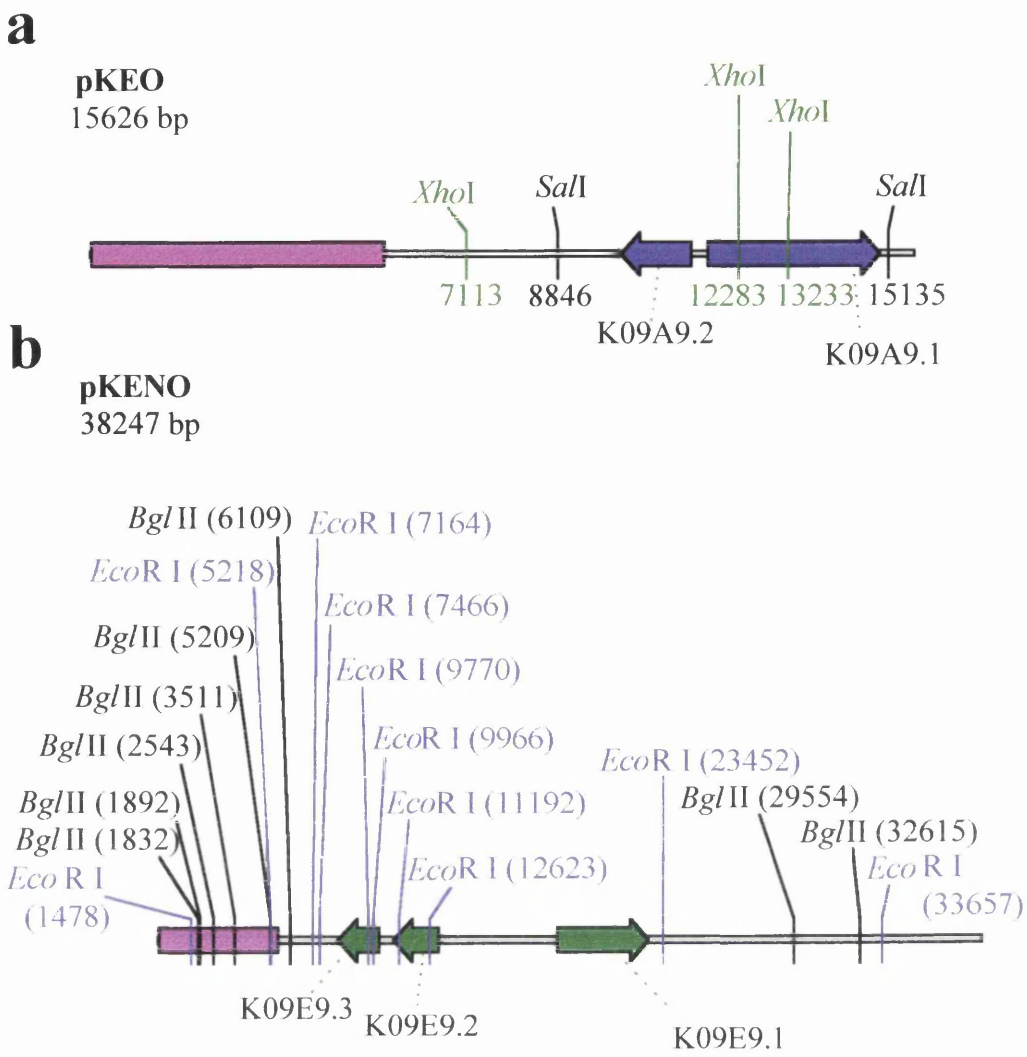
a
pKEO
15626 bp
XhoI
XhoI
XhoI
SalI
SalI
7113
8846
12283
13233
15135
K09A9.2
K09A9.1
b
pKENO
38247 bp
BglII (6109)
EcoR I (7164)
EcoR I (5218)
EcoR I (7466)
BglII (5209)
EcoR I (9770)
BglII (3511)
EcoR I (9966)
BglII (2543)
EcoR I (23452)
BglII (1892)
EcoR I (11192)
BglII (29554)
BglII (1832)
BglII (32615)
EcoR I (12623)
EcoR I (1478)
EcoR I (33657)
K09E9.3
K09E9.2
K09E9.1

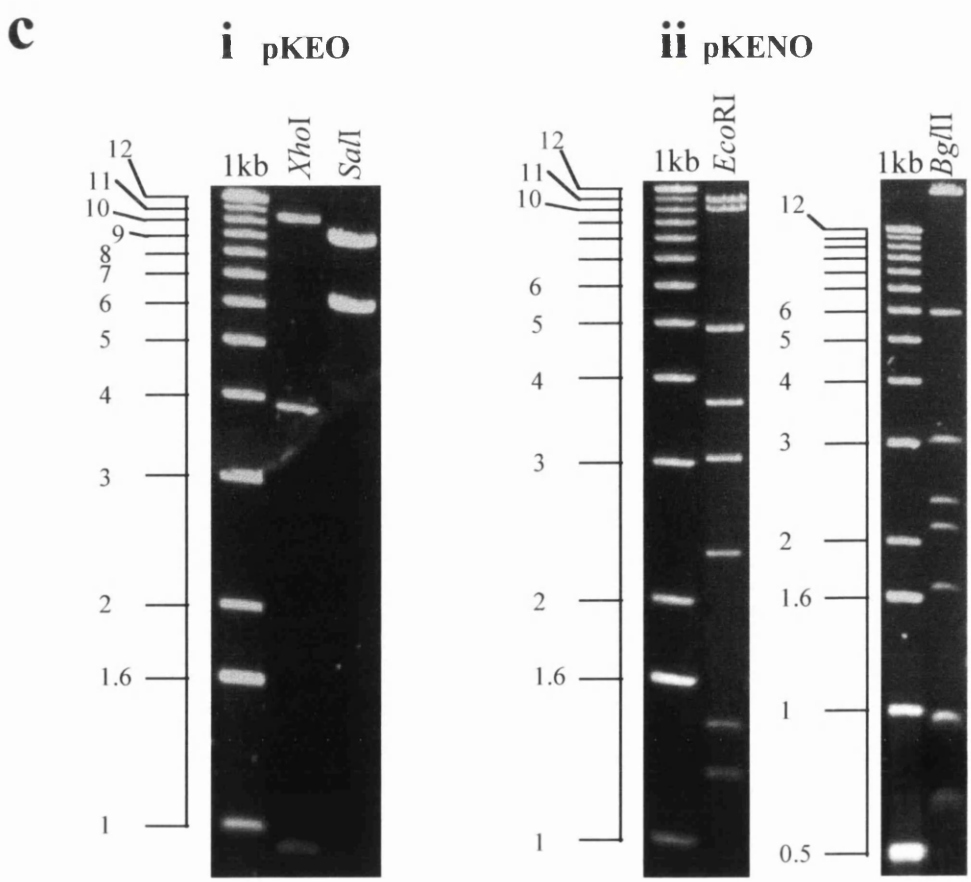
c
i pKEO
ii pKENO
1kb
XhoI
SalI
EcoRI
BglII
12
11
10
9
8
7
6
5
4
3
2
1.6
1
0.5

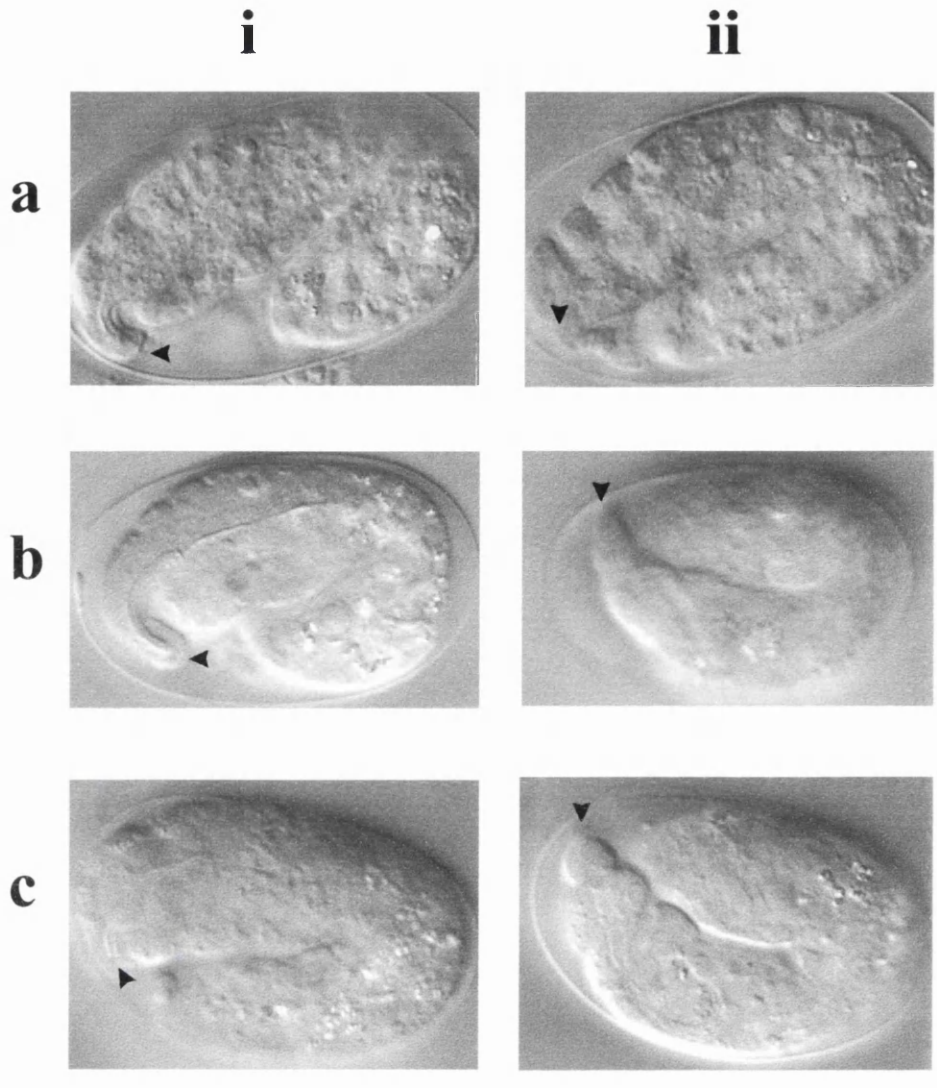

Figure 6.25

DIC images showing phenotypes of *ijDf1* homozygous mutants transformed with various cosmid groups or subclones

All embryos are positioned with the anterior to the left and the dorsal surfaces to the top of the images. In column **i,** an arrowhead indicates the anterior tip of the head and in column **ii,** an arrowhead indicates the posterior tip of the tail.

a Original 15 cosmid rescue

b pKEO plus cosmid C02C6 rescue

c Phenotype achieved by pKENO plus cosmid C02C6 injections

also showed an effect even though this was not as pronounced as the previous cosmid group rescue (Figure 6.25c). These results point to the genes in the overlap as being involved in rescuing the elongation defect along with a component of C02C6 but there may also be another aspect of K09E9 and possibly K09A9 which can also contribute partially to rescue. Since the genes in the overlap of the genomic sequence of these two cosmids do not share any significant homology with any genes outwith the genomic overlap, it seems that the partial rescue effect resulting from the pKENO plus C02C6 injections differs from the rescue effect resulting from the pKEO plus C02C6 injections. It appears that more than one set of genes can affect this mutant phenotype and it therefore seems that the elongation defect is a complex compound effect.

6.8. Implications of partially deleted K09A9 and K09E9 cosmids on previous results.

The large deletions in the genomic sequences contained within the K09A9 and K09E9 cosmids were not detected until after the cosmid rescue injections had been completed and the K09A9.1 and K09A9.2 genes had been subcloned. It has already been mentioned above that PCR was used to ensure that the correct genes were present within pKA1 and pKA2, and the same primers were used to detect these 'overlap' genes in the partially deleted K09A9 and K09E9 cosmids (Figure 6.26). The overlap genes were found to be present in both partially deleted cosmids which may be a significant result as the deleted cosmids also achieved rescue along with cosmid C02C6 which was present in an undeleted form. The presence of other genes outside the K09A9/K09E9 genomic sequence overlap were not tested in the partially deleted K09A9 and K09E9 cosmids. I also examined the restriction digest pattern of the deleted cosmids using different restriction endonucleases and deduced that the region of deletion was outwith the overlap between the genomic sequences contained within the K09A9 and K09E9 cosmids. To summarise, although rescuing cosmids K09A9 and K09E9 were injected in a partially deleted form, the genes from the genomic overlap between these two cosmids were present in the injected cosmids. They were also shown to be present in the plasmids pKA1 and pKA2 which did not give rescue in any combination along with cosmid C02C6. For simplicity I will henceforth use the cosmid name to denote the *C.elegans* genomic sequences contained within that cosmid.

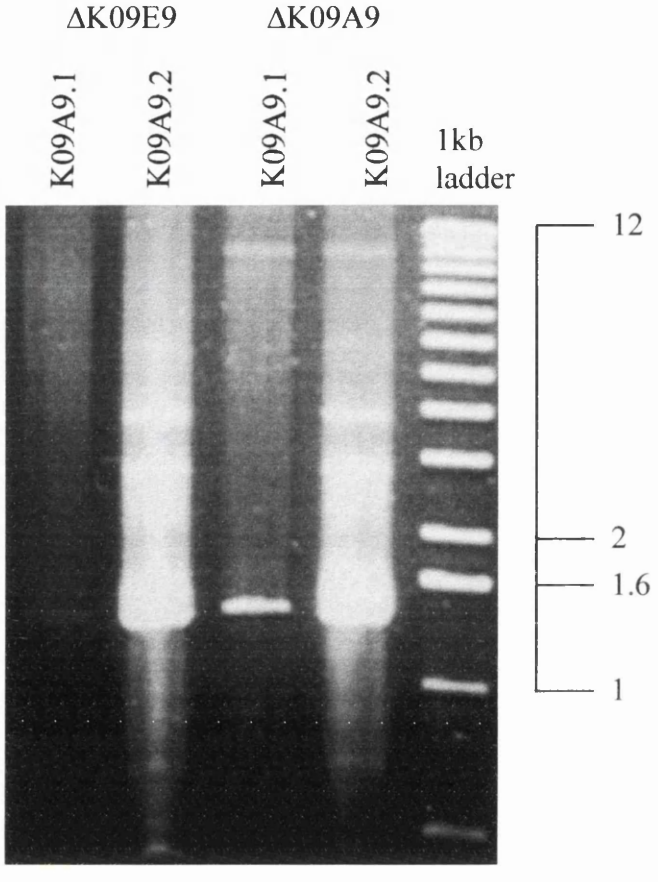

Figure 6.26

Gel showing the presence of coding sequences from genes K09A9.1 and K09A9.2 in deleted cosmids K09E9 and K09A9

K09A9.1 lanes contain a 1.45kb amplified fragment of the coding sequence of the predicted gene K09A9.1. K09A9.2 lanes contain the entire coding sequence of the predicted gene K09A9.2 (1.38kb). ΔK09E9 lanes contain DNA amplified from the deleted K09E9 cosmid and ΔK09A9 lanes contain DNA amplified from the deleted K09A9 cosmid.
The gel shows the presence of both genes in both deleted cosmids although the K09A9.1 band in the deleted K09E9 cosmid is faint.

Sample marker bands from 1kb ladder are shown to the right of the gel in kb. Above the 2kb band, all subsequent higher bands differ by 1kb in size up to the largest band of 12kb which is shown.

6.9. RNA interference of genes within the K09A9/K09E9 overlap and the cosmid C02C6

6.9.1. Background of RNA interference

A relatively new reverse genetic tool in *C.elegans* is that of RNA interference (RNAi) which can specifically inhibit the function of the gene under study and allow the 'null' phenotype of the gene to be observed. This is achieved by injecting double stranded RNA, corresponding to the gene in question, into an adult hermaphrodite and then examining the progeny of that animal for any effect. It was first reported that antisense RNA towards specific genes in *C.elegans* could phenocopy a null mutation in a gene when expressed from a transgene and that sense transcripts were also effective in producing the targeted phenotype (Fire *et al.*, 1991). This effect was also found by Guo and Kemphues in 1995 during attempts to use antisense RNA to block gene expression in the maternal germ line. They observed that injecting both antisense and sense RNA separately into adult hermaphrodites induced phenocopies of a mutation in the target gene in the progeny of the injected animals. Many subsequent studies have shown that double stranded RNA (dsRNA) is much more potent at causing interference than either single strand alone and it is thought that the presence of tiny amounts of dsRNA present in single stranded RNA preparations may actually be the cause of the interference seen (Fire *et al.*, 1998). RNAi has shown to be specific when tested for many genes for which the null phenotype is known, for example, *unc-22* and *mec-3* (Fire *et al.*, 1998). Several aspects of RNAi are unusual. Firstly, interference can cross cell boundaries as injection of dsRNA into the gonads and the intestine produce the same effects and more recently it was found that simply soaking the worms in dsRNA could induce specific interference of the essential maternal gene *pos-1* (Tabara *et al.*,1998). Secondly, interference can not only be observed in the injected animal but can frequently be seen in a high proportion or in all of its progeny. It has also been found that the DNA template used to produce the RNA can be genomic and that the presence of intronic sequences seem to have no effect on interference although it is vital that exon sequence is present. The mechanism of this process is not fully understood as yet. Only a few molecules of dsRNA are required per cell to induce an effect which suggests that there may be an amplification or catalytic step in the interference process. It is known that

RNA transcripts of a target gene fail to accumulate after RNAi and in some cases of RNA-mediated co-suppression in plants, gene silencing correlates with an increased turnover of both the transgenic and endogenous gene transcripts (Jacobs *et al.*, 1997). It is possible that there is a role for RNA-associated gene silencing in the wild type system as a defence against invading viruses or as a method to switch off specific genes in response to physiological or developmental cues (Jorgensen *et al.*, 1998; Montgomery and Fire, 1998).

6.9.2. RNAi of genes in the K09A9/K09E9 cosmid overlap and in the C02C6 cosmid

As a final test to examine the predicted genes in the overlap of cosmids K09A9 and K09E9 and in C02C6, I decided to produce dsRNA towards a region of each gene and then inject the dsRNAs in different combinations to observe their effects. Even though a combination of these genes were enough to rescue the early elongation defect in *ijDf1*, this does not mean that their deletion alone is sufficient to create the phenotype seen. dsRNA was prepared for the predicted overlap genes: K09A9.1 and K09A9.2, and for the genes in C02C6: C02C6.1(*dyn-1*), and predicted genes, C02C6.2 and C02C6.3, as detailed in section 2.17. Figure 6.27 shows the positions of the genomic sequence used to generate RNA in the 5 genes and the sizes of the single stranded and double stranded RNA prepared for each gene. The combinations of dsRNA were injected into wild type hermaphrodites which were then transferred singly to new plates at regular intervals in order to examine the brood phenotypes and look for any resulting lethality. Table 6.4 details the combinations of dsRNA injected and the resulting phenotype seen. I found that if I injected dsRNA of every gene except *dyn-1*, there was no overall phenotype produced, but if *dyn-1* dsRNA was injected alone, I observed over 80% embryonic death in the progeny of the injected animals and the other 20% were very small, dumpy and slow growing. *dyn-1* encodes a homologue of vertebrate dynamin which is required for endocytosis, acting to pinch vesicles off from the plasma membrane (Clark *et al.*,1997; Labrousse et al, 1998). The dead embryos from *dyn-1* RNAi were variable, but the vast majority arrested as amorphous lumps of cells with no distinguishing features or tissues (Figure 6.28a). The most likely explanation for this is that *dyn-1* RNAi inhibits both maternal and zygotic *dyn-1* function resulting in a more

Figure 6.27

RNA interference (RNAi) using genes in the genomic overlap of K09A9 and K09E9 cosmids, and in cosmid C02C6

Positions of primers used to generate DNA fragment templates for RNA interference (RNAi) and single and double stranded RNA fragments corresponding to these templates for each target gene
Details of the RNAi protocols are given in section 2.17.

a Schematic diagram of the complete genomic sequence contained within cosmid K09A9 with the positions of the 6 predicted genes indicated as arrows. Genes from the K09A9/K09E9 genomic overlap are denoted by blue arrows and the positions of the primers used to amplify the DNA fragment templates for RNA in the RNAi experiments are shown in pink.

b Schematic diagram of the complete genomic sequence contained within cosmid C02C6 with the positions of the 3 predicted genes indicated as blue arrows. Positions of the primers used to amplify the DNA fragment templates for RNA in the RNAi experiments are shown in pink.

c Agarose gel showing the single stranded RNA (T3 and T7 lanes) and double stranded RNA (ds lanes) generated from the amplified DNA fragments from each gene. The gene name is above the lanes containing corresponding RNA.

Sizes of DNA fragments amplified from each gene (which will correspond to the size of the generated RNA):

K09A9.1: 1.45kb
K09A9.2: 1.38kb
C02C6.1: 1.48kb
C02C6.2: 1.03kb
C02C6.3: 1.77kb

a

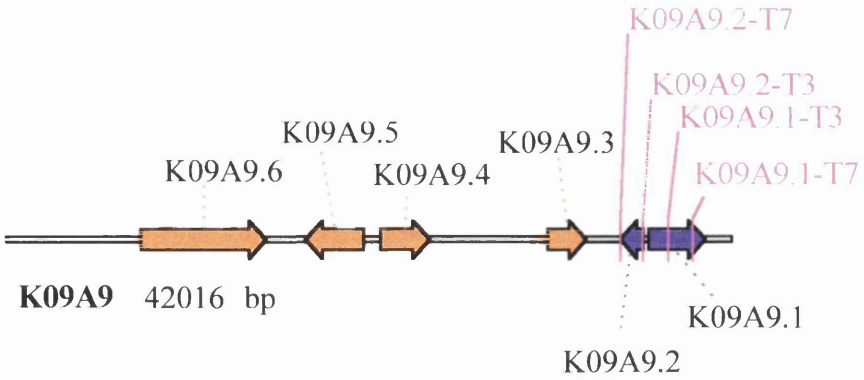
K09A9.2-T7
K09A9.2-T3
K09A9.1-T3
K09A9.1-T7
K09A9.5
K09A9.3
K09A9.6
K09A9.4
K09A9 42016 bp
K09A9.1
K09A9.2

b

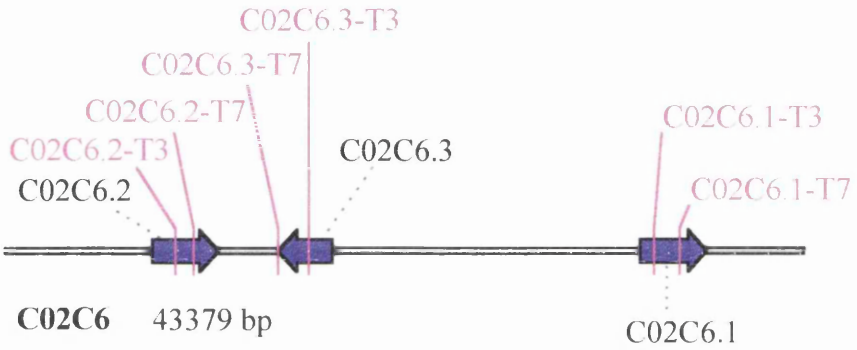
C02C6.3-T3
C02C6.3-T7
C02C6.2-T7
C02C6.1-T3
C02C6.2-T3
C02C6.3
C02C6.2
C02C6.1-T7
C02C6.1
C02C6 43379 bp

c

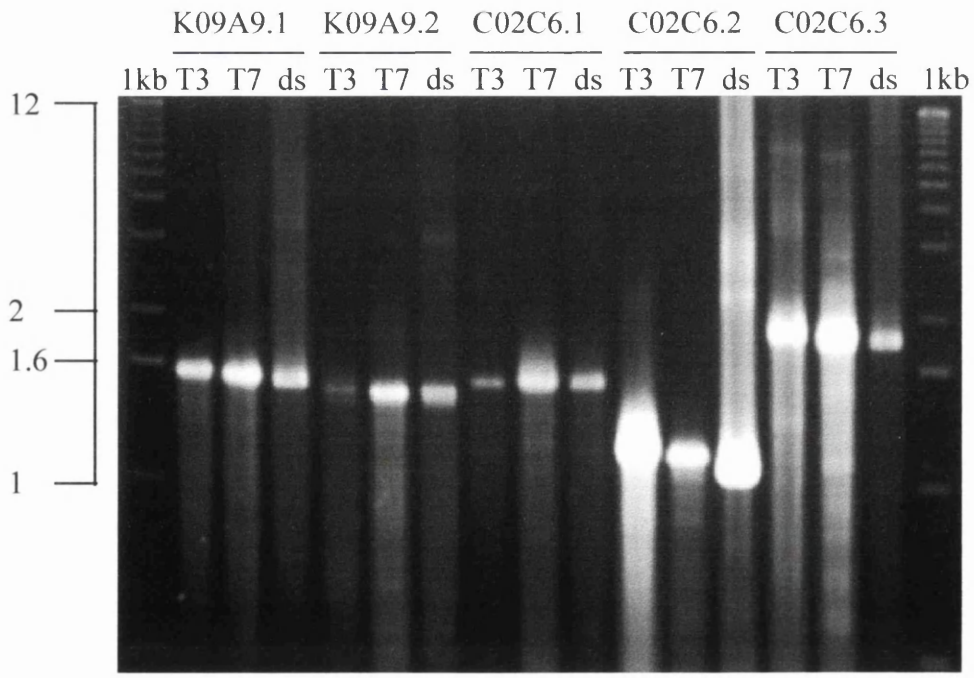
K09A9.1
K09A9.2
C02C6.1
C02C6.2
C02C6.3
1kb T3 T7 ds T3 T7 ds T3 T7 ds T3 T7 ds T3 T7 ds 1kb
12
2
1.6
1

Figure 6.28

DIC images of phenotypes obtained from *dyn-1* RNAi and phenotypes of *dyn-1(ky51)* and *dyn-1(cq4)* homozygotes.

In images **b** and **d**, the anterior is towards the left of the image.

a An embryo from an wild type hermaphrodite injected with double stranded RNA corresponding to a region of sequence from the *dyn-1* gene.

b Larvae from an wild type hermaphrodite injected with double stranded RNA corresponding to a region of sequence from the *dyn-1* gene. The larvae are trapped in their old cuticle, indicated with arrows in both images. Scale bar is 10μm in both cases.

c Terminal arrest phenotype of an embryo produced from a *dyn-1(ky51)* homozygote which was raised and maintained at 25°C.

d Terminal arrest phenotype of a *dyn-1(cq4)* homozygous embryo.

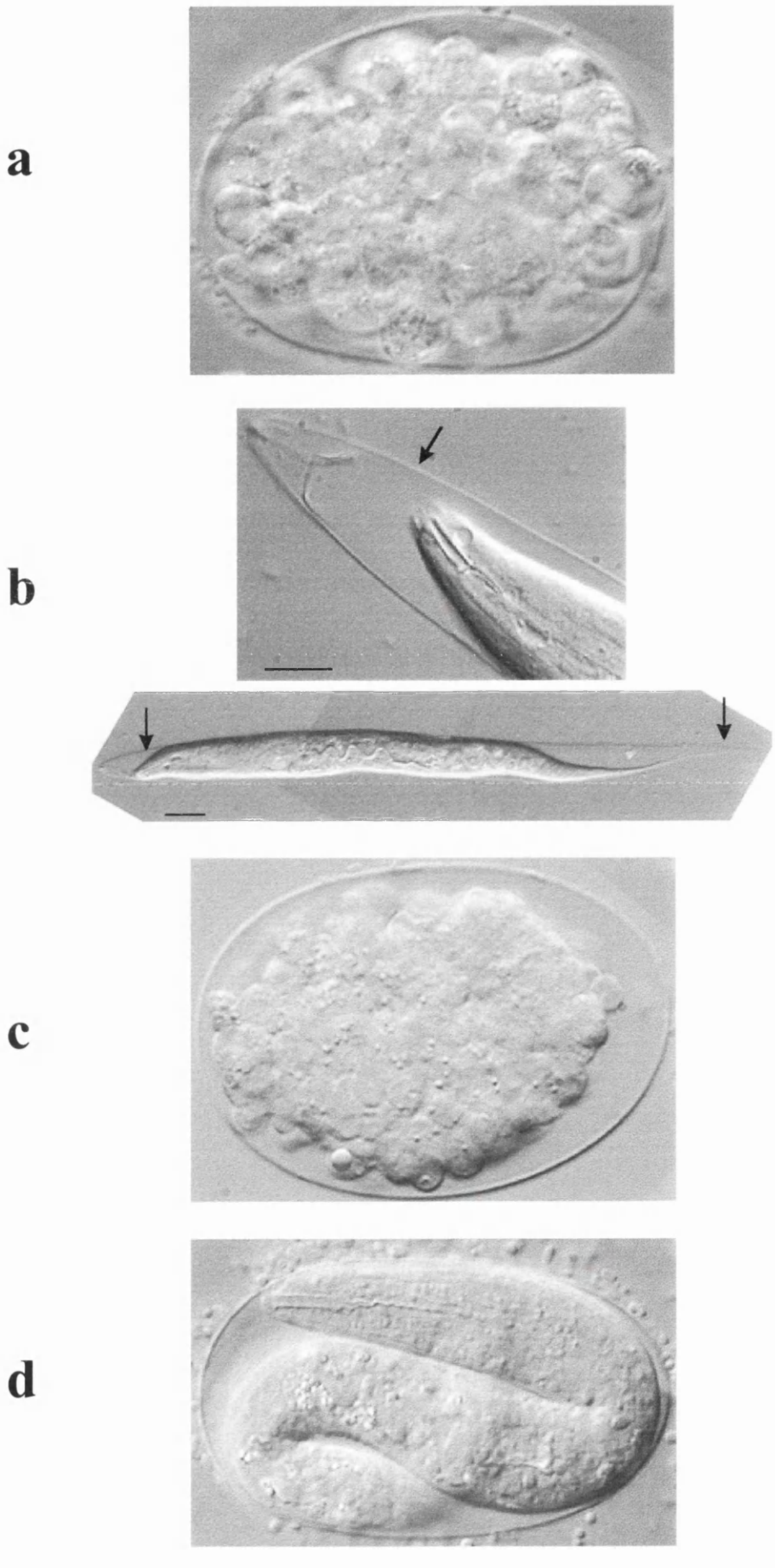
a
b
c
d

severe phenotype than that seen in *ijDf1* homozygotes where maternal dynamin will be present from the heterozygous parent.

Table 6.4

Results of RNAi for genes K09A9.1, K09A9.2, C02C6.1 (*dyn-1*), C02C6.2 and C02C6.3 injected into wild type hermaphrodites

dsRNA injection combinations	Concentration of dsRNA injected (ng/µl)	Phenotypes seen in F1 generation	If lethality, arrest phenotypes seen
C02C6.1 (*dyn-1*)	300	78% embryonic lethality (n=1277), other progeny small, dumpy, slow growing. Some Egl	82% amorphous, lumpy 'blobs' 7% irregular 3-fold 11% irregular 2-fold (n=194)
C02C6.1 (*dyn-1*)	30	70% embryonic lethality (n=1253), other progeny small, slow growing, dumpy, Egl.*	91% amorphous, lumpy 'blobs' 3% irregular 3-fold 6% irregular 2-fold (n=211)
K09A9.1 and .2, C02C6.2 and .3	300 each	<1% dead embryos and slightly lumpy larvae. No definite phenotype	variable
All combinations including C02C6.1 (*dyn-1*)	300 each	as C02C6.1 alone*	as C02C6.1 alone
All combinations not including C02C6.1 (*dyn-1*)	300 each	<1% dead embryos and slightly lumpy larvae. No definite phenotype	variable

* In the RNA combinations including C02C6.1 (*dyn-1*), it was noted that a high proportion of larvae were mid-moult, seemingly trapped in their shed cuticle (Figure 6.28b). They appeared lethargic or paralysed

In order to check that the *dyn-1* RNAi embryos were the result of removing both maternal and zygotic dynamin, I observed the temperature-sensitive allele *dyn-1(ky51)* and a null allele of dynamin, *dyn-1(cq4)* kindly sent to me by A.van der Bliek. *dyn-1(ky51)* homozygotes are paralysed when transferred to the restrictive temperature and this paralysis is reversible (Clark *et al.*,1997). This is due to the high demand on endocytosis at neuron synapses from the recycling of synaptic vesicles. At the restrictive temperature, the amount of dynamin present is significantly reduced and endocytosis is therefore halted. I raised *dyn-1(ky51)* homozygotes at the restrictive temperature of 25°C and then observed the phenotype of their progeny produced at the same temperature which would have no, or a greatly reduced amount of, maternal or zygotic dynamin. These hermaphrodites produced a small brood including embryonic lethals as well as other small, lethargic progeny. The majority of embryos arrested at the same stage as *dyn-1* RNAi embryos (Figure 6.28c). Dynamin functions maternally in endocytosis of the yolk proteins which provide essential nourishment for the developing embryos (B.Grant, pers. comm.). In contrast, animals homozygous for the *dyn-1(cq4)* null arrest as 3-fold embryos or L1 stage larvae (Figure 6.28d). I then performed RNAi with the predicted genes K09A9.1 and K09A9.2 in hermaphrodites heterozygous for *dyn-1(cq4)* and subsequently examined their homozygous *dyn-1(cq4)* progeny for any effects. I did not observe any difference between the *dyn-1(cq4)* null homozygous progeny of the injected *dyn-1(cq4)* null heterozygotes, and homozygote *dyn-1(cq4)* null embryos from non-injected heterozygote animals.

6.9. Discussion

ijDf1 is a deficiency which deletes around 1.6Mb of the genome and extends from around position 18 to position 23.5 on the X chromosome,. Animals homozygous for the deficiency arrest as 1.5-fold stage embryos with an underdeveloped pharynx and a limited degree of movement. The basement membrane between the muscle and hypodermis appears to be as wild type and myosin staining shows that muscle sarcomeres are in the correct position, although the organisation of myosin within each sarcomere seems less uniform than wild type. This could reflect an actual defect or simply be the result of the presence of fully developed muscle in a much shorter space than wild type due to the lack of elongation in *ijDf1* mutant embryos. MH4 staining,

however, is absent from the hypodermis which would seem to indicate some defect in the intermediate filaments of the hypodermis which mediate muscle-cuticle attachment from around the 2-fold stage. In fact there is a predicted gene deleted by *ijDf1* present across cosmids W10G6 and F52E10 which encodes an intermediate filament protein (Dodemont *et al.*, 1994). It is possible that this protein is the target of the MH4 antibody in the hypodermis. The presence of basement membrane between the hypodermis and muscle however show that these tissues are properly aligned and closely apposed. As normal muscle function is required for proper elongation, this apparent defect in the muscle-hypodermis association may contribute to the elongation defect seen in *ijDf1* homozygotes (Waterston, 1989; Williams and Waterston, 1994). Another possible role for intermediate filaments is the anchorage of the circumferentially oriented actin filament bundles in the hypodermis during elongation (Costa *et al.*, 1998). If intermediate filaments were necessary to maintain proper actin microfilament organisation during elongation then the absence of an intermediate filament structural protein may prevent full elongation. It is possible that the deletion of the W10G6.3 gene which encodes an intermediate filament protein could prevent significant elongation past 2-fold in 'rescued' *ijDf1* homozygotes. Another gene thought to be involved in intermediate filament function is *jam-1* which encodes the protein recognised by the MH27 monoclonal antibody (M.Koeppen, pers. comm.). This gene encodes a protein homologous to human trychohyalin which organises intermediate filaments and RNAi experiments with *jam-1* produce embryos which arrest at the 2-3-fold stage. The hypodermis undergoes fusions, almost to the terminal stage but often the hypodermal fusions are not complete. *ijDf1* mutants synthesise and secrete cuticle with essentially the same pattern as fully elongated wild type embryos, and the furrows seen in the cuticle may reflect circumferential orientation of actin fibres during embryogenesis as in wild type embryos (Costa *et al.*, 1997). The secretion of a cuticle in these *ijDf1* homozygotes suggests that completed hypodermal fusions are not necessary for this process.

The study of overlapping deficiencies uncovered a possible region of *ijDf1* containing genes involved in this early elongation process and subsequent injection of cosmids from this region partially rescued the phenotype so that transformed embryos arrest at a much later stage in elongation. The rescue phenotype was an arrest at around 2.5-fold elongation, often associated with a very narrow anterior and an apparently more

developed pharynx than *ijDf1* homozygotes. There are aspects of this phenotype which are similar to *mnDf43* homozygotes, although *ijDf1* rescued embryos do not rupture suggesting that *mnDf43* deletes a gene or genes involved in enclosure/cuticle synthesis which *ijDf1* does not delete. The smallest area that rescued this phenotype was the overlap of the two cosmids K09E9 and K09A9 plus the cosmid C02C6. The non-overlap region of K09E9 plus C02C6 also gave a partial rescue effect although this was not as pronounced.

From the published sequences of the *C.elegans* genomic DNA contained within cosmids K09A9 and K09E9, two genes are predicted within the genomic overlap of the two cosmids: K09A9.1 which is similar to a serine/threonine kinase, and K09A9.2 which is similar to the rat RAS-related gene, Rab-14. C02C6 contains two genes predicted by GENEFINDER, C02C6.2 and C02C6.3 (containing sequences similar to leucine-rich repeats), and a cloned gene C02C6.1, or *dyn-1* which encodes a homologue of mammalian dynamin, an 100kDA GTPase necessary for clathrin-mediated endocytosis (Clark *et al.*,1997). There are several possible connections between these various genes. Dynamin regulates endocytic coated-vesicle formation and is expressed in neurons primarily and also in the pharynx, intestine and reproductive tissues. The abundance of dynamin in neurons is thought to reflect the need for a high rate of endocytosis due to the recycling of synaptic vesicles (Labrousse *et al.*.,1998). Dynamin expression has not been observed in the hypodermis although it is thought to be expressed ubiquitously as it appears to be the only dynamin gene in *C.elegans* (Clark *et al.*, 1997). There is a dynamin-related gene, *drp-1,* also present in *C.elegans* which encodes a protein with 32% identity to dynamin (A.Labrousse, pers comm). This identity is distributed over most of the proteins except for a few highly divergent domains which may confer functional specificity, and DRP-1 is thought to regulate mitochondrial morphology. My observations that *dyn-1* RNAi can result in animals 'trapped' in their cuticle may indicate that it has some function in moulting which is thought to involve coated-pit mediated endocytosis (Yochem *et al.*, 1999). Rab proteins are small GTPases regulating membrane traffic in eukaryotic cells and recently an epithelial-specific member of this family, Rab17, has been identified which may be involved in transcellular transport between the apical and basolateral surfaces of polarised cells (Lütcke et al, 1993; Zacchi et al, 1998). Interestingly, another member of the family, *rab-3* also appears to be involved in the trafficking of synaptic vesicles and

another three rab genes in *C.elegans*, *rab-5*, *rab-7* and *rab-11*, are thought to be involved in receptor-mediated endocytosis (Iwasaki *et al.*, 1997; Y.Zhang, pers. comm.). However, it is difficult to say how these findings fit into the mechanism of elongation and it may be possible that the genes responsible for rescue of the early elongation defect in these cosmids have unique functions in morphogenesis which have not been uncovered as yet.

A possible role for the predicted K09A9.2 gene in embryonic elongation is in the organisation of the actin cytoskeleton. Small GTPases from the Rho subfamily of the Ras superfamily have been implicated in the regulation of actin cytoskeleton organisation in many different cells and organisms (Hall, 1998; Schmidt and Hall, 1998). *In vitro* studies on vertebrate fibroblasts have shown that the activation of Rho results in the assembly of contractile actin-myosin filaments called stress fibres; activation of Rac, another member of the Rho family, results in the production of actin-rich lamellipodia; and activation of Cdc42, a third member of the Rho family, stimulates the production of actin-rich filopodia (Ridley and Hall, 1992; Ridley *et al.*, 1992; Kozma *et al.*, 1995; Nobes and Hall, 1995). It has also been found that there is significant interaction between these GTPases as Ras and Cdc42 can activate Rac, and Rac can activate Rho (Ridley *et al.*, 1992; Nobes and Hall; 1995). As discussed in section 1.7.5.3, the contractile actin microfilaments of *C.elegans* appear to be anchored at the adherens junctions of hypodermal cells by a putative catenin-cadherin system which mediates elongation (Costa et al, 1998). It has been found that Rho and Rac are required for the establishment of cadherin-mediated cell-cell adhesion in human epithelial cells and for the actin reorganisation necessary for the stabilisation of cadherins at intercellular junctions (Braga *et al.*, 1997). It seems quite likely therefore that small GTPases may also play a role in the circumferential organisation of actin microfilaments in the *C.elegans* embryo and possibly in the anchoring of these microfilaments at adherens junctions in hypodermal cells.

It is interesting that genes contained in the K09E9/K09A9 overlap and C02C6 are sufficient to rescue the early elongation defect (and underdeveloped pharyngeal defect) in *ijDf1* but the RNAi results indicate that only one of these genes, *dyn-1* shows a phenotype when its function is disrupted. Firstly, it must be remembered that RNAi is a new and not well understood tool for phenocopying a gene knock-out and although results for many genes have been shown to be specific and reproducible (Fire *et al.*,

1998), a negative result is not very informative. The results for the *dyn-1* RNAi phenotype were shown to be comparable to the phenotype obtained when maternal and zygotic dynamin were removed, or greatly reduced, in the temperature shift experiment, but there could be many aspects of the sequences used for the other genes which prevented the production of an actual null phenocopy. Also, the methods used to produce dsRNA may not have worked uniformly for all genes and so there could have been differences in the injected concentrations of the different RNAs. If the RNAi results were an actual indication of the null phenotypes of these genes, then I would expect the deficiency to remove other similar genes which, in wild type worms, would compensate for the 'knock-out' of the rescuing genes by RNAi. Using the WU-Blast 1.4 blastn sequence homology search, I searched for sequence alignment between the genes contained in C02C6 and in the K09A9/K09E9 overlap and other sequences contained within the *ijDf1* deficiency and no significant homology was found. WU-Blast 1.4 is based on NCBI-Blast version 1.4 (Gish and States, 1993; Altschul and Gish, 1996). This leads me to believe that either the RNAi results were not indicative of the null phenotypes of the genes examined, except *dyn-1*, or that the phenotype seen in *ijDf1* homozygotes is the result of an extremely complex compound effect of many deleted genes. This may be the reason why there was also some degree of cosmid rescue with the non-overlap rescue of K09E9 plus C02C6. It is possible that the disruption of several pathways is responsible for the *ijDf1* phenotype and that, while replacing genes in some of these pathways gives significant repair, the removal of these genes alone is not sufficient to create the phenotype observed.

The relationships between genes that have emerged from the characterisation of this deficiency are much more complex than expected. I can not discard the possibility that other cosmids may also have rescued the phenotype to the same extent if they had been injected in their entirety rather than in the deleted forms discovered in retrospect. It is possible that a process necessary for the initiation of elongation or for terminal differentiation of the pharynx, requires the proper function of a common pathway with several gene components. There may also be a degree of redundancy which has been seen so often in *C.elegans* with various genes compensating for the loss of others (Culotti *et al.*, 1981; Johnson *et al.*, 1988; Ferguson and Horvitz, 1989). This could explain why more than one combination of genes can repair the *ijDf1* early elongation defect. No clear cut explanation of rescue has arisen from this characterisation other

than the fact that more than one gene is required for rescue, and the common factor in all rescue combinations has been an element of the cosmid C02C6. Because the K09A9/K09E9 overlap in combination with C02C6 is sufficient to rescue the early elongation defect, it would be of interest to check the predicted positions of the genes contained therein and to subclone them again with a larger upstream flanking region in each clone. The injections of these clones along with C02C6 may show which gene is involved in the rescue, if it is only one of these genes, and further injections with subclones of the genes in C02C6 could possibly provide rescue at the gene level. Although the removal of these genes may not be sufficient to cause the *ijDf1* phenotype, the study of rescuing genes could give an insight into how several aspects of elongation are controlled and unearth complex interactions that would otherwise have remained hidden.

Chapter 7
Concluding discussion

7.1. Summary of results

The work presented in this thesis is concerned with embryonic and postembryonic shape change and maintenance in the nematode *Caenorhabditis elegans*. I have shown that many different factors are involved in these processes as well as elucidating some of these factors through the characterisation of mutants and the observations of an antibody localisation pattern. The characterisation of three embryonic lethal mutants defective in elongation suggests that the presence of a seemingly correctly fused hypodermis is not enough to drive normal elongation and that there are factors such as cell adhesion or the presence of certain GTPases or protein kinases which are involved in the dynamic process of embryonic shape change. The localisation of DPY-7, a cuticular collagen necessary for postembryonic shape maintenance, has been analysed using the monoclonal antibody, DPY7-5a. This has shown where DPY-7 is localised within hypodermal cells before secretion, when it is first translated, when it is secreted, and has given an indication of the position of DPY-7 within the multilayered structure of the cuticle. The comparison of localisation patterns in wild type animals and in strains producing only mutant DPY-7 has given an indication of the cause of the mutant phenotype and the comparison of DPY7-5a staining patterns between wild type and non-*dpy-7* mutants may yet uncover further collagen interactions.

7.2.1. Embryonic lethal mutations causing defective morphogenesis

Three mutants, that had been generated in two separate genetic screens for embryonic lethal mutants defective in morphogenesis, were phenotypically and genetically characterised. Two of these mutations were shown to be the result of deficiencies, *ijDf1* in the X chromosome, and *ijDf2* in chromosome V. The third, *w4* was mapped genetically to an area of chromosome I between *dpy-5* and *unc-75* although it was not established if this mutation was the result of a point mutation or a deletion.

ijDf2 homozygotes arrest as amorphous lumps of cells prior to any elongation and many of these arrested embryos have loose cells floating about inside the eggshell. Certain components of muscle, basement membrane, intestine, pharynx and muscle:hypodermis attachment structures are present at arrest and the embryos twitch in an uncontrolled manner. Defects in embryogenesis were seen before the precomma stage as *ijDf2* homozygote embryos showed loose aggregations of cells rather than the tightly packed spheroid of cells seen before enclosure in the wild type embryo. For this reason, it was suggested that *ijDf2* may delete a gene or genes involved in general cell adhesion, and this defect in turn would disrupt hypodermal morphogenesis when hypodermal cells are migrating around the embryo during enclosure and in the processes of body elongation and hypodermal cell fusion. Hypodermal cells were shown to be present around the surface of the embryo although they were completely disorganised and it was not clear if there were gaps in this hypodermal coverage. There were mono- and multi-nucleate hypodermal cells present and a seemingly correct total number of hypodermal nuclei. These cells were not organised into wild type positions, however, and the total number of hypodermal cells was less than the normal number at hatch, indicating a possible hyperfusion defect in the hypodermis. Although the *ijDf2* homozygote phenotype resembled gastrulation-defective embryos in several respects, some components of the pharynx and intestine were present internally, as were the body wall muscles and so this indicated that gastrulation had occurred to some extent (Knight and Wood, 1998). It is possible that gastrulation is not completed normally in *ijDf2* homozygotes, possibly due to a cell adhesion defect, although it is initiated and the internalisation of a number of cells has occurred. The *ijDf2* deficiency was mapped both genetically and molecularly and was shown to delete 2.2Mb at the centre of chromosome V from around position -0.9 to position 0.7 on the genetic map. A deficiency, *sDf30,* that almost completely overlaps *ijDf2,* shows apparently normal gastrulation and enclosure of hypodermal cells and arrests at the 1.5- to 2-fold stage of elongation. It is apparent therefore that the gene or genes involved in the earlier, possible cell adhesion role, are present in the area of the genome that is deleted by *ijDf2* but not by *sDf30.*

ijDf1 homozygotes appear to develop normally until the comma stage of embryogenesis. At this stage they appear to halt the elongation process while wild type embryos of the same age elongate normally to the 3-fold stage. *ijDf1* homozygotes

arrest at the 1.5-fold stage of elongation with an apparently normal number of hypodermal nuclei. Some *ijDf1* homozygotes appear to have arrested with too few fusions in the dorsal hypodermis although all of them express collagen genes and secrete a cuticle. Components of the pharynx, intestine, basement membrane and muscles were shown to be present at arrest and the embryos twitch actively inside the eggshell although the movement is 'jerky' and uncontrolled. The monoclonal antibody, MH4, recognises intermediate filaments which are components of hemidesmosomes, specialised hypodermal structures which anchor muscle cells to the cuticle. The MH4 staining pattern was shown to be absent from the hypodermis and, interestingly, the *ijDf1* deficiency does delete a predicted gene, W10G2.3, which encodes an intermediate filament protein (Dodemont *et al.*, 1994). The *ijDf1* deficiency was mapped to the right arm of the X chromosome from position 18 to position 23.5, and deletes 1.6Mb of the genome. Two overlapping deficiencies, *mnDf17* and *mnDf43*, were characterised and compared to *ijDf1*, and a region of the physical map was implicated as a likely region to contain the gene or genes involved in the early elongation process. It was found that two groups of two cosmids from this region could rescue the early elongation defect and produce embryos that arrested at over the 2-fold stage of elongation. One of these cosmids in each rescue pair was C02C6 and the other rescuing cosmid was either K09A9 or K09E9. The genomic sequence contained within these two latter cosmids overlapped and this overlap contained two predicted genes, encoding a serine/threonine kinase-like protein, and a Ras-like GTPase respectively. It was found that this overlap alone injected with C02C6 also gave rescue of the early elongation defect and so one or both of these genes was involved in restoring the elongation defect of *ijDf1*.

It was proposed that, since GTPases of the Ras superfamily have been implicated in actin cytoskeletal organisation and the production of contractile stress fibres in fibroblasts, the Ras-like GTPase may be a likely candidate for a gene involved in the elongation process (Hall, 1998). There are three predicted genes in C02C6 but only one of these *dyn-1* encodes a protein with significant homology to any known protein (Clark *et al.*, 1997). DYN-1 is a homologue of vertebrate dynamin which is a small GTPase involved in coated pit endocytosis. It does not appear to be expressed in the hypodermis although the absence of any close homologues in *C.elegans* suggests that the protein should be present ubiquitously. The main role of dynamin in *C.elegans* is in the recycling of synaptic vesicles and it is present at high levels in neurons (Clark

et al., 1997; Labrousse *et al.*, 1998). It has also been suggested that dynamin is involved in endocytosis of yolk proteins necessary for nourishment of the developing embryo (B.Grant pers. comm.). It is possible that dynamin is present in hypodermal cells and has as yet remained undetected there. However, the role that dynamin plays, if any, in the rescue of the early elongation phenotype of *ijDf1* is unknown. The predicted gene encoding the intermediate filament protein is present outwith the area targeted for rescue of the early elongation phenotype. However, it is very possible that this gene has a role to play in the later stages of elongation as correct muscle-hypodermis attachment, mediated by the intermediate filaments, is an essential prerequisite to complete elongation.

Both *ijDf1* and *ijDf2* were zygotic lethal mutations isolated from an EMS genetic screen for mutants defective in embryonic elongation carried out in our laboratory (I.Johnstone, pers.comm.). Genetic mapping and molecular data subsequently showed both these mutations to be very large deficiencies, *ijDf1* deleting 1.6Mb and *ijDf2* deleting 2.2Mb of the genome. This was unexpected considering the previous data both in *C.elegans* and in other organisms where over 90% of EMS mutation events resulted in a single G/C→A/T substitution (Anderson, 1995; Li *et al.*, 1998). The purpose of our mutant screens was to select for embryonic lethal mutations affecting morphogenesis, which has been shown to be a complex process depending on the normal functioning of several different tissues. There are reports of very few single genes which have been mutated to completely disrupt elongation. It is very possible that severe elongation disruptions may be caused by mutations in several different gene combinations and by selecting for these defects, we have automatically been biasing our search towards deficiencies. The larger the deficiency, the more likely it is that it will delete two genes involved in the elongation process and thus produce an elongation defective phenotype. Between 15% and 30% of the 19,099 predicted genes in the genome are thought to be essential (Johnsen and Baillie, 1997). Selecting for embryonic lethal mutants in a screen may bias the outcome towards a higher possibility of obtaining deficiencies. Also, two genes which would produce viable phenotypes if deleted separately may produce a lethal phenotype when deleted together.

The third elongation defective mutant which was characterised was given to us from a screen carried out by Joel Rothman. *w4* was mapped to the right arm of chromosome I, between *dpy-5* and *unc-75* and closer to *unc-75* but a more precise

location was not determined. The majority of *w4* homozygotes, around 75%, arrest as embryos with a pronounced rupture of internal tissues at the lower ventral surface. Since this is the point of ventral closure of the hypodermal cells in wild type embryos, it seems that the *w4* hypodermis does not enclose properly at this point and as elongation begins, internal tissues are forced out through the ventral opening. From time-course studies it can be seen that the amount of exuded tissue increases greatly after the comma stage until, at arrest, the embryo is very ruptured. The pharynx, muscles, basement membrane, intestine and hemidesmosomes all appear to be present in their correct positions and seem equivalent to wild type, except that the internal structures often extend outwith the embryo at the site of rupture. Hypodermal cells are present in approximately the correct number with an apparently wild type number of nuclei, however the site of rupture suggests that the most ventral hypodermal cells, the P cells do not form proper junctions with their contralateral neighbours. These homozygotes do secrete a cuticle which can be seen under Nomarski microscopy, and when using an antibody, DPY7-5a, which recognises the DPY-7 cuticular collagen. Around 25% of *w4* homozygotes elongate to around 2.5 fold and hatch as lumpy-dumpy larvae. Most of these hatched mutants have dorsal and ventral bulges, especially at the anterior, a detached and fused buccal cavity, branched alae at the level of the bulges, and occasionally a blocked rectum. These mutants move slowly across a surface and die within 2-3 days of hatching without growing any larger, presumably due to starvation. Interestingly, Costa *et al.* (1998) characterised mutations in a gene, *hmr-1* which maps to between *dpy-5* and *unc-75* on chromosome I and encodes a homologue of classical cadherin. *hmr-1* homozygotes arrest as embryos and appear to be defective in hypodermal enclosure also, although the rupture appears to be towards the anterior in these embryos. A very small proportion (around 2%) of *hmr-1* homozygotes enclose but do not elongate normally, arresting with dorsal bulges. It is possible that *w4* is an allele of *hmr-1* although cosmid rescue of the *w4* phenotype was not obtained by injecting a group of cosmids including one containing the wild type *hmr-1* gene.

7.2.2. Characterisation of the staining pattern of DPY7-5a, a monoclonal antibody specific to the cuticular collagen DPY-7

The control of body morphogenesis is taken over by the multilayered cuticle at the 3-fold stage of embryonic elongation and the cuticle is responsible for maintaining shape change for the rest of the life cycle. The structural components of the cuticle are synthesised in the hypodermis and proteins known as collagens make up the majority of these components. Genetic studies have shown that some cuticular collagens are essential for maintaining shape as null mutants of the genes encoding these collagens have an altered postembryonic shape. Null mutations in other collagens do not produce a detectable phenotype under laboratory conditions, although mutant forms of these collagens can disrupt the organisation of the cuticle and cause an abnormal body shape. DPY-7 plays an significant role in the function of the *C.elegans* cuticle and the absence of DPY-7 in the cuticle results in a dumpy animal which is much shorter and broader than wild type. *dpy-7* is also among the earliest group of collagen genes to be expressed in the hypodermis at each stage of the life cycle, beginning embryonically at the precomma stage. A novel monoclonal antibody, DPY7-5a, which is specific to the carboxy terminal domain of DPY-7 was generated by I.Johnstone in our laboratory and I observed the spatial and temporal staining of this antibody embryonically and postembryonically. The DPY7-5a antibody was shown to be specific to DPY-7 by staining *dpy-7(qm63)* homozygotes which have the *dpy-7* locus deleted. These mutants showed no DPY7-5a staining at all. DPY7-5a showed an intracellular localisation of DPY-7 in hypodermal cells of the embryo from the precomma stage to around the 2.5 fold stage of development. This result coincided with the previous finding that *dpy-7* was expressed at the precomma stage of embryonic development (Johnstone and Barry, 1996). Staining was cytoplasmic and appeared to be present throughout the whole cell, although most of the staining was subapical, and it was absent from the nucleus. All hypodermal cells appeared to contain DPY7-5a staining although the seam cells appeared to show a less bright signal in some embryos. From the 2.5 fold stage to the 3-fold stage there was a switch from an intracellular to an extracellular location of the DPY7-5a antibody and at the 3-fold stage, staining was present extracellularly in circumferentially arranged bright bands, except over the seam cells where there was a complete absence of staining. These bright circumferentially arranged bands of DPY7-

5a staining coincided exactly with the annular ridges of the cuticle. This suggests that the DPY-7 collagen is in the cortical layer of the cuticle as this is the only layer to be patterned into annulae, and that DPY-7 is localised to a region of the annular ridges (Cox *et al.*, 1981a; Costa *et al.*, 1998). The intracellular pattern of localisation was only examined thoroughly during embryogenesis as in later stages, the secreted cuticle makes internal observation difficult. However, in stages where internal staining was observed postembryonically, it appeared to follow the same intracellular pattern and was present in hypodermal cells as expected. Extracellular staining of DPY7-5a was seen in all stages. In L1 and adult stages, there is a clear absence of DPY7-5a staining from above the seam cells and staining is only seen to either side of the alae, the cuticular structures which run longitudinally above the seam. In L2-L4 stages however, the annulae staining appears to traverse the borders of the seam cells and, in many cases, the annulae almost interdigitate above the seam. Since it has been reported that annulae are absent from above the seam cells at all stages, this may indicate some movement of the DPY-7 collagen over cell boundaries. It appears that the DPY-7 protein is only completely absent or undetectable over the seam cells at stages where there are alae present.

All collagens have conserved blocks of Gly-X-Y repeats, and point mutations which cause glycine substitutions in these repeats in collagens essential for the maintenance of shape usually result in shape defects when homozygous. It was previously thought that these mutant phenotypes were due to the absence of the wild type collagen in the cuticle rather than the presence of the mutant collagen as the mutations are recessive and the phenotypes are very similar to the null phenotype of each particular collagen gene (Johnstone *et al.*, 1992; Johnstone, 1994; Kramer, 1997). I examined the pattern of the DPY7-5a antibody in mutants homozygous for the *dpy7(e88)* mutation which results in a Gly-X-Y repeat glycine substitution. The internal staining pattern during embryogenesis was as wild type, but when the intracellular-extracellular switch occurred there was a noticeable decrease in the amount of DPY-7 collagen secreted into the cuticle. There was some extracellular DPY7-5a staining, however, which indicates that a proportion of the mutant collagen does enter the cuticle. This observation suggests that although the dumpy phenotype produced in this mutant may be due mostly to the absence of wild type DPY-7 collagen in the cuticle, there still may be a component of the phenotype which is due to the presence of mutant DPY-7 collagen in the cuticle. To ensure that this reduction in extracellular DPY7-5a staining

was not simply a facet of the dumpy phenotype, I stained *dpy-13(e458)* homozygotes. DPY-13 is another collagen essential for postembryonic shape maintenance and the *dpy-13(e458)* homozygotes represent the null phenotype. Intracellular DPY7-5a staining was as wild type in *dpy-13(e458)* homozygote embryos and the intracellular-extracellular switch occurred as normal. Extracellular staining of all larval stages and the adult stage was in the same pattern as wild type except that the bands of staining, representing annulae, were much closer together, around half the distance apart of wild type annulae. Costa *et al.* (1997), reported that it is the circumferentially aligned actin microfilaments within hypodermal cells that pattern the cuticle, giving rise to annulae. Since these actin microfilaments are independent of the cuticle, it would seem likely that there would be the same amount of actin filaments and thus annulae in a wild type and a dumpy animal. For this reason, the annulae should be closer together in the dumpy animal, and the shorter the animal, the closer together the annulae should be. I found that this indeed appeared to be true when comparing *dpy-13(e458)* homozygotes with wild type animals of the same stage.

The DPY7-5a antibody is a useful tool when examining postembryonic shape change as it may give an indication of the reason for particular phenotypes and the organisation of the cuticle in wild type worms. It may also shed some light on the temporal expression of collagen genes in the hypodermis by staining collagens that are expressed at the same time and those expressed in the later temporal waves.

7.2. Future work

7.2.1. Cosmid rescue of *ijDf2* early enclosure/cell adhesion defect

In order to identify precisely which gene or genes are deleted by *ijDf2* to produce the unelongated arrest phenotype, the endpoints of the *ijDf2* and *sDf30* deficiencies would have to be mapped more finely on the physical map. *ijDf2* extends further right than *sDf30* and may also extend further to the left. It is possible that the gene or genes of interest are deleted by a region of *ijDf2* which is deleted by it and not *sDf30*. Overlapping groups of cosmids corresponding to this area could be injected into *ijDf2* heterozygotes with the same markers used for indicating transgenic larvae and embryos as were used in the cosmid rescue of *ijDf1* (section 6.5). The resulting rescue

should produce *ijDf2* homozygote embryos that elongate to an equivalent length to *sDf30* homozygotes. This may give a clearer indication of what process is being affected in *ijDf2* homozygotes and how it relates to morphogenesis.

7.2.2. Rescue of the *ijDf1* early elongation phenotype at the gene level

I showed that the overlap of genomic sequence between the cosmids K09A9 and K09E9 along with the cosmid C02C6 produced rescue of the *ijDf1* early elongation defect. Rescue was not obtained, however, when the two predicted genes contained in this overlap were subcloned and injected together with the C02C6 cosmid. This may have been for several reasons, one of which being that there may not have been enough upstream flanking sequence contained along with the gene coding sequence in the subclones. In order to narrow down the number of genes involved in this early elongation process, it would be beneficial to subclone these two predicted genes again, with larger flanking sequences, and to try to achieve the early elongation defect rescue at the gene level. This would show which of these predicted genes was involved in this process, or that both were involved. There are three predicted genes in C02C6 and so these could be subcloned also and different combinations of genes could be injected in an attempt to rescue the early elongation phenotype using gene subclones.

7.2.3. The involvement of an intermediate filament component coding gene in the elongation process

Although the cosmid W10G6 was not in the region targeted for rescue of the early elongation phenotype, there is a strong possibility that it could influence the later stages of elongation as it contains the gene W10G6.3 which encodes an intermediate filament component. Intermediate filaments are important components of hemidesmosomes, structures in the hypodermis which function in the attachment of muscles through the hypodermis to the cuticle. Muscle attachment to the hypodermis has been shown to be an important feature in the elongation process from 2- to 3-fold and mutants defective in muscle:hypodermis attachments usually arrest as lumpy, improperly elongated embryos (Rogalski *et al.*, 1993; Williams and Waterston, 1994; Gupta *et al.*, 1997). Staining *ijDf1* homozygotes with the MH4 antibody, which

recognises an unknown component of hemidesmosomes, showed a complete absence of staining in the hypodermis although the staining patterns of this antibody in other structures were present. This indicates some defect in the hypodermal muscle attachment structures, probably due to the absence of W10G6.3 gene, and so may have an effect on the later stages of *ijDf1* homozygote elongation. In order to investigate this, the cosmids W10G6 and F52E10, or the subcloned W10G6.3 gene could be injected into *ijDf1* heterozygotes along with the K09A9/K09E9 overlap plus C02C6 cosmids which are known to rescue the early elongation defect seen, and the resulting transformed *ijDf1* homozygotes could be observed for changes in the degree of rescue.

7.2.4. Testing whether *w4* is an allele of *hmr-1*

The theory that *w4* may be an allele of *hmr-1* because of the proximity of the loci and the similarity of the phenotypes produced by homozygous mutants, could be tested by a complementation test or by attempting to rescue the *w4* phenotype by injection of an *hmr-1* subclone. Attempted rescue using the W02B9 cosmid or an *hmr-1* subclone would be carried out by injecting *w4* heterozygotes using the same marker genes as in section 6.5 and then monitoring transformed lines for any rescue of the embryonic lethal phenotype. If the injected DNA rescues the embryonic lethal phenotype, then the co-injected *dpy-7*::GFP fusion construct marker would not be present or expressed in dead embryos, but if the injected DNA did not rescue the embryonic lethal phenotype then expression of the *dpy-7*::GFP transgene would be present in a percentage of arrested embryos equivalent to the transformation frequency of the line.

7.2.5. Electron microscopy of the cuticle of hatched *w4* homozygotes

In order to investigate whether the defects seen in *w4* homozygotes are purely due to hypodermal abnormalities, an investigation of the cuticle of hatched homozygotes could be undertaken. *w4* hatched homozygotes have branched alae and a lumpy, short appearance with dorsal and ventral bulges so the cuticle may be weak or defective in certain areas. Serial sections of the cuticle at these areas of abnormal body shape would help to elucidate whether these abnormalities simply reflected defects in

the underlying hypodermal cells or whether they are due to actual structural defects in the cuticle.

7.2.6. Determining the precise point of DPY-7 secretion during embryogenesis

It is known that the cuticle is secreted at the 3-fold stage of embryogenesis but analysis of the actual process of secretion of the DPY-7 cuticular collagen may help to elucidate the stages of this process. Synchronised embryonic cultures can be obtained by cutting open gravid hermaphrodites and selecting 2-cell stage embryos. These synchronised cultures could be left to develop until the 2-fold stage of embryogenesis in an appropriate buffer and then sample specimens taken every 10 minutes, fixed and stained with the DPY7-5a monoclonal antibody. In this way, the precise time of cuticle secretion, estimated from the secretion of the DPY-7 collagen, can be observed and the transition from intracellular to extracellular staining could be monitored much more closely. Once the secretion time is known more accurately, embryos could be stained at smaller time points and the secretion process could be observed more clearly. This analysis would indicate whether there is a specific area where cuticle secretion begins, or whether it is a more uniform process, it would also elucidate whether DPY-7 collagen is secreted along an annular ridge at various points at the same time or whether there is a focal point from which cuticle secretion spreads.

7.2.7. Precise subcellular localisation of DPY-7 collagen in the hypodermis

I have reported the intracellular localisation of DPY-7 as observed using immunofluorescence microscopy but a much more accurate subcellular localisation could be obtained using electron microscopy. Serial sections of embryos throughout the stages of elongation stained with the DPY7-5a monoclonal antibody may show subtle changes in the position of DPY-7 within cells, from the time of translation to the time of secretion. Electron microscopy would indicate which organelles DPY-7 co-localises with and if this changes throughout embryonic development. This may elucidate aspects of the cuticle formation process and could even indicate a route from the intracellular position of the DPY-7 collagen to the apical surface in preparation for secretion.

7.2.8. DPY7-5a staining pattern in collagens expressed at the same time during development

Many aspects of cuticular collagen synthesis and organisation are still unknown including whether collagen trimers are made up of collagen chains from only one or more than one collagens. It is known that collagen genes are expressed in temporal waves during development but the reason for this organisation still remains unclear (Johnstone and Barry, 1996). *dpy-7* is expressed at the same time as several other collagen genes, including *dpy-2* and *dpy-10* and so it would be interesting to look at the DPY7-5a staining pattern in embryos homozygous for *dpy-2* or *dpy-10* null alleles (J.Muriel, pers comm.). This may indicate previously hidden interactions between collagens expressed at the same time and may help provide an explanation as to why collagens are expressed in this manner.

Appendices

Appendix 3.1
Measurements of the distance between annulae/DPY7-5a bands in N2 and CB458 strains in μm

N2

young adults:

A)

1.178	1.149	1.157	1.157	0.930	1.178	1.149	1.178	1.140	1.283
1.178	1.053	1.283	1.283	1.053	1.178	1.538	1.157	1.283	1.283
1.283	1.178	1.029	1.140	1.183	1.140	1.140	1.183	1.183	1.178
1.157	1.538	1.149	1.178	1.302	1.410	1.404	1.178	1.428	1.140

B)

0.723	0.818	0.903	0.639	0.723	0.903	0.723	0.723	0.818	0.723
0.818	0.723	0.639	0.998	0.998	0.542	0.818	0.903	0.639	0.818
0.903	0.818	0.818	0.998	0.903	0.639	0.818	1.029	0.818	0.818
0.903	0.723	0.818	1.098	0.903	1.029	1.098	0.818	0.972	0.542
1.098	0.972	0.571	0.818	0.808	0.818	0.639	0.930	0.745	0.903
0.930									

C)

0.972	0.903	0.903	0.930	0.894	0.894	0.651	1.149	1.029	0.808
0.894	1.022	0.808	1.029	1.157	0.688	0.930	1.022	0.651	0.903
1.149	0.777	0.903	1.029	0.930	1.149	1.022	0.808	0.777	0.894
0.808	0.903	1.157	0.777	0.894	1.029	0.651	0.903	1.178	1.149
0.903	0.930	0.894	0.894	0.930	0.894	0.903	1.029		

D)

1.083	1.178	1.091	0.930	1.091	0.977	1.083	1.178	0.977	0.903
0.930	0.977	1.029	1.178	0.857	1.083	1.091	0.977	1.083	1.178
1.029	1.083	1.157	1.091	1.083	1.178	1.091	1.083	1.083	0.977
1.091	0.930	0.977	1.083	0.903	0.977	1.303	0.894	1.258	1.083
1.083	1.142	1.022	0.930	1.091	1.283	0.857	1.142		

E)

1.029	0.930	1.083	1.029	1.178	1.083	1.157	1.211	1.083	0.930
1.333	1.283	1.178	1.303	1.178	1.083	1.333	1.157	1.178	1.333
1.083	0.972	1.553	1.178	1.178	1.211	1.083	0.903	1.303	1.091
1.083	1.083	1.083	1.083	1.178	1.178	1.091	1.178	1.091	0.972
1.178	1.083	1.083	0.930	1.211	1.178	1.083	1.091		

Appendix 3.1 (continued)
Measurements of the distance between annulae/DPY7-5a bands in N2 and CB458 strains in μm

N2 old adults

A)

1.498	1.459	1.431	1.639	1.379	1.669	1.378	1.639	1.431	1.741
1.379	1.669	1.431	1.741	1.431	1.498	1.384	1.379	1.493	1.547
1.431	1.547								

B)

1.778	1.456	1.376	1.494	1.494	1.778	1.456	1.494	1.376	1.302
1.778	1.333	1.580	1.315	1.580	1.580	1.580	1.494	1.494	1.660
1.456	1.615	1.778	1.456	1.543	1.428	1.615	1.543	1.494	1.376
1.660	1.778	1.456	1.376	1.494	1.580	1.376	1.315	1.494	1.494
1.660	1.580	1.494	1.660	1.494	1.376	1.714			

C)

1.660	1.494	1.899	1.737	1.778	1.859	1.778	1.954	1.600	1.899
1.615	1.778	1.494	1.615	2.063	1.376	1.806	2.063	1.494	1.302
1.899	1.660	1.428	2.019	1.580	1.494	2.182	1.737	1.456	2.141
1.737	1.456	1.859	1.737	1.580	1.615	1.737	1.859	1.494	1.704
1.553	1.615	1.580	1.778	1.615	1.778	1.615			

CB458 [*dpy-13(e458)*] adults

A)

0.746	0.572	0.572	0.746	0.640	0.859	0.746	0.859	0.462	0.859
0.572	0.572	0.405	0.689	0.859	0.820	0.746	0.640	0.462	0.923
0.640	0.640	0.543	0.724	0.724	0.820	0.640	0.640	0.543	

B)

0.689	0.572	0.820	0.810	0.746	0.859	0.859	0.746	0.810	0.859
0.746	0.820	0.689	0.572	0.820	0.640	0.859	0.820	0.640	0.746
0.820	0.572	0.572	1.000	0.746	0.859	0.820	0.640	0.572	0.746
0.820	0.746	0.820	1.208	0.572	0.923	0.746	0.689	0.923	0.859
0.859	0.653	0.810	0.689	0.689					

Appendix 4.1
Percentage of L1 and embryonic death in broods from heterozygous *w4*/+ hermaphrodites. All broods maintained at 20°C except where stated.

Within each brood				Within dead progeny	
Number of dead embryos	Number of dead L1s	Number of viable progeny	Percentage death	Percentage L1 death	Percentage embryonic death
91	28	0	100*	24	76
34	10	124	26	23	77
35	18	130	29	34	66
32	8	99	29	20	80
40	10	92	35	20	80
31	18	110	31	37	63
32	5	91	29	13	86
20	2	46	32	9	91
23	2	49	34	8	92
11	0	55	17	0	100
22	2	59	29	8	92
16	1	51	25	6	94
20	4	57	30	16	84
11	1	24	33	8	92
7	1	27	23	12	88
27	2	78	27	7	93
17	6	72	24	26	74
12	10	82	21	45	55
36	11	89	35	23	77
17	15	90	26	47	53
18	4	59	27	18	82
12	4	38	30	25	75
6	3	39	19	33	67
11	7	38	32	39	61
15	5	82	20	25	75
21	7	69	29	25	75
24	10	86	28	29	71
8	7	27	36	47	53
7	8	32	32	53	47
6	6	38	24	50	50
8	11	28	40	58	42
14	4	57	33	22	78
12	12	68	26	50	50
7	1	48	14	12	88

*Parent hermaphrodite was maintained at 13°C as incubator was not working properly and so a *w4* homozygote must have escaped death. This brood was not included when calculating the average percentage death.

Appendix 4.2

ZE316 MT465 cross - raw data:
F2 recombinants

Brood number	Dumpy recombinants (dpy-5 homozygotes)			Blister recombinants (bli-2 homozygotes)			Uncoordinated recombinants (unc-32 homozygotes)		
	number of dead progeny	number of live progeny	percentage ZE316 death	number of dead progeny	number of live progeny	percentage ZE316 death	number of dead progeny	number of live progeny	percentage ZE316 death
1	0	ND	0	24	87	22	16	46	26
2	0	ND	0	25	87	22	12	47	20
3	0	ND	0	39	101	28	0	ND	0
4	0	ND	0	36	100	26	14	42	25
5	0	ND	0	14	68	17	0	ND	0
6	0	ND	0	20	36	36	25	56	31
7	7	88	7*	18	73	20	19	52	27
8	0	ND	0	33	122	21	19	68	22
9	0	ND	0	22	62	26	25	71	26
10	0	ND	0	20	81	20	21	67	24
11	0	ND	0	18	58	24	23	62	27
12	0	ND	0	0	ND	0	0	ND	0
13	17	48	26	18	65	22	10	48	17
14	0	ND	0	30	89	25	0	ND	0
15	0	ND	0	0	ND	0	21	57	27
16	23	62	67	36	129	22	12	32	27
17	0	ND	0	32	97	25	8	30	21
18	0	ND	0				28	87	24

* Very low percentage of death but embryos were checked under high magnification (X1000) and found to have the ZE316 phenotype

Appendix 4.3

dpy-5+unc-101/+w4+ three-factor cross raw data

Brood number	Dpy-non-Unc recombinants			Unc-non-Dpy recombinants		
	number of dead progeny	number of living progeny	percentage death	number of dead progeny	number of living progeny	percentage death
1	0	ND	0	0	ND	0
2	16	60	21	9	63	13
3	15	42	26	0	ND	0
4	22	82	21	30	91	25
5	0	ND	0	0	ND	0
6	11	52	17	0	ND	0
7	17	31	35	9	44	17
8	0	ND	0	20	47	30
9	0	ND	0	0	ND	0
10	15	68	18	0	ND	0
11	0	ND	0	0	ND	0
12	9	29	24	33	72	31
13	14	75	16	0	ND	0
14	12	30	29	0	ND	0
15	20	51	28	21	63	25
16	24	91	21	0	ND	0
17	0	ND	0	15	47	24
18	15	50	23	0	ND	0
19	20	57	26	9	21	30
20	0	ND	0	0	ND	0
21	7	39	15	0	ND	0
22	10	24	29	0	ND	0
23	12	44	21	0	ND	0
24	5	23	18	0	ND	0
25	4	12	25	0	ND	0
26	15	46	25	0	ND	0
27	5	24	17	7	17	29
28	8	52	13	0	ND	0
29	0	ND	0	24	58	29
30	5	12	29	19	54	26
31	0	ND	0	16	42	28
32	0	ND	0	18	52	26
33	15	32	32	14	26	35
34	0	ND	0	0	ND	0
35	25	69	27	19	40	32
36	0	ND	0			
37	0	ND	0			
38	27	64	30			
39	18	74	20			
40	18	78	19			
41	19	63	23			
42	16	60	21			
43	14	50	22			

Appendix 4.4a
F2 progeny phenotypes from Line2 of *w4* cosmid injections

Brood	number of dead embryos	Total number of larvae	number of Uncs	number of Rollers	percentage Uncs
A	29	84	1	9	0.9
B	49	91	0	8	0
C	29	58	1	9	1.1

Appendix 4.4b
F3 progeny phenotypes from Line 2 of *w4* cosmid injections

Brood	number of dead embryos	Total number of larvae	number of Uncs	number of Rollers	percentage Uncs
A1	sterile adult				
A2	27	95	2	21	1.6
A3	sterile adult				
A4	44	98	4	7	2.8
A5	32	102	1	27	0.7
A6	sterile adult				
A7	sterile adult				
A8	26	63	2	9	2.2
A9	31	78	2	32	1.8
B1	17	50	2	17	3.0
B2	17	66	2	7	2.4
B3	sterile adult				
B4	sterile adult				
B5	sterile adult				
C1	13	32	0	4	0
C2	sterile adult				
C3	sterile adult				
C4	sterile adult				

Appendix 4.4c

F4 Progeny phenotypes from F3s including Uncs from Line2 of *w4* cosmid injections

brood no	Roller phenotype	number of dead embryos	Total number of larvae	number of Uncs	percentage Uncs
A1.1	yes	sterile adult			
A1.2	yes	sterile adult			
A1.3	yes	sterile adult			
A1.4	yes	47	84	2	1.5
A1.5	yes	27	47	0	0
A1.6	yes	sterile adult			
A1unc1	no	13	48	N/A	N/A
A2.1	yes	33	70	2	1.9
A2.2	yes	sterile adult			
A2.3	yes	sterile adult			
A2.4	yes	20	101	0	0
A2.5	yes	sterile adult			
A2unc1	no	30	122	N/A	N/A
A2unc2	yes	23	101	N/A	N/A
A2unc3	no	29	96	N/A	N/A
A3.1	yes	31	129	5	3.1
A3.2	yes	24	114	4	2.9
A3.3	yes	36	103	4	2.8
A3.4	yes	25	59	0	0
A3.5	yes	sterile adult			
A4.1	yes	55	116	4	2.3
A4.2	yes	sterile adult			
A4.3	yes	30	93	2	1.6
A4.4	yes	29	80	2	1.8
A4.5	yes	sterile adult			
A4unc1	no	20	59	N/A	N/A
A5.1	yes	31	61	3	3.3
A5.2	yes	54	108	3	1.9
A5.3	yes	30	78	5	4.6
A5.4	yes	34	83	3	2.6
A5.5	yes	25	68	2	2.2
A5unc1	yes	28	71	N/A	N/A
B1.1	yes	sterile adult			
B1.2	yes	19	48	3	4.5
B2.1	yes	sterile adult			
B2.2	yes	39	106	4	2.8
B2.3	yes	45	97	3	2.1
B2.4	yes	32	68	2	2.0
B2.5	yes	25	101	2	1.6

Appendix 5.1

Percentage death in 33 broods from *ijDf1* heterozygote hermaphrodites. All broods were maintained at 20°C.

Number of dead embryos	Number of viable L1 larvae	Total progeny	Percentage death
33	75	108	30
32	76	108	30
28	72	100	28
29	63	92	32
24	58	82	29
12	54	66	18
16	52	68	24
33	61	94	35
14	42	56	25
25	84	109	23
24	86	110	22
36	73	109	33
28	71	99	28
39	96	135	29
20	69	89	22
16	65	81	20
15	59	74	20
20	64	84	24
17	56	73	223
18	56	74	24
24	81	105	23
17	78	95	18
23	53	76	30
11	50	61	18
19	71	90	21
26	68	94	28
23	58	81	28
28	57	85	33
25	50	75	33
20	66	86	23
30	88	118	25
15	76	91	16
28	75	103	27

Average death = 25.5±0.88%
Total number of progeny scored = 2971

Appendix 5.2a

Tabulated representation of chromosomal assignment STS multiplex PCR gels for *ijDf2*.

In all cases, 1 indicates the presence of the STS marker band, and 0 indicates its absence. Each lane on the gel represented one embryo.

embryo	hP4 (LG I)	maP1 (LG II)	mgP21 (LG III)	sP4 (LG IV)	bP1 (LG V)
1	1	0	0	1	0
2	0	0	1	1	0
3	1	0	1	0	0
4*	1	1	0	1	1
5	1	1	1	1	0
6	1	1	0	0	0
7	1	1	0	1	0
8	0	0	1	1	0
9	1	1	1	1	0
10	0	1	1	1	0
11	0	1	0	1	0
13	1	0	0	1	0
14	0	1	1	1	0
15	1	0	1	1	0
16	1	0	1	1	0
17	1	0	1	1	0
21	1	1	1	1	0
22	0	1	1	1	0
23	1	0	1	1	0
24	1	1	1	1	0
25	1	1	1	1	0
26	1	1	1	1	0
27	1	1	1	1	0
28	1	0	1	1	0
29	1	1	1	1	0
30	1	1	0	0	0
31	0	1	1	1	0
32	1	1	0	1	0
33	1	1	0	1	0
34	1	1	1	1	0
35	0	1	1	0	0
36	0	1	0	1	0
37	0	1	1	1	0
38	1	0	1	0	0
39	1	1	1	1	0
40	0	0	1	0	0
41	0	0	1	1	0
42	1	1	1	1	0
43	1	1	0	1	0
44	1	0	1	0	0
45	1	1	1	1	0
46	1	1	1	0	0
47	1	1	0	0	0
48	1	1	1	1	0
49	0	1	1	0	0
50	0	1	0	0	0
51	0	1	1	1	0
TOTAL	32/47	33/47	34/47	35/47	1/47

Appendix 5.2a continued

Reactions: 12, 18, 19 and 20 failed.
The number of bP1 bands may have been underestimated as on some gels, the control bP1 band was quite faint. On gels with clear bP1 controls, however, the band was only seen once (* embryo 4). The *ijDf2* mutation is still clearly linked to Chromosome V comparing the incidence of bP1 bands with STS markers from the other chromosomes which were all present in approximately 75% of embryos (corresponding to 35 out of 47 embryos).

Appendix 5.2b

Tabulated representation of gels showing chromosome V mapping data for *ijDf2* using STS markers on the right and centre of chromosome V.

1 indicates the presence of a STS marker band, and 0 indicates the absence of the band. STS markers are placed in the order that they appear on chromosome V, from left to right (stP192 being the farthest left in this group). Each lane on the gel represented one embryo.

embryo	stP192	bP1	stP6	stP108	stP105	stP128
1	0	0	0	1	1	1
2	0	0	0	0	1	1
3	0	0	0	1	1	1
4	0	0	0	1	1	1
5*	1	1	1	1	1	1
6	0	0	0	1	1	1
7	0	1	1	1	1	1
8	0	0	0	1	1	1
9	0	0	0	0	1	1
10	0	0	0	1	1	1
11	0	0	0	0	0	1
12	0	0	0	0	1	1
13	0	0	0	0	1	1
14	0	0	0	1	1	1
15	0	0	0	1	1	1
16	0	1	1	1	1	1
17	0	0	1	1	1	1
18	0	0	0	1	1	1
19	0	0	0	0	1	1

29 gel lanes contained no bands either due to a failed PCR reaction or absence of the STS markers tested in the embryo.
*embryo 5 was probably a dead RW7000 embryo as it had all STS markers in the region. (from later results I know that stP192 is deleted in ijDf2). Occasionally, the RW7000 strain gives death or sick larvae due to the high number of Tc1 insertions.

Appendix 5.2c

Tabulated representation of gels showing chromosome V mapping data for *ijDf2* using STS markers on the left and centre of chromosome V.

1 indicates the presence of a STS marker band, and 0 indicates the absence of the band. STS markers are placed in the order that they appear on chromosome V, from left to right (stP3 being the farthest left in this group). Each lane on the gel represented one embryo.

embryo	stP3	stP192	bP1	stP6	stP18
1	1	0	0	0	0
2	1	0	0	0	0
3	0	0	0	0	1
4	0	0	0	1	1
5	0	0	0	0	1
6	0	0	0	1	1
7	0	0	0	1	1
8	0	0	0	1	1
9	0	0	0	1	1
10	0	0	0	0	1
11	1	0	0	0	0
12	0	0	0	0	1
13	0	0	0	1	1
14	0	0	0	0	1
15	1	0	0	0	0
16	0	0	0	1	1
17	0	0	0	1	1
18	0	0	0	1	1
19	0	0	0	1	1
20	0	0	0	1	1
21	1	0	0	0	0
22	0	0	0	1	1
23	0	0	0	1	1
24	0	0	0	0	1

137 gel lanes contained no bands either due to a failed PCR reaction or absence of the STS markers tested in the embryo.

Appendix 5.2d
Tabulated representation of gels showing chromosome V mapping data for *ijDf2* using STS markers on chromosome V.

1 indicates the presence of a STS marker band, and 0 indicates the absence of the band. STS markers are placed in the order that they appear on chromosome V, from left to right (stP3 being the farthest left in this group). Each lane on these gels represented a pool of 10 embryos.

embryo pool	stP3	stP192	stP23	bP1	stP6	stP128
1*	1	1	1	1	1	1
2	1	0	0	1	1	1
3	0	0	0	0	0	1
4	0	0	0	1	1	1
5	0	0	0	1	1	1
6	1	0	0	0	0	1
7	0	0	0	0	1	1
8§	1	0	1	1	1	1
9§	1	0	1	1	1	1
10	0	0	0	1	1	1
11	1	0	0	1	1	1
12	1	0	0	0	0	1
13	0	0	0	0	0	1
14	0	0	0	1	1	1
15	0	0	0	0	1	1
16	0	0	0	1	1	1
17	0	0	0	1	1	1
18	1	0	0	0	1	1
19	0	0	0	0	1	1
20	0	0	0	0	0	1
21	1	0	1	1	1	1
22	1	0	1	1	1	1
23	1	0	1	1	1	1
24	1	0	0	1	1	1
25	0	0	0	1	1	1
26	1	0	0	0	1	1
27	0	0	0	0	0	1
28	0	0	0	0	1	1
29	0	0	0	1	1	1
30	0	0	0	0	0	1
31	0	0	0	0	0	1

3 lanes contained bands which were too faint to distinguish properly.
*The pool of 10 probably an RW7000 death as all STS markers are present

Appendix 6.1

Percentage death in 33 broods from *ijDf1* heterozygote hermaphrodites. All broods were maintained at 20°C.

Number of dead embryos	Number of viable L1 larvae	Total progeny	Percentage death
35	89	124	28
32	86	118	27
30	80	110	27
13	40	53	24
16	45	61	26
17	40	57	30
13	42	55	24
16	36	52	31
15	48	63	24
12	36	48	25
21	43	64	33
25	43	68	37
14	53	68	20
14	39	53	26
22	38	60	37
18	53	71	25
14	49	63	22
20	49	69	29
46	134	180	26
32	65	97	33
29	51	80	36
21	48	69	30
16	47	63	25
15	52	67	22
18	58	76	24
14	43	57	24
29	59	88	33
18	68	86	21
17	52	69	25
15	46	61	24
11	37	48	23
25	69	94	26
29	67	96	30

Average death = 27.2±0.79%
Total number of progeny scored = 2488

Appendix 6.2

Tabulated representation of gels showing mapping data for *ijDf1* using STS markers on the X chromosome. (continued on the next two pages)

1 indicates the presence of a STS marker band, and 0 indicates the absence of the band. STS markers are placed in the order that they appear on the X chromosome, from left to right (stP41 being the farthest left). Each lane on the gel represents one embryo.

Embryo	stP41	stP40	stP33	stP129	stP72	stP2
1	1	1	0	0	0	0
2	1	1	1	0	0	0
3	1	1	0	0	0	0
4	1	1	0	0	0	0
5	1	1	1	1	0	0
6	1	1	1	1	0	0
7	1	1	1	0	0	0
8*	1	1	1	1	1	1
9	1	0	0	0	0	0
10	1	1	0	0	0	0
11	1	1	0	0	0	0
12	1	1	0	0	0	0
13	1	1	1	0	0	0
14	1	1	0	0	0	0
15	1	1	1	0	0	0
16	1	1	0	0	0	0
17	1	1	0	0	0	0
18	1	1	1	1	1	0
19	1	1	1	1	1	0
20	1	1	1	0	0	0
21*	1	1	1	1	1	1
22	1	0	0	0	0	0
23	1	1	0	0	0	0
24	1	1	0	0	0	0
25	1	1	0	0	0	0
26	1	1	0	0	0	0
27	1	1	0	0	0	0
28	1	1	0	0	0	0
29?	1	0	0	0	0	1
30	1	0	0	0	0	0
31	1	1	0	0	0	0
32	1	1	1	0	0	0
33	1	1	1	1	1	0
34	1	1	1	0	0	0
35	1	0	0	0	0	0
36	1	1	0	0	0	0
37	1	1	1	1	0	0
38*	1	1	1	1	1	1
39	1	0	0	0	0	0
40	1	1	1	1	0	0
41	1	1	1	1	0	0
42	1	1	1	0	0	0
43?	1	1	0	1	1	0

Embryo	stP41	stP40	stP33	stP129	stP72	stP2
44	1	1	0	0	0	0
45	1	1	0	0	0	0
46	1	1	0	0	0	0
47	1	1	1	1	1	0
48	1	1	1	0	0	0
49	1	1	0	0	0	0
50	1	1	1	0	0	0
51	1	1	1	1	0	0
52	1	1	0	0	0	0
53	1	1	0	0	0	0
54	1	0	0	0	0	0
55	1	0	0	0	0	0
56	1	1	0	0	0	0
57	1	1	0	0	0	0
58	1	0	0	0	0	0
59	1	1	1	1	0	0
60	1	1	1	0	0	0
61	1	1	1	1	0	0
62	1	1	0	0	0	0
63	1	1	1	1	0	0
64	1	1	0	0	0	0
65	1	1	0	0	0	0
66	1	0	0	0	0	0
67	1	1	1	0	0	0
68	1	0	0	0	0	0
69	1	1	1	0	0	0
70	1	1	1	0	0	0
71	1	1	1	0	0	0
72	1	1	0	0	0	0
73	1	1	1	1	0	0
74	1	0	0	0	0	0
75	1	1	0	0	0	0
76	1	1	0	0	0	0
77	1	1	0	0	0	0
78	1	1	1	0	0	0
79	1	1	1	0	0	0
80	1	1	1	0	0	0
81	1	1	0	0	0	0
82	1	1	0	0	0	0
83	1	0	0	0	0	0
84	1	1	1	0	0	0
85*	1	1	1	1	1	1
86	1	1	1	0	0	0
87	1	1	0	0	0	0
88	1	1	1	1	0	0
89	1	1	1	0	0	0
90	1	1	0	0	0	0
91	1	0	0	0	0	0
92	1	0	0	0	0	0
93	1	1	1	0	0	0
94	1	1	1	0	0	0
95	1	1	0	0	0	0
96	1	1	1	1	0	0
97	1	1	0	0	0	0
98	1	1	1	0	0	0
99	1	1	0	0	0	0

Embryo	stP41	stP40	stP33	stP129	stP72	stP2
100	1	0	0	0	0	0
101	1	1	1	0	0	0
102	1	1	1	0	0	0
103	1	1	0	0	0	0
104	1	1	0	0	0	0
105	1	0	0	0	0	0
106	1	1	1	1	0	0
107	1	0	0	0	0	0
108	1	0	0	0	0	0
109	1	1	1	1	0	0
110	1	0	0	0	0	0
111	1	1	1	0	0	0
112?	1	1	1	0	0	1
113	1	0	0	0	0	0
114	1	0	0	0	0	0
115	1	1	1	1	0	0
116	1	0	0	0	0	0
117	1	0	0	0	0	0
118	1	1	1	1	0	0
119	1	0	0	0	0	0
120	1	0	0	0	0	0
121	1	0	0	0	0	0
122	1	1	0	0	0	0
123	1	0	0	0	0	0
124	1	1	0	0	0	0
125	1	1	0	0	0	0
126	1	0	0	0	0	0
127	1	1	0	0	0	0
128	1	1	1	0	0	0
129	1	0	0	0	0	0
130	1	1	1	1	0	0
131	1	0	0	0	0	0

* may be RW7000 homozygotes which have died as embryos. RW7000 animals are very slow growing and there is occasional embryonic and larval lethality.
? These are strange combinations of markers which could only be explained by double recombination events or the embryos carrying two recombinant chromosomes, each with different STS markers.

References

Aberle,H., Butz,S., Stappert,J., Weissig,H., Kemler,R., and Hoschuetzky,H. (1994). Assembly of the cadherin-catenin complex in vitro with recombinant proteins. *Journal of Cell Science* **107**, 3655-3663.

Abrahante,J.E., Miller,E.A., and Rougvie,A.E. (1998) Identification of heterochronic mutants in *Caenorhabditis elegans*: temporal misexpression of a collagen::green fluorescent protein fusion gene. *Genetics* **149**, 1335-1351.

ACeDB: Durbin,R. and Thierry-Mieg,J., unpublished software. Documentation, code, and data are available from anonymous ftp. servers at lirmm.lirmm.fr/pub/acedb/, ftp.sanger.ac.uk/pub/acedb/, and ncbi.nlm.nih.gov/repository/acedb/.

Adams, E. (1978). Invertebrate collagens. Marked differences from vertebrate collagens appear in only a few vertebrate groups. *Science* **202**, 591-598.

Albertson,D.G. (1984). Formation of the first cleavage spindle in nematode embryos. *Developmental Biology* **101**, 61-72.

Albertson,D.G., and Thomson,J.N. (1976). The pharynx of *Caenorhabditis elegans*. *Philosophical Transactions of the Royal Society (London) Series B. Biological Sciences* **275**, 299-325.

Allen,B.G., and Walsh,M.P. (1994). The biochemical basis of the regulation of smooth muscle contraction. *Trends in Biochemical Science* **19**, 362-368.

Altschul,S.F., and Gish,W. (1996). Local alignment statistics. *Methods in Enzymology* **266**, 460-480.

Ambros,V. (1989). A hierarchy of regulatory genes controls a larva-to-adult developmental switch in *C.elegans*. *Cell* **57**, 49-57.

Ambros,V., and Horvitz,H.R. (1984). Heterochronic mutants of the nematode *Caenorhabditis elegans*. *Science* **226**, 409-416.

Ambros,V., and Horvitz,H.R. (1987). The *lin-14* locus of *Caenorhabditis elegans* controls the time of expression of specific postembryonic developmental events. *Genes and Development* **1**, 389-414.

Anderson,P. (1995). Mutagenesis. In: *Methods in Cell Biology: Volume 48.* Caenorhabditis elegans: *Modern Biological Analysis of an Organism*, 31-58. Edited by Epstein,H.F., and Shakes,D.C. Academic Press.

Apodaca,A., Katz,L.A., and Mostov,K.E. (1994). Receptor-mediated transcytosis of IgA in MDCK cells is via apical recycling endosomes. *Journal of Cell Biology* **125**, 67-86.

Aroian,R.V., Koga,M., Mendel,J.E., Ohshima,Y., and Sternberg,P.W. (1990). The *let-23* gene necessary for *Caenorhabditis elegans* vulval induction encodes a tyrosine kinase of the EGF receptor subfamily. *Nature* **348**, 693-699.

Austin,J., and Kimble,J. (1987). *glp-1* is required in the germ line for regulation of the decision between mitosis and meiosis in *Caenorhabditis elegans*. *Cell* **51**, 589-599.

Bamburg,J.R., Bray,D., and Chapman,K. (1986). Assembly of microtubules at the tip of growing axons. *Nature* **321**, 788-790.

Barnes,T.M., Kohara,Y., Coulson,A., and Hekimi,S. (1995). Meiotic recombination, non-coding DNA and genomic organization in *Caenorhabditis elegans*. *Genetics* **141**, 159-179.

Barr,P.J. (1991). Mammalian subtilisins: the long-sought dibasic processing endoproteases. *Cell* **66**, 1-3.

Barroso,M., and Sztul,E.S. (1994). Basolateral to apical transcytosis in polarised cells is indirect and involved BFA and trimeric G protein sensitive passage through the apical endosome. *Journal of Cell Biology* **124**, 83-100.

Beitel,G.J., Clark,S.G., and Horvitz,H.R. (1990). *Caenorhabditis elegans ras* gene *let-60* acts as a switch in the pathway of vulval induction. *Nature* **348**, 503-509.

Beitel,G.J., Tuck,S., Greenwald,I., and Horvitz,H.R. (1995). The *Caenorhabditis elegans* gene *lin-1* encodes an ETS-domain protein and defines a branch in the vulval induction pathway. *Genes and Development* **9**, 3149-3162.

Bennett,V., and Gilligan,D.M. (1993). The spectrin-based membrane skeleton and micron-scale organization of the plasma membrane. *Annual Review of Cell Biology* **9**, 27-66.

Bement,W.M., Forscher,P., and Mooseker,M.S. (1993). A novel cytoskeletal structure involved in purse string wound closure and cell polarity maintenance. *Journal of Cell Biology* **121**, 565-578.

Bergmann,D.C., Crew,J.R., Kramer,J.M., and Wood,W.B. (1998). Cuticle chirality and body handedness in *Caenorhabditis elegans*. *Developmental Genetics* **23**, 164-174.

Betchaku,T., and Trinkaus,J.P. (1978). Contact relations, surface activity, and cortical microfilaments of marginal cells of the enveloping layer and of the yolk syncytial and yolk cytoplasmic layers of *Fundulus* before and during epiboly. *Journal of Experimental Zoology* **3**, 381-426.

Bettinger,J.C., Lee,K., and Rougvie,A.E. (1996). Stage-specific accumulation of the terminal differentiation factor LIN-29 during *Caenorhabditis elegans* development. *Development* **122**, 2517-2527.

Blaxter,M. (1998). *Caenorhabditis elegans* is a nematode. *Science* **282**, 2041-2045.

Bornstein,P., and Traub,W. (1979). The chemistry and biology of collagen. In: *The Proteins* vol.4, 411-632. Third edition. Edited by Neurath,H., and Hill,R.L. Academic Press, New York.

Bradley,B., and Morgan,K.G. (1987). Alterations in cytoplasmic calcium sensitivity during porcine coronary-artery contractions as detected by aequorin. *Journal of Physiology* **385**, 437-448.

Braga,V.M.M., Machesky,L.M., Hall,A., and Hotchin,N.A. (1997). The small GTPases rho and rac are required for the establishment of the cadherin-dependent cell-cell contacts. *Journal of Cell Biology* **137**, 1421-1431.

Brenner,S (1974). The genetics of *Caenorhabditis elegans*. *Genetics* **77**, 71-94.

Bucher,E.A., and Seydoux,G. (1994). Gastrulation in the nematode *Caenorhabditis elegans*. *Seminars in Developmental Biology* **5**, 121-130.

Burke,D.T., Carle,G.F., and Olson,M.V. (1987). Cloning of large segments of exogenous DNA into yeast by means of artificial chromosome vectors. *Science* **236**, 806-812.

The *C.elegans* Sequencing Consortium (1998). Genome sequence of the nematode *C.elegans*: a platform for investigating biology. *Science* **282**, 2012-2018.

Cassada,R.C., and Russell,R.L. (1975). The dauer larva, a post-embryonic developmental variant of the nematode *Caenorhabditis elegans*. *Developmental Biology* **46**, 326-342.

Chalfie,M., and White,J. (1988). The nervous system. In: *The Nematode* Caenorhabditis elegans, 337-391. Edited by Wood,W.B. Cold Spring Harbor Laboratory Press, Cold Spring Harbor, New York.

Chalfie,M., Horvitz,H.R., and Sulston,J.E. (1981). Mutations that lead to reiterations in the cell lineages of *C.elegans*. *Cell* **24**, 59-69.

Chalfie,M., Tu,Y., Euskirchen,G., Ward,W., and Prasher,D. (1994). Green fluorescent protein as a marker for gene expression. *Science* **263**, 802-805.

Chanal,P., and Labouesse,M. (1997). A screen for genetic loci required for hypodermal cell and glial-like cell development during *Caenorhabditis elegans* embryogenesis. *Genetics* **146**, 207-226.

Chen,L., Krause,M., Sepanski,M., and Fire,A. (1994). The *Caenorhabditis elegans* MYOD homologue HLH-1 is essential for proper muscle function and complete morphogenesis. *Development* **120**, 1631-1641.

Cheng,S., Fockler,C., Barnes,W.M., and Higuchi,R. (1994). Effective amplification of long targets from cloned inserts and human genomic DNA. *Proceedings of the National Academy of Sciences (USA)* **91**, 5695-5699.

Church,D., Guan,K.-L., and Lambie,E.J. (1995). Three genes of the MAP kinase cascade, *mek-2, mpk-1/sur-1* and *let-60 ras*, are required for meiotic cell cycle progression in *Caenorhabditis elegans*. *Development* **121**, 2525-2535.

Clark, S.G., Stern,M.J., and Horvitz,H.R. (1992). *C.elegans* cell-signalling gene *sem-5* encodes a protein with SH2 and SH3 domains. *Nature* **356**, 340-344.

Clark,S.G., Shurland,D.-L., Meyerowitz,E.M., Bargmann,C.I., and van der Bliek,A.M. (1997). A dynamin GTPase mutation causes a rapid and reversible temperature-inducible locomotion defect in *C.elegans*. *Proceedings of the National Academy of Sciences (USA)* **94**, 10438-10443.

Clarke, H.F., Brentrup,D., Schneitz,K., Beiber,A., Goodman,C., and Noll,M. (1995). *Dachsous* encodes a member of the cadherin superfamily that controls imaginal disc morphogenesis in *Drosophila*. *Genes and Development* **9**, 1530-1542.

Condic,M.L., Fristrom,D., and Fristrom,J.W., (1991). Apical cell shape changes during *Drosophila* imaginal leg disc elongation: a novel morphogenetic mechanism. *Development* **111**, 23-33.

Costa,M., Draper,B.W., and Priess,J.R. (1997). The role of actin filaments in patterning the *Caenorhabditis elegans* cuticle. *Developmental Biology* **184**, 373-384.

Costa,M., Raich,W. Agbunag,C., Leung,B., Hardin,J., and Priess,J.R. (1998). A putative catenin-cadherin system mediates morphogenesis of the *Caenorhabditis elegans* embryo. *Journal of Cell Biology* **141**, 297-308.

Coulson,A.R., Huynh,C., Kozono,Y., and Shownkeen,R. (1995). The physical map of the *Caenorhabditis elegans* genome In: *Methods in Cell Biology: Volume 48.* Caenorhabditis elegans: *Modern Biological Analysis of an Organism*, 534-550. Edited by Epstein,H.F., and Shakes,D.C. Academic Press.

Coulson,A.R., Sulston,J., Brenner,S., and Karn,J. (1986). Toward a physical map of the genome of the nematode *C.elegans*. *Proceedings of the National Academy of Sciences (USA)* **83**, 7821-7825.

Coulson,A.R., Waterston,R.H., Kiff,J.E., Sulston,J.E., and Kohara,Y. (1988). Genome linking with yeast artificial chromosomes. *Nature* **335**, 184-186.

Coulson,A.R., Kozono,Y., Lutterbach,B., Shownkeen,R., Sulston,J., and Waterston,R. (1991). YACs and the *C.elegans* genome. *BioEssays* **13**, 413-417.

Cox,G.N., and Hirsh,D. (1985). Stage-specific patterns of collagen gene expression during development of *Caenorhabditis elegans*. *Molecular and Cellular Biology* **5**, 363-372.

Cox,G.N., Laufer,J.S., Kusch,M., and Edgar,R.S. (1980). Genetic and phenotypic characterisation of roller mutants of *Caenorhabditis elegans*. *Genetics* **95**, 317-339.

Cox,G.N., Kusch,M., and Edgar,R.S. (1981a). Cuticle of *Caenorhabditis elegans*: its isolation and partial characterisation. *Journal of Cell Biology* **90**, 7-17.

Cox,G.N., Kusch,M., DeNevi,K., and Edgar,R.S. (1981b). Temporal regulation of cuticle synthesis during development of *Caenorhabditis elegans*. *Developmental Biology* **84**, 277-285.

Cox,G.N., Straprans,S., and Edgar,R.S. (1981c). The cuticle of *Caenorhabditis elegans* II. Stage-specific changes in ultrastructure and protein composition during Postembryonic development. *Developmental Biology* **86**, 456-470.

Cox,G.N., Fields,C., Kramer,J.M., Rosenzweig,B., and Hirsh,D. (1989). Sequence comparisons of developmentally regulated collagen genes of *Caenorhabditis elegans*. *Gene* **76**, 331-344.

Culotti,J.G., von Ehrinstein,G., Culotti,M.R., and Russell,R.L. (1981). A second class of acetylcholinesterase-deficient mutants of the nematode *Caenorhabditis elegans*. *Genetics* **97**, 281-305

de Cuevas,M., Lee,J.K., and Spradling,A.C. (1996). α-spectrin is required for germline cell division and differentiation in the *Drosophila* ovary. *Development* **122**, 3959-3968.

Denich,K., Schierenberg,E., Isnenghi,E., and Cassada,R. (1984). Cell lineage and developmental defects of temperature-sensitive embryonic arrest mutants of the nematode *Caenorhabditis elegans*. *Wilhelm Roux's Archives of Developmental Biology* **193**, 164-179.

Deppe,U., Schierenberg,E., Cole,T., Krieg,C., Schmitt,D., Yoder,B., and von Ehrenstein,G. (1978). Cell lineages of the embryo of the nematode *Caenorhabditis elegans*. *Proceedings of the National Academy of Sciences (USA)* **75**, 376-380.

Dodemont,H., Riemer,D., Ledger,N., and Weber,K. (1994). Eight genes and alternative RNA processing pathways generate an unexpectedly large diversity of cytoplasmic intermediate filament proteins in the nematode *Caenorhabditis elegans*. *EMBO Journal* **13**, 2625-2638.

Dopf,J. and Horiagon,T.M. (1996). Deletion mapping of the *Aequorea victoria* green fluorescent protein. *Gene* **173**, 39-44.

Downie,J.R., and Pegrum,S.M. (1971). Organisation of the chick blastoderm edge. *Journal of Embryology and Experimental Morphology* **26**, 623-635.

Draper,B.W., Mello,C.C., Bowerman,B., Hardin,B., and Priess,J.R. (1996). MEX-3 is a KH domain protein that regulates blastomere identity in early *C.elegans* embryos. *Cell* **87**, 205-216.

Dubreuil,R.R., Byres,Y.J., Stewart,C.T., and Kiehart,D.P. (1990). A β-spectrin isoform from *Drosophila* (β_H) is similar in size to vertebrate dystrophin. *Journal of Cell Biology* **111**, 1849-1858.

Edgar,L.G., Wolf,N., and Wood,W.B. (1994). Early transcription in *Caenorhabditis elegans* embryos. *Development* **120**, 443-451.

Elgasaeter,A., Stokke,B.T., Mikkelsen,A., and Branton,D. (1986). The molecular basis of erythrocyte shape. *Science* **234**, 1217-1222.

Ellis,H.M., and Horvitz,H.R. (1986). Genetic control of programmed cell death in the nematode *C.elegans*. *Cell* **44**,817-829.

Engel,J., and Prockop,D.J. (1991). The zipper-like folding of collagen triple helices and the effects of mutations that disrupt the zipper. *Annual Review of Biophysics and Biophysical Chemistry* **20**, 137-152.

Ettensohn,C.A. (1985). Gastrulation in the sea urchin is accompanied by the rearrangement of invaginating epithelial cells. *Developmental Biology* **112**, 383-390.

Favre,R., Hermann,R., Cermola,M., Hohenberg,H., Müller,M., and Bazzicalupo,P. (1995). Immuno-gold-labelling of CUT-1, CUT-2 and cuticlin epitopes in *Caenorhabditis elegans* and *Heterorhabditis sp.* processed by high pressure freezing and freeze-substitution. *Journal of submicroscopic cytology and pathology* **27**, 341-347.

Fessler,J.H., Lunstrum,G., Duncan,K.G., Campbell,A.G., Sterne,R., Bachinger,H.P., and Fessler,L.I. (1984). Evolutionary constancy of basement membrane proteins. In: *The Role of Extracellular Matrix in Development*, 207-219. Liss, New York.

Ferguson,E., and Horvitz,H.R. (1989). The multivulva phenotype of certain *C.elegans* mutants results from defects in two functionally redundant pathways. *Genetics* **123**, 109-121.

Ferguson,K.C., Heid,P.J., and Rothman,J.H. (1996). The SL1 trans-spliced leader RNA performs an essential embrbyonic function in *Caenorhabditis elegans* that can also be supplied by SL2 RNA. *Genes and Development* **10**, 1543-1556.

Finney,M., and Ruvkun,G.B. (1990). The *unc-86* gene product couples cell lineage and cell identity in *C.elegans*. *Cell* **63**, 895-905.

Fire,A. (1986). Integrative transformation of *Caenorhabditis elegans*. *EMBO Journal* **5**, 2673-2680.

Fire,A. (1992). Histochemical techniques for locating *Escherichia coli* β-galactosidase activity in transgenic organisms. *Genetic Analysis - Techniques and Applications* **9**,152-160.

Fire,A., Harrison,S., and Dixon,D. (1990). A modular set of lacZ fusion vectors for studying gene expression in *Caenorhabditis elegans*. *Gene* **93**, 189-198.

Fire,A., Albertson,D., Harrison,S., and Moerman,D. (1991). Production of antisense RNA leads to effective and specific inhibition of gene expression in *C.elegans* muscle. *Development* **113**, 503-514.

Fire,A., Xu,S., Montgomery,M.K., Kostas,S.A., Driver,S.E., and Mello,C.C. (1998). Potent and Specific genetic interference by double-stranded RNA in *Caenorhabditis elegans*. *Nature* **391**, 806-811.

Fleig,R., and Sander,K., (1988). Honeybee morphogenesis: embryonic cell movements that shape the larval body. *Development* **103**, 525-534.

Fristrom,D. (1976). The mechanism of evagination of imaginal disks of *Drosophila melanogaster*. III. Evidence for cell rearrangement. *Developmental Biology* **54**, 163-171.

Fristrom, D. (1982). Septate junctions in imaginal discs of *Drosophila*: a model for the redistribution of septa during cell rearrangement. *Journal of Cell Biology* **94**, 77-87.

Fristrom,D. (1988). The cellular basis of epithelial morphogenesis. A review. *Tissue and Cell* **20**, 645-690.

Francis,R., and Waterston,R.H., (1991). Muscle cell attachment in *Caenorhabditis elegans*. *Journal of Cell Biology* **114**, 465-479.

Fuchs,E., and Weber,K. (1994). Intermediate filaments: structure, dynamics, function and disease. *Annual Review of Biochemistry*. **63**, 345-382.

Fujimoto,D., and Kanaya,S. (1973). Cuticlin: a noncollagen structural protein from *Ascaris* cuticle. *Archives of Biochemistry and Biophysics* **157**, 1-6.

Gatewood,B.K., and Bucher,E.A. (1997). The *mup-4* locus in *Caenorhabditis elegans* is essential for hypodermal integrity, organismal morphogenesis, and embryonic body wall position. *Genetics* **146**, 165-183.

Gendreau,S.B., Moskowitz,I.P.G., Terns,R.M., and Rothman,J.H. (1994). The potential to differentiate epidermis is unequally distributed in the AB lineage during early embryonic development in *Caenorhabditis elegans*. *Developmental Biology* **166**, 770-781.

George,S.E., Simokat,K., Hardin,J., and Chisholm,A.D. (1998). The VAB-1 eph receptor tyrosine kinase functions in neural and epithelial morphogenesis in *C.elegans*. *Cell* **92**, 633-643.

Gettner,S.N., Kenyon,C., and Reichardt,L.F. (1995). Characterization of *beta-pat-3* heterodimers, a family of essential integrin receptors in *C.elegans*. *Journal of Cell Biology* **129**, 1127-1141.

Gieger,B., and Ayalon,O. (1990) Cadherins. *Annual Review of Cell Biology* **8**, 307-332.

Gilchrist,E.J., and Moerman,D.G. (1992). Mutations in the *sup-38* gene of *Caenorhabditis elegans* suppress muscle-attachment defects in *unc-52* mutants. *Genetics* **132**, 431-442.

Gilleard,J.S., Barry,J.D., and Johnstone,I.L. (1997). *cis* regulatory requirements for hypodermal cell-specific expression of the *Caenorhabditis elegans* cuticle collagen gene *dpy-7*. *Molecular and Cellular Biology* **17**, 2301-2311.

Gilleard,J.S., Shafi,Y., Barry,J.D., and McGhee,J.D. (1999). ELT-3: A *Caenorhabditis elegans* GATA factor expressed in the embryonic epidermis during morphogenesis. *Developmental Biology* **208**, 265-280.

Gish,W., and States,D.J. (1993). Identification of protein coding regions by database similarity search. *Nature Genetics* **3**, 266-272.

Giuliano,K.A., and Taylor,D.L. (1995). Measurement and manipulation of cytoskeletal dynamics in living cells. *Current Opinion in Cell Biology* **7**, 4-12.

Godt,D., and Laski,F.A. (1995). Mechanisms of cell rearrangement and cell recruitment in *Drosophila* ovary morphogenesis and the requirement of *bric a brac*. *Development* **121**, 173-187.

Goffeau,A., Barrell,B.G., Bussey,H., Davis,R.W., Dujon,B., Feldmann,H., Galibert,F., Hoheisel,J.D., Jacq,C., Johnston,M., Louis,E.J., Mewes,H.W., Murakami,Y., Philippsen,P., Tettelin,H., and Oliver,S.G. (1996). Life with 6000 genes. *Science* **274**, 546-552.

Goh,P.-Y., and Bogaert,T. (1991). Positioning and maintenance of embryonic body wall muscle attachments in *C.elegans* requires the *mup-1* gene. *Development* **111**, 667-681.

Gong,M.C., Iizuka,K., Nixon,G., Browne,J.P., Hall,A., Eccleston,J..F., Sugai,M., Kobayashi,S., Somlyo,A.V., and Somlyo,A.P. (1996). Role of guanine nucleotide-binding proteins - ras-family or trimeric proteins or both - in Ca^{2+} sentisization of smooth muscle. *Proceedings of the National Academy of Sciences (USA)* **10**, 31-54.

Gotwals,P.J., and Fristrom,J.W. (1991). Three neighbouring genes interact with the *broad-complex* and the *stubble-stubbloid* locus to affect imaginal disc morphogenesis in *Drosophila*. *Genetics* **127**, 747-459.

Granato,M., Schnabel,H., and Schnabel,R. (1994). Genesis of an organ: molecular analysis of the *pha-1* gene. *Development* **120**, 3005-3017.

Greenwald,I. (1997). Development of the vulva. In: *C.elegans II*, 519-542. Edited by Riddle,D.L., Blumenthal,T., Meyer,B.J., and Priess,J.R. Cold Spring Harbor Laboratory Press.

Greenwald,I. (1998). LIN-12/Notch signalling: lessons from worms and flies. *Genes and Development* **12**, 1751-1762.

Gumbiner,B.M. (1993). Proteins associated with the cytoplasmic surface of adhesion molecules. *Neuron* **11**, 551-564.

Gumbiner,B.M. (1996). Cell adhesion: the molecular basis of tissue architecture and morphogenesis. *Cell* **84**, 345-357.

Guo,S., and Kemphues,K. (1995). *par-1*, a gene required for establishing polarity in *C.elegans* embryos, encodes a putative Ser/Thr kinase that is asymmetrically distributed. *Cell* **81**, 611-620.

Guo,X., Johnson,J.J., and Kramer,J.M. (1991). Embryonic lethality caused by mutations in basement membrane collagen of *C.elegans*. *Nature* **349**, 707-709.

Gupta,M.C., Graham,P.L., and Kramer,J.M. (1997). Characterization of α1(IV) collagen mutations in *Caenorhabditis elegans* and the effects of α1 and α2(IV) mutations on type IV collagen distribution. *Journal of Cell Biology* **137**, 1185-1196.

Hall,A. (1998). Rho GTPases and the actin cytoskeleton. *Science* **279**, 509-514.

Han,M., and Sternberg,P.W. (1990). *let-60*, a gene that specifies cell fates during *C.elegans* vulval induction, encodes a *ras* protein. *Cell* **63**, 921-931.

Han,M., Golden,A., Han,Y., and Sternberg,P.W. (1993). *C.elegans lin-45* raf gene participates in *let-60 ras*-stimulated vulval differentiation. *Nature* **363**,133-140.

Hardin,J. (1989). Local shifts in position and polarised motility drive cell rearrangement during sea urchin gastrulation. *Developmental Biology* **136**, 430-445.

Hartenstein,V., and Campos-Ortega,J.A. (1985). Fate mapping in wild-type *Drosophila melanogaster*. *Wilhelm Roux's Archives of Developmental Biology* **194**, 181-197.

Hecht,R.M., Berg-Zabelshansky,M., Rao,P.N., and Davis,F.M. (1987). Conditional absence of mitosis-specific antigens in a temperature sensitive embryonic-arrest mutant of *Caenorhabditis elegans*. *Journal of Cell Science* **87**, 305-314.

Hedgecock,E.M., and White,J.G. (1985). Polyploid tissues in the nematode *Caenorhabditis elegans*. *Developmental Biology* **107**, 128-138.

Hengartner,M.O., and Horvitz,H.R. (1994). *C.elegans* cell survival gene *ced-9* encodes a functional homolog of the mammalian proto-oncogene *bcl-2*. *Cell* **76**, 665-676.

Hengartner,M.O., Ellis,R.E., and Horvitz,H.R. (1992). *C.elegans* gene *ced-9* protects cells from programmed cell death. *Nature* **356**, 494-499.

Herman,R.K. (1995). Mosaic analysis. In: *Methods in Cell Biology: Volume 48.* Caenorhabditis elegans: *Modern Biological Analysis of an Organism*, 123-146. Edited by Epstein,H.F., and Shakes,D.C. Academic Press.

Higgins,B.J., and Hirsh,D. (1977). Roller mutants of the nematode *Caenorhabditis elegans*. *Molecular and General Genetics* **150**, 63-72.

Hill,R.J., and Sternberg,P.W. (1992). The gene *lin-3* encodes an inductive signal for vulval development in *C.elegans*. *Nature* **358**, 470-476.

Hirsh,D., Oppenheim,D., and Klass,M. (1976). Development of the reproductive system of *Caenorhabditis elegans*. *Developmental Biology* **49**, 200-219.

Hogdkin,J.A., Horvitz,H.R., and Brenner,S. (1979). Nondisjunction mutants of the nematode *Caenorhabditis elegans*. *Genetics* **91**, 67-94.

Holder,N., and Klein,R. (1999). Eph receptors and ephrins: effectors of morphogenesis. *Development* **126**, 2033-2044.

Horner,M.A., Quintin,S., Domeier,M.E., Kimble,J., Labouesse,M., and Mango,S. (1998). *pha-4* an *HNF-3* homolog, specifies pharyngeal organ identity in *Caenorhabditis elegans*. *Genes and Development* **12**, 1947-1952.

Hresko,M.C., Williams,B.D., and Waterston,R.H. (1994). Assembly of body wall muscle and muscle cell attachment structures in *Caenorhabditis elegans*. *Journal of Cell Biology* **124**, 491-506.

Huttenlocher,A., Sandborg,R.R., and Horwitz,A. (1995). Adhesion in cell migration. *Current Opinion in Cell Biology* **7**, 697-706.

Hutter,H., and Schnabel,R. (1994). *glp-1* and inductions establishing embryonic axes in *Caenorhabditis elegans*. *Development* **120,** 2051-2064.

Hutter,H., and Schnabel,R. (1995a). Establishment of left-right asymmetry in the *C.elegans* embryo: a multistep process involving a series of inductive events. *Development* **121**, 3417-3424.

Hutter,H., and Schnabel,R. (1995b). Specification of anterior-posterior differences within the AB lineage in the *C.elegans* embryo: A polarising induction. *Development* **121**, 1559-1568.

Iwasaki,K., Staunton,J., Saifee,O., Noney,M., and Thomas,J.H. (1997). *aex-3* encodes a novel regulator of presynaptic activity in *C.elegans*. *Neuron* **18**, 613-622.

Jacobs,J.J.M.R., Litiere,K., van Dijk,V., van Eldik,G.J., van Montagu,M., Cornelissen,M. (1997). Post-transcriptional beta-1,3-glucanase gene silencing involves increased transcript turnover that is translation-independent. *Plant Journal* **12**, 885-893.

Janke,D.L., Schein,J.E., Ha,T., Franz,N.W., ONeil,N.J., Vatcher,G.P., Stewart,H.I., Kuervers,L.M., Baillie,D.L., and Rose,A.M. (1997). Interpreting a sequenced genome: towars a cosmid transgenic library of caenorhabditis elegans. *Genome Research* **7**, 974-985.

Janmey,P.A., Euteneuer,U., Traub,T., and Schliwa,M. (1991). Viscoelastic properties of vimentin comapared with other filamentous biopolymer networks. *Journal of Cell Biology* **113**, 155-160.

Johnsen,R.C., and Baillie,D.L. (1997). Mutation. In: *C.elegans II*, 79-96. Edited by Riddle,D.L., Blumenthal,T., Meyer,B.J., and Priess,J.R. Cold Spring Harbor Laboratory Press.

Johnson,C.D., Rand,J.B., Herman, R.K., Stern,B.D., and Russell,R.L. (1988). The acetylcholinesterase genes of *C.elegans* - identification of a third gene (*ace-3*) and mosaic mapping of a synthetic lethal phenotype. *Neuron* **1**, 165-173.

Johnstone,I.L., Shafi,Y., and Barry,J.D. (1992). Molecular analysis of mutations in the *Caenorhabditis elegans* collagen gene *dpy-7*. *EMBO Journal* **11**, 3857-3863.

Johnstone,I.L. (1994). The cuticle of the nematode *Caenorhabditis elegans*: a complex collagen structure. *BioEssays* **16,** 171-178.

Johnstone,I.L., and Barry,J.D. (1996). Temporal regulation of a precise gene expression pattern during nematode development. *EMBO Journal* **15**, 3633-3639.

Jorgensen,R.A., Atkinson,R.G., Forster,R.L.S., Lucas,W.J. (1998). Research: Botany - An RNA-based information superhighway in plants. *Science* **279**, 1486-1487.

Joshi,H.C., Chu,D., Buxbaum,R.E., and Heidemann,S.R. (1985). Tension and compression in the cytoskeleton of PC12 neurites. *Journal of Cell Biology* **101**, 697-705.

Junkersdorf,B., and Schierenberg,E. (1992). Embryogenesis in *C.elegans* after elimination of individual blastomeres or induced alteration of the cell-division order. *Wilhelm Roux's Archives of Developmental Biology* **202**, 17-22.

Kalb,J.M., Lau,K.K., Goszczynski,B., Fukushige,T., Moons,D., Okkema,P.G., and McGhee,J.D. (1998). *pha-4* is *Ce-fkh-1*, a *forkhead*/HNF-3α,β,γ homolog that functions in organogenesis of the *C.elegans* pharynx. *Development* **125**, 2171-2180.

Katz,W.S., Hill,R.J., Clansinin,T.R., and Sternberg,P.W. (1995). Different levels of the *C.elegans* growth factor LIN-3 promote distinct vulval precursor fates. *Cell* **82**, 297-307.

Keller,R.E. and Trinkaus,J.P. (1987). Rearrangement of enveloping layer cells without distribution of the epithelial permeability barrier as a factor in *Fundulus* epiboly. *Developmental Biology* **120**, 12-24.

Kemler,R., Ozawa,M., and Ringwald,M. (1989). Calcium-dependent cell adhesion molecules. *Current Opinion in Cell Biology* **1**, 892-897.

Kim,U.-J., Shizuya,H., de Jong,P.J., Birren,B., and Simon,M.I. (1992). Stable propagation of cosmid sized human DNA inserts in an F factor based vector. *Nucleic Acids Research* **20**, 1083-1085.

Kimble,J. (1981). Alteration in cell lineage following laser ablation of cells in the somatic gonad of *Caenorhabditis elegans*. *Developmental Biology* **87**,286-300.

Kimble,J., and Hirsh,D. (1979). The postembryonic cell lineages of the hermaphrodite and male gonads in *Caenorhabditis elegans*. *Developmental Biology* **70**, 396-417.

Kimble,J.E., and Sharrock,W.J. (1983). Tissue specific synthesis of yolk proteins in *Caenorhabditis elegans*. *Developmental Biology* **96**, 189-196.

Kimble,J.E., and Ward,S. (1988). Germ-line development and fertilization. In: *The Nematode* Caenorhabditis elegans, 191-213. Edited by Wood,W.B. Cold Spring Harbor Laboratory Press, Cold Spring Harbor, New York.

Kimura,K.D., Ito,M., Amano,M., Chihara,K., Fukata,Y., Nakafu,M., Yamamori,B., Feng,J., Nakano,T., Okawa,K., Iwamatsu,A., and Kaibuchi,K. (1996). Regulation of myosin phosphatase by Rho and Rho-associated kinase (Rho-kinase). *Science* **273**, 245-248.

Kimura,K.D., Tissenbaum,H.A., Liu,Y.X., and Ruvkun,G. (1997). *daf-2*, an insulin receptor-like gene that regulates longevity and diapause in *Caenorhabditis elegans*. *Science* **277**, 942-946.

Klass,M.R., and Hirsh,D. (1976). Nonaging developmental variant of *Caenorhabditis elegans*. *Nature* **260**, 523-525.

Knight,J.K., and Wood,W.B. (1998). Gastrulation initiation in *Caenorhabditis elegans* requires the function of *gad-1*, which encodes a protein with WD repeats. *Developmental Biology* **198**, 253-265.

Kornfield,K., Guan,K.-L., and Horvitz,H.R. (1995). The *Caenorhabditis elegans* gene *mek-2* is required for vulval induction and encodes a protein similar to the protein kinase MEK. *Genes and Development* **9**, 756-768.

Korsmeyer,S.J., Shutter,J.R., Veis,D.J., Merry,D.E., and Oltvai,Z.N. (1993). Bcl-2/Bax: A rheostat that regulates an anti-oxidant pathway and cell death. *Seminars in Cancer Biology* **4**, 327-333.

Koelle,M.R., Talbot,W.S., Segraves,W.A., Bender,M.T., Cherbas,P., and Hogness,D.S. (1991). The *Drosophila* EcR gene encodes an excysone receptor, a new member of the steroid receptor superfamily. *Cell* **67**, 59-77.

Kostrouchova,M., Krause,M., Kostrouch,Z., and Rall,J.E. (1998). CHR3: a *Caenorhabditis elegans* orphan nuclear hormone receptor required for proper epidermal development and moulting. *Development* **125**, 1617-1626.

Kozma,R., Ahmed,S. Best,A., and Lim,L. (1995). The Ras-related protein CDC42HS and Bradykinin promote formation of peripheral actin microspikes and filopodia in swiss 3T3 fibroblasts. *Molecular and Cellular Biology* **15**, 1942-1952.

Kramer,J.M. (1994a). Genetic analysis of extracellular matrix in *C.elegans*. *Annual Review of Genetics* **28**, 95-116.

Kramer,J.M. (1994b). Structures and functions of collagens in *Caenorhabditis elegans*. *FASEB Journal* **8**, 329-336.

Kramer,J.M. (1997). Extracellular matrix. In: *C.elegans II*, 471-500. Edited by Riddle,D.L., Blumenthal,T., Meyer,B.J., and Priess,J.R. Cold Spring Harbor Laboratory Press.

Kramer,J.M., and Johnson,J.J. (1993). Analysis of mutations in the *sqt-1* and *rol-6* collagen genes of *Caenorhabditis elegans*. *Genetics* **135**, 1035-1045.

Kramer,J.M., Cox,G.N., and Hirsh,D. (1985). Expression of the *Caenorhabditis elegans* collagen genes *col-1* and *col-2* is developmentally regulated. *Journal of Biological Chemistry* **260**, 1945-1951.

Kramer,J.M., Johnson,J.J., Edgar,R.S., Basch,C., and Roberts,S. (1988). The *sqt-1* gene of *C.elegans* encodes a collagen critical for organismal morphogenesis. *Cell* **55**, 555-565.

Kramer,J.M., French,R.P., Park,E.-C., and Johnson,J.J. (1990). The *Caenorhabditis elegans rol-6* gene, which interacts with the *sqt-1* collagen gene to determine organismal morphology, encodes a collagen. *Molecular and Cellular Biology* **10**, 2081-2089.

Kusch,M., and Edgar,R.S. (1986). Genetic studies of unusual loci that affect body shape of the nematode *Caenorhabditis elegans* and may code for cuticle structural proteins. *Genetics* **113**, 621-639.

Labouesse,M. (1997). A deficiency screen based on the monoclonal antibody MH27 to identify genetic loci required for morphogenesis of the *C.elegans* embryo. *Developmental Dynamics* **210**, 19-32.

Labouesse,M., Sookhareea,S., and Horvitz.,H.R. (1994). The *Caenorhabditis elegans* gene *lin-26* is required to specify the fates of hypodermal cells and encodes a presumptive zinc-finger transcription factor. *Development* **122**, 2359-2368.

Labouesse,M., Hartwieg,E., and Horvitz,H.R. (1996). The *Caenorhabditis elegans* LIN-26 protein is required to specify and/or maintain all non-neuronal ectodermal cell fates. *Development* **122**, 2579-2588.

Labrousse,A.M., Shurland,D.-L., and van der Bliek,A.M. (1998). Contribution of the GTPase domain to the subcellular localization of dynamin in the nematode *Caenorhabditis elegans*. *Molecular Biology of the Cell* **9**, 3227-3239.

Lackner,M.R., Kornfield,K., Miller,L.M., Horvitz,H.R., and Kim,S.K. (1994). A MAP kinase homologue, *mpk-1*, is involved in ras mediated induction of vulval cell fates in *Caenorhabditis elegans*. *Genes and Development* **8**, 160-173.

Lam,G.T., Jiang,C., and Thummel,C.S. (1997). Coordination of larval and prepupal gene expression by the DHR3 orphan receptor during *Drosophila* metamorphosis. *Development* **124**, 1757-1769.

Lassandro,F., Sebastiano,M., Zei,F., and Bazzicalupo,P. (1994). The role of dityrosine formation in the crosslinking of CUT-2, the product of a second cuticlin gene of *Caenorhabditis elegans*. *Molecular and Biochemical Parasitology* **65**, 147-159.

Laure,L., Ohsugi,M., Hirchenhain,J., and Kemler,R. (1994). E-cadherin null mutant embryos fail to form a trophectoderm epithelium. *Proceedings of the National Academy of Sciences (USA)* **91**, 8263-8267.

Lee,J.K., Coyne,R.S., Dubreuil,R.R., Goldstein,L.S.B., and Branton,D. (1993). Cell shape and interaction defects in α-spectrin mutants of *Drosophila melanogaster*. *Journal of Cell Biology* **123**, 1797-1809.

Lee,R.C., Feinbaum,R.L., and Ambros,V. (1993). The *C.elegans* heterochronic gene *lin-4* encodes small RNAs with antisense complementarity to *lin-14*. *Cell* **75**, 843-854.

Levitan,D., and Greenwald,I. (1995). Facilitation of *lin-12*-mediated signalling by *sel-12*, a *Caenorhabditis elegans S182* Alzheimer's disease gene. *Nature* **377**, 351-354.

Levy,A.D., Yang,J., and Kramer,J.M. (1993). Molecular and genetic analyses of the *Caenorhabditis elegans dpy-2* and *dpy-10* collagen genes: a variety of molecular alterations affect organismal morphology. *Molecular Biology of the Cell* **4**, 803-817.

Li,X. and Greenwald,I. (1998). Additional evidence for an eight-transmembrane-domain topology for *Caenorhabditis elegans* and human presenilins. *Proceedings of the National Academy of Sciences (USA)* **95**, 7109-7114.

Li,H.X., Yang,H., Li,J.X., Hu,Y.P., Wang,X.P., Hao,G.R., Fu,J.L. (1998). EMS-induced mutant frequency and spectrum in bone marrow of D6-2 transgenic mice. *Science in China Series C - Life Sciences* **41**, 286-292.

Liu,Z., and Ambros,V. (1991). Alternative temporal control systems for hypodermal cell differentiation in *Caenorhabditis elegans*. *Nature* **350**, 162-164.

Liu,Z., Kirch,S., and Ambros,V. (1995). The *Caenorhabditis elegans* heterochronic gene pathway controls stage specific transcription of collagen genes. *Development* **121**, 2471-2478.

Luna,E.J., and Hitt,A.L. (1992). Cytoskeleton-plasma membrane interactions. *Science* **258**, 955-964.

Lundquist,E.A., and Herman,R.K. (1994). The *mec-8* gene of *Caenorhabditis elegans* affects muscle and sensory neuron function and interacts with three other genes: *unc-52, smu-1* and *smu-2*. *Genetics* **138**, 83-101.

Lundquist,E.A., Herman,R.K., Rogalski,T.M., Mullen,G.P., Moerman,D.G., and Shaw,J.E. (1996). The *mec-8* gene of *C.elegans* encodes a protein with two RNA recognition motifs and regulates alternative splicing of *unc-52* transcripts. *Development* **122**, 1601-1610.

Lütcke,A., Jannson,S., Parton,R.G., Chavrier,P., Valencia,A., Hyber,L., Lehtonen,E., and Zerial,M. (1993). Rab-17, a novel small GTPase, is specific for epithelial cells and is induced during cell polarization. *Journal of Cell Biology* **121**, 553-564.

Madl,J.E., and Herman,R.K. (1979). Polyploids and sex determination in *Caenorhabditis elegans*. *Genetics* **93**, 393-402.

Mango,S.E., Lambie,E.J., and Kimble,J. (1994a). The *pha-4* gene is required to generate the pharyngeal primordium of *Caenorhabditis elegans*. *Development* **120**, 3019-3031.

Mango,S.E., Thorpe,C.J., Martin,P.R., Chamberlain,S.H., and Bowerman,B. (1994b). Two maternal genes, *apx-1* and *pie-1* are required to distinguish the fates of equivalent blastomeres in the early *Caenorhabditis elegans* embryo. *Development* **120**, 2305-2315.

Martin,P., and Lewis,J. (1992). Actin cables and epidermal movement in embryonic wound healing. *Nature* **360**, 179-183.

McCombie,W.R., Adams,M.D., Kelley,J.M., Fitzgerald,M.G., Utterback,T.R., Khan,M, Dubnick,M., Kerlavage,A.R., Ventre,J.C., and Fields,C. (1992). *Caenorhabditis elegans* expressed sequence tags identify gene families and potential disease gene homologues. *Nature Genetics* **1**, 124-131.

McCormack,S.A., Viar,M.J., and Johnson,L.R. (1992). Migration of IEC-6 cells: a model for mucosal healing. *American Journal of Physiology* **263**, G426-435.

McDowall,J.S., and Rose,A. (1997). Alignment of the genetic and physical maps in the *dpy-5 bli-4 (I)* region of *C.elegans* by the serial cosmid rescue of lethal mutations. *Molecular and General Genetics* **255**, 78-95.

McGhee,J.D. (1995). Cell fate decisions in the early embryo of the nematode *Caenorhabditis elegans*. *Developmental Genetics* **17**, 155-166.

McKeown,C., Pratis,V., and Austin,J. (1998). The *sma-1* gene encodes a β_{Heavy}-spectrin required for *C.elegans* morphogenesis. *Development* **125**, 2087-2098.

Mellman,I. (1996). Endocytosis and molecular sorting. *Annual Review of Cell and Developmental Biology* **12**, 63-84.

Mello,C., and Fire,A. (1995). DNA transformation. In:*Methods in Cell Biology: Volume 48.* Caenorhabditis elegans: *Modern Biological Analysis of an Organism*, 452-482. Edited by Epstein,H.F., and Shakes,D.C. Academic Press.

Mello,C.C., Draper,B.W., and Priess,J.R. (1994). The maternal genes *apx-1* and *glp-1* and establishment of dorsal-ventral polarity in the early *C.elegans* embryo. *Cell* **77**, 95-106.

Mello,C.C., Kramer,J.M., Stinchcomb,D., and Ambros,V. (1991). Efficient gene transfer in *C.elegans*: Extrachromosomal maintenance and integration of transforming sequences. *EMBO Journal* **10**, 3959-3970.

Meneely,P.M., and Herman,R.K. (1981). Suppression and function of X-linked lethal and sterile lethal mutations in *C.elegans*. *Genetics* **97**, 65-84.

Mickey,K.M., Mello,C.C., Montgomery,M.K., Fire,A., and Priess,J.R. (1996). An inductive interaction in 4-cell stage *C.elegans* embryos involves APX-1 expression in the signalling cell. *Development* **122**, 1791-1798.

Miller,D.M., and Shakes,D.C. (1995). Immunofluorescence microscopy. In: *Methods in Cell Biology: Volume 48.* Caenorhabditis elegans: *Modern Biological Analysis of an Organism*, 365-394. Edited by Epstein,H.F., and Shakes,D.C. Academic Press.

Miller,D.M., Ortiz,I., Berliner,G.C., and Epstein,H.F. (1993). Differential localization of two myosins within nematode thick filaments. *Cell* **34**, 477-490.

Miller,L.M., Gallegos,M.E., Morisseau,B.A., and Kim,S.K. (1993). *lin-31*, a *Caenorhabditis elegans* HNF-3/*fork head* transcription factor homolog, specifies three alternative cell fates in vulval development. *Genes and Development* **7**, 933-947.

Milner,M.J., and Muir,J. (1987). The cell biology of *Drosophila* wing metamorphosis *in vitro*. *Wilhelm Roux's Archives of Developmental Biology* **196**, 191-201.

Miura,M., Zhu,H., Rotello,R., Hartweig,E.A., and Yuan,J. (1993). Induction of apoptosis in fibroblasts by IL-1β converting enzyme, a mammalian homolog of the *C.elegans* cell death gene *ced-3*. *Cell* **75**, 653-660.

Moerman,D.G., and Waterston,R.H. (1984). Spontaneous unstable *unc-22* IV mutations in *Caenorhabditis elegans* var. Bergerac. *Genetics* **108**, 859-877.

Moerman,D.G., Hutter,H., Mullen,G.P., and Schnabel,R. (1996). Cell autonomous expression of perlecan and plasticity of cell shape in embryonic muscle of *Caenorhabditis elegans*. *Developmental Biology* **173**, 228-242.

Mohler,W.A., Simske,J.S., Williams-Masson,E.M., Hardin,J.D., and White,J.G. (1998). Dynamics and ultrastructure of developmental cell fusions in the *Caenorhabditis elegans* hypodermis. *Current Biology* **8**, 1087-1090.

Montgomery,M.K., and Fire,A. (1998). Double-stranded RNA as a mediator in sequence-specific genetic silencing and co-suppression. *Trends in Genetics* **14**, 255-258.

Morgan,W.R., and Greenwald,I. (1993). Two novel transmembrane protein tyrosine kinases expressed during *Caenorhabditis elegans* hypodermal development. *Molecular and Cellular Biology* **13**, 7133-7143.

Morin,J.G., and Hastings,J.W. (1971). Energy transfer in a bioluminescent system. *Journal of Cellular Physiology* **77**, 31-318.

Morris,J.Z., Tissenbaum,H.A., and Ruvkun,G. (1996). A phosphatidylinositol-3-OH kinase family member regulating longevity and diapause in *Caenorhabditis elegans*. *Nature* **382**, 536-539.

Moskovwitz,I.P., Gendreau,S.B., and Rothman,J.H. (1994). Combinatorial specification of blastomere identity by *glp-1*-dependent cellular interactions in the nematode *Caenorhabditis elegans*. *Development* **120**, 3325-3338.

Mostov,K., Apodaca,G., Aroeti,B., and Okamoto,C. (1992). Plasma membrane protein sorting in polarized epithelial cells. *Journal of Cell Biology* **116**, 577-583.

Näthke,S.I., Hinck,L., Swedlow.J.R., Papkoff,J., and Nelson,W.J. (1994). Defining interactions and distributions of cadherin and catenin complexes in polarized cells. *Journal of Cell Biology* **125**, 1341-1352.

Nelson,W.J. (1992). Regulation of cell surface polarity from bacteria to mammals. *Science* **258**, 948-955.

Nigon,V. (1949). Les modalités de la reproduction et le déterminisme du sexe chez quelques nematodes libres. *Annales de Sciiences Naturelles -Zool.Biol.Anim.* **11**, 1-132.

Nishiwaki,K., Sano,T., and Miwa,J. (1993). *emb-5*, a gene required for the correct timing of gut precursor cell division during gastrulation in *Caenorhabditis elegans,* encodes a protein similar to the yeast nuclear protein SPT6. *Molecular and General Genetics* **239**, 313-322.

Nobes,C.D., and Hall,A. (1995). Rho, Rac, and CDC42 GTPases regulate the assembly or multimolecular focal complexes associated with actin stress fibers, lamellipodia, and filopodia. *Cell* **81**, 53-62.

Nusrat,A., Delp,C., and Madara,J.L. (1992). Intestinal epithelial restitution. Characterization of a cell culture model and mapping of cytoskeletal elements in migrating cells. *Journal of Clinical investigation* **89**, 1501-1511.

Oda,H., Tsukita,S., and Takeichi,M. (1998). Dynamic behaviour of the cadherin-based cell-cell adhesion system during *Drosophila* gastrulation. *Developmental Biology* **203**, 435-450.

Ogg,S., Paradis,S., Gottlieb,S., Patterson,G.I., Lee,L., Tissenbaum,H.T., and Ruvkun,G. (1997). The Fork head transcription factor DAF-16 transduces insulin-like metabolic and longevity signals in *C.elegans*. *Nature* **389**, 994-999.

Okamoto,H., and Thomson,J.N. (1985). Monoclonal antibodies which distinguish certain classes of neuronal and supporting cells in the nervous tissue of the nematode *Caenorhabditis elegans*. *Journal of Neuroscience* **5**, 643-653.

Page,B.D., Zhang,W., Steward,K., Blumenthal,T., and Priess,J.R. (1997). ELT-1, a GATA-like transcription factor, is required for epidermal cell fates in *Caenorhabditis elegans* embryos. *Genes and Development* **11**, 1651-1661.

Park,Y,-S, and Kramer,J.M. (1994). The *C.elegans sqt-1*and *rol-6* collagen genes are co-ordinately expressed during development, but not at all stages that display mutant phenotypes. *Developmental Biology* **163**, 112-124.

Parker,R.E. (1991). Introductory Statistics for Biology, Second Edition, Cambridge University Press.

Piexoto,C.A., and de Souza,W. (1994). Freeze-fracture characterization of the cuticle of adult and dauer forms of *Caenorhabditis elegans*. *Parasitology Research* **80**, 53-57.

Peixoto,C.A., de Melo,J.V., Kramer,J.M., and de Souza,W. (1998). Ultrastructural analyses of the *Caenorhabditis elegans rol-6(su1006)* mutant, which produces abnormal cuticle collagen. *Journal of Parasitology* **84**, 45-49.

Peters,K., McDowall,J., and Rose,A.M. (1991). Mutations in the *bli-4(I)* locus of *Caenorhabditis elegans* disrupt both adult cuticle and early larval development. *Genetics* **129**, 95-102.

Pettitt,J., Wood,W.B., and Plasterk,R.H.A. (1996). *cdh-3*, a gene encoding a member of the cadherin superfamily funtions in epithelial cell morphogenesis in *Caenorhabditis elegans*. *Development* **122**, 4149-4157.

Plasterk,R.H.A. (1995). Reverse genetics: From gene sequence to mutant worm. In: *Methods in Cell Biology: Volume 48.* Caenorhabditis elegans: *Modern Biological Analysis of an Organism*, 59-80. Edited by Epstein,H.F., and Shakes,D.C. Academic Press.

Platt,H.M. (1994). Forward. In: *The phylogenetic systematics of free-living nematodes*, i-ii. Edited by Lorenzen,S. The Ray Society, London.

Podbilewicz,B., and White,J.G. (1994). Cell fusions in the developing epithelia of *C.elegans*. *Developmental Biology* **161**, 408-424.

Powell-Coffman,J.A., Knight,J., and Wood,W.B. (1996). Onset of *C.elegans* gastrulation is blocked by inhibition of embryonic transcription with an RNA polymerase antisense RNA. *Developmental Biology* **178**, 472-483.

Priess,J.R., and Hirsh,D.I. (1986). *Caenorhabditis elegans* morphogenesis: The role of the cytoskeleton in elongation of the embryo. *Developmental Biology* **117**, 156-173.

Priess,J.R., and Thomson,J.N. (1987). Cellular interactions in early *C.elegans* embryos. *Cell* **48**, 241-250.

Priess,J.R., Schnabel,H., and Schnabel,R. (1987). The *glp-1* locus and cellular interactions in early *C.elegans* embryos. *Cell* **51**, 601-611.

Prieto,A.L., and Crossin,K.L. (1995). Cell-cell adhesion molecules in epithelial-mesenchymal transformations. *Acta Anatomica* **154**, 21-33.

Prockop,D.J., Constantinou,C.D., Dombrowski,K.E., Hojima,Y., Kadler,K.E. Kuivaniemi,H., Tromp,G., and Vogel,B.E. (1989). Type I procollagen: the gene-protein system that harbors most of the mutations causing osteogenesis imperfecta and probably more common heritable disorders of connective tissue. *American Journal of Medical Genetics* **34**, 60-67.

Radice,G.P. (1980). The spreading of epithelial cells during wound closure in *Xenopus* larvae. *Developmental Biology* **76**, 26-46.

Ramachandran,G.N. (1967). Structure of collagen at the molecular level. In: *Treatise on Collagen,* 103-183. Edited by Ramachrandran,G.N. Academic Press, New York.

Ramachandran,G.N., and Ramakrishnan,C. (1976). Molecular structure. In: *Biochemistry of Collagen,* 45-81. Edited by Ramachandran,G.N., and Reddi,A.H. Plenium Press, New York.

Riddle,D.L. (1997). Genetic and environmental regulation of dauer larva development. In: *C.elegans II*, 739-768. Edited by Riddle,D.L., Blumenthal,T., Meyer,B.J., and Priess,J.R. Cold Spring Harbor Laboratory Press.

Ridley,A.J., and Hall,A. (1992) The small GTP-binding protein Rho regulates the assembly of focal adhesions and actin stress fibres in response to growth factors. *Cell* **70**, 389-399.

Ridley,A.J., and Hall,A., (1994). Signal transduction pathways regulating Rho-mediated stress fibre formation: requirement for a tyrosine kinase. *EMBO Journal* **13**, 2600-2610.

Ridley,A.J., Patterson,H.F., Johnston,C.L., Diekmann,D., and Hall,A. (1992). The small GTP-binding protein Rac regulates growth-factor induced membrane ruffling. *Cell* **70**, 401-410.

Rimm,D.L., Koslov,E.R., Kebriaei,P., Cianci,C.D., and Morrow,J.S. (1995). α1 (E)-Catenin is an actin-binding and -bundling protein mediating the attachment of F-actin to the membrane adhesion complex. *Proceedings of the National Academy of Sciences (USA)* **92**, 8813-8817.

Ristoratore,F., Cermola,M., Nola,M., Bazzicalupo., and Favre,R. (1994). Ultrastructural immuno-localisation of CUT-1 and CUT-2 antigenic sites in the cuticles of the nematode *Caenorhabditis elegans*. *Journal of Submicroscopic Cytology and Pathology* **26**, 437-443.

Rodman,J.S., Mercer,R.W., and Stahl,P.D. (1990). Endocytosis and transcytosis. *Current Opinion in Cell Biology* **2**, 664-672.

Rogalski,T.M., Williams,B.D., Mullen,G.P., and Moerman,D.G. (1993). Products of the *unc-52* gene in *Caenorhabditis elegans* are homologous to the core protein of the mammalian basement membrane heparan sulfate proteoglycan. *Genes and Development* **7**, 1471-1484.

Rosenbluth,R.E., Cuddeford,C., and Baillie,D.L. (1985). Mutagenesis in *Caenorhabditis elegans*. II. A spectrum of mutational events induced with 1500 R of gamma-radiation. *Genetics* **109**, 493-511.

Rougvie,A.E., and Ambros,V. (1995). The heterochronic gene *lin-29* encodes a zinc finger protein that controls a terminal differentiation event in *Caenorhabditis elegans*. *Development* **121**, 2491-2500.

Rushforth,A.M., Saari,B., and Anderson,P. (1993). Site-selected insertion of the transposon Tc1 into a *Caenorhabditis elegans* myosin light chain gene. *Molecular and Cellular Biology* **13**, 902-910.

Sambrook,J., Fritsch,E.F., and Maniatis,T. (1989). *Molecular Cloning: A Laboratory Manual*, Second Edition, Cold Spring Harbor, Cold Spring Harbor Laboratory Press.

Schmidt,A. and Hall,M.N. (1998). Signalling to the actin cytoskeleton. *Annual Review of Cell and Developmental Biology* **14**, 305-338.

Schnabel,H., and Schnabel,R. (1990). An organ-specific differentiation gene, *pha-1*, from *Caenorhabditis elegans*. *Science* **250**, 686-688.

Schnabel,R., and Priess,J.R. (1997). Specification of cell fates in the early embryo. In: *C.elegans II*, 361-382. Edited by Riddle,D.L., Blumenthal,T., Meyer,B.J., and Priess,J.R. Cold Spring Harbor Laboratory Press.

Schoenwolf,G.C., and Alvarez,I.S. (1989). Roles of neuroepithelial cell rearrangement and division in shaping of the avian neural plate. *Development* **106**, 427-439.

Sebastiano,M., Lassandro,F., and Bazzicalupo,P. (1991). *cut-1* a *Caenorhabditis elegans* gene coding for a dauer-specific noncollagenous component of the cuticle. *Developmental Biology* **146**, 519-530.

Shapiro,L., Fannon,A.M., Kwong,P.D., Thompson,A., Lehmann,M.S., Grübel,G., Legrand,J.-F., Als-Neilsen,J., Colman,D.R., and Hendrickson,W.A. (1995). Structural basis of cell-cell adhesion by cadherins. *Nature* **374**, 327-337.

Sharma-Kishore,R., White,J.G., Southgate,E., and Podbilewicz,B. (1999). Formation of the vulva in *Caenorhabditis elegans*: a paradigm for organogenesis. *Development* **126**, 691-699.

Shaw,L.M., and Olsen,B.R. (1991). FACIT collagens: diverse molecular bridges in extracellular matrices. *Trends in Biochemical Science* **16**, 191-194.

Sibley,M.H., Graham,P.L., von Mende,N., and Kramer,J.M. (1994). Mutations in the α2(IV) basement membrane collagen gene of *Caenorhabditis elegans* produce phenotypes of differeing severities. *EMBO Journal* **13**, 3278-3285.

Singh,R.N., and Sulston,J.E. (1978). Some observations on moulting in *Caenorhabditis elegans*. *Nematologica* **24**, 63-71.

Simons,K., and Wandinger-Ness,A. (1990). Polarised sorting in epithelia. *Cell* **62**,207-210.

Solnica-Krezel,L., and Driever,W. (1994). Microtubule arrays of the zebrafish yolk cell: organization and function during epiboly. *Development* **120**, 2443-2455.

Sonnhammer,E.L.L., and Durbin,R. (1997). Analysis of protein domain families in *Caenorhabditis elegans*. *Genomics* **46**, 200-216.

Spieth,J., Shim,Y.H., Lea,K., Conrad,R., and Blumenthal,T. (1991). *elt-1*, an embryonically expressed *Caenorhabditis elegans* gene homologous to the GATA transcription factor family. *Molecular and Cellular Biology* **11**, 4651-4659.

Spooner,B.S., Ash,J.F., Wrenn,J.T., Frater,R.B., and Wessels,N.K. (1973). Heavy meromyosin binding microfilaments involved in cell and morphogenetic movements. *Tissue and Cell* **5**, 37-46.

Stern,M.J., Marengere,L.E.M., Daly,R.J., Lowenstein,E.J., Kokel,M., Batzer,A.G., Olivier,P., Pawson,T., and Schlessinger,J. (1993). The human GRB2 and *Drosophila* Drk genes can functionally replace the *Caenorhabditis elegans* cell signalling gene *sem-5*. *Molecular Biology of the Cell* **4**, 1175-1188.

Sternberg,P.W., and Horvitz,H.R. (1986). Pattern formation during vulval development in *C.elegans*. *Cell* **44**, 761-772.

Stinchcomb,D.T., Shaw,J.E., Carr,S.H., and Hirsh,D. (1985). Extrachromosomal DNA transformation of *Caenorhabditis elegans*. *Molecular and Cellular Biology* **5**, 3484-3496.

Strähle,U., and Jesuthasan,S. (1993). Ultraviolet irradiation impairs epiboly in zebrafish embryos: evidence for a microtubule independend mechanism of epiboly. *Development* **119**, 909-919.

Strickland,D.K., Kounnas,M.Z., and Argraves,W.S. (1995). LDL receptor-related protein: a multiligand receptor for lipoprotein and proteinase catabolism. *FASEB Journal* **9**, 890-898.

Sulston,J.E., and Hodgkin,J. (1988). Methods. In: *The Nematode* Caenorhabditis elegans, 587-606. Edited by Wood,W.B. Cold Spring Harbor Laboratory Press, Cold Spring Harbor, New York.

Sulston,J.E., and Horvitz,H.R. (1977). Post-embryonic cell lineages of the nematode, *Caenorhabditis elegans*. *Developmental Biology* **56**, 110-156.

Sulston,J.E., and White,J.G. (1980). Regulation and cell autonomy during postembryonic development of *Caenorhabditis elegans*. *Developmental Biology* **78**, 577-597.

Sulston,J.E., Schierenberg,E., White,J., and Thomson,J. (1983). The embryonic cell lineage of the nematode *Caenorhabditis elegans*. *Developmental Biology* **100**, 64-119.

Sulston,J., Du,Z., Thomas,K., Wilson,R., Hillier,L., Staden,R., Halloran,N., Green,P., Thierry-Mieg,J., Qiu,L., Dear,S., Coulson,A., Craxton,M., Durbin,R., Berks,M., Metstein,M., Hawkins,T., Ainscough,R., and Waterston,R. (1992). The *C.elegans* genome sequencing project: A beginning. *Nature* **356**, 37-41.

Sweeton,D., Parks,S., Costa,M., and Wieschaus,E. (1991). Gastrulation in *Drosophila*: The formation of the ventral furrow and posterior midgut invaginations. *Development* **112**, 775-789.

Tabara,H., Grishok,A., and Mello,C.C. (1998). RNAi in *C.elegans*: Soaking in the genome sequence. *Science* **282**, 430-431.

Takeichi,M. (1991). Cadherin cell adhesion receptors as a morphogenetic regulator. *Science* **251**, 1451-1455.

Tanti,J.F., Gremeauz,T., Grillo,S., Calleja,V., Klippel,A., Williams,L.T., VanObberghen,E., and LeMarchandBrustel,Y.(1996). Overexpression of a constitutively active form of phosphatidylinositol-3-kinase is sufficient to promote Glut4 translocation in adipocytes. *Journal of Biological Chemistry* **271**, 25227-25232.

Thomas,G.H., and Kiehart,D.P. (1994). β_{Heavy}-spectrin has a restricted tissue and subcellular distribution during *Drosophila* embryogenesis. *Development* **120**, 2039-2050.

Thomas,G.H., Newbern,E.C., Korte,C.C., Bales,M.A., Muse,S.V., Clark,A.G., and Kiehart,D.P. (1997). Intragenic duplication and divergence in the spectrin superfamily of proteins. *Molecular Biology and Evolultion* **14**, 1285-1295.

Thomas,G.H., Zarnescu,D.C., Juedes,A.E., Bales,M.A., Londergan,A., Korte,C.C., and Kiehart,D.P. (1998). *Drosophila* β_{Heavy}-spectrin is essential for development and contributes to specific cell fates in the eye. *Development* **125**, 2125-2134.

Thomas,J.H., Stern,M.J., and Horvitz,H.R. (1990). Cell interactions coordinate the development of the *C.elegans* egg-laying system. *Cell* **62**, 1041-1052.

Thornberry,N.A., Bull,H.G., Calaycay,J.R., Chapman, K.T., Howard,A.D., Kostura,M.J., Miller,D.K., Molineaux,S.M., Weidner,J.R., Aunins,J., Elliston,K.O., Ayala,J.M., Casano,F.J., Chin,J., Ding,J.F., Egger,L.A., Gaffney,E.P., Limjuco,G., Palyha,O.C., Raju,S.M., Rolando,A.M., Salley,J.P., Yamin,T., Lee,T.D., Shivley,J.E., MacCross,M.M., Mumford.R.A., Schmidt,J.A., and Tocci,M.J. (1992). A novel heterodimeric cysteine protease is required for interleukin-1β processing in monocytes. *Nature* **356**, 768-774.

Toker,A., and Cantley,L.C. (1997). Signalling through the lipid products of phosphatidylinositol-3-OH kinase. *Nature* **387**, 673-676.

Trinkaus,J.P. (1951). A study of the mechanism of epiboly in the egg of *fundulus heteroclitus*. *Journal of Experimental zoology* **118**, 269-319.

Trinkaus,J.P. (1984). Mechanism of *Fundulus* epiboly- a current view. *American Zoologist* **24**, 673-688.

van der Keyl,H., Kim,H., Espey,R., Oke,C.V., and Edwards,M.K. (1996). *Caenorhabditis elegans sqt-3* mutants have mutations in the *col-1* collagen gene. *Developmental Dynamics* **201**,86-94.

Vaux,D.L., Weissman,I.L., and Kim,S.K. (1992). Prevention of programmed cell death in *Caenorhabditis elegans* by human *bcl-2*. *Science* **258**, 1955-1957.

von Kalm,L., Fristrom,D., and Fristrom,J. (1995). The making of a fly leg: a model for epithelial morphogenesis. *BioEssays* **17**, 693-702.

von Mende,N., Bird,D.McK., Albert,P.S., and Riddle,D.L. (1988). *dpy-13*: a nematode collagen gene that affects body shape. *Cell* **55**, 567-576.

Watson,B.D. (1965). The fine structure of the body wall and the growth of the cuticle in the adult nematode *Ascaris lumbricoides*. *Quarterly Journal of Microbiological Science* **106**, 83-91.

Waterston,R.H. (1988). Muscle. In: *The Nematode* Caenorhabditis elegans, 281-335. Edited by Wood,W.B. Cold Spring Harbor Laboratory Press, Cold Spring Harbor, New York.

Waterston,R.H. (1989). The minor myosin heavy-chain, MHC A, of *Caenorhabditis elegans* is necessary for the initiation for thick filament assembly. *EMBO Journal* **8**, 3429-3436.

Waterston,R., Martin,C., Craxton,M., Huynh.C., Coulson,A., Hillier,A., Durbin,R., Green,P., Shownkeen,R., Halloran,N., Metzstein,M., Hawkins,T., Wilson,R., Berks,M., Du,Z., Thomas,K., Thierry-Mieg,J., and Sulston,J. (1992). A survey of expressed genes in the nematode *Caenorhabditis elegans*. *Nature Genetics* **1**, 114-123.

White,J. (1988). The anatomy. In: *The Nematode* Caenorhabditis elegans, 81-122. Edited by Wood,W.B. Cold Spring Harbor Laboratory Press, Cold Spring Harbor, New York.

White,J.,Southgate,E., Thomson,J.N., and Brenner,S. (1986). The structure of the ventral nerve cord of *Caenorhabditis elegans*. *Philosophical Transactions of the Royal Society (London) Series B. Biological Sciences* **275**, 327-348.

Williams,B.D. (1995). Genetic mapping with polymorphic sequence-tagged sites. In: *Methods in Cell Biology: Volume 48.* Caenorhabditis elegans: *Modern Biological Analysis of an Organism*, 81-96. Edited by Epstein,H.F., and Shakes,D.C. Academic Press.

Williams,B.D., and Waterston,R.H. (1994). Genes critical for muscle development and function in *Caenorhabditis elegans* identified through lethal mutations. *Journal of Cell Biology* **124**, 475-490.

Williams,B.D., Schrank,B., Huynh,C., Shownkeen,R., and Waterston,R.H. (1992). A genetic mapping system in *Caenorhabditis elegans* based on polymorphic sequenced-tagged sites. *Genetics* **131**, 609-624.

Williams-Masson,E.M., Malik,A.N., and Hardin,J. (1997). An actin-mediated two-step mechanism is required for ventral enclosure of the *C.elegans* hypodermis. *Development* **124**, 2889-2901.

Williams-Masson,E.M., Heid,P.J., Lavin,C.A., and Hardin,J. (1998). The cellular mechanism of epithelial rearrangement during morphogenesis of the *Caenorhabditis elegans* dorsal hypodermis. *Developmental Biology* **204**, 263-276.

Wilson,P.A., and Keller,R.E. (1991). Cell rearrangement during gastrulation of *Xenopus*: Direct observation of cultured explants. *Development* **105**, 155-166.

Wissmann,A., Ingles,J., McGhee,J.D., and Mains,P.E. (1997). *Caenorhabditis elegans* LET-502 is related to Rho-binding kinases and human myotonic dystrophy kinase and interacts genetically with a homolog of the regulatory subunit of smooth muscle myosin phosphatase to affect cell shape. *Genes and Development* **11**, 409-422.

Wood,W.B. (1988). Embryology. In: *The Nematode* Caenorhabditis elegans, 215-241. Edited by Wood,W.B. Cold Spring Harbor Laboratory Press, Cold Spring Harbor, New York.

Wrischnik,L.A. and Kenyon,C.J. (1997). The role of *lin-22*, a *hairy/Enhancer of split* homolog, in patterning the peripheral nervous system of *C.elegans*. *Development* **124**, 2875-2888.

Wu,Y., and Han,M. (1994). Suppression of activated Let-60 Ras defines a role of *Caenorhabditis elegans sur-1* MAP kinase in vulval differentiation. *Genes and Development* **8**, 147-159.

Wu,Y., Han,M., and Guan,K.-L. (1995). MEK-2, a *Caenorhabditis elegans* MAP kinase kinase, functions in Ras-mediated vulval induction and other developmental events. *Genes and Development* **9**, 742-755.

Xue,D., and Horvitz,H.R. (1995). Inhibition of the *Caenorhabditis elegans* cell-death protease CED-3 by a CED-3 cleavage site in baculovirus p35 protein. *Nature* **377**, 248-251.

Xue,D., Shaham,S., and Horvitz,H.R. (1996). The *Caenorhabditis elegans* cell-death protein CED-3 is a cysteine protease with substrate specificities similar to those of the human CPP32 protease. *Genes and Development* **10**, 1073-1083.

Yang,J., and Kramer,J.M. (1994). *In vitro* mutagenesis of *Caenorhabditis elegans* cuticle collagens identifies a potential subtilisin-like protease cleavage site and demonstrates that carboxyl domain dilsulfide bonding is required for normal function but not assembly. *Molecular and Cellular Biology* **14**, 2722-2730.

Yochem,J., and Greenwald,I. (1989). *glp-1* and *lin-12*, genes implicated in distinct cell-cell interactions in *Caenorhabditis elegans*, encode similar transmembrane proteins. *Cell* **58**, 553-563.

Yochem,J., Tuck,S., Greenwald,I., and Han,M. (1999). A gp330/megalin-related protein is required in the major epidermis of *Caenorhabditis elegans* for completion of moulting. *Development* **126**, 597-606.

Young,P.E., Richman,A.M., Ketchum, A.S. and Kiehart,D.P. (1993). Morphogenesis in *Drosophila* requires nonmuscle myosin heavy chain function. *Genes and Development* **7**, 29-41.

Yuan,J., Shaham,S., Ledoux,S., Ellis,H.M., and Horvitz,H.R. (1993). The *C.elegans* cell death gene *ced-3* encodes a protein similar to mammalian interleukin-1β converting enzyme. *Cell* **75**, 641-652.

Zacchi,P., Stenmark,H., Parton,R., Orioli,D., Lim,F., Giner,A., Mellman,I., Zerial,M., and Murphy,C. (1998). Rab17 regulates membrane trafficking through apical recycling endosomes in polarized epithelial cells. *Journal of Cell Biology* **140**, 1039-1053.

Zackson,S.L. (1984). Cell lineage, cell-cell interaction, and segment formation in the ectoderm of a glossiphoniid leech embryo. *Developmental Biology* **104**, 143-160.

Zhu,J., Hill,R.J., Heid,P.J., Fukuyama,M., Sugimoto,A., Priess,J.R., and Rothman,J.H. (1997). *end-1* encodes an apparent GATA factor that specifies the endoderm precursor in *Caenorhabditis elegans* embryos. *Genes and Development* **11**, 2883-2896.

Zwaal,R.R., Ahringer,J., van Leunen,H.G.A.M., Rushforth,A., Anderson,P., and Plasterk,R.H.A. (1996). G proteins are required for spatial orientation of early cell cleavages in *C.elegans* embryos. *Cell* **86**, 619-629.

Zwaal,R.R., Broeks,A., van Meurs,J., Groenen,J.T.M., and Plasterk,R.H.A. (1993). Target-selected gene inactivation in *Caenorhabditis elegans* by using a frozen transposon insertion mutant bank. *Proceedings of the National Academy of Sciences (USA)* **90**, 7431-7435.